INFORMATION TO USERS

This manuscript has been reproduced from the microfilm master. UMI films the text directly from the original or copy submitted. Thus, some thesis and dissertation copies are in typewriter face, while others may be from any type of computer printer.

The quality of this reproduction is dependent upon the quality of the copy submitted. Broken or indistinct print, colored or poor quality illustrations and photographs, print bleedthrough, substandard margins, and improper alignment can adversely affect reproduction.

In the unlikely event that the author did not send UMI a complete manuscript and there are missing pages, these will be noted. Also, if unauthorized copyright material had to be removed, a note will indicate the deletion.

Oversize materials (e.g., maps, drawings, charts) are reproduced by sectioning the original, beginning at the upper left-hand corner and continuing from left to right in equal sections with small overlaps.

Photographs included in the original manuscript have been reproduced xerographically in this copy. Higher quality 6" x 9" black and white photographic prints are available for any photographs or illustrations appearing in this copy for an additional charge. Contact UMI directly to order.

ProQuest Information and Learning
300 North Zeeb Road, Ann Arbor, MI 48106-1346 USA
800-521-0600

Université d'Ottawa · University of Ottawa

SUBMERGED VANE PERFORMANCE IN STRONGLY CURVED NARROW CHANNEL BENDS

ADAM VOISIN

A thesis

submitted under the supervision of

Dr. R. D. Townsend

in partial fulfillment of the requirements for the degree of

Master of Applied Science in Civil Engineering

Department of Civil Engineering

University of Ottawa

Ottawa, Canada

K1N 6N5

July, 2001

ACKNOWLEDGMENTS

I would like to thank my supervisor, Dr. R. Townsend for his invaluable guidance, encouragement, constant interest, and availability throughout the course of this research.

Much of the construction of the experimental apparatus was done with the assistance of Mr. Bob Moore. His help is greatly appreciated. I am also grateful to the Civil Engineering support staff for their excellent service.

Furthermore, I would like to express appreciation to Dr. R. Frenette, Jason Bettez for their useful comments and suggestions.

Finally, I would like to thank my family for their support and encouragement throughout this work.

ABSTRACT

This thesis reports on a laboratory study which examines the effectiveness of submerged vanes for the control of erosion in strongly curved narrow channel bends. Submerged vanes are thin flow-training structures that protrude above the channel bed to a height of approximately 0.2 to 0.5 times the flow depth. They have lengths of 1 to 4 times their height, and are typically angled between 5 and 30 degrees to the free-stream flow direction (counterclockwise, when viewed in plan, in a bend turning to the right). The vanes induce a secondary current which may be harnessed to counteract the centrifugally-induced helicoidal flow in channel bends. A reduction in the strength of the helicoidal current will in turn lead to a corresponding reduction in outer bank erosion.

Leopold and Wolman (1960) report that rivers of various sizes and geographical settings share a common curvature ratio, r/b = 3.0 (where: r = bend radius, and b = channel width). Many researchers associate the maximum river bend migration rate with this particular curvature ratio (Biedenharn et al. 1989; Begin 1986, 1981; Hickin and Nanson 1975, 1986). Most of the previous laboratory research on submerged vanes has been performed at the University of Iowa. The two Iowa test channels incorporated bend sections with r/b = 5.37 and 6.75. These values are sufficiently higher than the aforementioned r/b value to render them inappropriate for properly representing streams or rivers that experience the highest rates of bend migration. The current work attempts to address this deficiency by investigating the (laboratory) case where submerged vanes are employed in channel bends with r/b = 2.95 and b/d = 3.05 (where: d = flow depth).

Physical model testing was performed to determine the effects of several parameters which affect submerged vane performance, namely: submerged vane height H, length L, angle to main flow direction α, vane streamwise spacing δ_s, vane transverse spacing from outer bank δ_n, and bend angle φ. Two bend angles were examined in this study. The majority of testing was performed in a 90° bend, and a limited number of tests were performed in a 135° bend with the same radius. The experimental data indicate that the greater bend angle results in less efficient submerged vane operation. Previous analyses of submerged vane performance (Odgaard and Lee 1984; Odgaard and Wang, 1991a) do not adequately describe our conditions since they assume that the transverse channel bed slope is *linear*, and that the channel is hydraulically *wide* (b/d < 10). The transverse bed slope observed in the present study was highly *non-linear*, and the experimental channel is hydraulically *narrow*. Accordingly, a unique empirical method of analysis was developed and is presented herein.

The results indicate that vane height, angle to the main flow direction and transverse spacing from outer bank have the greatest influence on submerged vane performance. Vane length and streamwise spacing have less influence on their performance. The optimum submerged vane configuration incorporates vanes with height and length of $H/d_i = 0.33$ and $L/b = 0.35$, respectively. These vanes should be spaced at a distance of $\delta_n/b = 0.24$ from the outer bank, be installed at $\alpha = 2°$ to the main flow direction, and have a streamwise spacing of $\delta_s/b = 0.70$. The trends exhibited by each parameter examined on vane performance are examined herein.

TABLE OF CONTENTS

LIST OF SYMBOLS

A_V	vane density
b	channel width
B	function of Coulomb friction factor and ratio of lift force to drag force for a bed particle
c_D	drag coefficient
c_L	lift coefficient
d	local flow depth
$\bar{d}$	cross-sectional average depth
d_c	depth of flow at channel centreline
d_i	initial flow depth (prior to scouring)
d_s	vertical distance between initial bed elevation and final bed elevation for zones of scour
$(d_s)_{ave}$	average of all negative bed elevation changes
d_0	normal flow depth
D	median grain size diameter
D_s	average of all d_s
D_{50}	grain size for which 50% by weight is finer
f	Darcy-Weisbach friction factor
f_V	function (eq. 2.43)
$\mathbf{F_D}$	densimetric Froude number
F	vane function, shear stress
F_D	horizontal drag force
F_L	horizontal lift force
F_{min}	minimum vane function
g	gravitational acceleration
G	function (eq. 2.59)
H	vane height
k	factor of order 2/3; turbulence kinetic energy
L	vane length
m	velocity profile exponent
n	axis perpendicular to s-axis and positive toward concave (outer) bank
p	pressure

q_n volumetric bed-load transport per unit width in the n-direction

q_s volumetric bed-load transport per unit width in the s-direction

Q discharge

r radius from centre of bend curve

r_c radius from curve centre to channel centreline

r_e effective bend radius

r_{e0} effective radius associated with S_{n0}

r_i radius from curve centre to inner bank

r_o radius from curve centre to outer bank

r_v radial distance from vortex core

s axis along channel centreline and positive in the streamwise direction

S longitudinal slope of water surface

S_n transverse bed slope

S_{n0} non-zero objective transverse bed slope

S_o outer bank transverse bed slope

$(S_o)_{ave}$ average outer bank transverse bed slope

T_c torque on flow caused by centrifugally-induced secondary current

T_v torque on flow caused by thin flat vane

u time-averaged velocity component in s-direction

u_{ap} vane approach velocity

u_{cr} critical velocity for sediment movement

$\bar{u}$ depth-averaged value of v

$\bar{u}_c$ depth averaged mean velocity at channel centreline

u_{ave} cross-sectional average velocity

u_* shear velocity

v time-averaged velocity component in n-direction

v_b near-bed transverse velocity component

v_{bv} near-bed transverse velocity component induced by vane

v_θ vortex tangential velocity (perpendicular to its core axis)

w time-averaged velocity component in z-direction

z axis perpendicular to s-axis and positive vertically upward

Greek Symbols

α	vane angle of incidence with flow
α_e	vane effective angle of incidence with flow caused by downwash
α_{max}	maximum angle tested
α'	vane geometrical angle of incidence with flow (see eq. 2.31)
β	change in vane effective angle of incidence with flow caused by downwash, factor arising from averaging process (eqs. 2.50 & 2.51)
Γ	vortex horizontal circulation
δ_b	spacing between bank and vane
δ_n	transverse spacing between vanes
δ_s	streamwise spacing between vanes
ε	eddy viscosity
η	angle that the near-bed velocity forms with the mean flow direction
κ	von Kármán's constant
λ	interaction coefficient
φ	bend angle included in computation
φ_e	effective bend angle included in computation
ρ	fluid density
ρ_s	bed sediment particle density
θ	Shields' parameter
τ_{cr}	critical shear stress for sediment movement
τ_0	bed shear stress in streamwise direction
ψ	aspect ratio (vane height/length)
ε	rate of turbulence kinetic energy dissipation

Subscripts

b	refers to near-bed value
c	refers to channel bend centreline value
n	refers to transverse direction
s	refers to streamwise direction
S	refers to free-surface component
V	refers to value induced by vane
z	refers to vertical direction

LIST OF FIGURES

LIST OF TABLES

CHAPTER ONE

INTRODUCTION

1.1 Statement of the Problem

In 1981, the final report of work done in the United States under the Streambank Erosion Control Evaluation and Demonstration Act of 1974 (Section 32, Public Law 93-251) was submitted to the Congress by the U.S. Army Corps of Engineers (U.S. Army Corps of Engineers, 1981). The report concluded that streambank erosion is a major problem which affects many American streams and waterways, resulting in serious economic losses of private and public lands, bridges, etc. Of course, if the problem is a major one in the United States, then it is also likely to be a major problem in Canada and elsewhere, where rivers and streams are a common feature of the geographical makeup. According to the study, approximately 17% of America's 5,540,000 km of streams and waterways are in need of erosion protection. It was estimated that by using conventional bank protection methods, costs would exceed $1 billion (1981 USD) annually.

A river may experience varied causes of erosion at different locations along its length. Also, the erosion processes that occur in large rivers are generally quite different from those occurring in small streams. In order to study these different erosion processes, two types of laboratory research are required. The first type, which is used to determine the relative effectiveness of various streambank protection methods, consists of tests which are universal in nature, and strives to model a broad range of field conditions. The second type is used to model the effectiveness of various streambank protection measures for a particular field condition. Both research approaches serve to reinforce our knowledge of streambank erosion, causes, and controls, and inevitably lead to full-scale performance studies in the field. The research presented herein is of the former type.

The damages resulting from streambank erosion encompass direct or indirect loss of income, or reduction in environmental quality. The U.S. Army Corps of Engineers (1981) recognizes three categories of damages: land loss, sediment, and others. *Land loss* is the most obvious damage; however, the term refers

to more than simple channel enlargement or migration onto valuable property. One may argue that, in the case of channel migration, the land owner on the receding side (usually the inner bank) is gaining property; however, this is not the case. The land that is left behind is usually uncompacted, coarse, unfertile soil which is lower in elevation. Because it is rarely as valuable as the land which was eroded, the land exchange resulting from bend migration generates a net economic loss. Furthermore, if the stream defines a real estate boundary, the resurvey and litigation required to settle disputes incur additional costs. Lastly, land loss also incorporates that land which is underutilized due to the threat of streambank migration.

Damage resulting from *sedimentation* may be less obvious since it usually occur far from the erosion site, but these are also substantial. An increase in suspended sediment increases water treatment costs, a reduction in the operating life of machinery, and adversely affects shellfish quality, recreational use, and the aesthetic value of the river. The sediment deposited from suspension requires increased dredging costs to ensure navigable depths in harbours and waterways. Higher costs are also associated with the increased size of reservoirs required to accommodate the sediment influx. Also, when channel bed material that has been stable for several years in resuspended, it releases compounds containing nutrients like phosphorous and nitrogen. These nutrients result in increased vegetation and organism growth which, in turn, stimulate the eutrophication process and degrades water quality. *Other damages* include those losses incurred when structures located at a river's edge are made unsafe because of the erosion triggered in their immediate vicinity. Also, increased costs are associated with the over-design of any structure which can not tolerate the effects of erosion because of the potential threat to human life (i.e., floodwall, bridge, water treatment plant). Lastly, eroded streambanks are usually unsightly and contribute to reduced environmental quality.

Despite the complexity of river morphological processes, Leopold and Wolman (1960) report a marked similarity in curvature ratios, r/b, among various rivers of greatly-differing sizes. They indicate that, in a sample of 50 rivers, the median and mean r/b are 2.7 and 3.1, respectively. Also, approximately two-thirds of the values fall between 1.5 and 4.3, and one-quarter fall between 2.0 and 3.0. In fact, Leopold and Wolman note that the ratio is so similar among rivers of various sizes that, without looking at the scale on a planimetric map, it is impossible to determine whether the river is large or small. It is also interesting that the maximum rate of river bend migration is often associated with $r/b = 3.0$ (Biedenharn et al., 1989; Begin, 1981, 1986; Hickin and Nanson, 1975, 1986). Hickin and Nanson (1975) showed that the maximum migration rate occurs at $r/b = 3$ and declines rapidly on either side of this value. Of several

data from 18 river reaches, the median migration rate is approximately 2 channel widths per century, and only 10% of the rates exceed 5.5 channel widths per century.

Previous experimentation on the use of submerged vanes to control and reduce scour, though unquestionably valuable, has nonetheless left a large research gap. Literature indicates that the bulk of past research was performed at the Iowa Institute of Hydraulic Research, University of Iowa (Odgaard and Wang, 1991b, 1990; Odgaard and DeWitt, 1989; Odgaard and Spoljaric, 1989, 1986a, 1986b; Odgaard and Mosconi, 1987; Odgaard and Lee, 1984; and Odgaard and Kennedy, 1983). The two Iowa test channels that incorporated bends had $r/b = 5.37$ and 6.75. These values are sufficiently outside of the r/b range to render them inappropriate for properly representing natural river conditions. Furthermore, they inadequately represent those rivers which experience the highest rates of bend migration. The current work attempts to address this deficiency by investigating the (laboratory) case where $r/b \approx 3.0$. Submerged vanes are employed in channel bends wherein $r/b = 3.0$ and $b/d << 10$.

The problem of river bank scour is the result of complex interactions which are dependent on streamflow characteristics, sediment transport capacity of the stream, river bank stability and the effects of man's activities. Because of the vertical velocity gradient, flow through a river bend has a maximum longitudinal velocity at the free surface and a minimum at the channel bed. In the river bend, this gradient results in a difference in centrifugal acceleration which is defined by u^2/r (where u = local longitudinal velocity, and r = bend radius). The vertically differing centrifugal acceleration induces a *spiral motion* (counterclockwise when looking downstream in a bend curving to the right) in the direction normal to that of the primary flow. This spiral motion is also referred to as the *helicoidal motion*, *transverse circulation*, or perhaps most commonly, the *secondary current*. The secondary current tends to erode, or scour the outer bank by moving the sediment at the channel bed laterally from the outer bank to the inner bank. This process, once initiated, is further exaggerated as the newly deepened section near the outer bank allows the heavily concentrated longitudinal flow to attack the bank at an even greater intensity.

As the channel approach flow attacks a submerged vane, a high pressure zone forms at the upstream face, and a low pressure zone forms at the downstream face. The pressure differential across a vane induces a current over the top of the latter which is carried downstream by the longitudinal flow as a helicoidal vortex. This vortex is responsible for changes in the near-bed velocity, shear stress, and hence, the bed topography in the vicinity of the vanes. The vane-induced helicoidal current may be used in a channel

bend to reduce or completely eliminate the naturally-developed centrifugally-induced secondary current. A reduction in the natural secondary current leads to a reduction in (or possible cessation of) outer-bank scour.

To date, two vane design methods have been developed (Odgaard and Lee, 1984; Odgaard and Wang, 1991a). The older of the two is based on the use of vanes to reduce or eliminate channel transverse bed slope, while the newer method is based on the elimination of transverse bed shear stress. For the channel conditions examined in the present study, neither method is directly applicable. The first method assumes that the transverse bed slope is *linear*, which is only appropriate for a *wide* channel condition ($b/d > 10$). The second method assumes that the channel is *wide* in the reduction of the three-dimensional equations of motion. The transverse bed slope observed in the present narrow channel study was highly non-linear. Accordingly, a unique empirical method of analysis was developed and is presented herein. The method is based on the application of various failure criteria to the data collected.

1.2 Outline of Thesis

Chapter two of the thesis is divided into two main sections. The first section, in addition to describing the 'vane' concept, also reviews the more traditional river bank stabilization methods, including: bank protection, dikes, grade-control structures, cutoffs, and bendway weirs. The second section presents the two analyses and design methods related to the application of submerged vanes. The first method deals with elimination of transverse bed slope, and the second deals with elimination of transverse shear stress. Obviously, the principles behind the two analyses are intimately related; however, they are separately developed.

Chapter three describes the experimental apparatus, including the bend test sections used, depth and velocity-measurement devices, and the submerged vanes employed. Also presented therein are the physical modelling considerations. It is shown that our laboratory conditions model natural conditions more accurately than the channels used in the earlier similar-type studies.

In chapter four, the conditions which governed the testing program are discussed. These required either preliminary experimentation or thorough investigation to determine their relative importance and impact. They included: sediment characteristics, channel slope, velocity, vane sizes used, vane angles investigated, vane placement, channel bend angles, and test duration. The sediment characteristics were

determined by uniformity and size criteria, which would not result in rippling or armouring of the streambed. The channel slope was then selected based on the sediment characteristics and the requirement of uniform flow depth in the test section. All tests were done at the critical velocity for initiation of sediment movement. The vane and channel bend properties are discussed and finally, an explanation for the selected test duration is given.

Chapter five includes: the experimental procedures followed, the related parametric study and the method of analysis. This is followed by detailed discussions on the effects of vane height, vane length, vane angle, vane streamwise spacing, vane transverse spacing from outer bank, vane aspect ratio (height/length), and bend angle on submerged vane performance. The section on vane height examines its effect on vane performance for narrow, intermediate-length and long vanes. Likewise, the section on vane length examines its effect on vane performance for short, intermediate-height, and tall vanes. The sections on vane angle and streamwise spacing also examine their effects on vane performance for vanes of various heights and lengths. Discussions are given on the effects of local scour and on design practicality. Finally, a summary of the optimum design configuration is given at the end of the chapter. The summary, conclusions and research needs are presented in chapter six.

CHAPTER TWO

LITERATURE REVIEW

2.1 Introduction

The control of sediment transport is a problem that has captured the interest of many river engineers. It involves the management of two natural river processes: streambank erosion and aggradation. Either may be induced or exaggerated by human activities and both result in adverse fluvial conditions. Excessive scour of the outer bank of a river bend causes undermining and bank failure, which accelerates lateral and downstream river bend migration. Excessive deposition at the inner bank of a river bend reduces flow area, and thus, reduces the capacity of the river to convey flood flows. In addition, it may interfere with navigation.

Streambanks can be protected or restored either by increasing resistance of the bank to erosion or by decreasing the energy of the water at the point of contact with the bank (i.e., by deflecting the flow). All river stabilization and rectification works are done for the same reason, and that is to shape a river into a single channel which follows a path of easy bends of reverse curvature, and to fix it permanently on that alignment. There are two primary functions of river stabilization and rectification (Petersen, 1986):

(*i*) to prevent bank erosion and the subsequent loss of land that threatens life and property, and

(*ii*) to improve stream alignment, cross-sectional shape, and depth to reduce flood stage and to improve navigation conditions.

A secondary function is to concentrate flows in relatively deep narrow channels to reduce transpiration, evaporation, and seepage losses in arid and semiarid areas. Some objectives of stabilization and rectification works include:

(*i*) preventing the need for periodic setback of levees,

(*ii*) preventing damage or loss of property and crops on the overbank,

(*iii*) preventing damage to bridges and utility lines crossing a river,

(*iv*) preventing flanking of locks on a canalized river, and

(*v*) providing an adequate channel for commercial navigation.

A successful river training work will control the river, not by forcing it through unnatural conditions, but by guiding it along a natural alignment with a channel cross-section that accommodates the river's water/sediment regime. Four traditional and two contemporary types of river stabilization works will be discussed in this section. The traditional types include *bank protection*, *dikes*, *grade-control structures*, and *cutoffs*; the contemporary types are *bendway weirs* and *submerged vanes*.

2.1.1 Bank Protection

Traditionally, river banks have been stabilized with many different material types and procedures, including: riprap (Chang, 1988), rock trenches (Petersen, 1986), mattresses (*ibid.*), gabions (*ibid.*), soil-cement blocks (*ibid.*), and cribs (Schiechtl and Stern, 1997). These methods must all be installed from above the design high water stage to well below the expected scour. They should also accommodate various unpredictable events, such as erratic hydrologic phenomena, changes in flood plain vegetation, unforseen settlement, channel-bed aggradation, accumulation of trash and debris, etc.

While these traditional methods are generally simple to design and work very effectively, they are usually costly, require labor-intensive installation procedures, and are unsightly. To overcome these problems, river engineers have developed bioengineered bank stabilization methods which control erosion and stabilize soil by installing hardy herbaceous (i.e., grassy) or woody (i.e., trees and shrubs) vegetation (Przedwojski et al., 1995).

2.1.1.1 Rock Riprap

Because of its effectiveness and availability, rock riprap is a common bank protection material (Fig. 2.1). It is capable of accommodating minor undermining of the bank toe, since it is composed of loose stones and can therefore settle to fill those areas where the scour has occurred. Its stability depends on factors such as the stone size, grading, weight, shape, and layer thickness. It is preferable to use hard, durable angularly-shaped rock. The design size is based on tractive force theory, and the size distribution should be well-graded (i.e., having good representation of all particle sizes) so that smaller stones will fill the

cavities between the larger stones. The layer thickness is usually 30 cm or the diameter of the largest stone, whichever is greater. Rock riprap is either placed on a filter blanket or directly on the prepared slope and is installed by hand or by machine. as long as layer thickness uniformity is ensured. and no segregation in size occurs.

A filter layer may be required below the riprap layer to prevent the water from removing bank material through the voids. It may be composed of a layer of finer gravel (size range from 6 mm to 75 mm) or a plastic filter cloth. If there exists a great size disparity between the riprap material and the filter material. then multiple filter layers may be required in gradually decreasing sizes.

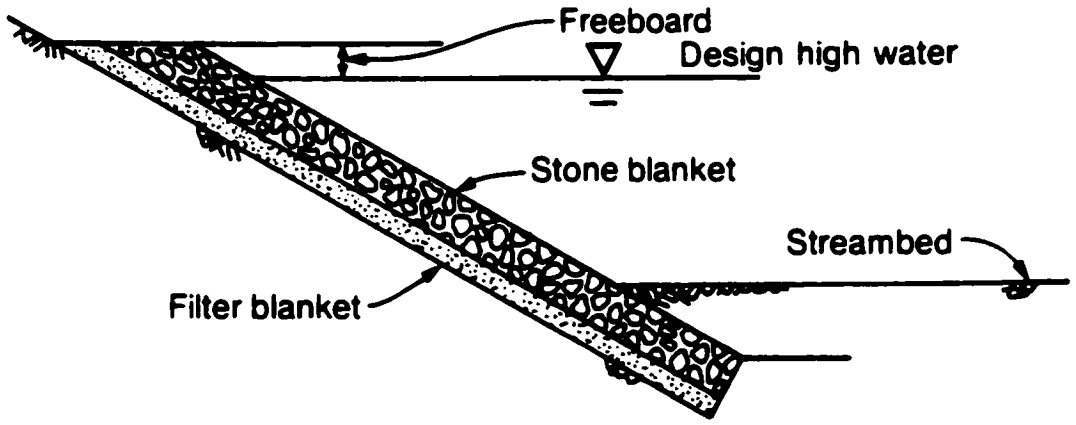

Figure 2.1: Riprap bank protection (Chang, 1988).

2.1.1.2 Rock-filled Trenches

Rock-filled trenches (Fig. 2.2) may be used in conjunction with other bank stabilization methods (Petersen. 1986). The procedure requires a trench to be dug (parallel to the river bank) at a point beyond which the protection is required. The trench is then filled with stone. The flow will erode the river bank until it reaches the trench. at which point. the stones will dislodge and roll down the bank. thus protecting it. The quantity of rock in the trench depends on the desired layer thickness and the depth to be protected. Because trench-fill revetments can be constructed with standard construction equipment, such as bulldozers and excavators, their construction is relatively quick and economical.

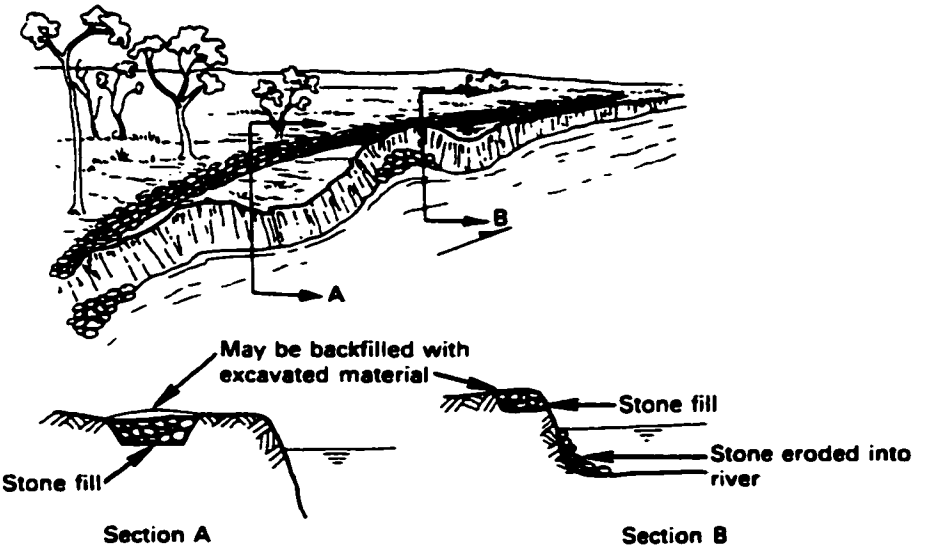

Figure 2.2: Standard rock-filled trench with cross-sections (Petersen, 1986).

2.1.1.3 Soil-cement Blocks

Soil-cement blocks (Fig. 2.3) are used where rock riprap is unavailable, and where the soil lends itself to this technique. Joglekar (1971) determined that soils with the following ranges of gradation will result in the optimal strength and durability:

Sand content ($0.05 < D_{50} < 2$ mm)	60 - 80%
Silt content ($0.005 < D_{50} < 0.05$ mm)	12 - 25%
Clay content ($D_{50} < 0.005$ mm)	8 - 15%

The optimum cement content ranges from 9 to 10% by weight of soil. Soil-cement block bank protection is popular in semiarid regions where construction is facilitated by often-dry rivers. Also, because the native soil is used in the process, the bank does not take on an unsightly appearance.

2.1.1.4 Mattresses

Mattress revetments (Fig. 2.4) may be constructed of many different types of materials, including: wood, asphalt, and concrete. They are installed from above the high water stage to beyond the toe of the bank. Generally, they are fabricated on dry land and then sunk in place from a work barge. Wood mattresses

are made of woven wood planks which are sunk under the weight of wooden cribs which house large quantities of rock. Since they are constructed in sections which are linked together, they are articulated, which allows them to accommodate gaps and settlements below them. Concrete mattresses are also articulated since they are constructed of linked slabs. They are very expensive, but are warranted where heavy reinforcement is required or where continuing construction justifies such an investment.

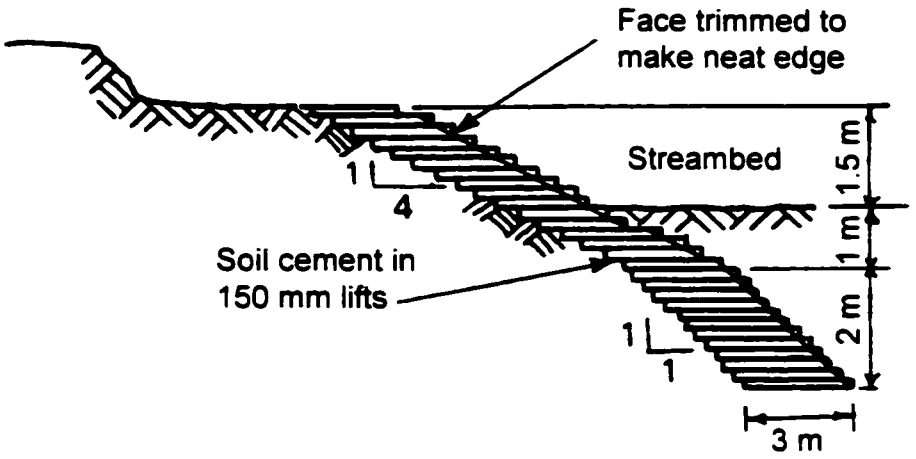

Figure 2.3: Typical section of soil cement bank protection (Petersen, 1986).

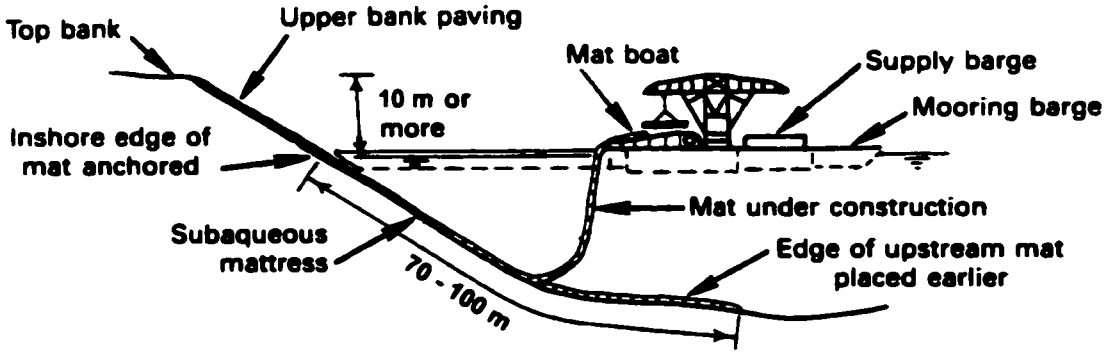

Figure 2.4: Concrete mattress installation (Petersen, 1986; source: U.S. Army Corps of Engineers, Vicksburg District).

2.1.1.5 Bioengineered Bank Protection

Today, much emphasis is placed on the environmental compatibility of the river stabilization technique to be chosen. This has led to a proliferation of bioengineered bank protection techniques. These usually involve the introduction of live green cuttings which will take root in the bank soil, thereby stabilizing it. Several techniques have been developed, including: live cribwalls, live fascines, live staking, tree revetments, vegetative cover, branch packing, and brush layering (Schiechtl and Stern, 1997). A few methods will be discussed in the following sections:

Live cribwalls (Fig. 2.5) are hollow box-like structures made of timber or log members which are placed on/in the bank slope (Schiechtl and Stern, 1997). The structure is filled with a suitable backfill material between several layers of live branch cuttings, which root inside the crib structure and extend into the slope. Once the live cuttings root and become established, the subsequent vegetation takes over the structural functions of the wood members. The cribs are often countersunk into the bank. Live cribwalls provide long-term protection and are best used as part of a system which includes a component to deter undercutting at the bed/bank interface, such as rock riprap or gabions.

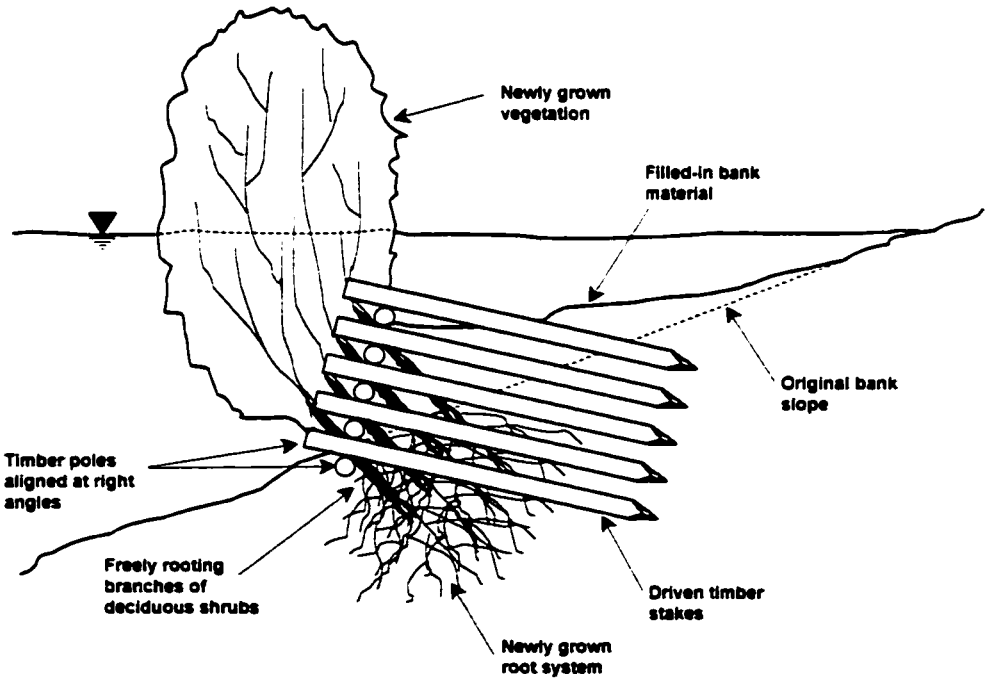

Figure 2.5: Live cribwall (after Schiechtl and Stern, 1997).

Vegetative cover (Fig. 2.6) is the most commonly used tool for bank protection, particularly in small, low velocity tributaries. It has the advantage of being self-propagating and self-repairing. Vegetation provides two levels of protection (Thompson and Green, 1994). First, the root system reinforces the bank soil and increases the overall bank stability by forming a subsurface interweaving network. Secondly, the stalks, stems, branches and foliage provide resistance to the flow by absorbing flow energy. Vegetative cover also protects the bank against rainfall runoff and trampling forces. It must be checked however, that the vegetative system does not become exceedingly overgrown in a small river upstream of a bridge with piers and abutments protruding into the flow. If this happens, the channel cross-section may become reduced to a level where the velocities are increased beyond those for which the bridge support structures were designed. This could result in subsequent undermining and bridge failure. Vegetative cover may be used in conjunction with many other river stabilization methods.

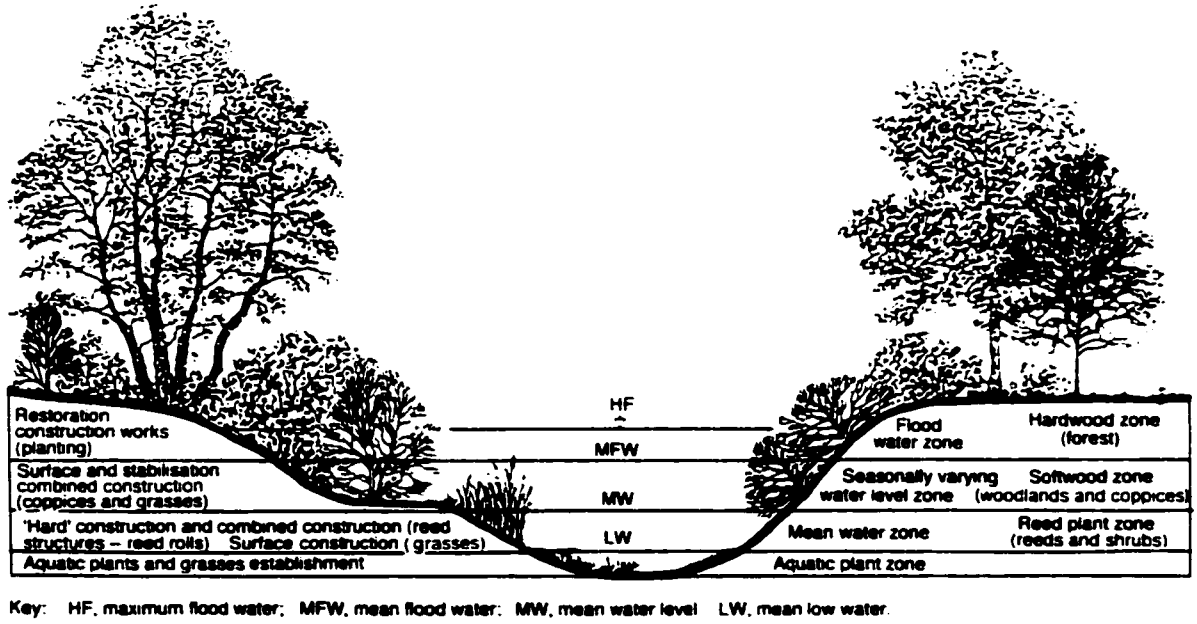

Figure 2.6: Idealized watercourse cross-section showing water management and vegetation zones and appropriate bioengineering measures (Schiechtl and Stern, 1997).

Live fascines (or wattling bundles) (Fig. 2.7) are long bundles of live branch cuttings bound together in long rows and placed in shallow trenches following the contour on bank slopes (Schiechtl and Stern, 1997). Typically, when willow species or cottonwood are used, and when the fascines are properly installed, they will root and quickly begin to stabilize slopes. Usually, once the slope is stabilized, natural

vegetative recruitment follows. This method requires very little site disturbance which is beneficial on very unstable slopes.

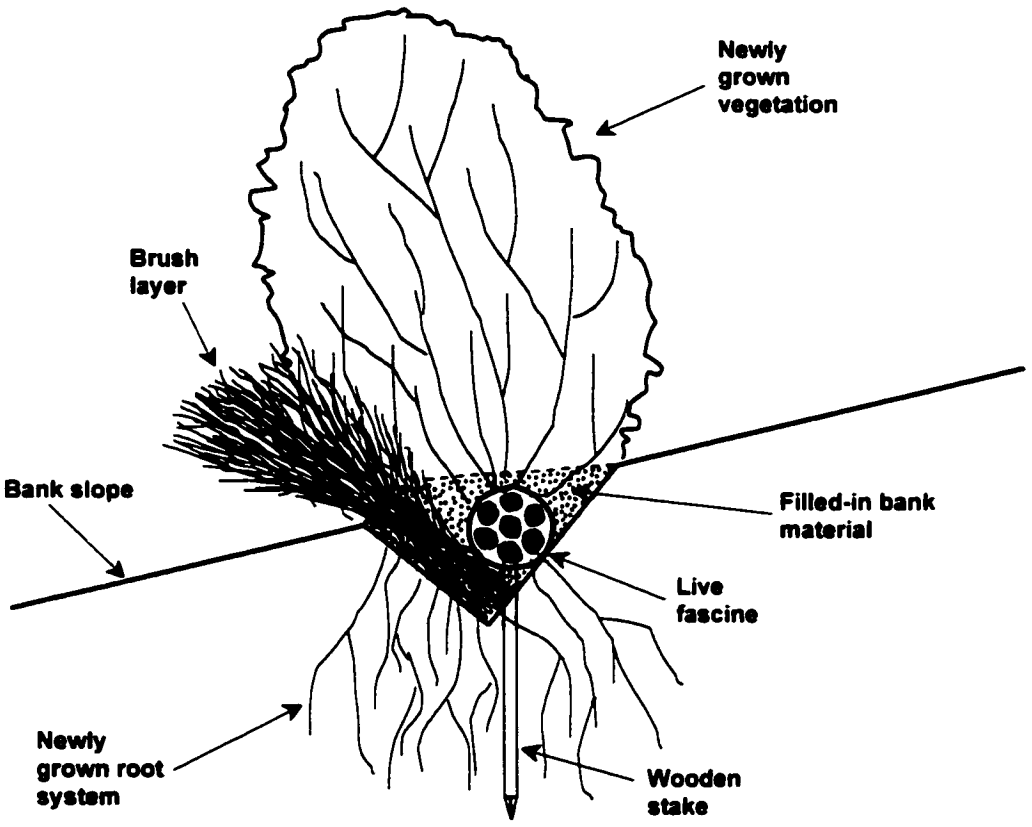

Figure 2.7: Live fascine (after Schiechtl and Stern, 1997).

2.1.2 Dikes

Dikes (Fig. 2.8) are river training structures that extend out from the bank into the flow perpendicularly or at a slight angle (usually downstream). They are also known as groins (or groynes), spurs, spur dikes, or transverse dikes, and represent a very widely used type of training works. They are either permeable or impermeable, and serve one or more of the following functions:

(*i*) training a river along a desired course,

(*ii*) creating a region of low velocity flow to induce siltation,

(*iii*) protecting the bank by keeping the flow away, and/or

(*iv*) contracting a wide river channel usually for the improvement of depth for navigation.

Permeable dikes allow flow through them at reduced velocities, thereby preventing bank erosion and causing deposition of suspended sediment from the flow. Experience has shown that these are more effective than their impermeable counterparts, especially in silt and sand rivers. They are cost effective, especially where rock riprap is unavailable and in deep rivers where impermeable dikes are expensive. The other advantage of permeable dikes over impermeable dikes is that they do not interfere as severely with the flow, which results in less intensive eddies and less severe local scour holes.

Dike lengths range from about one hundred to several hundred meters into the flow, their spacing ranges from 1.5 to 6 times their length, and their heights are based on the required freeboard above them. They may be made of many different types of materials. Permeable timber pile dikes for example, are, by definition, made of wood piles, which are placed in one or more rows and then linked together with wire fence. The design relies on the fence mesh collecting debris which would reduce the open area through which the water can pass, thereby further restricting velocities. The base of the piles and fence may be further protected by dumped rock. Although there are many variations of dike design, they are all based on the same principle, and that is to reduce flow near the bank and induce siltation between them.

Impermeable dikes are completely solid and are designed to attract, repel or deflect the flow away from the bank along a desired flow course. They are usually made of masonry or dumped stone. The stone used in dumped stone dikes is well graded, and therefore has fines which fill the voids between the larger components. Because impermeable dikes induce significant scour, they must be protected (usually with large stones) in the critical areas, which are normally the toe and head of the dikes.

Vane dikes (Fig. 2.9) (not to be confused with the topic of the current thesis - submerged vanes) are low, longitudinal stone-filled structures, with crown elevations above the low-water stage. Their crowns are low enough that at high flows they are submerged. They are angled slightly into the longitudinal flow (clockwise when viewed in plan), and placed at a small distance out from the concave bank in a bend. In their design, it is expected that at low flows, there will be very low velocities behind the vanes which will induce deposition and vegetative growth, and thus protect the bank. In the Lower Mississippi River, vane dikes have been used to partially close chutes and restrict crossings (Petersen, 1986). They extend to 4 m to 5 m above the average low water stage, are approximately 360 m long, have approximately 200 to 350 m between the ends of adjacent dikes, and are angled 10° toward the channel thalweg.

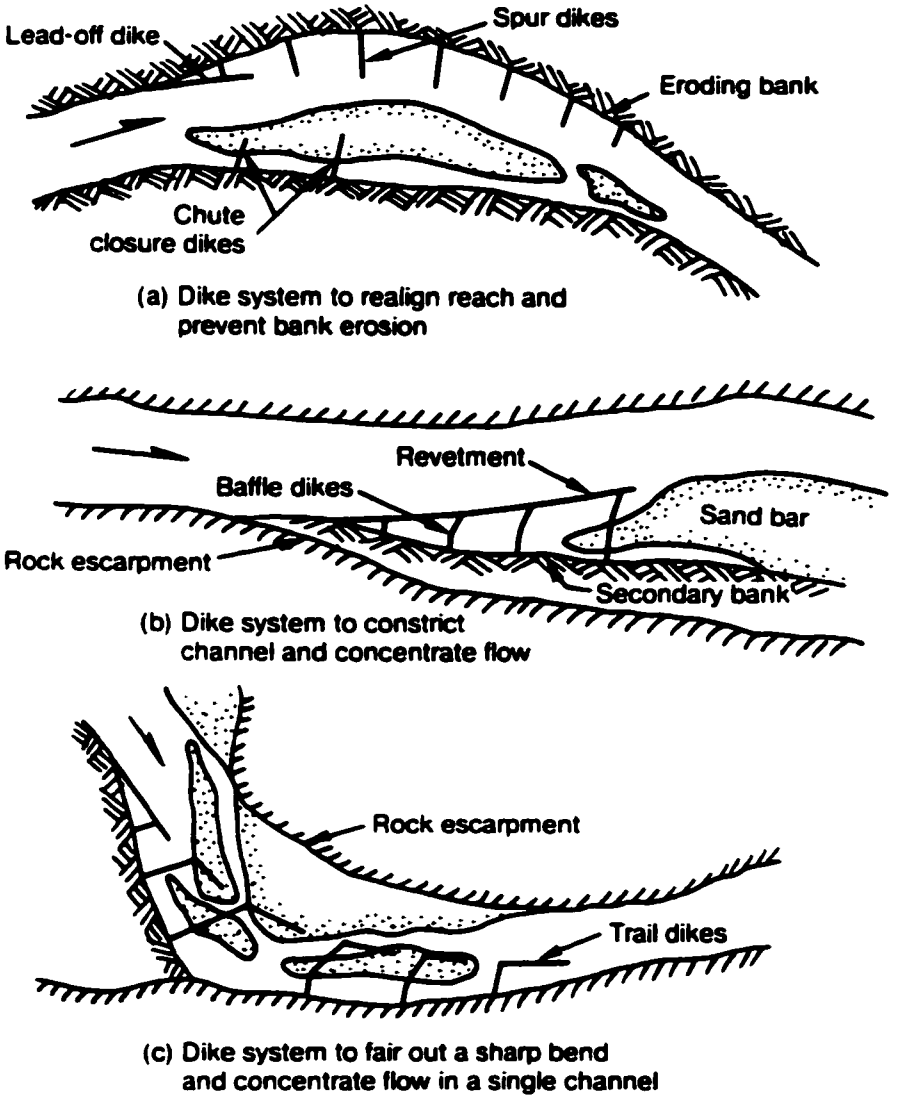

Figure 2.8: Various dike systems (Petersen, 1986).

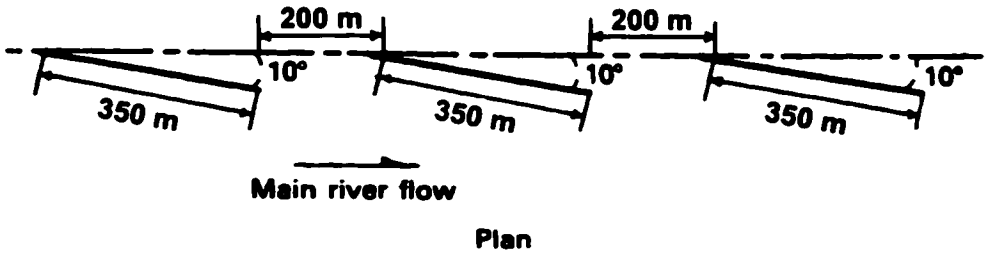

Figure 2.9: Stone vane dike system as used in the Mississippi River (Petersen, 1986; after Winkley, 1971).

2.1.3 Grade-Control Structures

Grade-control structures including drop structures, stabilizers, weirs, barrages and check dams are generally constructed normal to the channel flow and traverse the channel bed. They are used in river channels to induce and maintain a slope which is flatter than the slope of the terrain. Stabilizers (Fig. 2.10) are sediment control structures which are used slightly downstream of an area requiring stabilization. They operate by backing the water up behind them, thus reducing velocities and lessening the scour which would normally occur around certain structures such as bridge piers and abutments. The crest of the structure normally traverses the entire channel width, and the ends are keyed into the banks and protected against scour. The downstream end of the stabilizer which acts like a spillway is under the attack of high velocities and therefore requires adequate protection.

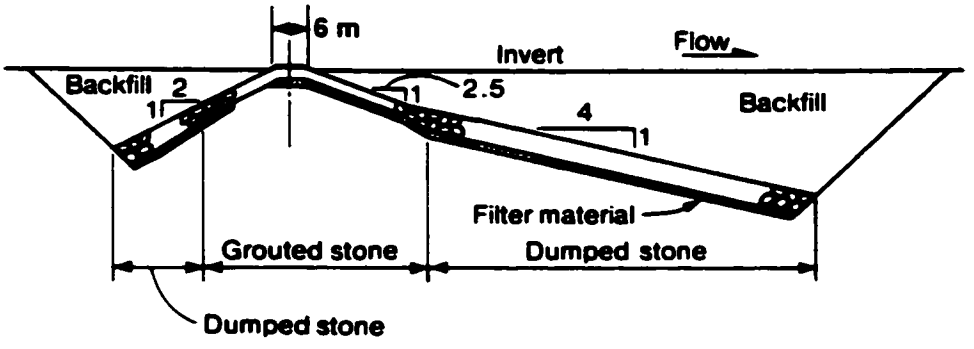

Figure 2.10: Typical stabilizer (Chang, 1988; after U.S. Army Corps of Engineers, 1970).

Stabilizers may be constructed of grouted or ungrouted rock, sheet piling, or a concrete sill. Although grade-control structures stabilize channel reaches upstream of them, they tend to induce changes in the channel regime downstream. Either a longitudinal channel slope change or local scour increase (or both) may occur. A change in longitudinal channel slope may be induced by an imbalance in sediment transport in the river reach, and it ceases when a dynamic equilibrium is reached. To prevent drastic longitudinal slope changes, a series of grade-control structures may be used to span the changes over a greater distance. Channel protection is necessary if intense flow conditions are unavoidable downstream of the structure.

2.1.4 Cutoffs

A cutoff (Fig. 2.11) is a short channel cut across the neck of a river bend, either by natural processes, or by man. The river will naturally form a cutoff at long, looping bends, or man will excavate a cutoff to improve river alignment for navigation or as a flood control measure. Although Europeans have been using man-made cutoffs for some time, they are relatively recent in the United States. The concept of excavating a limited pilot channel of relatively small cross-sectional area and then letting the river develop and enlarge the excavated cut to full channel dimensions was first suggested in 1930 by General H. B. Ferguson, Corps of Engineers, and was used later on the Lower Mississippi River under his direction (Matthes, 1948). It has been found that it is easier to maintain the alignment of a properly located cutoff than it is to protect the bank of a long bend.

The cutoffs which have been used on the Mississippi River have resulted in several feet of flood stage reduction along many miles of the river (Matthes, 1948). Many of those who use the cutoffs for navigation originally opposed their construction since they involved negotiating higher velocities; however, they soon accepted the compromise when they realized the benefits of traveling shorter distances.

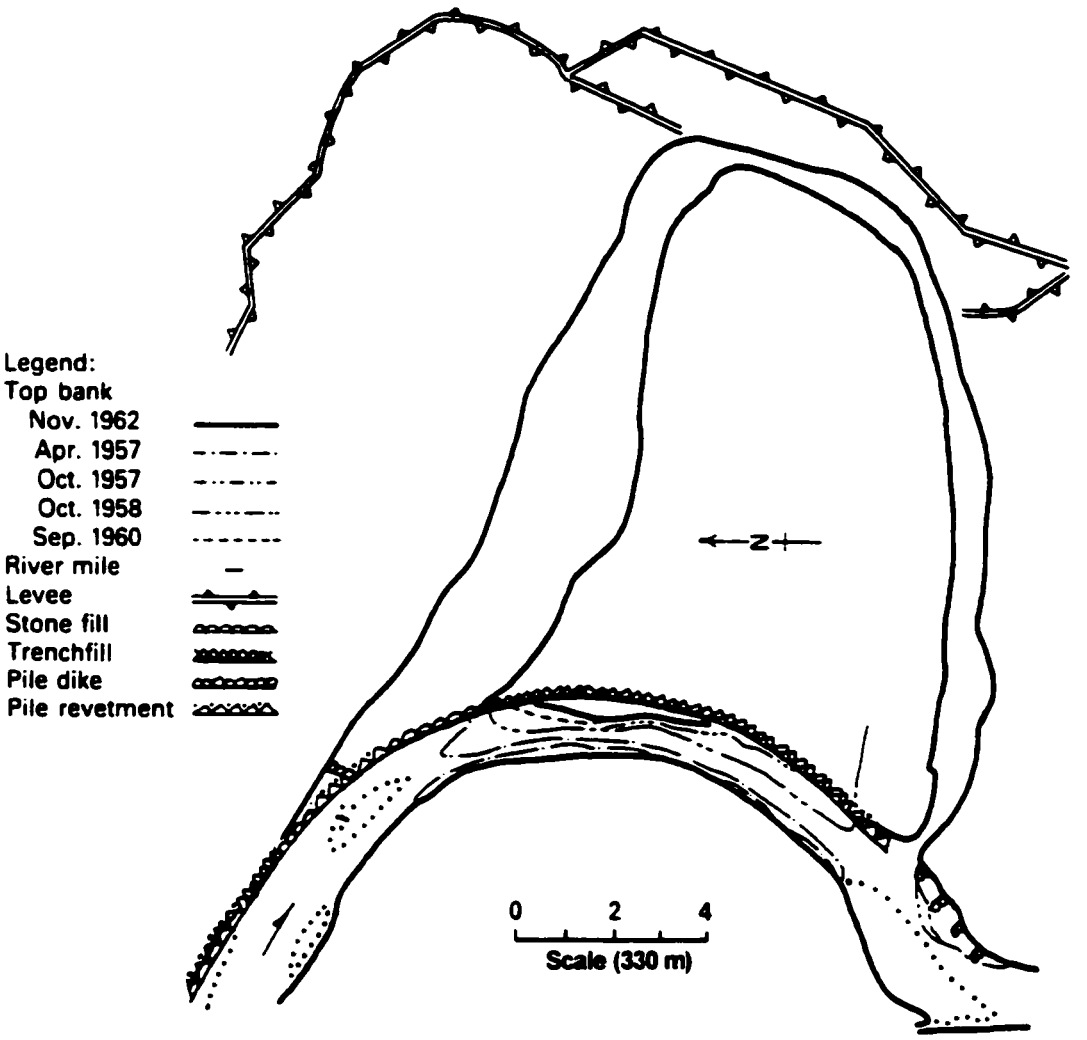

Figure 2.11: Brodie Bend cutoff, kilometer 220, Arkansas River (Peteresen, 1986; after Petersen, 1963).

2.1.5 Bendway Weirs

In 1989, the U.S. Army Corps of Engineers installed the first *bendway weir* field in the outside of a channel bend of the Mississippi River (Derrick, 1997). Since then, many more of these structures have been built in other problem bends of the river. Bendway weirs are submerged, rock structures placed on the bed of a navigation channel beneath passing traffic. They protrude out from the bank (usually the concave bank) at an angle of 20 to 30 degrees upstream of a line drawn perpendicularly from the bank (Fig. 2.12). They are designed such that they eliminate the natural centrifugal secondary current in bends and redistribute flow for the desired sediment management (Davinroy, 1990). Because they are angled upstream, the water that passes over them is redirected away from the outer bank and toward the inner part of the bend. By redistributing the velocity in such a way so as to encourage bed material deposition on the outside of the bend, and scour on the inside of the bend (at the stream ends of the weirs), they produce a wider and safer navigation channel through the bend.

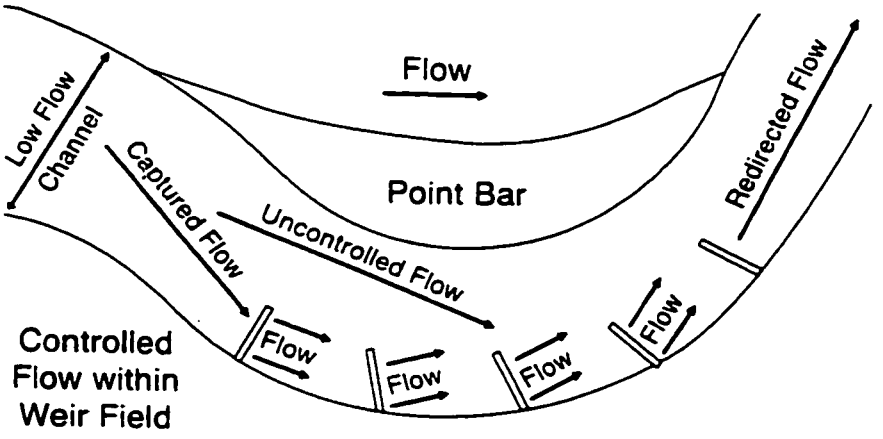

Figure 2.12: Illustration of bendway weir concept (Derrick, 1997).

Bendway weir construction is simple and cost effective since it requires only a work barge to dump rock along the specified line. Their length is normally as long as practicable constraints will allow, and they are longitudinally spaced at a distance approximately equal to the width of the bend. Although their height should not be compromised, they are usually low-profile, having a crest which does not extend past 25% of the mean river stage.

The bendway weir concept is novel and seems to have very few, if any, drawbacks. In 1994, personnel from St. Louis District, the Lower Mississippi River Valley Division, the U.S. Fish and Wildlife Service, the Illinois and Missouri Departments of Conservation, and the University of Southern Illinois Fisheries

Department conducted a study on the environmental effects of bendway weirs. Their results showed that the bends in the Mississippi River with bendway weirs experienced a fivefold increase in fish population accompanied by an increase in the number of fish species populating the bend. Other native species are also thriving. In fact, an endangered species of bird, the Least Tern, has found a place to nest on the point bars formed by the bendway weirs.

2.1.6 Submerged Vanes

Submerged vanes have recently been developed to remedy the scour/deposition problem. Although submerged vane-like structures have been used in the past (Potapov and Pyshkin, 1947; Potapov, 1950, 1951; Chabert et al., 1961; Jansen et al., 1979), very little has been documented on their design and performance until recently. At the time of this writing, most of the work on submerged vanes has been performed at the Iowa Institute of Hydraulic Research, where the first attempts to develop a theoretical design basis were made by Odgaard and Kennedy (1983) and Odgaard and Spoljaric (1986a).

Submerged vanes are small, thin, flow-training structures designed to modify the near-bed flow pattern and redistribute flow and sediment transport within the channel cross-section. They are vertical foils typically installed at an angle of 15-25° to the free-stream flow direction (i.e., counterclockwise, when viewed in plan, in a bend turning to the right), and have an initial height (i.e., before bed deformation) of 0.2 to 0.4 times the local water depth (Odgaard and Wang, 1991a). The vane induces a secondary current, which arises because the pressure difference between the upstream high pressure zone and downstream low pressure zone causes flow over the top of the vane (Fig. 2.13). The helicoidal flow which develops as the vortex is carried downstream by the predominant longitudinal flow resulting in changes in the near-bed velocity, the bed shear stress, and bed topography in the vicinity of the vane.

In a river bend, if the vane-induced secondary current is strong enough to completely counteract the centrifugally-induced secondary current (which is caused by the difference in centrifugal acceleration along a vertical line in the flow because of the nonuniform vertical velocity profile), then no predominant helicoidal flow will occur in the bend, and thus, the water and sediment will flow through the bend as if it were straight. The obvious benefit is the immediate cessation of attack by the centrifugally-induced secondary current on the outer bank, and consequently, improved bank stabilization.

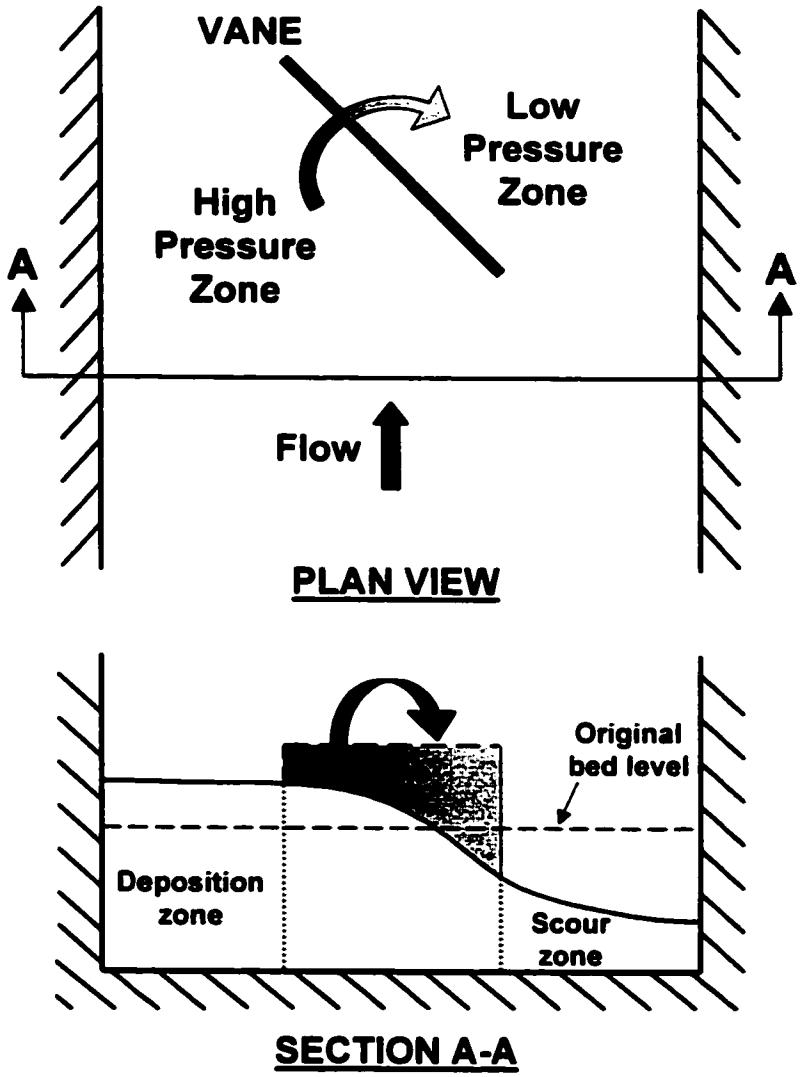

Figure 2.13: Flow over top of vane.

2.2 Submerged Vane Theory

To date, two usable analyses have been developed to aid in vane design (Odgaard and Lee, 1984; Odgaard and Wang, 1990, 1991a). Obviously, both are intimately associated with the vanes' ability to alter the primary and secondary currents and therefore their ability to alter the shear stresses acting on the channel bed. The first analysis (Odgaard and Lee, 1984) focuses more specifically on the vanes' ability to alter the channel transverse bed slope in a bend, while the second analysis (Odgaard and Wang, 1990, 1991a) concerns the vanes' ability to alter transverse shear stresses in the bend. A third, and more complex analysis has been performed by Sinha and Marelius (2000). These authours developed a numerical model which solves the fully three-dimensional Reynolds-averaged Navier-Stokes equations in conjunction with the standard two-equation k-ε (k is turbulence kinetic energy, and ε is its rate of dissipation) turbulence model. The complexity of the model does not lend itself well to the formulation of simple design relations, which is the focus of the current work: therefore, it will not be treated in any further detail.

2.2.1 Analysis Based on Changes in Transverse Bed Slope

2.2.1.1 Bed Slope Relations

The goal of the analysis, which is based on the changes in transverse bed slope (caused by transverse sediment movement under the influence of radial bed shear stress), is to develop relations that may be used to design a vane system for the protection of river banks. The assumption is made that it is the outer bank in the bend which requires protection against undermining by the high velocities in its vicinity. The vane system should be designed to reduce the near-bank depth and velocity to below allowable values.

Based on the Darcy-Weisbach resistance law, Odgaard (1984) has shown that the radial distribution of depth-averaged mean velocity in the fully-developed part of a constant-radius river curve can be described by:

$$\frac{\bar{u}}{\bar{u}_c} = \left(\frac{d}{d_c}\right)^k \left(\frac{r_c}{r}\right)^{1/2} \qquad (2.1)$$

where:

r = radius from curve centre,
r_c = radius from curve centre to channel centreline,
$\bar{u}$ = depth-averaged mean velocity at r,
$\bar{u}_c$ = depth-averaged mean velocity at r_c,
d = depth of flow at r,
d_c = depth of flow at r_c, and
k = factor of order 2/3.

It is often assumed that d_c is equal to the cross-sectional average depth, $\bar{d}$. Also, it is assumed that the variation of depth can be taken to be linear in the radial direction. Therefore, the slope of the transverse bed profile can be described by:

$$S_n = \frac{d - \bar{d}}{r - r_c} \tag{2.2}$$

or:

$$d = \bar{d} + S_n (r - r_c) \tag{2.3}$$

where: S_n = radial, or transverse bed slope, which is related to the primary flow variables by:

$$S_n = 4.8 \sqrt{\theta}\, \mathbf{F_D} \frac{\bar{d}}{r_c} \tag{2.4}$$

in which the Shields (Shields, 1936) parameter, θ, is defined as:

$$\theta = \frac{\tau_0}{\left(\frac{\rho_s}{\rho} - 1 \right) \rho g D} \tag{2.5}$$

and the densimetric Froude number, $\mathbf{F_D}$, is defined as:

$$\mathbf{F_D} = \frac{u_{ave}}{\sqrt{\frac{\rho_s - \rho}{\rho} g D}} \tag{2.6}$$

where:

τ_0 = bed shear stress,
ρ = fluid density,
ρ_s = bed sediment particle density,
g = gravitational acceleration,

D = median grain size of bed material, and
u_{ave} = cross-sectional average velocity.

Substitution of eq. 2.3 into eq. 2.1 yields the relationship between S_n and $\bar{u}$:

$$S_n = \frac{\bar{d}}{r - r_c}\left[\left(\frac{\bar{u}}{\bar{u}_c}\right)^{1/k}\left(\frac{r}{r_c}\right)^{1/2k} - 1\right] \tag{2.7}$$

Hence, by eq. 2.7, a criterion for $\bar{u}$ is equivalent to a criterion for S_n. The design objective for a system of vanes can be evaluated in terms of a maximum allowable transverse bed slope. The transverse bed slope may be reduced or eliminated if the secondary current in the channel bend is likewise reduced or eliminated.

The vane effectiveness is primarily a function of the drag and lift induced by the approach flow, as well as the vane height compared to the flow depth. The drag and lift forces are the sums of the pressure and viscous forces that act parallel and normal, respectively, to the free-stream flow direction. The drag and lift depend on the vane aspect ratio, ψ, (height/length); and angle of incidence with free-stream flow, α (Odgaard and Spoljaric, 1989). The optimum vane system design has, as a maximum, the moment caused by the lift force about the centroid of the channel cross-section and has, as a minimum the drag force on the vane. A sufficiently large drag force would increase the overall channel roughness, which would adversely alter the general river flow characteristics. Also, the vanes should be placed in such a way that they do not create interference with one another, which would reduce the overall effectiveness of the vane system.

2.2.1.2 Vane Function

The flow in a curved channel is under the influence of centrifugal acceleration, which is associated with (*i*) spiral motion of flow, and (*ii*) superelevation of the water surface. The latter is often very small and may be neglected. The former, is also known as the *helical current*, *transverse circulation*, or perhaps most commonly, the *secondary current*. The secondary current has a flow direction which is normal to that of the primary longitudinal flow. It owes its existence to the difference in centrifugal acceleration u^2/r (u is the local longitudinal velocity) along a vertical line in the flow because of the vertical profile of u in viscous fluids (Fig. 2.14).

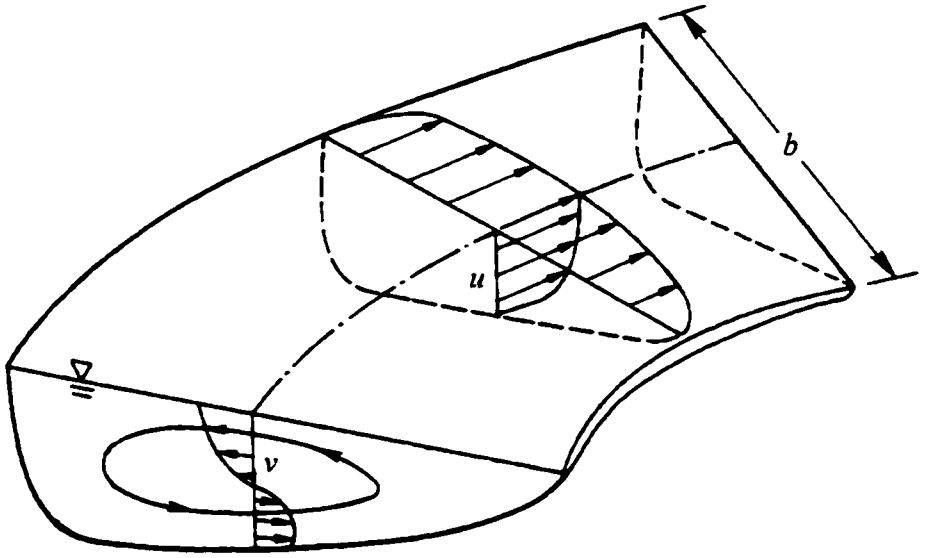

Figure 2.14: Definition sketch of flow in a curved channel (Chang, 1988).

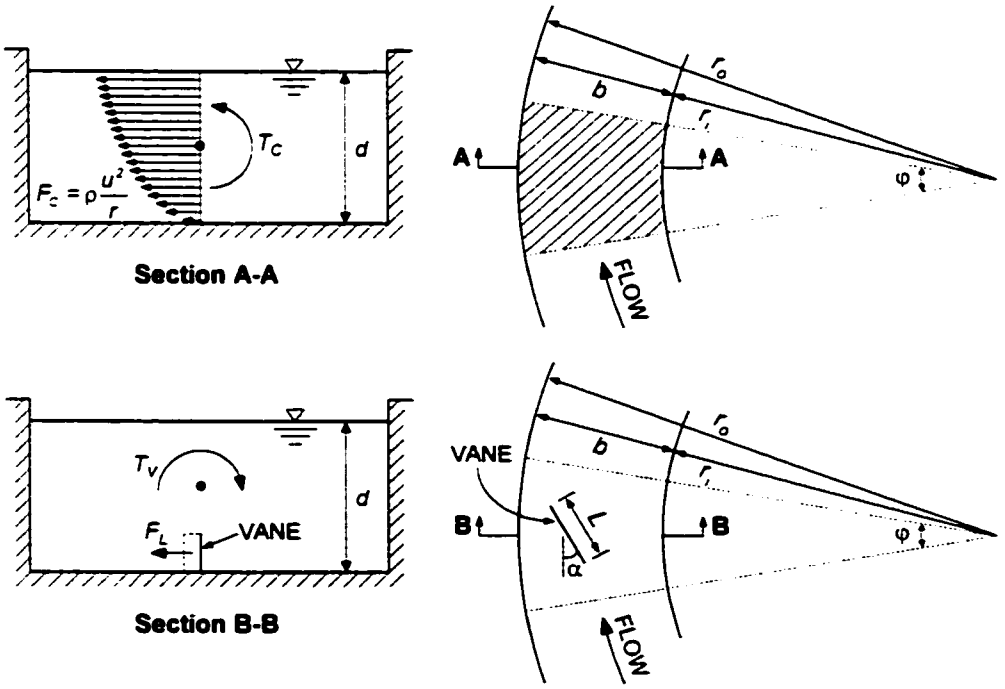

Figure 2.15: Definition sketch of torque caused by centrifugal acceleration (Section A-A) and by vanes (Section B-B) (after Odgaard and Mosconi, 1986).

In a rectangular channel with fully developed flow, constant radius bend, and power law velocity distribution , the torque T_c (Fig. 2.15) that causes the secondary current is given by (Odgaard, 1984):

$$T_c = \frac{1}{2}\rho \bar{u}^2 \frac{m+1}{m(m+2)} d^2 b \varphi \tag{2.8}$$

where:

φ = included bend angle,
b = channel width, and
m = velocity profile exponent.

It should be noted that neither the lateral bed shear stress, nor the superelevation caused by the centrifugal acceleration are shown in Fig. 2.15. The value of m may be related to the Darcy-Weisbach friction factor, f, by (Zimmerman and Kennedy, 1978):

$$m^2 = \frac{8\kappa^2}{f} \tag{2.9}$$

where: κ = von Kármán's constant (typically $\kappa = 0.4$ for clear water conditions). Since:

$$f = \frac{4\tau_o}{\frac{1}{2}\rho \bar{u}^2} \tag{2.10}$$

and

$$\tau_0 = \gamma R S \tag{2.11}$$

it follows that:

$$m = \frac{\kappa \bar{u}}{\sqrt{gRS}} \tag{2.12}$$

where: S = longitudinal slope of water surface, and R = hydraulic radius. A thin flat vane exerts a torque, T_v, on the flow that is given by (Odgaard, 1984):

$$T_v = \frac{1}{4} c_L \rho \bar{u}^2 L d^2 \left(\frac{H}{d}\right)^{\frac{(2+m)}{m}} \left[\frac{(m+1)^2}{m(m+2)} - \frac{m+1}{m}\frac{H}{d}\right] N \tag{2.13}$$

where:

c_L = lift coefficient (= $2\pi \sin \alpha$; where α is the vane's angle of attack with the mean flow),
L = vane length,
H = vane height, and
N = number of vanes.

It follows that, by equating the torque induced by natural river bend flow, T_C, with that induced by the vanes, T_V, the net secondary current can be eliminated, and no transverse bed slope will develop. By doing so:

$$\frac{NHL}{r_c \varphi b} = \frac{2F}{c_L}\left(\frac{r_c}{d}\right)^{-1} \tag{2.14}$$

where: F = *vane function* which is a function of the velocity profile exponent, m, and the *submergence ratio*, H/d, and is given by eq. 2.15. It should be noted that the above relationship treats the channel cross-section globally and assumes that the *entire* secondary current may be eliminated. In reality however, the net secondary current may not be totally eliminated, but rather significantly reduced, and there may still exist minor helices whose impacts are not considered herein.

$$F = \frac{1}{\left(\frac{H}{d}\right)^{2/m}\left[(m+1)-(m+2)\left(\frac{H}{d}\right)\right]} \tag{2.15}$$

and has been plotted in Fig. 2.16. Equation 2.14 yields the total vane lifting surface per channel bed surface area, $NHL/(r_c \varphi b)$, in terms of the vane function, F; the lift coefficient, c_L; and the radius-depth ratio, r_c/d. It can be seen in Fig. 2.16, that F increases as m decreases; therefore, the required lifting area likewise increases as m decreases (*note*: a lower m is associated with higher frictional resistance). Therefore, the required optimum vane area is minimized when F is minimized.

By differentiating eq. 2.15 with respect to H, the vane function minimum is found to be at $H/d = 2(m+1)/(m+2)^2$. Substituting this into eq. 2.15 gives the minimum vane function value, F_{min}, as:

$$F_{min} = \frac{m+2}{m(m+1)}\left[\frac{2(m+1)}{(m+2)^2}\right]^{-2/m} \tag{2.16}$$

For each value of m, there are corresponding values of F_{min} and H/d. And it can be shown that vane function is relatively insensitive to variations in submergence over a broad range of H/d values. For example, at $m = 5$, the minimum value of the vane function occurs at $H/d = 0.24$ and has the value $F_{min} = 0.41$ (Table 2.1, Fig. 2.16). All values of F which are within 20% of the minimum fall within the range of $0.09 \le H/d \le 0.46$. In other words, as long as the water depth is between 2 and 11 times the vane height, the vane function will be reasonably close to its minimum.

2.2.1.3 Effective Bend Radius

Equation 2.14 was developed based on the assumption that the flow is fully-developed in a constant-radius bend; however, most natural river bends do not have constant radii, nor is the flow fully-developed. Therefore, eq. 2.14 is inadequate. To address this problem, the *effective bend radius* concept can be applied if the channel's transverse bed slope is known. The effective radius, r_e, is that which, if the flow was fully-developed in a constant-radius bend, would produce the same transverse bed slope as that in the natural channel. Making the appropriate substitution, eq. 2.4 becomes:

$$S_n = 4.8\sqrt{\theta}\,\mathbf{F_D}\frac{\bar{d}}{r_e} \tag{2.17}$$

The torque associated with the centrifugal force (eq. 2.8), T_c, may be applied to the effective bend radius method if the bend angle, φ, is replaced with the effective bend angle, φ_e which corresponds to the effective bend radius. Again, equating the torque induced by the centrifugal current, T_c, (eq. 2.8 with $\varphi = \varphi_e$) with that induced by the vanes, T_v, (2.13), gives:

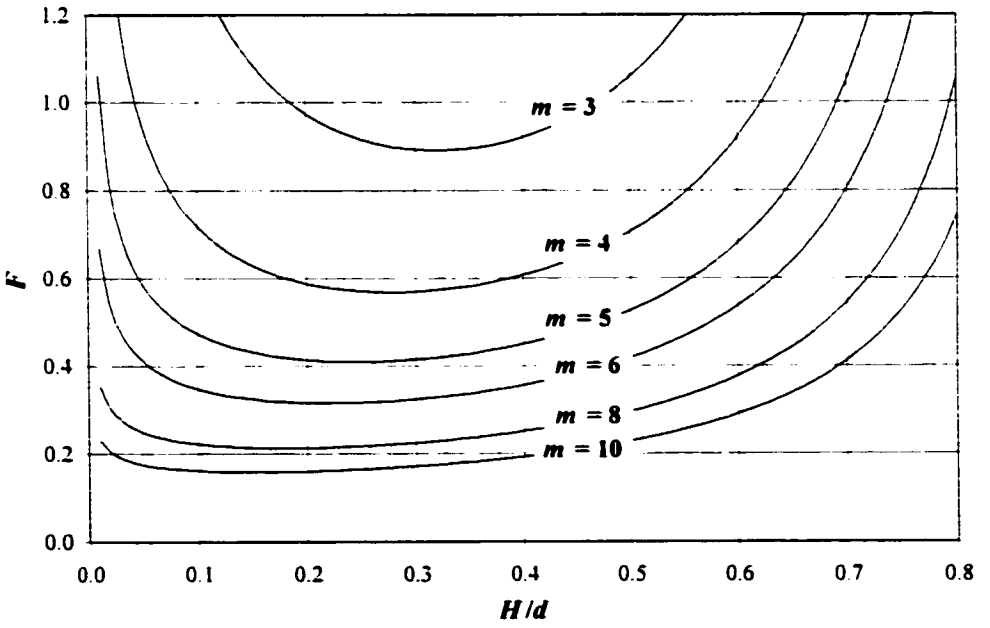

Figure 2.16: Vane function, F, as a function of the submergence ratio, H/d, and the velocity profile exponent, m.

Table 2.1: Minimum values of vane function, F.

m	Minimum value of F, $F = F_{min}$	Value of H/d at which $F = F_{min}$	Value of F which is 20% greater than F_{min}, $F = 1.2F_{min}$	Lower limit of submergence for which $F = 1.2F_{min}$		Upper limit of submergence for which $F = 1.2F_{min}$		Range of d/H for which $F \le 1.2F_{min}$
				H/d	d/H	H/d	d/H	
3	0.89	0.32	1.07	0.16	6	0.50	2	2 - 6
4	0.57	0.28	0.68	0.12	9	0.48	2	2 - 9
5	0.41	0.24	0.49	0.09	11	0.46	2	2 - 11
6	0.32	0.22	0.38	0.07	15	0.44	2	2 - 15
8	0.21	0.18	0.26	0.04	23	0.41	2	2 - 23
10	0.16	0.15	0.19	0.03	34	0.39	3	3 - 24

$$\frac{NHL}{r_e \varphi_e b} = \frac{2F}{c_L}\left(\frac{r_e}{d}\right)^{-1} \tag{2.18}$$

or since $r_e\varphi_e = r_c\varphi$:

$$\frac{NHL}{r_c \varphi b} = \frac{2F}{c_L}\left(\frac{r_e}{d}\right)^{-1} \tag{2.19}$$

Equations 2.14 and 2.19 were developed based on the total elimination of secondary current and the consequent prevention of transverse bed slope development. Practical considerations may not allow, or require such a design. A narrow and/or shallow channel may impose space restrictions on the vane design. For instance, the vane design for bank protection in a narrow shallow channel may dictate that the vanes be so high that they interfere with navigation through the bend of a major shipping throughway. In this case, shorter and perhaps more numerous vanes may be required, or, it may be feasible to allow for a non-zero objective transverse bed slope. Or, it may be possible to use only enough vanes (or vane area) to keep bank-shear stresses below the critical value for sediment movement. If the maximum acceptable transverse bed slope is S_{n0}, then the vanes must induce a torque capable of achieving this. According to eq. 2.17, the effective radius must be increased from r_e to r_{e0}, where:

$$r_{e0} = 4.8\sqrt{\theta}\,\mathbf{F_D}\frac{\bar{d}}{S_{n0}} \tag{2.20}$$

The lifting surface area, NHL, required to produce the objective transverse bed slope would be the difference between the lifting surface required for zeroing S_n and that required for zeroing S_{n0}:

$$NHL = \frac{2F}{c_L} r_c \varphi b d \left(\frac{1}{r_e} - \frac{1}{r_{e0}} \right) \tag{2.21}$$

2.2.1.4 Lift Coefficient

For ideal two-dimensional flow around a thin flat vane, the Kutta condition (Sabersky and Acosta, 1964) gives the lift coefficient as:

$$c_L = 2\pi \sin\alpha \tag{2.22}$$

In reality, the flow around a vane is not ideal, nor two-dimensional. Furthermore, as α increases, flow separation occurs, increasing the drag and reducing the lift. It has been noted (Odgaard and Lee, 1984) that a decrease in vane aspect ratio, ψ (= H/L), results in a decrease in c_L relative to the value given in eq. 2.22. This is due in part to the formation of tip vortices which trail the upper edge of the vane and induce a downward motion, or *downwash*, in the flow over the vane. The downwash tends to alter the direction of the free-stream direction, resulting in an effective angle of attack, α_e, which is smaller than the actual angle of attack, α, by a magnitude of β, or:

$$\alpha_e = \alpha - \beta \tag{2.23}$$

Since nothing is known about the value of β for small-aspect-ratio foils which are 'end-attached', the only recourse the engineer has is to resort to research performed by Bertin and Smith (1979) on the value of β for a finite-span airfoil in undisturbed free-stream air. They determined that:

$$\beta = \frac{c_L}{\pi (H/L)} \tag{2.24}$$

Substituting eq. 2.24 into eq. 2.23 yields:

$$\alpha = \alpha_e + \frac{c_L}{\pi (H/L)} \tag{2.25}$$

For two airfoils which have the same lift coefficient and effective angle of attack, but with differing aspect ratios, H_1/L_1 and H_2/L_2, their geometric angles of attack, α_1 and α_2, are related by the equation:

$$\alpha_2 = \alpha_1 + \frac{c_L}{\pi} \left(\frac{L_2}{H_2} - \frac{L_1}{H_1} \right) \tag{2.26}$$

Bertin and Smith (1979) verified eqs. 2.25 and 2.26 for airfoils having $\psi \geq 1$. It is currently assumed that, for a bottom-attached flat plate with a large aspect ratio, the relationship $c_L = 2\pi \sin\alpha$ applies and the

downwash angle is one half that given by eq. 2.24 (since a bottom-attached vane has only one edge with tip vortices).

The angle to be used in determining the lift coefficient is not the geometrical angle, but rather the angle of the vane as seen by the fluid; therefore, a nomenclature revision is necessary here. In the analysis, the vane angle used in the design relationships was α; however, α refers to the geometrical angle and *not* the appropriate vane angle as seen by the approaching fluid. For the remainder of this section, the geometrical vane angle will be referred to as α′ (rather than α), and the angle (as seen by the fluid) to be used in the following design relations will be α.

The centrifugal acceleration of flow in the bend causes the near-bed velocity distribution to be skewed toward the inner bank. This further affects the vane angle as seen by the fluid. Falcon (1979) gives the angle that the near-bed velocity forms with the mean flow direction (Fig 4.5), η, as:

$$\eta = \tan^{-1}\left(\frac{\tau_n}{\tau_0}\right) \tag{2.27}$$

where: τ_n is the radial component of the bed shear stress, τ_0. Substituting (Falcon, 1979):

$$\tau_0 = \rho \bar{u}^2 \left(\frac{\kappa^2}{m^2}\right) \tag{2.28}$$

and:

$$\tau_n = \frac{\rho \bar{u}^2 (m+1)}{m(m+2)} \left(\frac{d}{r_c}\right) \tag{2.29}$$

into eq. 2.27 yields:

$$\eta = \tan^{-1}\left[\frac{1}{\kappa^2} \frac{m(m+1)}{m+2} \frac{d}{r_c}\right] \tag{2.30}$$

Hence, the angle α to be used in the calculation of c_L for a vane which is placed at an angle α′ with the free-stream flow is given by:

$$\alpha = \alpha' + \eta \tag{2.31}$$

2.2.2 Analysis Based on Changes in Transverse Shear Stress

The upstream face of the vane experiences high pressure on the upstream side and low pressure on the downstream side. This induces a vertically upward velocity component on the upstream and a vertically downward velocity component on the downstream side. The result is the generation of a vortex sheet which travels downstream away from the vane under the influence of the main channel longitudinal flow, producing a helicoidal flow structure. This helicoidal flow induces its own transverse bed shear stresses which may be used to counteract the transverse shear stresses arising from the naturally-developed secondary current in a channel bend. The following analysis is based on this premise (Odgaard and Wang, 1991a).

The strength of the steady, potential vortex decays downstream because of viscous diffusion. Lamb (1932) describes the vortex's tangential velocity (perpendicular to its core axis) in an *unbounded* flow field as

$$v_\theta = \frac{\Gamma}{2\pi r_v}\left[1 - \exp\left(-\frac{u}{4\varepsilon s} r^2\right)\right] \tag{2.32}$$

where:

s = downstream distance,
Γ = horizontal circulation at $s = 0$,
r_v = radial distance from core of vortex, and
ε = eddy viscosity.

However, actual open channel flow is bounded by the channel bed, sides and free surface. The value of v_θ for a *bounded* flow field may be obtained by using the method of images. The transverse component of v_θ (perpendicular to the z-axis) at a distance z from the stream bed is

$$v_n = \sum_{i=1}^{\infty} (-1)^{i-1} \frac{\Gamma}{2\pi r_i}\left[1 - \exp\left(-\frac{u}{4\varepsilon s} r_i^2\right)\right]\frac{z_i - z}{r_i} + \sum_{j=1}^{\infty} (-1)^{j-1} \frac{\Gamma}{2\pi r_j}\left[1 - \exp\left(-\frac{u}{4\varepsilon s} r_j^2\right)\right]\frac{z_j - z}{r_j} \tag{2.33}$$

where:

r_i = distance from core of vortex i,
r_j = distance from core of vortex j,
z_i = vertical distance from stream bed to core of vortex i, and
z_j = vertical distance from stream bed to core of vortex j.

The first summation of eq. 2.33 includes contributions from the images *above the free surface* and the second summation includes the contributions from the images *below the stream bed.* The pressure difference between the pressure and suction sides of the vane causes the vortex core to be slightly below the top elevation of the vane. Several researchers (Milne-Thomson, 1966; Odgaard and Spoljaric, 1989; Wang, 1990) have shown that the core is about 0.2 times the vane height below the top elevation of the vane. The horizontal circulation is related to the horizontal lift force, F_L, that the vane *exerts on the flow* (Fig. 2.17). The lift force has an equal magnitude and opposite direction as the force *exerted on the vane by the flow*, which, according to the Kutta-Joukowskii theorem (Sabersky and Acosta, 1964), is proportional to the vertical circulation around the vane associated with the shift of the rear stagnation point to the trailing edge of the vane. By Helmholz's second theorem (Currie, 1974), this vertical circulation is equal to the horizontal circulation, Γ; therefore:

$$F_L = \rho \Gamma u H \tag{2.34}$$

From the velocity field thus calculated, the near-bed transverse velocity component is obtained with $z = 0$:

$$v_{V} = \frac{F_L}{\pi \rho u H} \sum_{j=1}^{\infty} \frac{(-1)^{j+1}}{r_j} \left[1 - \exp\left(-\frac{u}{4 \varepsilon s} r_j^2 \right) \right] \frac{z_j}{r_j} \tag{2.35}$$

where the subscript n refers to the transverse direction and the subscript V refers to the velocity associated with the vane. The assumption in eq. 2.35 is that there are as many vortices above the stream bed as there are below. Now that the transverse near-bed velocity is known, the transverse bed shear stress can be calculated. Assuming that τ_{Vn} has the same ratio to the streamwise bed shear stress, τ_{bs}, as v_V to the streamwise near-bed velocity, u_b (Odgaard and Wang, 1991a):

$$\frac{\tau_{Vn}}{\tau_{bs}} = \frac{v_V}{u_b} \tag{2.36}$$

The power-law streamwise velocity distribution may be adopted (Odgaard and Wang, 1991):

$$u = \frac{m+1}{m} \left(\frac{z}{d} \right)^{1/m} \bar{u} \tag{2.37}$$

where the value of m is given in eq. 2.12. With this velocity profile, the vane-approach velocity averaged over the vane height, $\bar{u}_V$, the vane-approach velocity at the bed, u_b, and the streamwise bed shear stress, τ_{bs}, are related to $\bar{u}$ as:

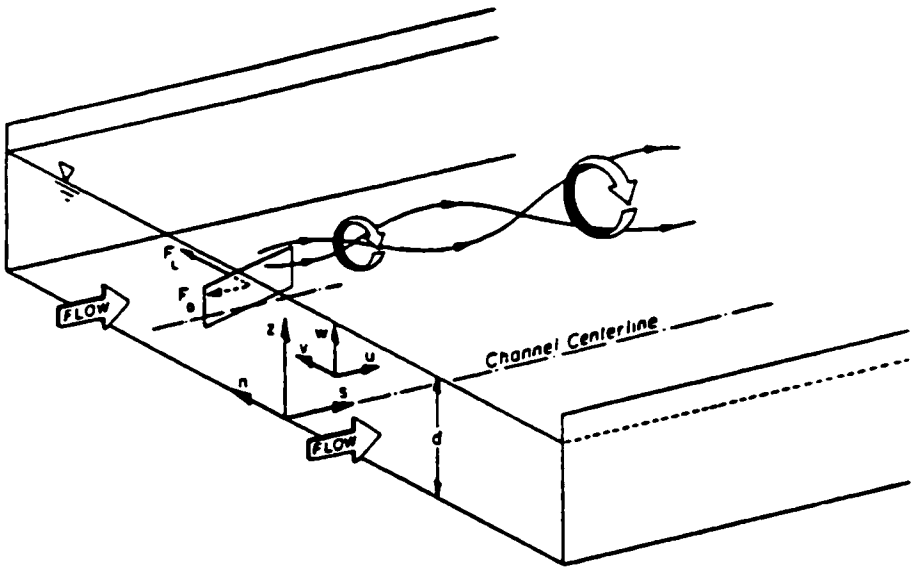

Figure 2.17: Definition sketch of flow structure around vane (Odgaard and Wang, 1991a).

$$\bar{u}_V = \bar{u}\left(\frac{H}{d}\right)^{1/m} \tag{2.38}$$

$$u_b = \frac{\bar{u}}{k} \tag{2.39}$$

and:

$$\tau_{bs} = \frac{\rho \kappa^2 \bar{u}^2}{m^2} \tag{2.40}$$

The eddy viscosity, ε, controls the downstream decay of τ_{Vn} and v_V, and may be obtained from the power law and an assumed linearly distributed primary-flow shear stress, so that:

$$\varepsilon = \frac{\kappa^2 \bar{u} d}{6m(1 + 1/m)(1 - 1/2m)(1 - 1/3m)} \tag{2.41}$$

By substituting eq. 2.35 into 2.36, the transverse bed shear stress is:

$$\tau_{Vn} = F_L f_V \tag{2.42}$$

where:

$$f_V = \frac{k\kappa^2}{\pi m^2 H} \frac{\bar{u}}{u_{ap}} \sum_{j=1}^{\infty} \frac{(-1)^{j-1}}{r_j} \left[1 - \exp\left(-\frac{\bar{u}}{4\varepsilon s} r_j\right)\right] \frac{z_j}{r_j} \tag{2.43}$$

It follows that the streamwise component of the vane induced bed shear stress is:

$$\tau_{Vs} = F_D f_V \tag{2.44}$$

where: F_D = drag force associated with the lift force F_L. The drag force and lift force may be calculated by relating them to the dynamic pressure as:

$$F_L = \frac{1}{2} c_L \rho L \int_0^H u^2 \, dz \tag{2.45}$$

and:

$$F_D = \frac{1}{2} c_D \rho L \int_0^H u^2 \, dz \tag{2.46}$$

where: c_D = drag coefficient. Equation 2.37 may be substituted into eqs. 2.45 and 2.46 to obtain the lift and drag forces:

$$F_L = \frac{1}{2} \rho c_L H L \bar{u}^2 \frac{(m+1)^2}{m(m+2)} \left(\frac{H}{d} \right)^{2/m} \tag{2.47}$$

and:

$$F_D = \frac{c_D}{c_L} F_L \tag{2.48}$$

The lift coefficient, c_L, for a thin flat vane is given in section 2.2.1.4, and the associated drag coefficient is given by:

$$c_D = \frac{1}{2\pi} \frac{L}{H} c_L^2 \tag{2.49}$$

It has been noted that the vane has little impact beyond a transverse distance which is about three times the vane height. Therefore, a wider area is affected if more than one vane is used in an array (Figs. 2.18 and 2.19). Although a greater transverse circulation is induced with an array of vanes, the interaction of tip vortices results in a cumulative transverse circulation which is less than that which would be obtained by simple superposition of the individual vorticity fields. Wang (1989) shows that, for an array of equally sized, equally angled vanes, the total circulation may be obtained by adding the circulations from the individual vanes and then adjusting it by an interaction coefficient, λ, which is a function of the transverse vane spacing, δ_n, and vane dimensions H and L. With a transverse vane spacing of two to three times the vane height, λ is of the order of 0.9. A larger spacing results in a lower λ.

To maintain a desired induced transverse circulation and consequent induced bed shear stress downstream of a vane array, the array must be repeated in the downstream direction. The streamwise distance

between the arrays, δ_s, depends on the design objective, which includes lower limits in the objective induced stresses. The area-averaged induced bed shear stresses within a vane field consisting of equally-spaced vanes is:

$$\bar{\tau}_{Vn} = \frac{F_L \lambda \beta}{A_V} \tag{2.50}$$

and:

$$\bar{\tau}_{Vs} = \frac{F_D \lambda \beta}{A_V} \tag{2.51}$$

where:

$\bar{\tau}_{Vn}$ = area-averaged transverse component of vane induced bed shear stress,
$\bar{\tau}_{Vs}$ = area-averaged streamwise component of vane induced bed shear stress,
β = factor arising from averaging process (Wang, 1990), and
A_V = vane density ($= \delta_n \delta_s$).

It follows that, if the vane field covers an area A, and the total number of vanes is N, then $A_V = A/N$.

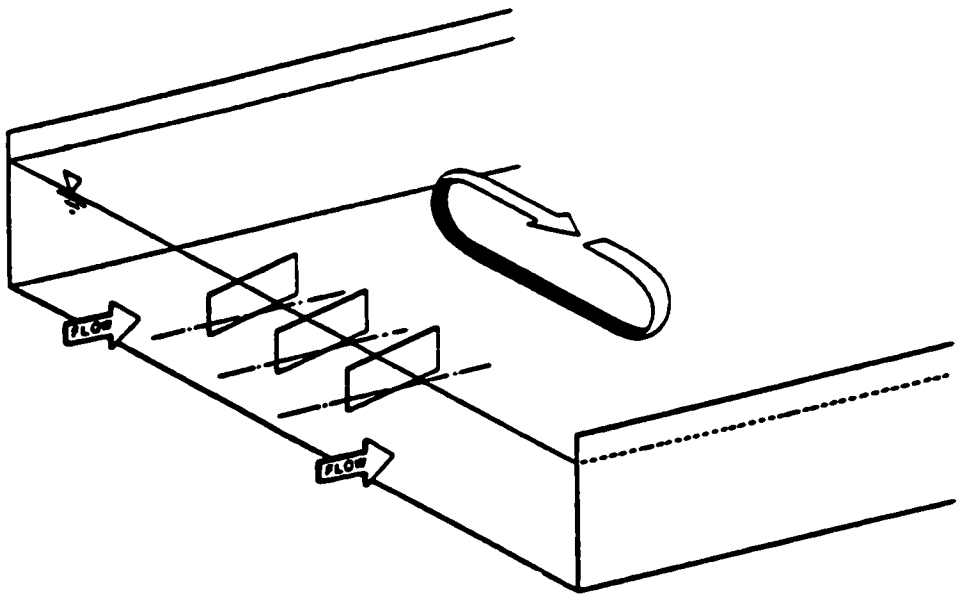

Figure 2.18: Vane-induced circulation by array of three vanes (Odgaard, 1991).

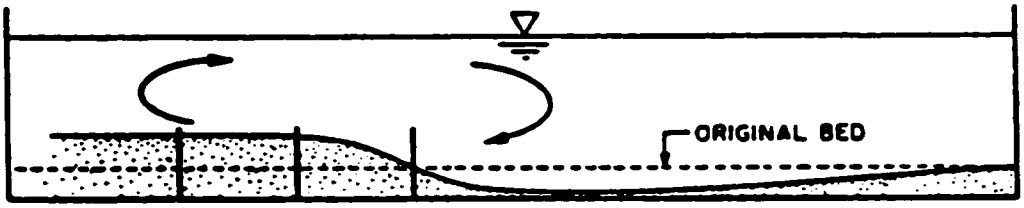

Figure 2.19: Change in bed profile induced by array of three vanes (Odgaard, 1991).

To determine the interaction between the vane-induced transverse shear stress and the natural secondary current-induced transverse shear stress, Odgaard and Wang (1991a) employ the three-dimensional equations of motion (Fig. 2.17):

$$u\frac{\partial u}{\partial s} + v\frac{\partial u}{\partial n} + w\frac{\partial u}{\partial z} + \frac{uv}{r} = -\frac{1}{\rho}\frac{\partial p}{\partial s} + F_s \tag{2.52}$$

$$u\frac{\partial v}{\partial s} + v\frac{\partial v}{\partial n} + w\frac{\partial v}{\partial z} - \frac{u^2}{r} = -\frac{1}{\rho}\frac{\partial p}{\partial n} + F_n \tag{2.53}$$

$$u\frac{\partial w}{\partial s} + v\frac{\partial w}{\partial n} + w\frac{\partial w}{\partial z} + g = -\frac{1}{\rho}\frac{\partial p}{\partial z} + F_z \tag{2.54}$$

where s, n, and z refer to the downstream, lateral (positive toward outer bank), and vertical (positive up) coordinate, respectively; u, v, and w = time averaged velocity component in s-, n-, and z-direction, respectively; p = pressure; F_s, F_n, and F_z = shear stress component in s-, n-, and z-direction, respectively; and g = gravitational acceleration. The coordinate system has its origin at the channel bed transverse centerline. The flow and sediment equations (respectively) at equilibrium are:

$$\frac{\partial u}{\partial s} + \frac{1}{r}\frac{\partial (vr)}{\partial n} + \frac{\partial w}{\partial z} = 0 \tag{2.55}$$

and:

$$\frac{\partial q_s}{\partial s} + \frac{1}{r}\frac{\partial (q_n r)}{\partial n} = 0 \tag{2.56}$$

where:

q_s = volumetric bed-load transport per unit width in the s-direction, and

q_n = volumetric bed-load transport per unit width in the n-direction.

As r approaches infinity, eqs. 2.52 - 2.56 describe the flow in a straight channel. Odgaard and Wang (1991a) reduce the above equations by making the following assumptions. First, that in a river, the flow depth d is small compared to the width b, therefore, $d/b << 1$. Second, that the bend radius r is generally larger than b. In our particular conditions, the width ratio is not sufficiently small ($d/b = 0.305$) nor is

the curvature ratio sufficiently large ($r/b = 2.95$) to make these assumptions. Further development of the above equations leads to the following relationship for the vane-induced near-bed transverse shear stress, τ_{Vn}, required to completely counteract the shear stress from the natural secondary current:

$$\tau_{Vn} = \frac{\rho k(2m+1)(m+1)}{m^2[2m^2+k(m+1)]}\overline{u}^2\frac{d}{r} \tag{2.57}$$

Substituting area-averaged, vane-induced bed shear stress as given by eq. 2.50 into eq. 2.57 yields the following design vane density required to achieve this condition:

$$\frac{NHL}{A} = \frac{2}{c_L}\frac{d}{r}G \tag{2.58}$$

where:

$$G = \frac{k}{\beta\lambda}\frac{(2m+1)(m+2)}{m(m+1)[2m^2+k(m+1)]}\left(\frac{d}{H}\right)^{2/m} \tag{2.59}$$

and the area covered by the vane field, $A = r_c\varphi b$, as in eqs. 2.14 and 2.21.

CHAPTER THREE

EXPERIMENTAL APPROACH AND MODELLING CONSIDERATIONS

3.1 Introduction

To date, the majority of experimental research on submerged vanes has been done at the Iowa Institute of Hydraulic Research, University of Iowa (Odgaard and Wang, 1991b, 1990; Odgaard and DeWitt, 1989; Odgaard and Spoljaric, 1989, 1986a, 1986b; Odgaard and Mosconi, 1987; Odgaard and Lee, 1984; and Odgaard and Kennedy, 1983). The literature indicates that all of the laboratory research on submerged vanes has been conducted in essentially six different flumes (Table 3.1).

Table 3.1: Descriptions of previously used channels.

Channel Configu-ration	Cross-section Shape	Bend Angle, φ	Bend Radius, r (m)	Channel Width, B (m)	Curvature ratio, r/b	Flow Depth, d (m)	Width/Depth Ratio, B/d
Straight	Rectangular	N/A	N/A	0.61	N/A	$0.10 < d < 0.25$	$2.4 < B/d < 6.1$
Straight	Rectangular	N/A	N/A	1.50	N/A	$0.15 < d < 0.40$	$3.8 < B/d < 10.0$
Straight	Rectangular	N/A	N/A	1.83	N/A	0.15	12.2
Straight	Rectangular	N/A	N/A	2.44	N/A	$0.16 < d < 0.18$	$13.6 < B/d < 15.3$
Curved	Sloped walls	180°	13.1	2.44	5.37	0.1	24.4
Curved	Vertical outer wall-sloped inner wall	90°	13.1	1.94	6.75	$0.16 < d < 0.18$	$10.8 < B/d < 12.1$

Although submerged vanes are primarily designed to alter the secondary currents in *channel bends*, only two of the six channels described in Table 3.1 incorporate bend sections along their lengths. Moreover, the tests performed in these channels were for 'wide-channel' conditions only (Chow (1959) defines a wide channel as one with a width/depth ratio greater than 10). Since the majority of small eroding streams are 'narrow', there is an obvious gap in research contributions regarding submerged vane application. As stated earlier, **the aim of the current study was to address this limitation in submerged-vane research by investigating vane performance in narrow channel bends.** The

apparatus and equipment used in the study are described in the first part of this chapter. A discussion on model applicability is presented in the second part.

3.2 Experimental Setup

3.2.1 The Experimental Channel

The laboratory channel was constructed from acrylic sheet and has a cross-section measuring 0.305 m wide by 0.150 m deep. The channel comprises three sections: (*i*) an initial 'straight' (entrance) section, (*ii*) a 'bend' test section, and (*iii*) a 'final' straight (exit) section. Two bend test sections (having 90° and 135° angles) were employed in the study (Figs. 3.1 & 3.2). Both bends have inner and outer radii, r_i = 0.748 m and r_o = 1.053 m, respectively. The entrance straights for the 90° and 135° bends are 7.62 m and 10.16 m long, respectively. The exit straight is 7.62 m long for both bend test sections. Both bends have inverts set at 150 mm deeper than the invert of the entrance straight. This arrangement permits a 150 mm deep sand bed to be added to these two sections, such that the top of the sand bed matches the elevation of the channel bottom at the end of the entrance straight (Fig. 3.3).

The inlet to the channel is a large tank (Fig. 3.4) equipped with a series of mesh screens to help stabilize the flow by dissipating large eddies and thereby ensuring a reasonably uniform velocity distribution flow across the channel. Water is supplied to the tank through a 0.1 m diameter pipe. A perforated 'T' diffuser section at the end of this pipe distributes the flow evenly and minimizes turbulence in the tank. The water leaves the tank and enters the channel smoothly through a gradually-narrowing transition 'throat'. Preliminary transverse velocity measurements showed that the maximum velocity filament seemed to be uncharacteristically close to the channel bottom. It was believed that this occurred because the flow entrance into the channel was in fact too smooth and the flow was not turbulent enough to raise the maximum velocity filament off the channel floor. This was remedied by installing a simple 1 cm-diameter tube across the channel floor (perpendicular to the flow) immediately after the flow enters the channel. This feature induces sufficient turbulence to lift the maximum velocity filament off the channel floor to a more characteristic location closer to the free surface.

Given the range of hydraulic conditions examined in the study, the combination of the *bed tube* feature and the 7.62 m long entrance straight was considered sufficient to establish fully-developed and near-uniform flow conditions in the straight section upstream of the bend section. A series of calibration tests

confirmed that this was, in fact, the case. To avoid a sudden change from the hydraulically *smooth* (entrance) section to the *rough* (test) section, the final 1.72 m length of the entrance straight was lined with a (fixed) single layer of sand similar to that used in the test section (Fig. 3.4).

The downstream end of the channel is equipped with a 'mouth-jaw' adjustable tailgate used to control the flow profiles (i.e., depths) along the channel. Upon exiting the channel, the flow passes through a sediment trap and enters a large collection tank. The sediment trap is a sheet metal box having a screen bottom. The screen mesh size is 0.425 mm (i.e., #40 size) which is smaller than 99% of the particles in the test sand. The collection tank is equipped with baffle-plates to reduce turbulence and to ensure a tranquil water surface within the head-measurement well of the tank. A 45° sharp-edge triangular weir was installed at the end of the collection tank to measure the flowrate. After spilling through the triangular weir, water enters a large 380 m^3 underground sump and then is recirculated by means of a constant-rotational-speed (870 RPM) pump. The pump is capable of delivering a maximum flowrate of 0.315 m^3/s with a total head of 18.28 m. The entire channel (excluding the *inlet* and *outlet* tanks) sits on an adjustable-slope platform. The channel slope can be adjusted in both the longitudinal and transverse directions.

3.2.2 Depth and Velocity Measurement Devices

Water and bed surface elevations were measured with a point gauge mounted on a sturdy instrument carriage. The point gauge is accurate to 1 mm. The *mini-propeller-type velocity meter* and *Pitot tube* that were used to measure point velocities were capable of being mounted to the same instrument carriage as the point gauge. The *Streamflo-Series* propeller-type probe, manufactured by Nixon Instrumentations Ltd., was used for the velocity range of 5 to 70 cm/s when simple quick measurements were required. This probe was not used when high degrees of accuracy were required since the fluctuations of the analog display are too rapid to acquire a representative value. However, efforts were made to time-average several values, thus reducing the error involved. The total probe length is 0.468 m, and the head of the sensing probe consists of a fine-bladed PVC rotor (11.6 mm diameter) mounted on a hard stainless steel spindle. An insulated gold wire is contained within the tube of the probe and terminates 100 μm from the rotor blades' tips. When the rotor revolves under the influence of a conductive liquid (i.e., water), the measurable impedance between the gold wire and the tube changes slightly each time a rotor blade passes over a specific point on the tube. An analog indicator senses this variation and uses it to show the rotational speed in terms of frequency (Hz). The manufacturer of the analog indicator provided a specific

calibration curve for the probe to convert the blade frequency to actual velocity. This device has an associated error of ± 1.5% of the true velocity.

The 4-mm diameter Pitot tube was used when greater accuracy than what is obtainable from the propeller-type meters was required. For low velocities, when the pressure difference in the recording manometers was so small that minor errors in reading the water levels in the manometers contributed to large errors in the calculated velocities, a *Gaertner Cathetometer* having a 20-part vernier scale was used, enabling accuracy of 50 μm.

3.2.3 Vanes

The *vanes* were constructed from 0.5 mm-thick galvanized sheet metal. They were cut into rectangles having varying lengths and widths, which allowed for a thorough investigation of the effects of these parameters on vane performance. The dimensions and vane spacings will be discussed in a later chapter.

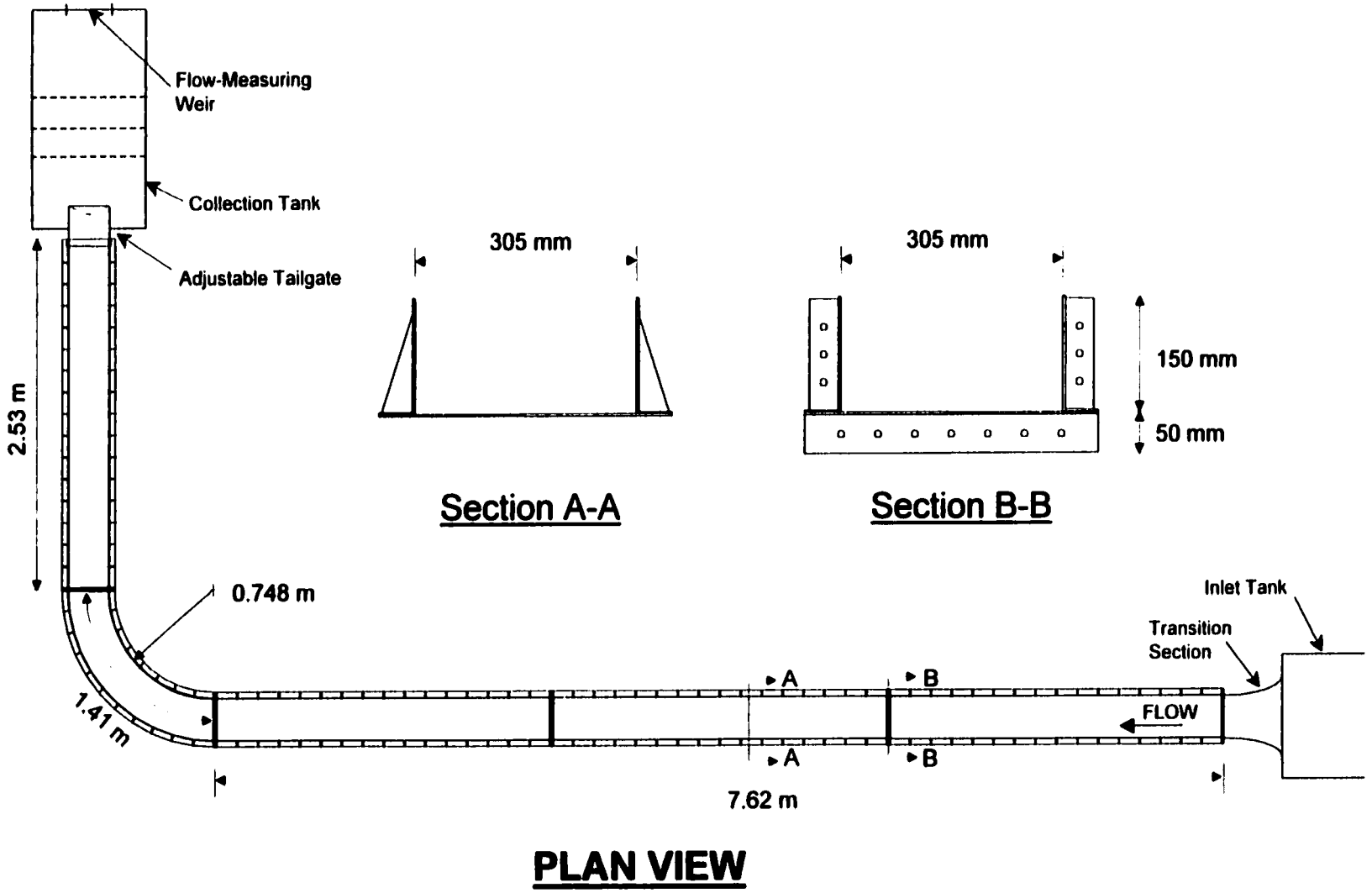

Figure 3.1: Experimental channel with 90° bend.

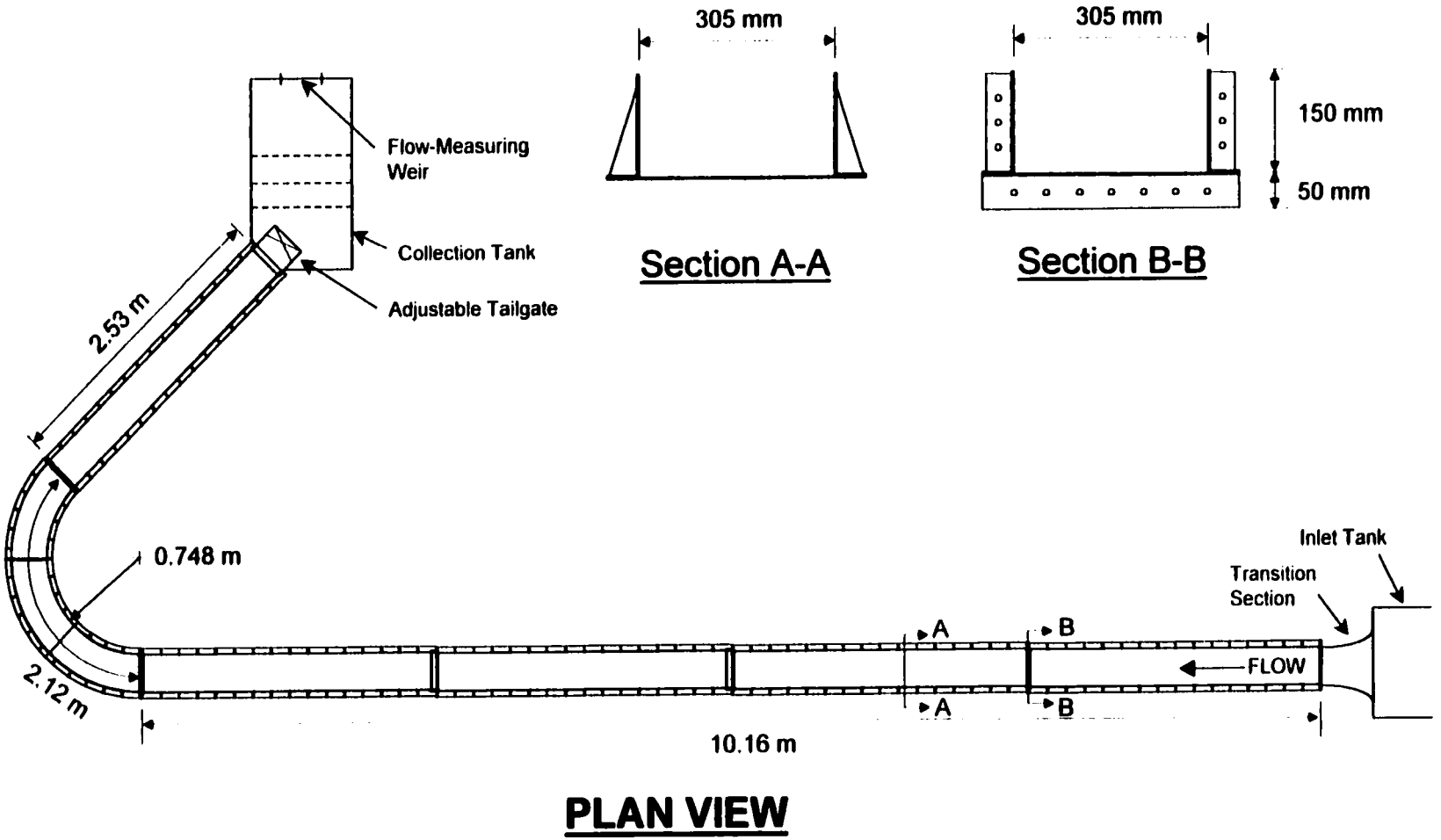

Figure 3.2: Experimental channel with 135° bend.

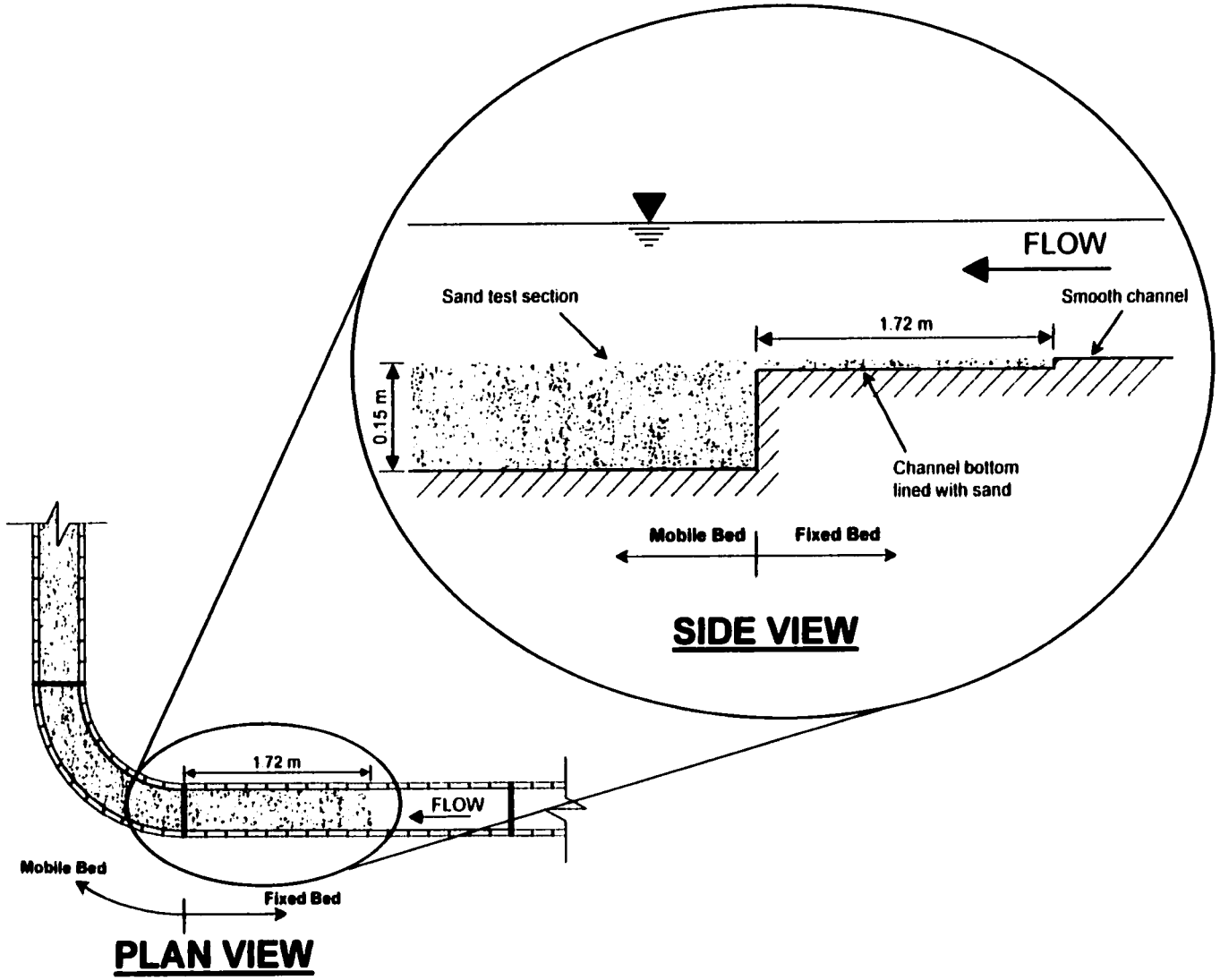

Figure 3.3: Fixed bed to mobile bed transition section.

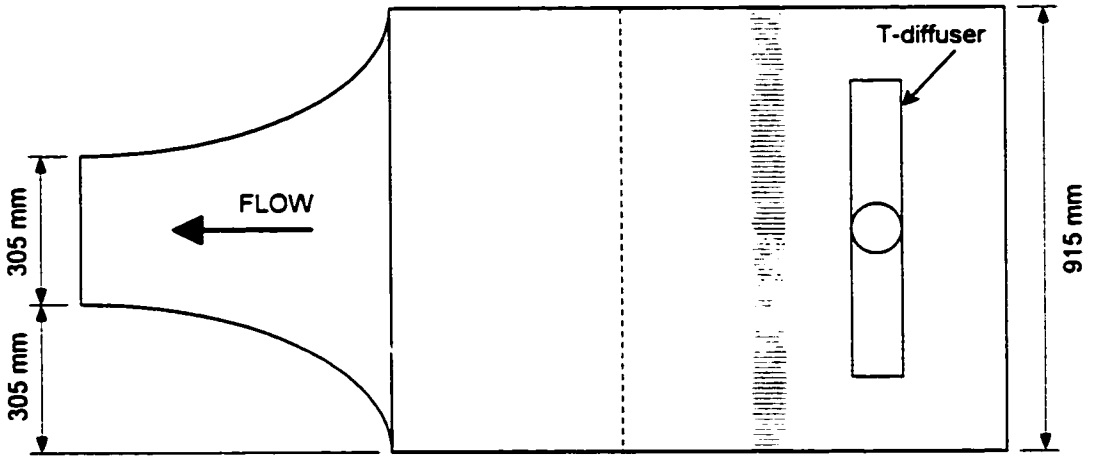

PLAN VIEW

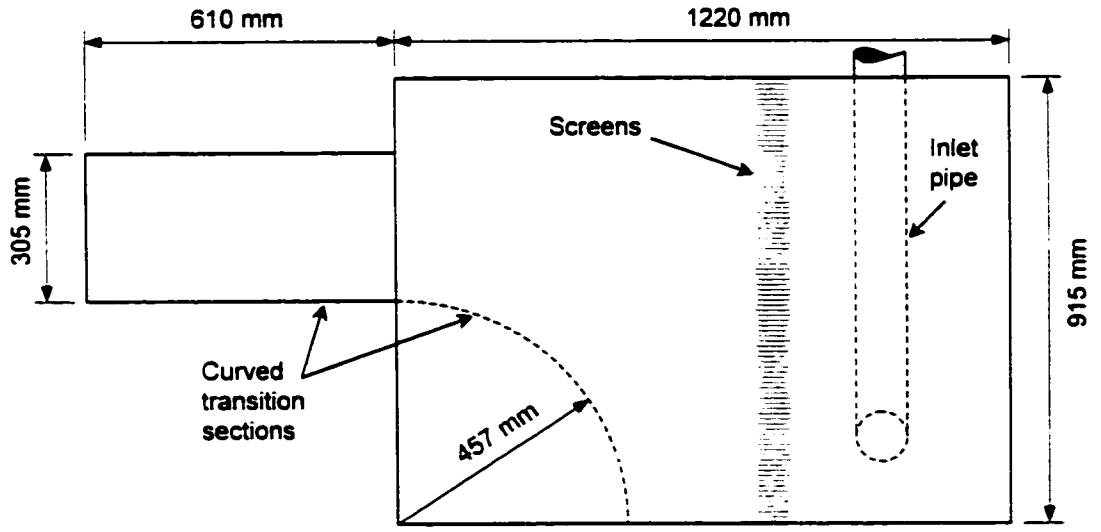

SIDE VIEW

Figure 3.4: Channel inlet tank details.

3.3 Modelling Considerations

3.3.1 Model Theory

As in the current study, when inertial and gravity forces are considered to be the dominant forces in the fluid motion, the Froude number of the model and prototype should be kept equal. If the same fluid is used in both, and they are both subjected to the same gravitational acceleration, then the various physical quantities can be derived based on the *Froude number law* if the prototype/model length ratio (scale), l_r, is known. The similarity between the hydraulic models and prototypes may be achieved in three basic forms

(*i*) *Geometric similarity*: implies similarity of form,

(*ii*) *Kinematic similarity*: implies similarity of motion, and

(*iii*) *Dynamic similarity*: implies similarity in forces involved in motion.

The various physical quantities have been grouped by their respective form of similarity and listed in Table 3.2.

Table 3.2: Ratios for the Froude number law (Hwang and Houghtalen, 1996).

Geometric Similarity		Kinematic Similarity		Dynamic Similarity	
Length	l_r	Time	$l_r^{1/2}$	Force	l_r^3
Area	l_r^2	Velocity	$l_r^{1/2}$	Mass	l_r^3
Volume	l_r^3	Acceleration	1	Work	l_r^4
		Discharge	$l_r^{5/2}$	Power	$l_r^{7/2}$
		Angular velocity	$l_r^{-1/2}$		
		Angular acceleration	l_r^{-1}		

3.3.2 Model Similarity

Our laboratory channel is unlike the five channels at the University of Iowa, in that it is relatively narrow ($b = 0.305$ m), deep ($d = 0.1$ m), and has a tight bend radius ($r_c = 0.901$ m). These conditions however, are not unlike those encountered in nature. For instance, at a scale, $l_r = l_p/l_m = 25$ (where: l = length,

subscript p and m refer to prototype and model quantities, respectively), a natural river would have the following properties:

Width

$$b_r = \frac{b_p}{b_m} = l_r = 25$$

$$b_p = b_m \cdot b_r = 0.305\ \text{m} \cdot 25 = 7.6\ \text{m}$$

Depth

$$d_r = \frac{d_p}{d_m} = l_r = 25$$

$$d_p = d_m \cdot d_r = 0.1\ \text{m} \cdot 25 = 2.5\ \text{m}$$

Radius

$$r_r = \frac{r_p}{r_m} = l_r = 25$$

$$r_p = r_m \cdot r_r = 0.901\ \text{m} \cdot 25 = 22.5\ \text{m}$$

Time (8 hr)

$$t_r = \frac{t_p}{t_m} = \sqrt{l_r} = \sqrt{25} = 5$$

$$t_p = t_m \cdot t_r = 8\ \text{hr} \cdot 5 = 40\ \text{hr}$$

Velocity

$$u_r = \frac{u_p}{u_m} = \sqrt{l_r} = \sqrt{25} = 5$$

$$u_p = u_m \cdot u_r = 0.285\ \text{m/s} \cdot 5 = 1.4\ \text{m/s}$$

Although the channel used in the current study is unlike any of those used previously, it can been seen that it nevertheless accurately represents a natural river bend at a length scale of 25. From the preceding calculations, the natural river bend would have a width of 7.6 m, a depth of 2.5 m, and a radius of 22.5 m. The result is a prototype (and model) radius-to-width ratio, $r_c/b = 2.95$. Leopold and Wolman (1960) report that although the sinuosities (ratio of valley slope to channel slope) vary greatly among different rivers in different geological conditions, there exists a definite trend in their r_c/b ratios. In fact, they found in a study of 50 different rivers, that two-thirds of the ratios were in the range 1.5 - 4.3, with a median value of 2.7. The two curved flumes used at the University of Iowa have r_c/b ratios of 5.4 and 6.8.

Simons (1971) reports that the U.S. Geological Survey tabulated 2950 river point velocities, and found that fewer than 1% exceeded 4 m/s; that the median velocity was 1.25 m/s; and that the mean velocity was

1.48 m/s. The model used in the current study represents a river with a mean velocity of approximately 1.4 m/s, which is considerably close to the mean velocity of 1.48 m/s as reported by Simons.

CHAPTER FOUR

EXPERIMENTAL BOUNDARY CONDITIONS

4.1 Introduction

Many experimental conditions were determined and set prior to experimental testing. These included: longitudinal channel bed slope, discharge, flow depth, velocity, bed material type and size, and the channel bend radius and angle. The longitudinal channel slope, flow depth, bed material type and size, and discharge were all kept constant throughout the entire testing program.

4.2 Sediment Characteristics

All experiments were run at or close to the threshold condition for bed material movement (i.e., where the shear stress ratio, τ_0/τ_{cr}, is kept close to unity). It is common practice in model design to attempt to scale the sediment geometrically according to the model-prototype scale ratio; however, when the length ratio is too large (i.e., when the prototype size is much larger than the model size), as it is in the current study, then it becomes impractical to do this. Therefore, other considerations in determining the sediment characteristics prevail. These considerations will be addressed below.

4.2.1 Sediment Size

According to García (1999), *ripples* form at sediment Reynolds numbers, $Re_* = u_* D_{50}/\nu \leq 11.6$, and according to Raudkivi (1990) they form with fine grained sediments, i.e., $D_{50} < 0.7$ to 0.9 mm. The size of the model used in this study is relatively small; thus, any ripples would be large compared to the bed profile elevations and vane dimensions. The ripples, which have a tendency to migrate downstream, would pass through the critical test areas in the channel, and thereby produce spurious results. Therefore, it is necessary that ripple formation is avoided. By applying García's condition, the sediment Reynolds number for the current conditions can be calculated and compared to his recommended limit of 11.6 to determine the possibility of ripple formation. By applying the following conditions:

- kinematic viscosity, $\nu = 1 \times 10^{-6}$ m^2/s,
- mean grain size, $D_{50} = 0.7$ mm (based on the lower limit of Raudkivi's second criterion),
- acceleration due to gravity, $g = 9.81$ m/s^2,
- initial flow depth (i.e., prior to scouring), $d_i = 0.1$ m
- hydraulic radius, $R = 0.06$ m (since R = flow area / wetted perimeter = [0.3 m × 0.1 m]/[2(0.1 m) +0.3 m]),
- streamwise slope, $S = 0.00065$ (based on preliminary calculations), and
- shear velocity, $u_* = \sqrt{g R S} = \sqrt{(9.81 \text{ m/s}^2)(0.06 \text{ m})(0.00065)} = 0.0196$ m/s

the sediment Reynolds number is:

$$\text{Re}_* = \frac{u_* D_{50}}{\nu}$$

$$\text{Re}_* = \frac{(0.0196 \text{ m/s})(0.0007 \text{ m})}{1 \times 10^{-6} \text{ m}^2/\text{s}}$$

$$\text{Re}_* = 13.7$$

A sediment Reynolds number, $\text{Re}_* = 13.7 > 11.6$ indicates that ripple formation will not occur. Preliminary tests were run at different flow rates and depths with a sand bed having $D_{50} = 0.7$ mm. The sand exhibited no tendencies to form ripples, and was therefore used throughout all the tests.

4.2.2 Sediment Uniformity

It is widely accepted that sediment gradation contributes significantly to the formation of scour patterns. The sediment gradation refers to the type of particle size distribution in a certain sediment. A sediment with a wide range of particle sizes is considered to be *nonuniform*, and that with a narrow range of sizes is considered to be *uniform*. The uniformity is quantified by the *geometric standard deviation*, σ_g, of the particle size distribution:

$$\sigma_g = \sqrt{\frac{D_{84.1}}{D_{15.9}}} \qquad \textbf{(4.1)}$$

where:

$D_{84.1}$ = particle size for which 84.1% of the sediment mixture is finer, and
$D_{15.9}$ = particle size for which 15.9% of the sediment mixture is finer.

Nonuniform sediment mixtures ($\sigma_g > 1.5$) consistently produce scour depths which are less than those produced by uniform sediments. Both the rate of scour and the maximum scour depth decrease with

increasing standard deviation. This trend is explained by the *armouring* effect. The armour layer develops as the finer particles are easily entrained into the flow and thus are transported away from the sediment mixture. This results in a coarser layer remaining which in turn is more resistant to scour. Many researchers report these findings, including Yaroslavtziev (1954), Jarocki (1961), Laursen (1963), Shen et al. (1966), Melville (1975), Kwan, (1988). As σ_g increases, so does the size of the particles in the remaining armour layer, which thus decreases the potential maximum scour depth. It is therefore desirable to use a uniform sediment in the test section to obtain results that are not falsified by a possible armour layer.

Washed quartz sand was obtained from a local quarry. Sieve analyses showed that it had a mean grain size, D_{50} = 0.7 mm and a geometric standard deviation, σ_g = 1.7, which would be classified as nonuniform. Therefore, the sand was screened in a large *Gilson* mechanical sieve to produce a more uniform material (Fig. 4.1). The result was a sand with D_{50} = 0.7 mm and σ_g = 1.3, which would be classified as uniform.

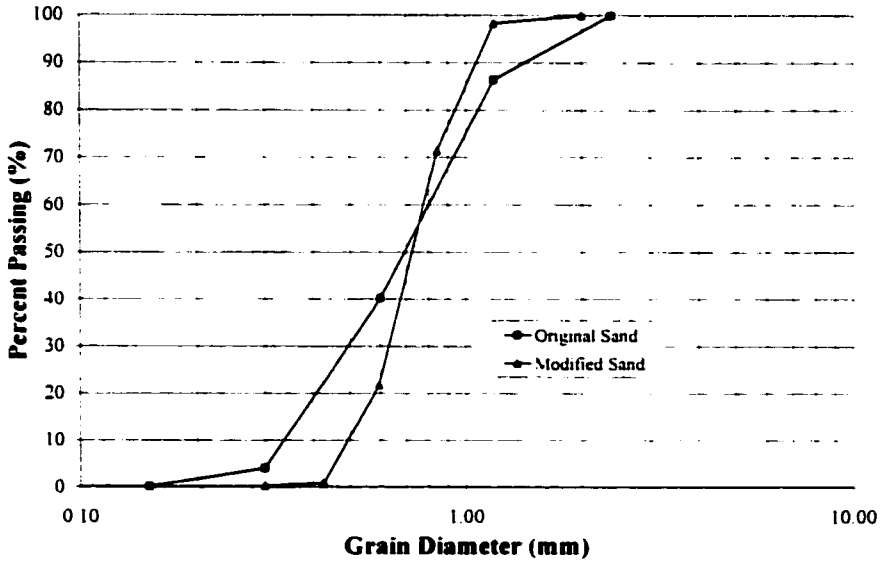

Figure 4.1: Gradation curves for original and modified sand.

4.3 Channel Slope

The channel slope was calculated based on conditions which would produce uniform flow with normal shear stress, τ_0, equal to the critical shear stress, τ_{cr}, for the initiation of sediment movement. Therefore, Shields' criteria may be applied for developing a relationship between the mean sediment size, the flow depth, and the channel slope. From section 4.2.1, the dimensionless sediment Reynolds number, $Re_* = 13.7$. Entering this value into Shields' curve (Fig. 4.2), yields a dimensionless shear stress of:

$$\tau_* = \frac{\tau_{cr}}{(\gamma_s - \gamma) D_{50}} = 0.033$$

Solving for the critical shear stress, τ_{cr}, yields:

$$\tau_{cr} = 0.033\,(2.65 - 1)\,(9810\ \text{kN/m}^3)\,(0.0007\ \text{m})$$
$$\tau_{cr} = 0.37\ \text{N/m}^3$$

Setting $\tau_{cr} = \tau_0$, and solving for the longitudinal slope, S, yields:

$$\tau_{cr} = \tau_0 = \gamma R S$$
$$\tau_{cr} = 0.37\ \text{N/m}^2 = (9810\ \text{kN/m}^3)\,(0.06\ \text{m})\,(S)$$
$$S = 0.00062$$

Thus, by setting the longitudinal slope, $S = 0.00062$, it will be possible to achieve a uniform flow depth of 0.1 m, which is coincident with the threshold conditions for sediment movement.

4.4 Velocity

All scour tests were done at the critical velocity for sediment movement. Unfortunately, there is much discussion in the research community on the exact definition of 'critical velocity' (Simons and Şentürk, 1977, pg. 399). The problem arises since there exists no true threshold condition beyond which motion begins spontaneously, but rather, a range of velocities over which the number of particles in motion increases gradually. Adding to the problem is that most definitions used in literature have relied on direct visual observations which in themselves are highly subjective. In the current study, the critical velocity was determined based on the mean velocity which would induce the movement of approximately 10 to 20% of the sand particles on the surface of the mobile bed. This velocity was 0.28 m/s, which corresponds reasonably well with recorded values of critical velocity for sand with $D_{50} = 0.7$ mm (Yang, 1996). At this velocity, with an initial flow depth, $d_i = 0.1$ m, the discharge was $Q = 0.0085\ \text{m}^3/\text{s}$.

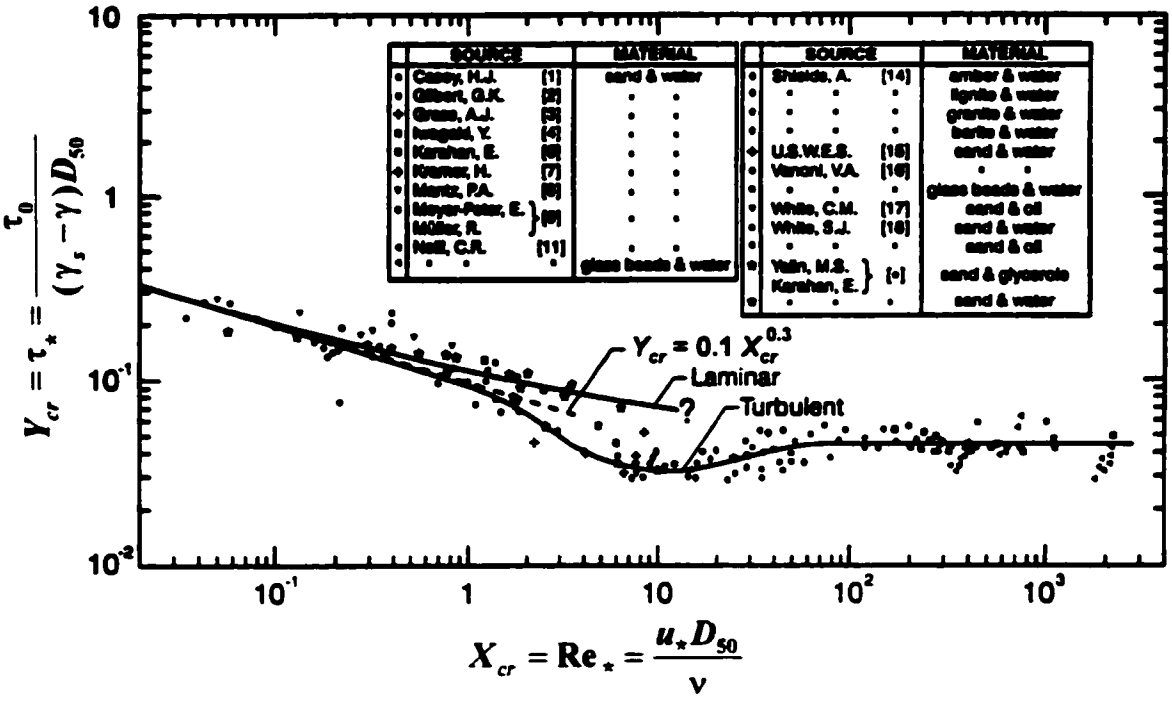

Figure 4.2: Shields' diagram (Yalin and Karahan, 1979).

4.5 Vane Sizes

Submerged vanes with heights, $H = 15, 25, 35, 50$, and 65 mm and lengths, $L = 50$, 100, and 150 mm were tested (Fig. 4.3). The corresponding range of aspect ratios (H/L) was $0.15 \leq \psi \leq 1.30$. (Table 4.1).

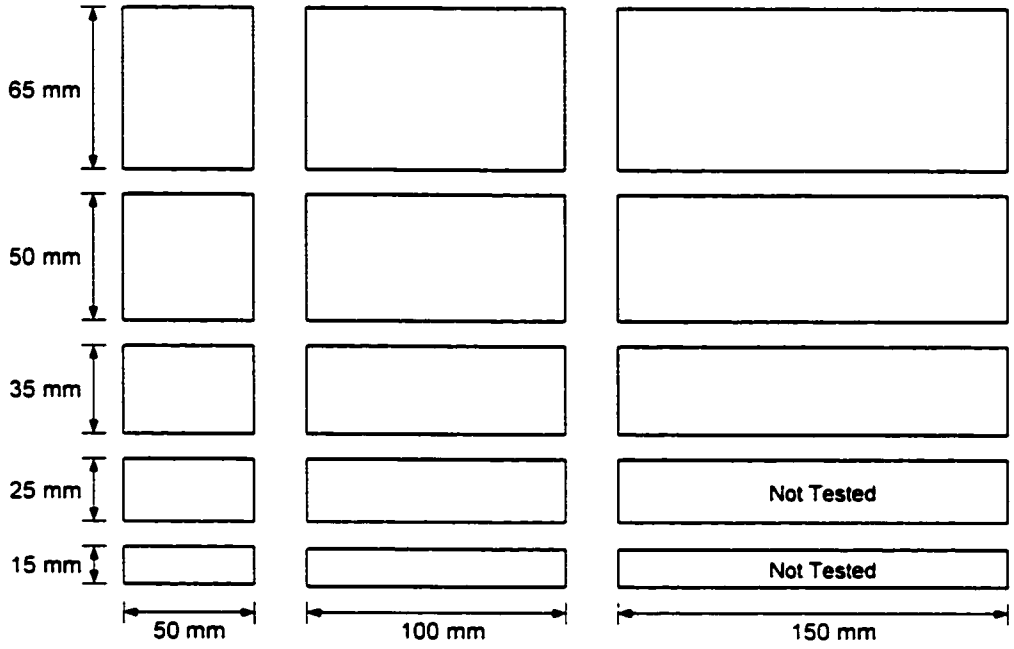

Figure 4.3: Dimensions of submerged vane sizes tested.

Table 4.1: Vane heights, lengths and aspect ratios examined in study.

Vane Height, H (mm)	Vane Length, L (mm)			
	50 (0.16)**	100 (0.33)	150 (0.49)	
65 (0.65)*	1.30	0.65	0.43	Aspect Ratio, ψ
50 (0.50)	1.00	0.50	0.33	
35 (0.35)	0.70	0.35	0.25	
25 (0.25)	0.50	0.25	N/A	
15 (0.15)	0.30	0.15	N/A	

* Values in parenthesis are heights nondimensionalized with initial flow depth (H/d_i)

** Values in parenthesis are lengths nondimensionalized with channel width (L/b)

4.6 Vane Angles

Submerged vanes were tested at angles, $\alpha = -4°, 0°, 4°, 8°, 12°$ and $16°$. The value of α is positive when the vane is installed at an angle set counter-clockwise (when viewed in plan) to the main flow direction (Fig. 4.4).

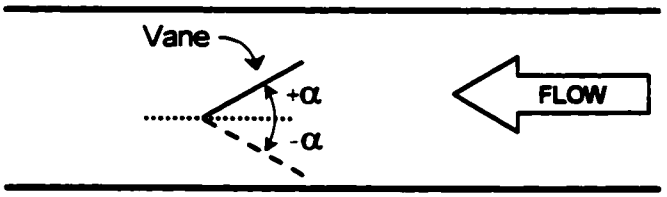

Figure 4.4: Definition sketch of vane angles.

Because the channel in the current study is hydraulically *narrow* (i.e., $b/d_i < 10$), the channel cross-section more closely approximates a square in which the secondary current may develop with greater efficiency. As a consequence, the direction of the near-bed flowlines has an incident flow angle, η, relative to a line drawn parallel to the channel wall (Fig. 4.5). η is given by:

$$\eta = \tan^{-1}\left[\frac{1}{\kappa^2}\,\frac{m(m+1)}{m+2}\,\frac{d}{r}\right] \qquad \textbf{(2.30)}$$

where: κ = von Kármán's constant ($\kappa = 0.4$ for clear water conditions), d = flow depth, r = channel radius, and m = velocity profile exponent which is given by:

$$m = \frac{\kappa \bar{u}}{\sqrt{gRS}} \qquad \textbf{(2.12)}$$

where: $\bar{u}$ = depth-averaged velocity, g = acceleration due to gravity, R = hydraulic radius, and S = longitudinal channel slope. The apparent near-bed flow angle, α', is directly related to the strength of the secondary current by:

$$\alpha' = \alpha + \eta \qquad \textbf{(2.31)}$$

For most of the earlier research on this subject, which was conducted at $d/r < 0.014$, η was less than approximately $10°$. In the current study, η is as high as $51°$. It should be noted that the vanes function by reducing the strength of the centrifugally-induced secondary current, thereby reducing η. It is the

presence of a large value of η (associated with strongly-curved narrow channels) which allows submerged vanes to operate at $\alpha < 0°$.

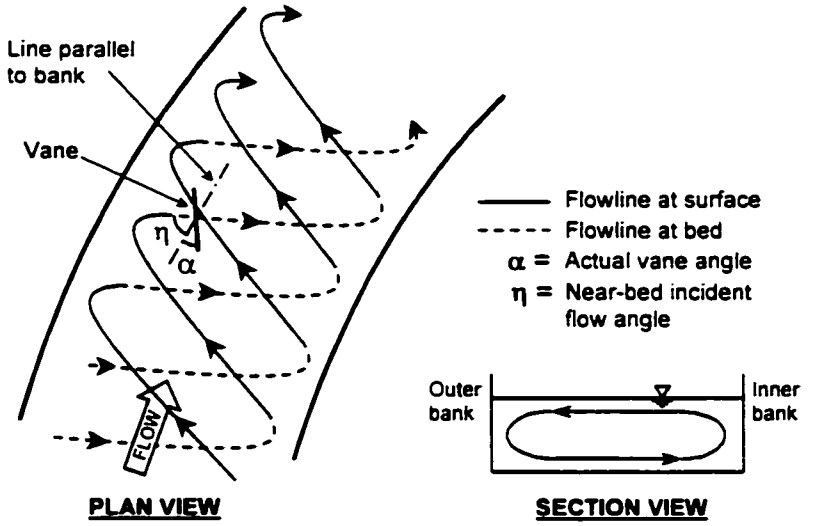

Figure 4.5: Illustration of near-bed incident flow angle.

4.7 Vane Placement

Much of the previous research was conducted on vanes placed in side-by-side *arrays* of two or more. This was believed to be unwarranted in our channel since it is narrow, and vane arrays of two or more would obstruct too much of the channel cross-section. For this reason, testing was restricted to a single array of vanes. The transverse distance from the channel's outer bank to the array (centreline) location was $\delta_n = 80$ mm, which resulted in the dimensionless ratio $\delta_n/b = 0.26$. The streamwise spacing between the vanes varied in the range 10 mm $\leq \delta_s \leq$ 40 mm ($0.33 \leq \delta_s/b \leq 1.31$).

Because of the variations in vane size and streamwise spacing, the vanes did not always end at the same streamwise location. To overcome this, it was decided that for any test, the last vane was the one which ended beyond 0.3 m past the end of the bend (Fig. 4.6).

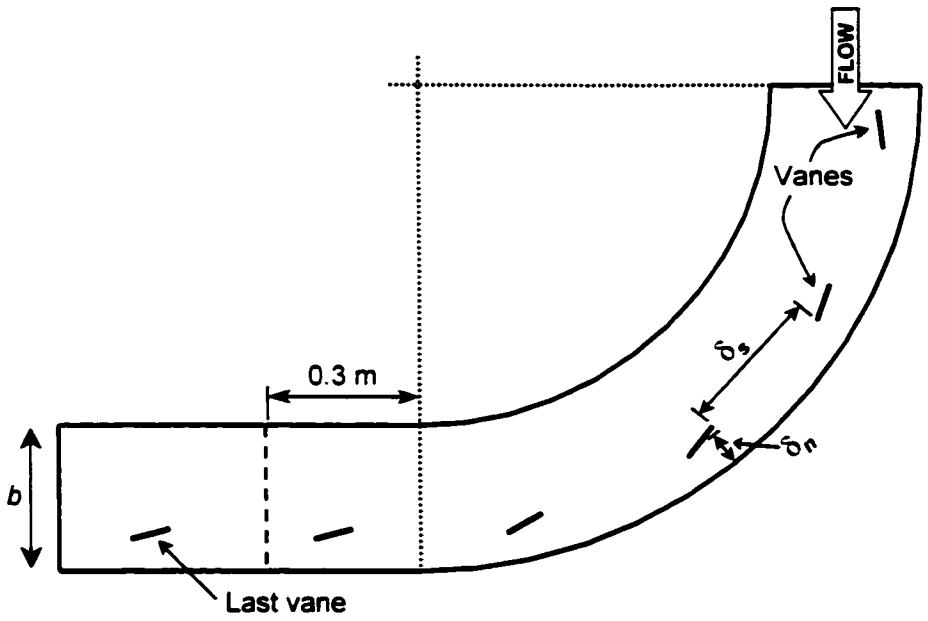

Figure 4.6: Typical vane placement (*note*: last vane is beyond 0.3 m past the end of the bend).

4.8 Bend Angle and Radius

Two bend angles were examined. Most of the testing program was conducted in a 90° bend. Because of time constraints, only a limited number of tests performed in the 90° bend were repeated in the 135° bend.

The radii to the inside and outside of the channel walls were $r_i = 0.748$ m and $r_o = 1.053$ m respectively; therefore, the radius to the channel centreline was $r_c = 0.901$ m. This results in a depth/radius ratio (which is commonly used to describe the degree of curvature) of $d_i/r_c = 0.11$. Previous studies were performed in channels with considerably weaker curvature, i.e., $d/r < 0.014$.

Another parameter commonly used to characterize natural rivers is the curvature ratio, r/b. In the current study, $r_c/b = 2.95$. This value is not only representative of typical r/b ratios reported in literature, it is also associated with very high bend migration rates. In a study conducted on fifty different rivers of varying sizes and physical settings, two-thirds of the r_c/b ratios were in the range 1.5 to 4.3, with a median value of 2.7 (Leopold and Wolman, 1960). Furthermore, for r_c/b ranging from 1.35 to 6.33, the maximum bend migration rate occurs at $r_c/b = 3.0$ (Begin, 1986).

4.9 Test Duration

It is common practice in sediment transport studies investigating maximum local scour phenomena, to allow tests to run until a quasi-equilibrium condition is reached. However, it is the nature of sediment transport that equilibrium is reached asymptotically only after a significant amount of time has elapsed. To overcome this, researchers often run tests to determine the time required for equilibrium, and then determine the value of the property they are examining (e.g., depth of pier scour, volume of sediment transport, etc.) at equilibrium. They may then determine the time required to reach say, 80% of the equilibrium value, run tests for that length of time and scale the remaining 20% up based on the determined ratios. This practice is ill-suited for the current study since the flow dynamics are highly three-dimensional and hence the time required to reach equilibrium conditions is not necessarily constant for all tests performed.

For many of the tests performed in this study, it was found that submerged vanes perform exceptionally well for the first 10 hours of model operation. In fact, most tests indicated that submerged vanes are capable of achieving 80% improvement (see eq. 5.1) in scour depth at the outer bank within this time. However, after approximately 10 hours, secondary flow effects become exaggerated and result in diminished submerged vane performance.

One common characteristic that occurred after 10 hours was the development of localized scour holes in the vicinity of the vanes. Once a scour hole would reach a certain size, flow separation would occur at the bed and would in turn further scour hole development, thereby aggravating the already-adverse situation. Another undesirable phenomenon was the continuous removal of sediment that occurred if a test was allowed to run for an extended duration. Therefore, one could argue that since vanes typically become ineffective after approximately 10 hours in our model conditions, they had proven themselves ineffective as bank stabilizers. However, it can be demonstrated that this is not the case by considering the following: first, the tests were conducted under a worst-case situation since no new sediment was introduced to replenish that which was removed from the test section during a test. In nature, sediment delivered from upstream enters a bend and is made available for sedimentation. This reduces the net loss of sediment through the vane field. Second, the sediment used in the experimental program was uniform ($\sigma_g = 1.3$), thus armouring did not take place. As discussed in section 4.2.2, armouring has the effect of stabilizing the channel bed and reducing scour depths, Third, the channel geometry allows for intensified sediment transport since it is very narrow, and therefore the cross-section more closely approximates a

square shape in which the secondary current can develop with greater efficacy. Furthermore, the r/b ratio is approximately equal to that which is associated with maximum bend migration (which occurs as a result of sediment removal from the outer bank) as was demonstrated in section 4.8. Finally, it may be that submerged vanes do not completely ameliorate the outer bank erosion process, but rather retard it significantly. This would not render the vanes ineffective, but on the contrary, it may result in them being considered as an attractive bank stabilization option since submerged vanes can be installed simply and inexpensively as a temporary measure until a more permanent one can be established.

CHAPTER FIVE

DATA ANALYSIS AND DISCUSSION

5.1 Introduction

Many of the analyses and design relationships for submerged vanes have been developed from extensive research performed at the University of Iowa (Odgaard and Wang, 1991b, 1990; Odgaard and DeWitt, 1989; Odgaard and Spoljaric, 1989, 1986a; Odgaard and Mosconi, 1987; Odgaard and Lee, 1984; and Odgaard and Kennedy, 1983). The literature indicates that all of the research was conducted in six flumes, only two of which incorporate bend sections. Both of the Iowa bends were located in hydraulically *wide* channels ($b/d > 10$) and possessed *weak* curvature ($r/b > 5.3$).

Both analyses that developed from the experiments on submerged vanes in curved channels were based on the conditions at the University of Iowa and therefore only satisfactorily describe wide channel bends with weak curvature (Odgaard and Lee, 1984; Odgaard and Wang, 1991a). The older of the two methods is based on the use of vanes to reduce or eliminate transverse bed slope, while the more recent method is based on elimination of transverse bed shear stress. The first method assumes that the transverse bed slope is linear (see eq. 2.2), which is only appropriate for a wide channel condition. The second method assumes that the channel is wide (i.e., $b/d > 10$) in the reduction of the three-dimensional equations of motion (see eqs. 2.57 & 2.58). The transverse bed slope observed in the present study was highly *non-linear*. Furthermore, our channel was hydraulically *narrow*. It follows therefore that neither method may be applied to the conditions in the current study. Being that this is the first study of submerged vane application in strongly curved narrow channels, it is believed that an empirical analysis will be sufficient to give a preliminary, yet conclusive overview of their performance under these conditions.

5.2 Experimental Procedure

Each of the scour tests was performed as follows:

1. The sand bed in the channel test section was leveled to an elevation equal to that of the upstream fixed-bed section.
2. Vanes with a given height and length were inserted vertically into the sand bed. Their angle was set and established with a specially-designed angle adjustment tool (Fig. 5.1). Vane placement continued to a point at least 0.3 m beyond the downstream end of the bend section (Fig. 4.6).
3. Water was admitted slowly to the flume.
4. All tests were performed under near-uniform ($d \approx d_0$) and clear-water ($u_*/u_{*_c} = u/u_c = 1$) flow conditions established in the test section.
5. After a period of 8 hours of continuous operation, the test was stopped and the water was slowly drained from the flume.
6. Bed elevations were measured with a point gauge at selected (grid) locations throughout the test section (Fig. 5.2).

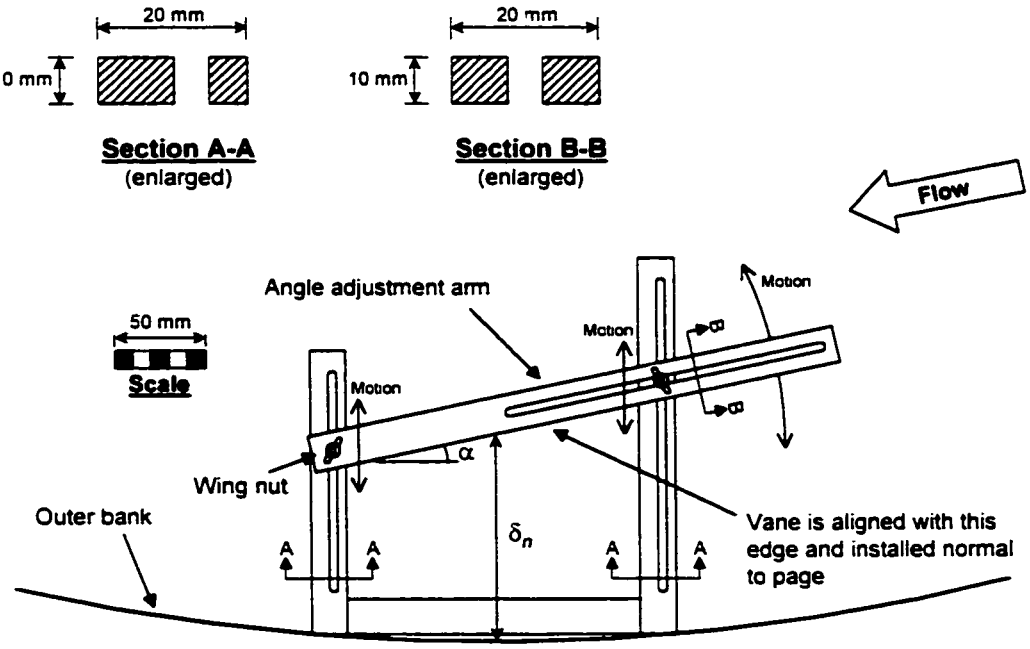

Figure 5.1: Vane angle adjustment tool (plan view).

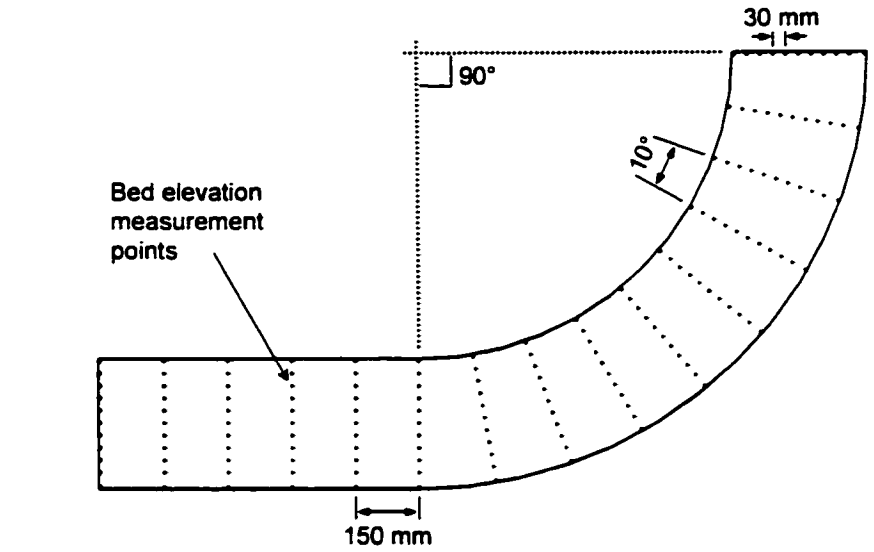

(a)

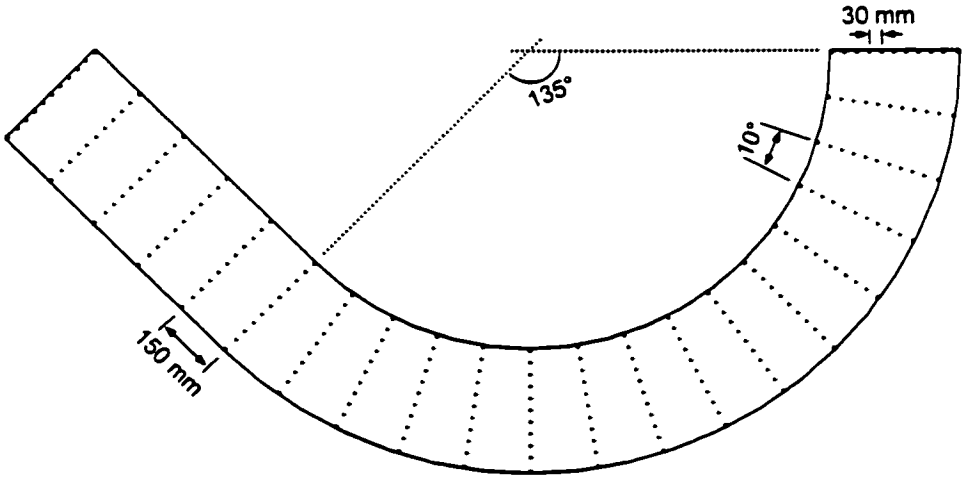

(b)

Figure 5.2: Bed elevation measurement points for: (a) 90° bend and (b) 135° bend.

5.3 Parametric Study

A parametric study was conducted to examine the effects of vane height, length, angle, streamwise spacing, transverse distance from outer bank, and bend angle. The first four parameters were examined over a wide range of values. Due to time constraints, the ranges for the last two parameters were limitted. In many of the previous 'wide-channel' studies, vanes were tested in lateral arrays of two or more. Because our channel was 'narrow', testing was restricted to a single row to avoid excessive blockage of the flow cross-section by vanes.

The parametric study examined the following ranges of boundary conditions:

(*i*) $0.15 \leq H/d_i \leq 0.65$

(*ii*) $0.16 \leq L/b \leq 0.49$

(*iii*) $-4° \leq \alpha \leq +16°$

(*iv*) $0.33 \leq \delta_i/b \leq 1.31$

(*v*) $0.23 \leq \psi \leq 1.30$

Tests were performed in the 90° bend for the vane sizes indicated in Fig. 4.3. For each vane, δ_i/b was initially fixed at 0.98 and tests were performed at $\alpha = -4°, 0°, 4°, 8°, 12°$, and 16°. Then, α was kept constant at 8° and tests were performed at $\delta_i/b = 0.33, 0.66$, and 1.31. At the end of this testing program, the bend angle was changed to 135° and the tests indicated in Table 5.1 were performed.

5.4 Method of Analysis

Successful vane operation is based on the premise that they will help stabilize a channel's outer bank by reducing movement of sediment from the outer bank toward the centre of the channel. This results in three positive effects: (*i*) reduction in channel bed scour depth at the outer bank, (*ii*) generation of a positive (transverse) bed slope at the outer bank, and (*iii*) net reduction of the bed scouring process through the bend. Based on these general observations and sound judgement, the five criteria employed in this study to evaluate the effectiveness of the various vane configurations tested were:

1. reduction in average scour depth at the outer bank,
2. generation of a positive transverse bed slope at the outer bank,

Table 5.1: Summary of all tests conducted in 135° bend.

Vane Length, L/b	Vane Height, H/d_i	Angle, α	Streamwise Spacing, δ_s/b
0.16	0.50	0	0.98
0.33	0.25	4	0.98
0.33	0.35	4	0.98
0.33	0.35	4	0.98
0.33	0.35	4	0.66
0.33	0.50	4	0.98
0.33	0.65	0	0.98
0.33	0.65	8	0.98
0.49	0.35	0	0.98
0.49	0.35	4	0.98
0.49	0.35	8	0.66
0.49	0.50	4	0.98
0.49	0.50	8	0.98
0.49	0.50	12	0.98
0.49	0.65	0	0.98
0.49	0.65	4	0.98
0.49	0.65	4	0.98
0.49	0.65	4	0.66
No Vanes	Test conducted at start of experimental program in compacted sand bed		
No Vanes	Test conducted at end of experiment program in compacted sand bed		
No vanes	Test conducted at end of experimental program in artificially uncompacted sand bed		

3. reduction in general scour throughout the bend,
4. avoidance of excessive local scouring in the vicinity of the vanes, and
5. practicality of vane size and spacing (relative to channel width and depth).

For any given vane size and arrangement to be considered successful, it must meet *all* of the above criteria.

Data were plotted graphically in three different ways to aid in the empirical analysis of submerged vane performance. The first series of graphs shows '*% Improvement*' (eq. 5.1) on the dependent axis and vane height (H/d_t), vane length (L/b), vane angle (α), or vane streamwise spacing (δ_v/b) on the independent axis. The second series shows the *average outer bank transverse bed slope*, $(S_o)_{ave}$ on the dependent axis and H/d_t, L/b, α, or δ_v/b on the independent axis. The third series of graphs shows the nondimensionalized *average scour depth*, D_v/d_t (where: D_v = the average of all d_v values, and d_v = vertical distance between initial bed elevation and final bed elevation for zones of scour (see Fig. 5.3) on the dependent axis and H/d_t, L/b, α, or δ_v/b on the independent axis.

Each graph shows three curves obtained by simple linear or 2nd order polynomial regression through the data. The top and bottom curves are plotted through the upper and lower boundaries of the data, respectively. The middle curve is plotted through the average of the data shown on the graph. This method was used to circumvent the problem which arises from the variability in the data. For instance, it can be seen in Fig. A.2, that the curves plotted individually through the four data sets would braid back and forth across the range of H/d_t values. The variability is not unexpected, but rather is inherent to sediment transport experimentation. Furthermore, as will be shown in a subsequent section, vane length (L/b) and streamwise spacing (δ_v/b) have only marginal impact on % Improvement, D_v/d_t and $(S_o)_{ave}$; therefore, curves plotted through various values of either L/b or δ_v/b (as in Fig. A.2) will naturally be very close together, and hence be more susceptible to crossing.

In the first series of graphs:

$$\%\ \text{Improvement} = \left(\frac{(d_o)_{max} - (d_o)_{ave}}{(d_o)_{max}} \right) \times 100\% \qquad \textbf{(5.1)}$$

where:

$(d_o)_{max}$ = maximum scour depth at outer bank for a 'no-vane' condition, and
$(d_o)_{ave}$ = average scour depth at outer bank for a 'with-vanes' condition.

By eq. 5.1, a 100% improvement in the outer bank scour condition would indicate that $(d_o)_{ave} = 0$, whereas a 0% improvement would indicate that $(d_o)_{ave} = (d_o)_{max}$. Furthermore, (*i*) if deposition occurs at the outer bank, then % Improvement will exceed 100%, and (*ii*) if $(d_o)_{ave} > (d_o)_{max}$, then % Improvement will be less than 0%.

In the second series of graphs, $(S_o)_{ave}$ is obtained by solving for the slope of the linear regression for the outer portion of each cross-section (Fig. 5.3) and then averaging them. The averaging process is used to smooth the data and thus produce more consistent trends. The result is, however, that in the upstream portion of the test section where the mobile-bed is usually quite stable, the average outer bank transverse bed slope is over-predicted. In the downstream portion, where the thalweg is usually deeper, it is under-predicted. Generally, $(S_o)_{ave} > 0$ is indicative of successful submerged vane operation; however, if the slope becomes too steep, it may be indicative of excessive channel thalweg deepening. Thalweg deepening is closely related to the amount of sediment being removed from the test section; thus, if it becomes excessive, it may incur a failure of criterion #3 above.

In the third series of graphs, D_s/d_i is obtained by averaging all *negative* bed elevation changes only and then nondimensionalizing them by the initial flow depth (d_i = 0.10 m). The average scour depth, D_s quantifies the severity of *scouring* throughout the channel, irrespective of the amount of deposition which occurs elsewhere in the test section. The data were arranged according to the three graph types, and then examined based on the three corresponding vane performance criteria. Performance thresholds were determined to identify, on any graph, ranges of successful and unsuccessful submerged vane operation (Table 5.2).

The failure thresholds were developed based on knowledge gained throughout the testing program. After performing numerous tests, the relative performance of each one became evident by simple observation. Judgement was then used to isolate 'threshold tests' which were close to what could be considered failure. The bed profiles (i.e., outer bank scour depth, transverse bed slope, and average scour depth throughout the bend) from these tests were then analyzed and the failure thresholds given in Table 5.2 were extracted therefrom.

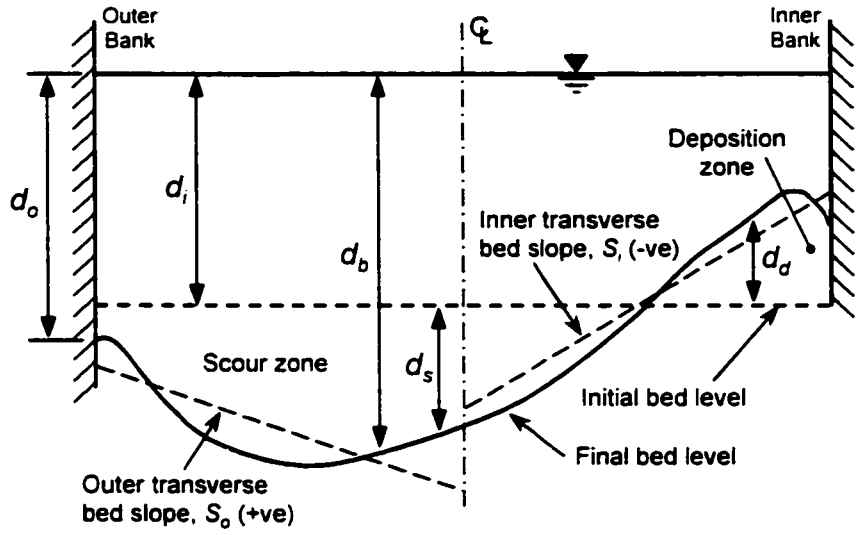

Figure 5.3: Typical channel cross-section showing inner and outer bank transverse bed slopes.

Table 5.2: Vane performance criteria and corresponding graph types.

Criterion	Graph Type	Failure Threshold
1. Reduction in average scour depth at the outer bank	% Improvement vs. *parameter*†	% Improvement < 90%
2. Generation of a positive transverse bed slope at the outer bank	$(S_n)_{ave}$ vs. *parameter*†	$(S_n)_{ave} < 0.05$
3. Reduction in average scour depth throughout the bend	$(D_v)/d_i$ vs. *parameter*†	$(D_v)/d_i < -0.13$

† *parameter* refers to any one of the following: H/d_i, L/b, α, or δ_i/b

5.5 90° Bend

As was previously indicated, the majority of the testing program was conducted in the 90° bend, with several selected tests conducted in the 135° bend. The 90° bend results are presented herein; the 135° bend results are presented in a subsequent section.

5.5.1 Effect of Vane Height

Narrow vanes ($L/b = 0.16$), intermediate-length vanes ($L/b = 0.33$), and long vanes ($L/b = 0.49$) of varying heights were examined. The results presented herein are summarized in Table 5.3.

5.5.1.1 Narrow Vanes ($L/b = 0.16$)

Narrow vanes having heights of $H/d_i = 0.15, 0.25, 0.35, 0.50$, and 0.65 were examined. The graphs used in the analysis (Figs. A.1 - A.6) appear in Appendix A. Figure A.1 shows the data for narrow vanes operated at various angles to the main flow direction and Fig. A.2 shows the data for narrow vanes operated at various streamwise spacings. The average curve in Fig. A.1 has its maximum at $H/d_i = 0.47$ which corresponds to 93% improvement. From this graph, the so-called 'range of successful operation' is $0.31 < H/d_i < 0.59$. Likewise, the average curve in Fig. A.2 has its maximum at $H/d_i = 0.44$ which corresponds to 97% improvement. The range of successful operation is $0.23 < H/d_i < 0.65$.

Figures A.3 and A.4 show average outer bank transverse bed slope, $(S_o)_{ave}$, versus H/d_i for the narrow vane case. Both graphs exhibit similar trends. In Fig. A.3, the average curve has its maximum at $H/d_i = 0.51$ which corresponds to $(S_o)_{ave} = 0.07$. The range of successful operation is $0.32 < H/d_i < 0.65^*$ (*note*: * is used to indicate that the range of successful operation extends beyond the tested boundaries). In Fig. A.4, the average curve has its maximum at $H/d_i = 0.49$ which corresponds to $(S_o)_{ave} = 0.09$. The range of successful operation is $0.24 < H/d_i < 0.65^*$. Figures A.5 and A.6 show average scour depth, D_s/d_i, versus H/d_i for narrow vanes (*note*: D_s is an average of the elevations of scour zones *only*). Both curves show linear trends with negative slopes. This suggests that for narrow vanes, as the vane height increases for narrow vanes, so does the severity of the average scour depth. Figures A.5 and A.6 indicate that submerged vanes are ineffective when $H/d_i > 0.47$ and $H/d_i > 0.52$, respectively.

5.5.1.2 Intermediate-length Vanes ($L/b = 0.33$)

Intermediate-length vanes having heights of $H/d_i = 0.15, 0.25, 0.35, 0.50$, and 0.65 were examined in the next series of experiments. The graphs used in their analysis (Figs. A.7 - A.12) appear in Appendix A. Figure A.7 shows the data for intermediate-length vanes operated at various angles and Fig. A.8 shows the data for the same vanes operated at various streamwise spacings. The average curve in Fig. A.8 has its maximum at $H/d_i = 0.41$, which corresponds to 95% improvement. The range of successful vane

operation is $0.20 < H/d_t < 0.63$. The average curve in Fig. A.8 has its maximum at $H/d_t = 0.39$, which corresponds to 97% improvement. The range of successful vane operation is $0.16 < H/d_t < 0.62$.

Figure A.9 indicates that, for intermediate-length vanes operated at various angles to the main flow direction, the maximum average outer bank transverse bed slope occurs at $H/d_t = 0.43$, which corresponds to $(S_o)_{ave} = 0.085$. The range of successful vane operation corresponds to $0.20 < H/d_t < 0.65^*$. Figure A.10 indicates that for vanes operated at various streamwise spacings, maximum average outer bank transverse bed slope occurs at $H/d_t = 0.41$, which corresponds to $(S_o)_{ave} = 0.095$. The range of successful vane operation is $0.23 < H/d_t < 0.60$. Figures A.11 and A12 both show linear trends with negative slopes indicating that as vane height increases, the bed elevation decreases. In Fig. A.11, failure occurs at $H/d_t > 0.42$: in Fig. A.12, failure occurs at $H/d_t > 0.40$.

5.5.1.3 Long Vanes ($L/b = 0.49$)

Long vanes having heights of $H/d_t = 0.35$, 0.50, and 0.65 were examined next. The graphs used in their analysis (Figs. A.13 - A.18) appear in Appendix A. Figure A.13 shows the data for long vanes operated at various angles to the main flow direction and Fig. A.14 shows the data for long vanes operated at various streamwise spacings. The average curve in Fig. A.13 exhibits a near-linear decreasing trend with all average values above 90% improvement; therefore, the range of successful vane operation is $0.35^* < H/d_t < 0.65^*$. Likewise, the average curve in Fig. A.14 also exhibits a near-linear decreasing trend with all average values above 90% improvement. The range of successful vane operation is also $0.35^* < H/d_t < 0.65^*$.

Figure A.15 indicates that for long vanes operated at different angles to the main flow direction, the maximum average outer bank transverse bed slope occurs at $H/d_t = 0.50$, which corresponds to $(S_o)_{ave} = 0.073$. The range of successful vane operation is $0.35^* < H/d_t < 0.65^*$. Figure A.16 indicates that for long vanes operated at various streamwise spacings, the maximum average outer bank transverse bed slope occurs at $H/d_t = 0.57$, which corresponds to $(S_o)_{ave} = 0.093$. The corresponding range of successful vane operation is $0.35^* < H/d_t < 0.65^*$. Figures A.17 and A18 both show linear trends with negative slopes indicating that as vane height increases, the bed elevation decreases. In Fig. A.17, failure occurs at $H/d_t > 0.56$: in Fig. A.18, failure occurs at $H/d_t > 0.58$.

5.5.2 Effect of Vane Length

Figures B.1 - B.18 show the effects of vane length (L/b) on % Improvement, $(S_o)_{ave}$ and D_s/d_i. It can be seen that most trends tend to be near-horizontal, indicating that vane length has little effect on submerged vane performance.

5.5.2.1 Intermediate-height Vanes ($H/d_i = 0.35$)

The effects of vane length, L/b on % Improvement, $(S_o)_{ave}$ and D_s/d_i for intermediate-height vanes can be seen in Figs. B.1 - B.6. Both Figs. B.1 and B.2 show that vanes with H/d_i perform well across the entire range of lengths tested. They both indicate mild positive slopes indicating that as length increases, the improvement at the outer bank also improves marginally.

Figures B.3 - B.4 show the effects of L/b on $(S_o)_{ave}$ for vanes with $H/d_i = 0.35$. The trends are very similar to those exhibited in Figs. B.1 and B.2. Both trend lines are above the failure threshold ($(S_o)_{ave} = 0.05$) for this type of graph which again indicates that submerged vanes perform well across the entire range of lengths tested. Figure B.3 shows the trend that outer bank transverse bed slope increases with increasing vane length, while Fig. B.4 shows a near-horizontal slope. Figures B.5 and B.6 show the effects of L/b on D_s/d_i for vanes with $H/d_i = 0.35$. In both graphs, the trends have near-horizontal slopes with all values above the failure threshold ($D_s/d_i = -0.13$) which indicates that vane length has negligible effect on general scour depth for these vanes.

5.5.2.2 Intermediate-height Vanes ($H/d_i = 0.50$)

Figures B.7 - B.12 show the effects of vane length on % Improvement, $(S_o)_{ave}$, and D_s/d_i for vanes with $H/d_i = 0.50$. Figure B.7 shows a trend with a near-horizontal slope having all values above the failure threshold for this type of graph. Figure B.8 also has all values above the failure threshold; however, it exhibits a mild positive slope, indicating that as vane length increases, there is a marginal improvement in the outer bank scour condition. Figures B.9 and B.10 both show the effect of vane length on outer bank transverse bed slope. The trends in both graphs have near-horizontal slopes with all values above the threshold condition for failure. This indicates that vanes of all lengths tested perform well with respect to the outer bank transverse bed slope.

Table 5.3: Summary of submerged vane performance and design envelopes for the effect of vane height.

Criterion	Narrow Vanes (L/b = 0.16)		Intermediate-length Vanes (L/b = 0.33)		Long Vanes (L/b = 0.49)	
	Maximum Performance	**Range of Successful Operation**	**Maximum Performance**	**Range of Successful Operation**	**Maximum Performance**	**Range of Successful Operation**
#1	H/d_s = 0.47 % Improv. = 93%	0.31 < H/d_s < 0.59	H/d_s = 0.41 % Improv. = 95%	0.20 < H/d_s < 0.63	% Improv. > 90 %	0.35* < H/d_s < 0.65*
	H/d_s = 0.44 % Improv. = 97%	0.23 < H/d_s < 0.65	H/d_s = 0.39 % Improv. = 97%	0.16 < H/d_s < 0.62	% Improv. > 90%	0.35* < H/d_s < 0.65*
#2	H/d_s = 0.51 $(S_{ss})_{ave}$ = 0.070	0.32 < H/d_s < 0.65*	H/d_s = 0.43 $(S_{ss})_{ave}$ = 0.085	0.20 < H/d_s < 0.65*	H/d_s = 0.50 $(S_{ss})_{ave}$ = 0.073	0.35* < H/d_s < 0.65*
	H/d_s = 0.49 $(S_{ss})_{ave}$ = 0.090	0.24 < H/d_s < 0.65*	H/d_s = 0.41 $(S_{ss})_{ave}$ = 0.095	0.23 < H/d_s < 0.60	H/d_s = 0.57 $(S_{ss})_{ave}$ = 0.093	0.35* < H/d_s < 0.65*
#3	N/A	H/d_s < 0.47	N/A	H/d_s < 0.42	N/A	H/d_s < 0.56
	N/A	H/d_s < 0.52	N/A	H/d_s < 0.40	N/A	H/d_s < 0.58
Design Envelope		0.32 < H/d_s < 0.47		0.23 < H/d_s < 0.40		0.35 < H/d_s < 0.65

An interesting, but not surprising occurrence is observed in Figs. B.11 and B.12, which show the effect of vane length on the general scour depth for vanes with $H/d_t = 0.50$. Both graphs exhibit trends with near-horizontal slopes having all values slightly *below* the threshold for failure ($D_s/d_t = -0.13$). This is consistent with what was revealed in the examination of the effect of vane height on scour depth, which revealed that vanes typically fail when the height exceeds approximately $H/d_t = 0.50$ (see Table 5.3).

5.5.2.3 Tall Vanes ($H/d_t = 0.65$)

Figures B.13 - B.18 show the effect of vane length on % Improvement, $(S_o)_{ave}$ and D_s/d_t for tall vanes. The trends are all very similar to those for vanes with $H/d_t = 0.50$. Both Figs. B.13 and B.14 show trends with positive slopes which cross the failure threshold (% Improvement = 90%). It can be noted that in Fig. B.13, the vanes become ineffective when their length is $L/b < 0.40$, and in Fig. B.14, they become ineffective when their length is $L/b < 0.18$. The discrepancy between the two values arises because both slopes are considerably mild and straddle the failure threshold. Very minor experimental anomalies result in large variations in the length at which the vanes cross the failure threshold. Given these facts, coupled with the reality that many of the data are subject to experimental error, it will be assumed that tall vanes ($H/d_t = 0.65$) of all lengths fail in terms of % Improvement. This assumption, although drastic, is acceptable since it will result in more conservative design criteria.

Figures B.15 and B.16 show the effect of vane length on the average outer bank transverse bed slope for tall vanes. The positive slopes exhibited in both graphs are mild enough that they can be assumed to be near-horizontal. Therefore, vane length has no effect on $(S_o)_{ave}$ across the entire range of lengths tested for vanes with $H/d_t = 0.65$. This trend is consistent with that which was revealed in the analysis of vanes with $H/d_t = 0.50$.

Figures B.17 and B.18 show the effect of vane length on D_s/d_t for tall vanes. The trends are similar to those discussed in the analysis of vanes with $H/d_t = 0.50$. The trends in both graphs have near-horizontal slopes and have all values below the failure threshold. As was discussed, this is expected since previous analysis revealed that in terms of scour depth through the channel, vanes typically fail when $H/d_t > 0.50$.

5.5.3 Effect of Vane Angle

Tests were conducted on each vane at various angles to the main flow direction to determine the effect of α. The results are presented herein and summarized in Tables 5.4 and 5.5.

5.5.3.1 Narrow Vanes (*L/b* = 0.16)

For narrow vanes, Figs. C.1 - C.3 show the effects of submerged vane installation angle on % Improvement, $(S_o)_{ave}$, and D_r/d_r for narrow vanes. Figure C.1 shows that the maximum occurs at $\alpha = 3°$, which corresponds to 92% improvement. The range of successful operation is $-2° \le \alpha \le 8°$. Figure C.2 shows that the maximum occurs at $\alpha = 6°$, which corresponds to $(S_o)_{ave} = 0.06$. The range of successful operation is $1° \le \alpha \le 11.5°$. Figure C.3 shows that the submerged vanes are ineffective when $\alpha > 7.5°$. The graphs for narrow vanes show data more irregularly scattered than in the graphs for other vane lengths and heights. This indicates that α has a less consistent effect on narrow vane performance than on intermediate-length or long vane performance.

5.5.3.2 Intermediate-length Vanes (*L/b* = 0.33)

Figures C.4 - C.6 show the effects of vane angle on % Improvement, $(S_o)_{ave}$, and D_r/d_r for intermediate-length vanes. In Fig. C.4, the value of % Improvement tends to increase with increasing α. This curve indicates that submerged vanes with $L/b = 0.33$ fail at $\alpha < -1°$. A similar increasing trend can be seen in Fig. C.5. The value of $(S_o)_{ave}$ increases with increasing α and fails at $\alpha < 2°$. Figure C.6 shows the typical decreasing trend for D_r/d_r vs. α. It indicates that submerged vanes fail at $\alpha > 8°$.

5.5.3.3 Long Vanes (*L/b* = 0.49)

Figures C.7 - C.9 show the effects of vane angle on % Improvement, $(S_o)_{ave}$, and D_r/d_r for long vanes. Figure C.7 shows that the maximum occurs at $\alpha = 6.5°$, which corresponds to 96% improvement. The range of successful operation is $-4°^{*} \le \alpha \le 16°^{*}$. Figure C.8 shows that the maximum occurs at $\alpha = 10°$ and $(S_o)_{ave} = 0.08$. The range of successful operation is $-4°^{*} \le \alpha \le 16°^{*}$. Figure C.9 shows that long vanes fail at $\alpha > 10°$.

5.5.3.4 Intermediate-height Vanes (H/d_i = 0.35)

An interesting trend in % Improvement vs. α is revealed when Figs. C.10 (H/d_i = 0.35), C.13 (H/d_i = 0.50), and C.16 (H/d_i = 0.65) are examined in succession. In Fig. C.10, the trend is in the form of an 'increasing parabola', in Fig. C.13, the trend is in the form of a 'symmetrical parabola' and in Fig. C.16, the trend is in the form of a 'decreasing parabola'. This would indicate that shorter vanes require larger settings of α, whereas taller vanes require smaller settings of α to achieve the same results. Figure C.10 shows that the maximum occurs at α = 11°, which corresponds to 99.5% improvement. The range of successful operation is $-3° \leq \alpha \leq 16°^{*}$. A trend very similar to that indicated above can be seen when Figs. C.11 (H/d_i = 0.35), C.14 (H/d_i = 0.50), and C.17 (H/d_i = 0.65) are examined in succession. This reveals that shorter vanes require larger α settings to achieve the same result as larger vanes installed at smaller α. Figure C.11 shows that the maximum occurs at $\alpha > \alpha_{max}$ (where α_{max} = maximum angle tested), and that vanes with H/d_i = 0.35 fail at α < 0°. Figure C.12 shows that these vanes fail when α > 16°.

5.5.3.5 Intermediate-height Vanes (H/d_i = 0.50)

Figures C.13 - C.15 show the effects of submerged vane angle on % Improvement, $(S_o)_{ave}$, and D_v/d_i for intermediate-height vanes (H/d_i = 0.50). Figure C.13 shows that the maximum occurs at α = 4.5°, which corresponds to 98% improvement. The range of successful operation is $-4°^{*} \leq \alpha \leq 14°$. Figure C.14 shows that the maximum is at α = 6°, which corresponds to $(S_o)_{ave}$ = 0.09. The range of successful operation is $-4°^{*} \leq \alpha \leq 16°^{*}$. Figure C.15 shows that these vanes are ineffective when α > 3°.

5.5.3.6 Tall Vanes (H/d_i = 0.65)

Figures C.16 - C.18 show the effects of vane angle on % Improvement, $(S_o)_{ave}$, and D_v/d_i, for tall vanes. In Fig. C.16, the maximum occurs at α = -2.5°, which corresponds to 96% improvement. The range of successful operation is $-4°^{*} \leq \alpha \leq 7°$. Figure C.17 shows that the maximum occurs at α = 2°, which corresponds to $(S_o)_{ave}$ = 0.075. The range of successful operation is $-4°^{*} \leq \alpha \leq 11.5°$. Again, Fig. C.18 shows the typical decreasing linear trend in D_v/d_i vs. α. Theses vanes are ineffective when at α > 3°.

Table 5.4: Summary of submerged vane performance for the effect of vane angle (for various vane lengths).

Criterion	Narrow Vanes (L/b = 0.16)		Intermediate-length Vanes (L/b = 0.33)		Long Vanes (L/b = 0.49)	
	Maximum Performance	**Range of Successful Operation**	**Maximum Performance**	**Range of Successful Operation**	**Maximum Performance**	**Range of Successful Operation**
#1	$\alpha = 3°$ % Improv. = 92%	$-2° < \alpha < 8°$	N/A	$\alpha > -1°$	$\alpha = 6.5°$ % Improv. = 96%	$-4°° < \alpha < 16°°$
#2	$\alpha = 6°$ $(S_{ii})_{ave} = 0.060$	$1° < \alpha < 11.5°$	N/A	$\alpha > 2°$	$\alpha = 10°$ $(S_{ii})_{ave} = 0.080$	$-4°° < \alpha < 16°°$
#3	N/A	$\alpha < 7.5°$	N/A	$\alpha < 8°$	N/A	$\alpha < 10°$
Design Envelope		$1° < \alpha < 7.5°$		$2° < \alpha < 8°$		$-4° < \alpha < 10°$

5.5.4 Effect of Vane Streamwise Spacing

Tests were conducted on each vane at various values of streamwise spacing to determine the effect of δ_s/b. Variations in streamwise spacing tend to have fairly consistent effects on submerged vane performance. In general, the trends in the reduction of % Improvement and $(S_o)_{ave}$ with increase in vane streamwise spacing are both essentially linear. On the other hand, variation in vane streamwise spacing appears to have little effect on D_s/d_i. The results presented herein are summarized in Table 5.6.

5.5.4.1 Narrow Vanes (L/b = 0.16)

Figures D.1 - D.3 show the effects of streamwise spacing on % Improvement, $(S_o)_{ave}$, and D_s/d_i for narrow vanes. It can be seen in Fig. D.1 that the vanes fail the % Improvement criterion at $\delta_s/b > 1.25$, and in Fig. D.2, they do not fail the average outer bank transverse bed slope criterion for the range of streamwise spacings examined (although, by extrapolation, the graph indicates that failure would occur at approximately $\delta_s/b > 1.35$). Figure D.3 shows that the narrow vanes performed well, in terms of average scour depth, for all streamwise spacings examined.

5.5.4.2 Intermediate-length Vanes (L/b = 0.33)

Figures D.4 - D.6 show the effects of streamwise spacing on % Improvement, $(S_o)_{ave}$, and D_s/d_i for intermediate-height vanes. In Fig. D.4, it can be seen that the vanes fail the % Improvement criterion at $\delta_s/b > 1.15$, and in Fig. D.5, they can be seen to fail the average outer bank transverse bed slope criterion at approximately $\delta_s/b > 1.3$. Figure D.6 shows that intermediate-height vanes fail the scour depth criterion at $\delta_s/b = 0.9$.

5.5.4.3 Long Vanes (L/b = 0.49)

Figures D.7 - D.9 show the effects of streamwise spacing on % Improvement, $(S_o)_{ave}$ and D_s/d_i for long vanes. As can be seen in Figs. D.7 and D.8, the vanes do not fail either the % Improvement or outer bank transverse bed slope criteria over the entire range of δ_s/b tested. Although the trend in Fig. D.9 is nearly horizontal, it approaches the failure threshold for D_s/d_i at approximately $\delta_s/b = 1.30$.

Table 5.5: Summary of submerged vane performance for the effect of vane angle (for various vane heights).

Criterion	Intermediate-height Vanes ($H/d_i = 0.35$)		Intermediate-height Vanes ($H/d_i = 0.50$)		Tall Vanes ($H/d_i = 0.65$)	
	Maximum Performance	**Range of Successful Operation**	**Maximum Performance**	**Range of Successful Operation**	**Maximum Performance**	**Range of Successful Operation**
#1	$\alpha = 11°$ % Improv. = 99.5%	$-3° < \alpha < 16°$	$\alpha = 4.5°$ % Improv. = 98%	$-4°* < \alpha < 14°$	$\alpha = -2.5°$ % Improv. = 96%	$-4°* < \alpha < 7°$
#2	N/A	$0° < \alpha < 16°$	$\alpha = 6°$ $(S_{ii})_{ave} = 0.090$	$-4°* < \alpha < 16°*$	$\alpha = 2°$ $(S_{ii})_{ave} = 0.075$	$-4°* < \alpha < 11.5°$
#3	N/A	$\alpha < 16°*$	N/A	$\alpha < 3°$	N/A	$\alpha < 3°$
Design Envelope		$0° < \alpha < 16°$		$-4° < \alpha < 3°$		$-4° < \alpha < 3°$

5.5.4.4 Intermediate-height Vanes (H/d_t = 0.35)

Figures D.10 - D.12 show the effects of streamwise spacing on % Improvement, $(S_o)_{ave}$ and D_v/d_t for intermediate-height vanes. Again, Figs. D.10 and D.11 show that vanes with H/d_t perform well over the entire range of δ_v/b tested. Figure D.12 shows a linear, horizontal trend at $D_v/d_t \approx -0.10$, which is well above the failure threshold. Therefore, intermediate-height vanes perform well at any streamwise spacing below $\delta_v/b < 1.30$.

5.5.4.5 Intermediate-height Vanes (H/d_t = 0.50)

Figures D.13 - D.15 show the effects of streamwise spacing on % Improvement, $(S_o)_{ave}$ and D_v/d_t for intermediate-height vanes. Figure D.13 indicates that the intermediate-height vanes having $H/d_t = 0.50$ fail at $\delta_v/b = 1.30$. Figure D.14 shows that although $(S_o)_{ave}$ decreases with increasing δ_v/b, it is still above the failure threshold for all values of δ_v/b tested. In Fig. D.15, D_v/d_t decreases at a very mild slope with increasing δ_v/b. The near-horizontal slope is *below* the failure threshold for all values of δ_v/b. This phenomenon is similar to that described in Section 5.5.2.2 (i.e., vanes having $H/d_t > 0.50$ typically fail the average scour depth criterion).

5.5.4.6 Tall Vanes (H/d_t = 0.65)

Figures D.16 - D.18 show the effects of streamwise spacing on % Improvement, $(S_o)_{ave}$ and D_v/d_t for tall vanes. The trends seen share a marked similarity to those described in the preceding section. In fact, the only significant difference is that the % Improvement curve falls below the failure threshold at $\delta_v/b = 1.15$.

Table 5.6: Summary of submerged vane performance and design envelopes for vane streamwise spacing.

Criterion	Range of Successful Operation					
	Narrow Vanes ($L/b = 0.16$)	**Intermediate-length Vanes ($L/b = 0.33$)**	**Long Vanes ($L/b = 0.49$)**	**Intermediate-height Vanes ($H/d_i = 0.35$)**	**Intermediate-height Vanes ($H/d_i = 0.50$)**	**Tall Vanes ($H/d_i = 0.65$)**
#1	$\delta_v/b < 1.25$	$\delta_v/b < 1.15$	$\delta_v/b < 1.30^*$	$\delta_v/b < 1.30^*$	$\delta_v/b < 1.30$	$\delta_v/b < 1.15$
#2	$\delta_v/b < 1.30^*$	$\delta_v/b < 1.30$	$\delta_v/b < 1.30^*$	$\delta_v/b < 1.30^*$	$\delta_v/b < 1.30^*$	$\delta_v/b < 1.30^*$
#3	$\delta_v/b < 1.30^*$	$\delta_v/b < 0.90$	$\delta_v/b < 1.30$	$\delta_v/b < 1.30^*$	FAIL.	FAIL.
Design Envelope	$\delta_v/b < 1.25$	$\delta_v/b < 0.90$	$\delta_v/b < 1.30$	$\delta_v/b < 1.30$	FAIL.	FAIL.

5.5.5 Effect of Vane Transverse Spacing from Bank

A brief set of tests was conducted to examine the effect of vane transverse spacing from the outer bank on % Improvement, $(S_n)_{ave}$ and D_v/d_t. Four tests were conducted on submerged vanes with $H/d_t = 0.35$, $L/b = 0.33$, $\alpha = 4°$ and $\delta_v/b = 0.98$. The transverse spacings from the outer bank considered were δ_n/b = 0.13, 0.26, 0.36, and 0.49. The three graph types used in the analysis appear as Figs. 5.4 - 5.6.

Figure 5.4 reveals the trend that the outer bank scour depth condition worsens as the vanes are placed further from the outer bank. By applying the aforementioned failure criteria, the vanes fail when $\delta_n/b >$ 0.42. Figure 5.5 reveals the trend that the maximum $(S_n)_{ave}$ occurs at $\delta_n/b = 0.24$ (all tests in the main experimental program were performed at $\delta_n/b = 0.26$) and the range of successful vane operation is $0.16 < \delta_n/b < 0.34$. The scatter of data in Fig. 5.6 prevents any categorical conclusions to be drawn about the effect of δ_n/b: however, a linear trend was plotted through the points in an effort to gain some insight into its effect. Although the trend in Fig. 5.6 is weak, it shows that the average scour depth through the channel increases marginally with increasing space between the outer bank and the vanes: however, over the range of δ_n/b examined, the trend line does not fall below the failure threshold ($D_v/d_t = -0.13$). From this brief analysis of the effect of transverse vane spacing from the outer bank, it can be concluded that the optimum transverse distance from the outer bank is $\delta_n/b = 0.24$.

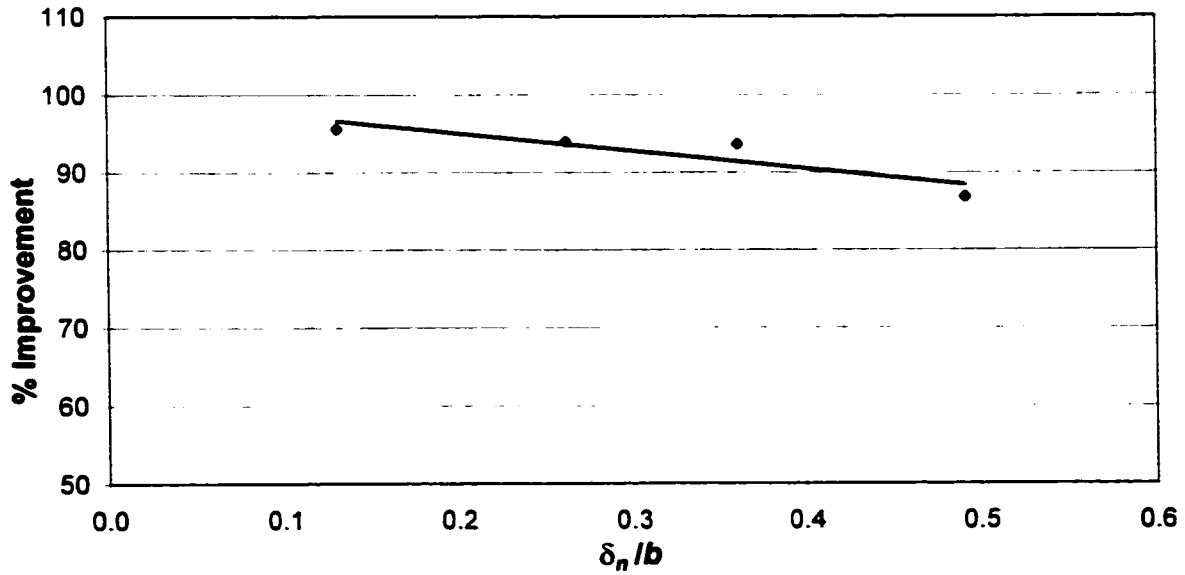

Figure 5.4: % Improvement vs. δ_n/b ($H/d_t = 0.35$, $L/b = 0.33$, $\alpha = 4°$, $\delta_v/b = 0.98$).

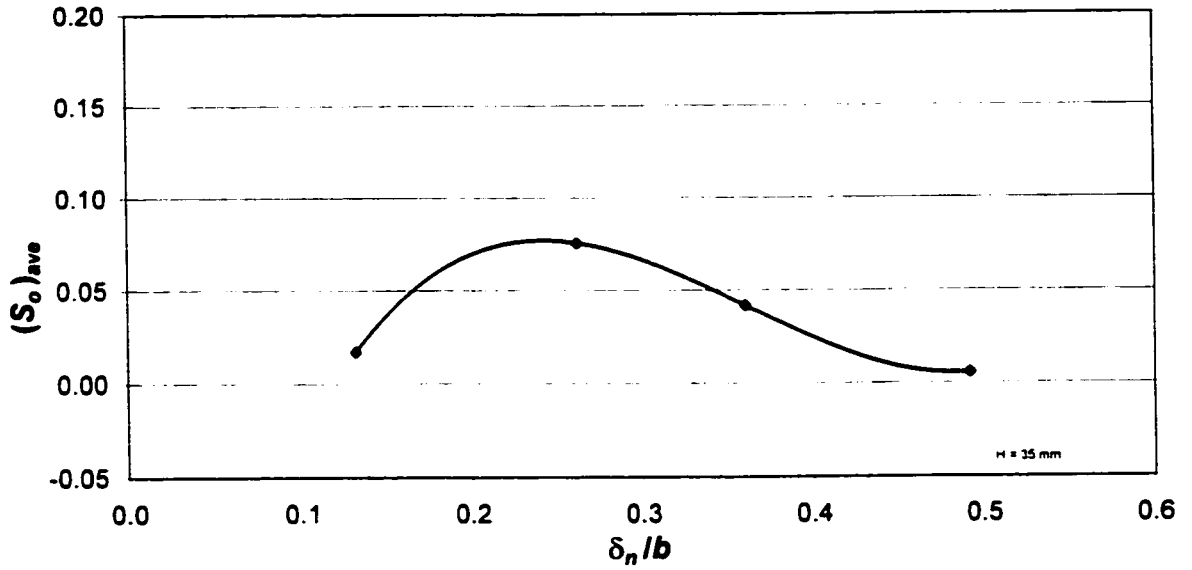

Figure 5.5: $(S_o)_{ave}$ vs. δ_n/b ($H/d_i = 0.35$, $L/b = 0.33$, $\alpha = 4°$, $\delta_s/b = 0.98$).

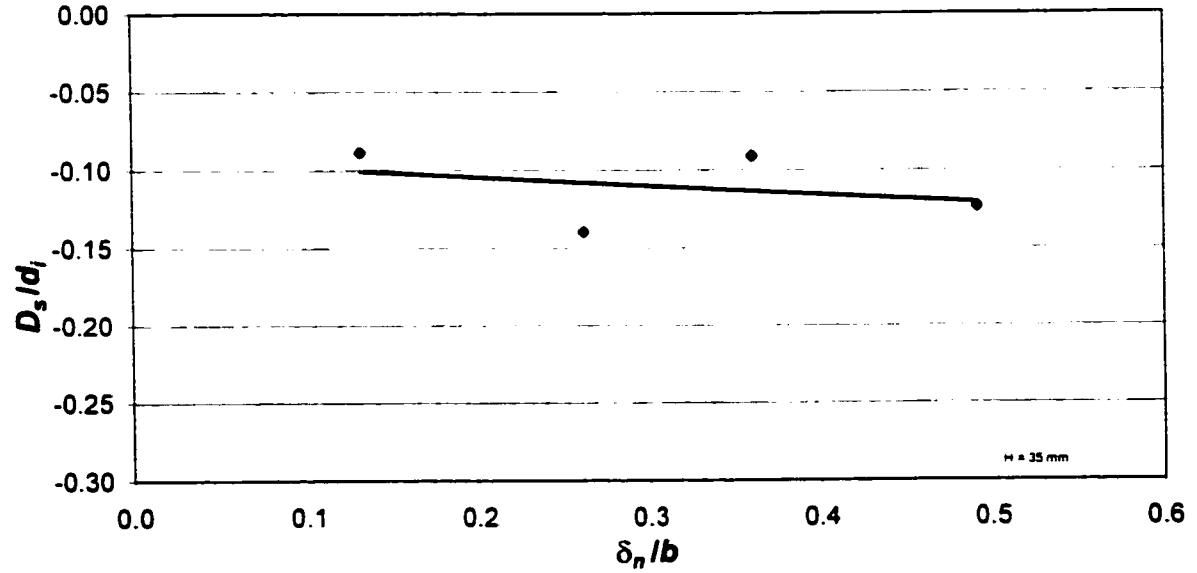

Figure 5.6: D_s/d_i vs. δ_n/b ($H/d_i = 0.35$, $L/b = 0.33$, $\alpha = 4°$, $\delta_s/b = 0.98$).

5.5.6 Local Scour

Local scour in the vicinity of the submerged vanes occurred in some tests. Not surprising, it was usually associated with vanes set at very large angles to the main flow direction, very tall and narrow or tall and long vanes, or vanes spaced excessively far apart. Furthermore, it was usually associated with the second vane (near the upstream end of the bend). Local scour, once initiated, tended to result in flow separation at the bed and contributed greatly to further scour hole development, thereby exacerbating the already-adverse situation. Since this scour hole would typically occur early on in the channel, its effects would persist throughout the entire test section, thereby reducing the effectiveness of the submerged vanes. Unfortunately, the presence of local scour is not revealed in the three main graph types discussed above. Therefore, the reader is directed toward Appendix F, wherein are presented topographic plots of every test conducted. These topographic plots show the profiles of the bed in the test section for each test, and hence, reveal areas of local scour. Each topographic plot shows solid and dashed lines. The solid lines are for zones of scour (i.e., $d_b/d_i > 1.0$) and the dashed lines are for zones of deposition (i.e., $d_b/d_i \leq 1.0$). The interval between the contours is $\Delta d = 0.05 d_i$, which corresponds to 5 mm in the test section. Submerged vane locations are also shown in each topographic plot. While the vanes are shown to scale in terms of length and streamwise spacing, they are not shown to scale in terms of vane angle (the actual dimensions, including α, are given in each figure caption). Illustrative samples are shown below.

Figure 5.7 shows an example of local scour associated with large vane angle ($\alpha = 12°$) to the main flow direction. It can be seen that the local scour is primarily associated with the second vane, and its effects persist throughout the remainder of the test section. Figure 5.8 shows an example of local scour associated with tall, narrow vanes ($H/d_i = 0.65$, $L/b = 0.16$), while Fig. 5.9 shows an example of local scour associated with tall, long vanes ($H/d_i = 0.65$, $L/b = 0.49$). Generally, the local scour that resulted for narrow vanes occurs halfway through the curved portion of the test section. Figure 5.10 shows an example of local scour associated with large streamwise vane spacing ($\delta_s/b = 0.98$). The local scour is clearly seen in the immediate vicinity of the second vane. Finally, Fig. 5.11 shows the results of a combination of tall, narrow vanes at large angle to the main flow direction ($H/d_i = 0.65$, $L/b = 0.16$, $\alpha = 16°$). The detrimental consequences of a poorly designed vane configuration are clearly seen in this figure.

A careful examination of the figures in Appendix F will reveal several failure criteria based on local scour avoidance. From a review of the topographic plots of narrow vanes ($L/b = 0.16$), it can be seen that most

configurations with $H/d_t \geq 0.50$ experience significant local scour (Figs. F.8d - F.9d). Likewise, from an examination of the topographic plots of long vanes ($L/b = 0.49$), it can be seen that most configurations with $H/d_t \geq 0.50$ experience significant local scour (Figs. F.24b - F.25d). Many of the topographic plots showing the results for tests run with large streamwise spacings ($\delta_t/b \geq 0.98$) show appreciable local scour (Figs. F.9d, F.11d, F.15d, F.17d-g, F.19d, F.23d, and F.25d). There does not seem to be any significant local scour trend for submerged vanes with $\delta_t/b < 0.98$. This indicates that local scour is a threat when $\delta_t/b \geq 1.0$. Local scour is also associated with large vane angles to the main flow direction (Figs. F.2e, F.4f, F.6f, F.8e-d, F.10e-f, F.16f, F.18f-h, F.20e, F.24e-f, and F.26e-f); therefore, to prevent such negative effects, vane configurations should be designed with $\alpha < 10°$.

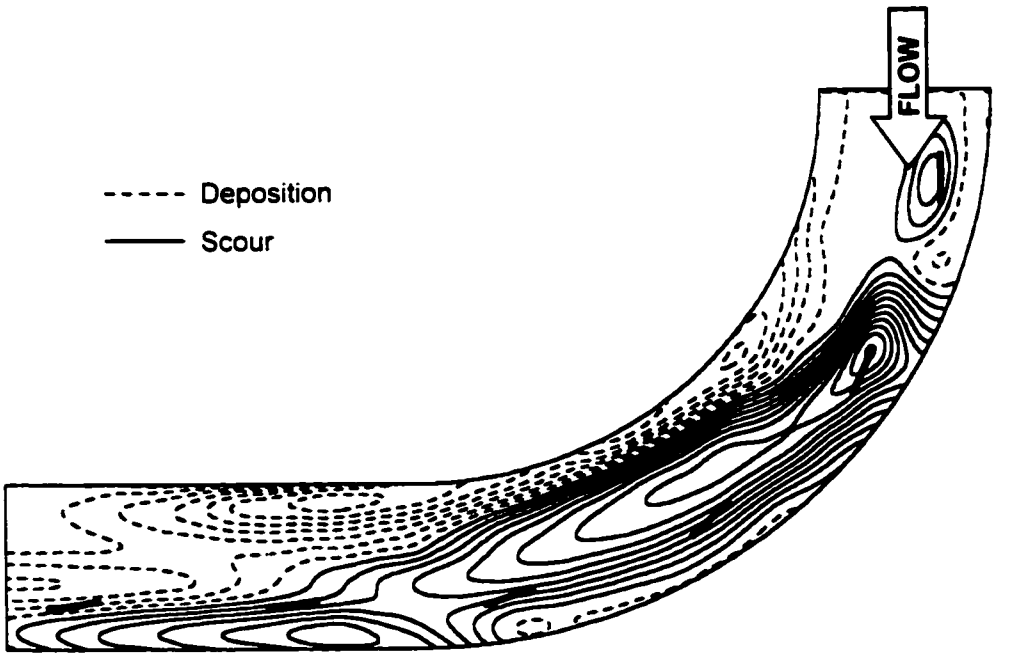

Figure 5.7: Example of local scour associated with large vane angle (H/d_t = 0.65, L/b = 0.33, α = 12°, δ_t/b = 0.98).

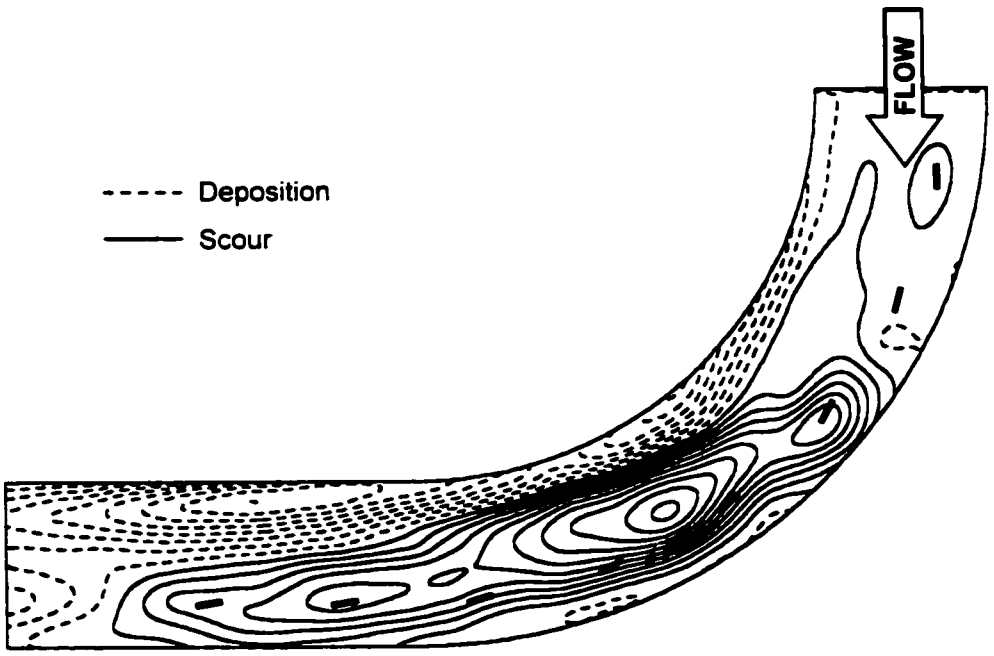

Figure 5.8: Example of local scour associated with tall, narrow vanes (H/d_t = 0.65, L/b = 0.16, α = 8°, δ_t/b = 0.66).

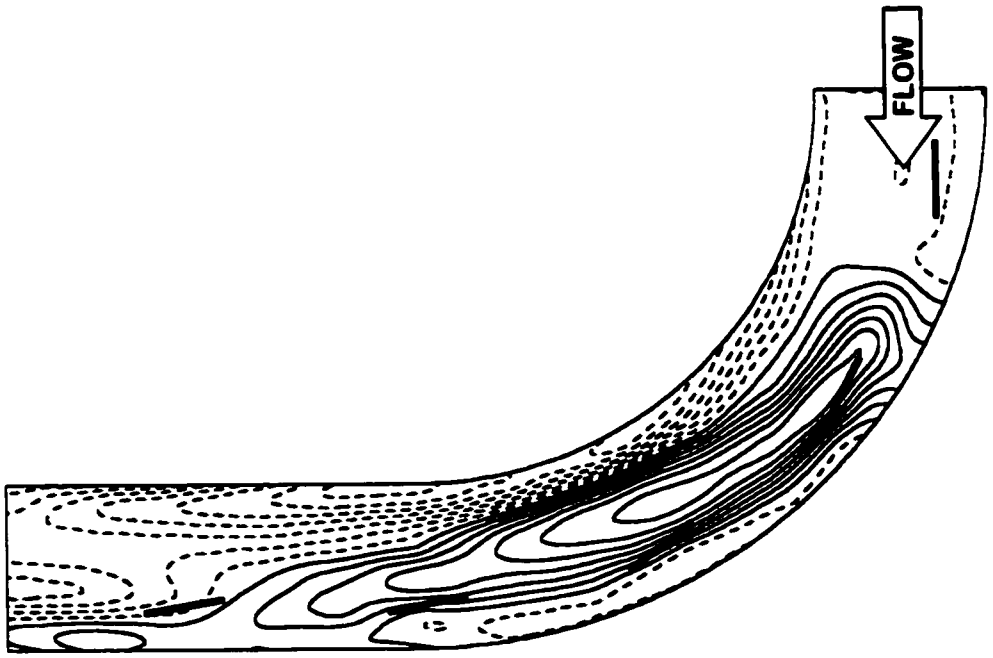

Figure 5.9: Example of local scour associated with tall, long vanes (H/d_t = 0.65, L/b = 0.49, α = 8°, δ_t/b = 0.98).

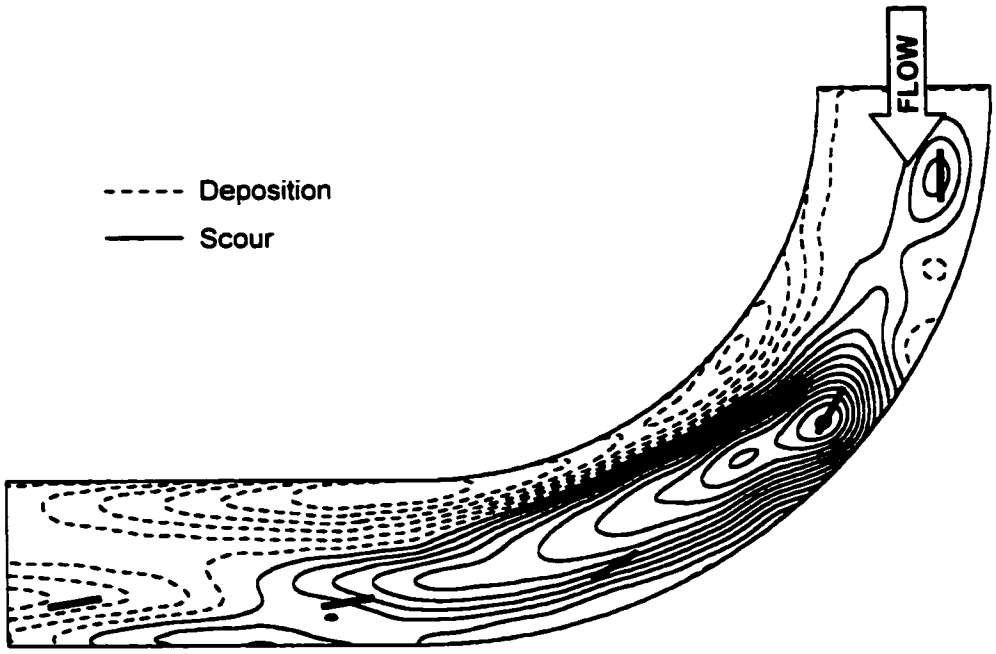

Figure 5.10: Example of local scour associated with large streamwise spacing ($H/d_t = 0.50$, $L/b = 0.33$, $\alpha = 8°$, $\delta_t/b = 1.31$).

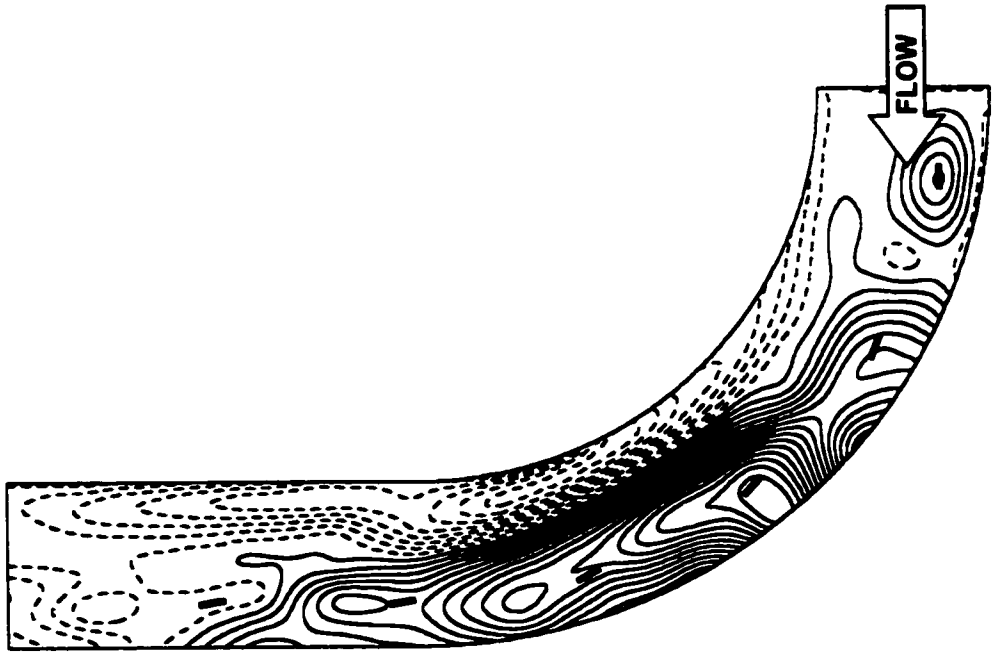

Figure 5.11: Example of local scour associated with tall, narrow vanes at large angle ($H/d_t = 0.65$, $L/b = 0.16$, $\alpha = 16°$, $\delta_t/b = 0.98$).

5.5.7 Aspect Ratio

Odgaard and Spoljaric (1989) state that vane angle (α) and aspect ratio (ψ) are the primary factors in the development of the vane 'lift' coefficient, c_L. The lift coefficient is related to the effectiveness of submerged vanes. Figures 5.12 through 5.14 show the effect of ψ on % Improvement, $(S_o)_{ave}$, and D_v/d_n, respectively. All three figures are similar in that they do not exhibit any pronounced trends. Therefore, it seems that in the current study the aspect ratio has little bearing on vane performance. The inability of ψ to affect vane performance would suggest that α is the predominant factor affecting c_L.

A feature not evident in Figs. 5.12 through 5.14 is the generation of local scour, which was discussed in the preceding section. As stated beforehand, local scour is associated with very tall and narrow vanes (i.e., large ψ). Therefore, in the design process large aspect ratio vanes should be avoided.

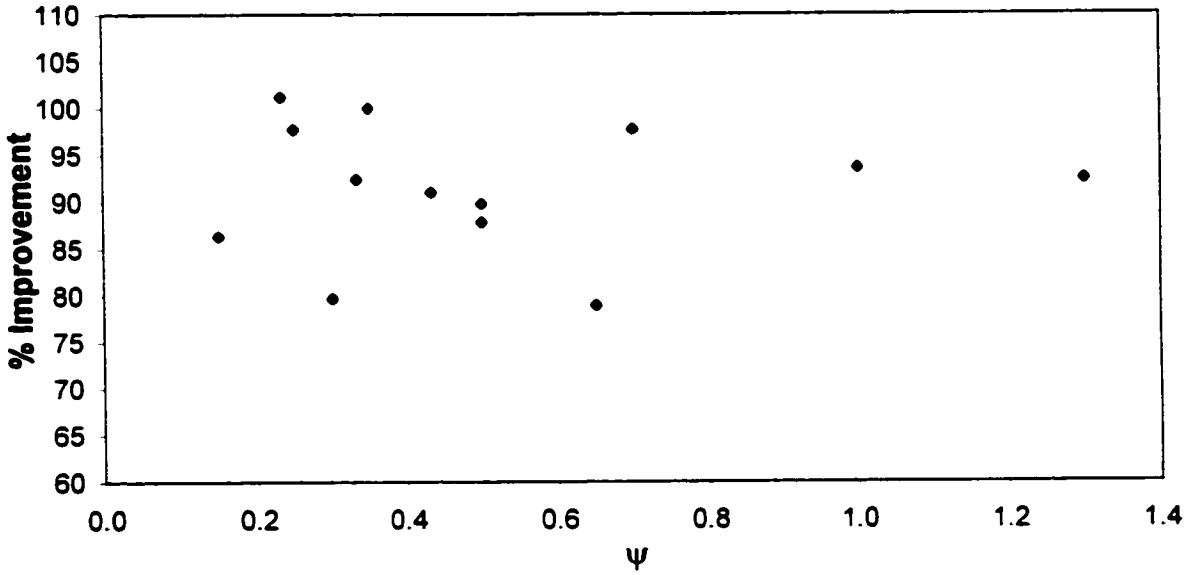

Figure 5.12: % Improvement vs. ψ ($\alpha = 8°$, $\delta_v/b = 0.98$).

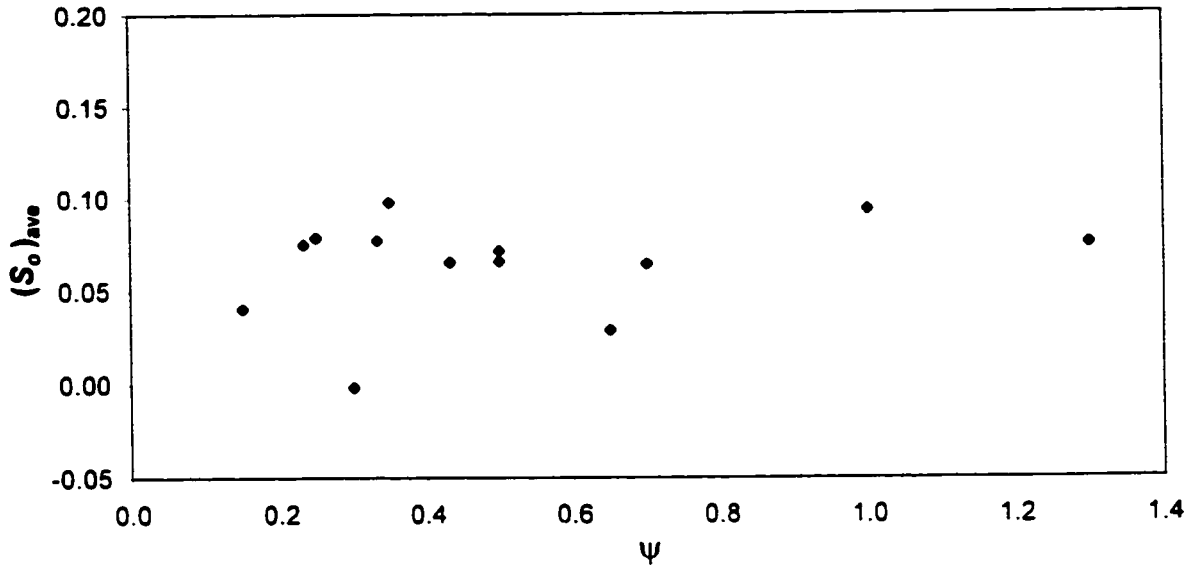

Figure 5.13: $(S_o)_{ave}$ vs. ψ (α = 8°, δ_f/b = 0.98).

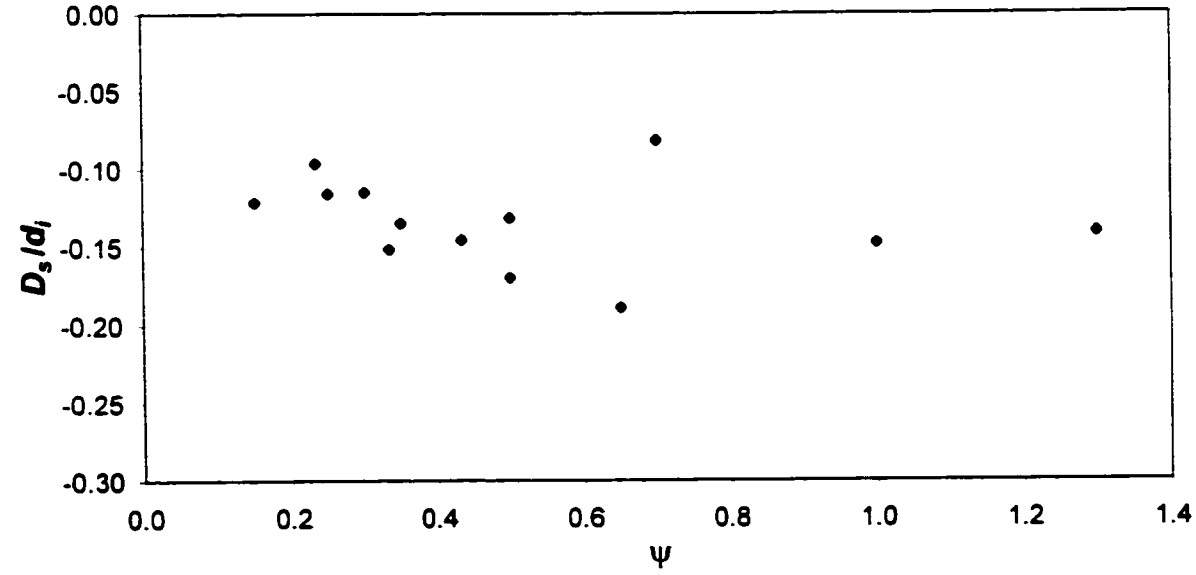

Figure 5.14: D_f/d_i vs. ψ (α = 8°, δ_f/b = 0.98).

5.6 Effect of Bend Angle

The tests conducted in the 135° bend were not intended to lead to a comprehensive set of design criteria, but rather, to lead to general conclusions about the effect of bend angle. Thus, a limited series of tests was performed in a 135° bend test section, and the results were graphically compared to the results obtained for the 90° bend. Appendix E contains the results for tests run in the 135° bend plotted on corresponding graphs showing results for the 90° bend. Most data for the 135° bend fall *below* the average of the corresponding data for the 90° bend. Appendix F.2 contains the topographic plots of all tests performed in the 135° bend.

5.6.1 Outer Bank Scour Depth (% Improvement)

Figures E.1 - E.10 show the results for the 135° bend plotted on graphs of % Improvement vs. H/d_t (Figs. E.1, E.2), L/b (Figs. E.3 - E.5) and α (Figs. E.6 - E.10). It is notable that almost all data for the 135° bend fall below the curve plotted through the average of the data for the 90° bend. The only exception is when the streamwise vane spacing is $\delta_s/b = 0.66$ (Figs. E2, E.3, E.5 - E.8). This indicates that, unlike in the 90° bend, there is a marked effect of streamwise spacing associated with the larger bend angle.

5.6.2 Outer Bank Transverse Bed Slope ($(S_o)_{ave}$)

Figures E.11 - E.21 show the results for the 135° bend plotted on graphs of $(S_o)_{ave}$ vs. H/d_t (Figs. E.11, E.12), L/b (Figs. E.13 - E.15) and α (Figs. E.16 - E.21). Similar to what is observed in the previous graphs of this kind, many data for the 135° bend fall below the curve plotted through the average of the data for the 90° bend; however, the trend is not as significant (i.e., the effects of vane height, length and angle on the transverse bed slope in the greater bend angle are not as significant). For instance, in Fig. E.11, three of six of the data are below the curve through the average of the data for the 90° bend; however, those that are above are only marginally higher, while those that are below are significantly lower. In Figs. E.13 and E.19, there are actually more data above the average curve than below. Figures E.12 - E.18, E.20 and E.21 show that the majority of 135° bend data are below the average curve for the 90° bend.

5.6.3 Scour Depth Through Channel (D_s/d_i)

Figures E.22 - E.31 show the results for the 135° bend plotted on graphs of D_s/d_i vs. H/d_i (Figs. E.22, E.23), L/b (Figs. E.24 - E.26) and α (Figs. E.27 - E.31). All data for the 135° bend fall below the curve through the average of the data for the 90° bend. This clearly indicates that the average scour depth through the 135° bend is greater than that for the 90° bend. A closer vane streamwise spacing (δ_s/b = 0.66) reduces the average scour depth (Figs. E.22 - E.24, E.26 - E.31); however, it is incapable of reducing it to a situation comparable to that for the 90° bend.

5.7 Design Considerations

Design practicality is based upon the use of sound judgement to achieve a balance between uneconomical over-design and unstable under-design. The over-designed submerged vane configuration would be characterized by excessively tall and long vanes spaced extremely close together. This situation would essentially be equivalent to a solid vertical wall adjacent to and protecting the channels bend's outer bank. One might assume that such a system, though over-designed, would work well, however, the opposite is true. The vanes would be so large that they would begin to act less as submerged vanes, and more like large roughness elements, which would simply reduce longitudinal velocities in the vicinity of the bank. The impact would be a decrease in effective flow area through the channel bend and hence an increase in corresponding mean flow velocity therein. The latter effect could have negative long-term consequences on the equilibrium of the entire channel reach.

The under-designed submerged vane configuration would be characterized by very narrow vanes spaced far apart. Such a design would be based on the above-stated conclusions that the effects of vane length and streamwise spacing are marginal compared to the effects of vane height and angle. However, as noted earlier, these types of vane configurations lead to excessive local scour. Therefore, care must be taken to ensure that a particular design is compatible with all of the aforementioned vane failure criteria.

Given the complexity of fluid and sediment transport phenomena in the vicinity of submerged vanes, and the discrepancies which arise between model and prototype systems, a precise set of exhaustive design guidelines can not be given based solely on this research. Rather, it is expected that the study results will give the reader a better understanding of the key parameters that influence (or do not influence) submerged vane performance in strongly curved narrow channels. Prior to any submerged vane design,

it would be prudent to examine the problem in a properly-scaled model of the river bend section of interest.

The key parameters in our model section were vane height (H/d_i), vane angle (α) and distance from the outer bank to the (vertical) centreline of the vane (δ_n/b). The experimental evidence suggests that vane length (L/b) and streamwise vane spacing (δ_s/b) had only marginal effects on submerged vane performance.

Based on this research, the optimum design configuration for the 90° bend was based on the following rationale: optimum vane length is determined by local scour considerations, since very narrow ($L/b \leq 0.16$) and very long ($L/b \geq 0.49$) vanes are both associated with local scour. Therefore intermediate-length vanes ($L/b = 0.33$) may be selected. From Table 5.3, the design envelope for these vanes is $0.23 < H/d_i < 0.40$. Based on criteria #1 and #2 (see Table 5.3), the maximum performance is achieved at $H/d_i \approx 0.40$; however, this value is too close to the upper limit of the design envelope. Therefore, the optimum vane height should be between the middle and upper limit of the envelope. Based on good judgement, $H/d_i \approx 0.35$ is selected. The vane angle is based on the design envelopes given in Tables 5.4 and 5.5. These design envelopes are $2° < \alpha < 8°$ and $-4° < \alpha < 3°$, respectively. When $\alpha = 2°$, both design envelopes are satisfied. Table 5.6 indicates that for intermediate-length vanes, the streamwise spacing should be $\delta_s/b < 0.90$. Again, based on good judgement, $\delta_s/b = 0.70$ is selected. The optimum distance from the outer bank to the centre of the vane is $\delta_n/b = 0.24$. The optimum design configuration is summarized in Table 5.7 and a topographic plot of vanes operation near the optimal configuration is shown in Fig. 5.15.

Table 5.7: Summary of optimum design configuration for test conditions (90° bend).

Parameter	Optimum Design Value
Length, L/b	0.33
Height, H/d_i	0.35
Angle to main flow direction, α	2°
Streamwise spacing, δ_s/b	0.70
Distance from outer bank to centre of vane, δ_n/b	0.24

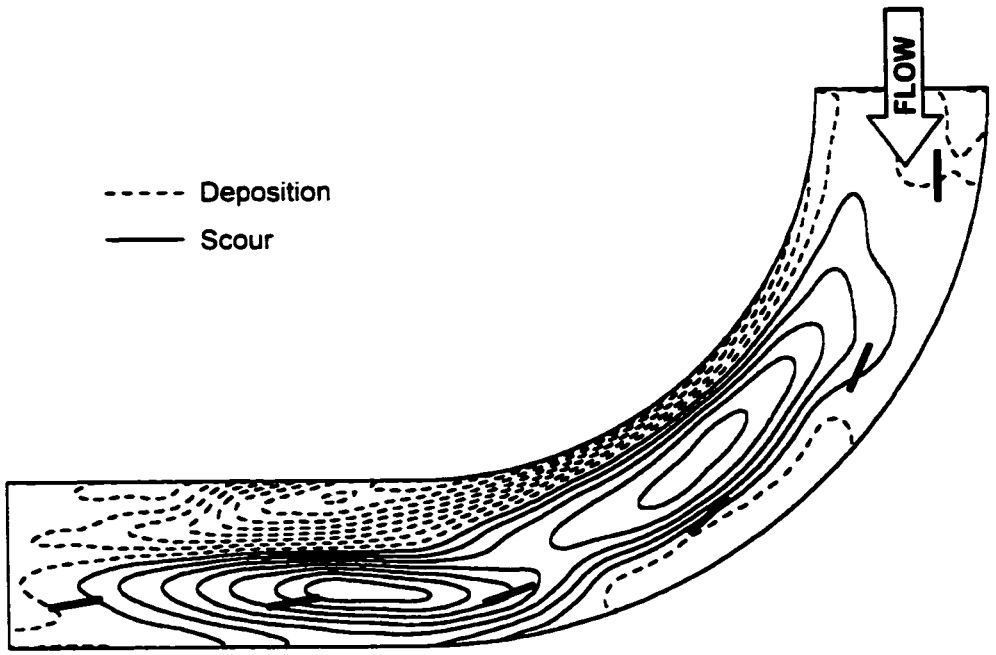

Figure 5.15: Example of vanes operating at the near-optimum configuration ($Hid_i = 0.35$, $L/b = 0.33$, $\alpha = 4°$, $\delta_v/b = 0.98$).

CHAPTER SIX

SUMMARY, CONCLUSIONS AND RESEARCH NEEDS

6.1 Summary

Although submerged vanes have been used in the past for river-bank stabilization (Potapov and Pyshkin, 1947; Potapov, 1950, 1951; Chabert et al., 1961; Jansen et al., 1979), very little had been documented on their analysis, design and performance until recently. At the time of this writing, most of the work on submerged vanes has been performed at the University of Iowa Institute of Hydraulic Research where two methods have been developed (Odgaard and Wang, 1991b, 1990; Odgaard and DeWitt, 1989; Odgaard and Spoljaric, 1989, 1986a, 1986b; Odgaard and Mosconi, 1987; Odgaard and Lee, 1984; and Odgaard and Kennedy, 1983). The first method is based on the premise that submerged vanes may be used to reduce the transverse bed slope in a channel bend (Odgaard and Lee, 1984). The second method is based on the premise that submerged vanes generate a helicoidal vortex which may be used to reduce the transverse bed shear stress (Odgaard and Wang, 1991a). Although both methods are obviously related in theory, they differ considerably in their development. The first method makes the assumption that the transverse bed slope is linear, while the second method makes the assumption that the channel is hydraulically wide. In our conditions, the transverse bed slope is not linear, nor is the channel wide; therefore, neither of the aforementioned design methods is directly applicable in this work.

There is a marked similarity in curvature ratios (r/b) among rivers of varying sizes and geographical locations. In a study conducted on fifty different rivers, two-thirds of the r/b were in the range 1.5 to 4.3, with a mean of 3.1 (Leopold and Wolman, 1964). Furthermore, the maximum bend migration rate occurs at $r/b \approx 3.0$ and declines rapidly on either side of this value (Biedenharn et al., 1989; Begin, 1986, 1981, Hickin and Nanson, 1975, 1986). Only two out of six of the experimental channels used in the earlier research at the University of Iowa incorporated bend sections along their lengths. These had $r/b = 5.37$ and 6.75. Our channel has $r/b = 2.95$, which is not only more representative of natural river conditions, but is also representative of bends with rapid migration rates.

Two bend angles were examined in this study. Most of the testing program was conducted in a 90° bend, and a limited number of tests were conducted in a 135° bend. Both bends shared the same inner and outer radii, namely r_i = 0.748 m, and r_o = 1.053 m, respectively. The corresponding radius to the channel centreline was r_c = 0.901 m, which results in the aforementioned curvature ratio r_c/b = 2.95.

Each test was run for 8 hr. After approximately 10 hr, some tests experienced adverse secondary flow effects which greatly decreased submerged vane effectiveness. It is not believed that this will translate to field conditions since our channel models a worst case situation for many reasons. Tests were performed for 'clear-water' conditions ($\tau_0 = \tau_{cr}$); therefore, sediment was not reintroduced to replenish that which was removed from the test section during a test. In nature, sediment which is delivered from upstream enters a bend, is made available for deposition and reduces the net loss of sediment through the vane field. Also, the sand used in the test section was uniform, thus armouring (which has the effect of stabilizing the channel and reducing scour depths) did not occur. Furthermore, the channel geometry allowed for intensified outer bank scour conditions because: (*i*) its narrow cross-section more closely approximated a square in which the secondary current could develop with greater efficiency than in a wide channel, and (*ii*) the curvature ratio, r_c/b, is approximately equal to that which is associated with high rates of lateral bend migration. Finally, it may be proven by field tests that submerged vanes in these conditions are more suited to retarding lateral bank migration rather than preventing it completely.

The two design methods discussed in Chapter five (Odgaard and Lee, 1984; Odgaard and Wang, 1991a) are inapplicable to our conditions since one makes the assumption that the channel transverse bed slope is linear, and the other makes the assumption that the channel is hydraulically wide. Therefore, an empirical method was developed for the conditions examined in this study. The new method is based on applying certain failure criteria to the experimental results to determine zones of optimum performance and design envelopes. The failure criteria are based on the vanes' ability to (*i*) reduce scour depth along the outer bank, (*ii*) reduce transverse bed slope at the outer bank, and (*iii*) reduce general erosion throughout the test section. Two further criteria were developed based on visual observation of the tests performed. These dealt with prevention of local scour in the vicinity of submerged vanes and design practicality (i.e., vane size and spacing). The application of these criteria is described in Chapter five.

6.2 Conclusions

Submerged vanes tend to perform well under a broad range of operating conditions. When they operate properly, they tend to shift the channel thalweg inward such that the outer bank experiences a reduction in scour depth, and a positive transverse bed slope is established. Our parametric study allowed isolated examination of each property tested (i.e., vane height, length, angle, streamwise spacing, bend angle, etc.). Upon examination of each parameter individually, a set of optimum design specifications may be given for the test conditions in the 90° bend. The optimum submerged vane configuration incorporates vanes with height and length of $H/d_i = 0.33$ and $L/b = 0.35$, respectively. These vanes should be spaced at a distance of $\delta_n/b = 0.24$ from the outer bank, be installed at $\alpha = 2°$ to the main flow direction, and have a streamwise spacing of $\delta_s/b = 0.70$. The trends exhibited by each parameter examined on vane performance are summarized below.

For the 90° bend, vane height, H/d_i, has a significant effect on submerged vane performance. The vanes tend to operate optimally when $0.25 < H/d_i < 0.50$. Tall vanes tend to perform well in terms of protecting the outer bank, and as well are associated with greater thalweg deepening throughout the test section. Also, tall vanes are typically associated with local scour and channel bed instability. Lastly, they are less economical because of increased material costs.

For the range examined in this study ($0.16 < L/b < 0.49$), vane length L/b seems to have marginal effect on their ability to protect the outer bank. However, vane length does influence the local scouring process. Very short ($L/b \leq 0.16$) and very long ($L/b \geq 0.49$) vanes result in local scouring in their vicinity. Vane angle has a significant effect on submerged vane performance; however, for narrow vanes ($L/b = 0.16$), the data are more scattered. As vane height increases, the required vane angle decreases to achieve the same degree of performance. Generally speaking, submerged vanes perform optimally when $0° \leq \alpha \leq 10°$. At larger angles, they tend to induce considerable scour hole development in the immediate vicinity of the vanes.

The results indicate that vane streamwise spacing, δ_s/b, has an effect, though marginal, on outer bank protection for the range examined ($0.33 \leq \delta_s/b \leq 1.31$). Based on % Improvement, $(S_o)_{ave}$, and D_s/d_i, all vane sizes (except intermediate-length vanes) performed well for all vane streamwise spacings tested. Only the results for intermediate-height vanes fell below the failure thresholds; however, this occurred

when $\delta_s/b > 0.90$. Despite this, vane streamwise spacing does have an impact on local scour development. Many vane installation configurations with $\delta_s/b \geq 0.98$ resulted in local scour hole formation.

Vane transverse spacing from the outer bank, δ_n/b, has a noticeable effect on % Improvement and $(S_o)_{ave}$. As δ_n/b increases, % Improvement decreases linearly (and fails when $\delta_n/b > 0.42$), and $(S_o)_{ave}$ reaches a maximum before it decreases. The range of operation for outer bank transverse bed slope is $0.16 < \delta_n/b < 0.34$, and the maximum occurs at $(S_o)_{ave}$ which corresponds with $\delta_n/b = 0.24$. There seems to be no effect of δ_n/b on D_s/d_t.

Generally speaking, the results for most vane configurations in the 135° bend fall below the results for the same configuration in the 90° bend. The exception is for those configurations with $\delta_s/b \leq 0.66$. This indicates that, unlike in the 90° bend, δ_s/b does have an influence on submerged vane performance for the greater bend angle. In fact, the closer spacing is required to achieve results equivalent to those from the 90° bend. The results indicate that vane local scour is only associated with very tall and narrow ($H/d_t \geq 0.50$ and $L/b \leq 0.16$) or tall and long vanes ($H/d_t \geq 0.50$ and $L/b \geq 0.49$), vanes set at large angles ($\alpha \geq 10°$), and vanes set at large streamwise spacings ($\delta_s/b \geq 0.98$). Scour usually occurred at the second vane (near the upstream end of the bend) and its effects persisted throughout the test section. Once initiated, local scour would cause flow separation at the bed and further aggravate the already-adverse situation.

The aspect ratio, ψ, seems to have no bearing on submerged vane performance. This is interesting since Odgaard and Spoljaric (1989) state that α and ψ are the primary factors in the development of the lift coefficient, c_L, which is a measure of the effectiveness of submerged vanes. The inability of ψ to affect vane performance suggests that in our 'narrow-channel' conditions, α is the dominant factor affecting c_L.

6.3 Research Needs

The current research is the first laboratory study of applying submerged vanes in strongly-curved narrow channels. The results presented herein describe the effects of several key parameters relating to submerged vane performance in such channels. To this end, a parametric study of these important parameters was performed. While the starting parameters were the same as those based on those reported in earlier works on this topic, our results indicate that some of those parameters found to be important under 'wide-channel' conditions, were not as important in the case of 'narrow-channels'. These were: vane length, vane streamwise spacing (in the 90° bend), and vane aspect ratio. Had this been known at

the outset, less effort would have been invested in their examination, and consequently more would have been invested in examining the more important parameters. The result was a less focused testing program that strove to determine general trends for several parameters, rather than one that strove to provide detailed submerged vane design relationships. Therefore, future research should address this. With greater understanding of the key parameters in this context, future research should concentrate on the impacts of vane height, vane angle, bend angle, and vane transverse spacing from outer bank.

Another disadvantage of our extensive testing program was that time limitations prevented most tests from being duplicated. It is not unlikely that some tests provided data outliers. Test duplication would have smoothed the data and given more accurate results. A more focused testing program could be comprised of additional tests on fewer parameters, therefore, more (or all) tests could be duplicated, and thus provide less scatter than sometimes encountered herein. Most of the tests in this study were performed in a 90° bend, and only a limited number of tests were performed in the 135° bend. Future research should address this limitation by extending the experimentation in the latter. Presumably, if vanes perform adequately in the channel with the greater bend angle, then they will also perform well in the channel with the lesser bend angle.

An interesting idea, which has yet to be examined, is the use of variably spaced and/or sized vanes. For instance, it may be that smaller vanes, vanes spaced further apart, or vanes at a smaller angle may be used in the upstream portion of the channel bend, and that larger vanes, vanes spaced closer or vanes at a larger angle may be used in the downstream portion of the bend. This may result in many benefits. It may be that local scour at the first and second vane would be reduced if these were smaller or installed at smaller angles. Also, the design would be more economical if smaller vanes could be used in one portion of the channel bend.

Lastly, the results from the current study should be used in performing a (prototype) study of submerged vanes in a natural river whose characteristics are similar to those examined in this laboratory study. This would provide a better understanding the model-prototype relationships for submerged vane performance in 'narrow-channel' conditions. Furthermore, this would complement the data acquired by the research community at large since only a limited number of field tests have been performed.

REFERENCES

Begin, Z. B., (1981), "Stream Curvature and Bank Erosion: a Model Based on the Momentum Equation", *Journal of Geology*, Vol. 89, pp. 497-504

Begin, Z. B., (1986), "Curvature Ratio and Rate of River Bend Migration - Update", *Journal of Hydraulic Engineering*, ASCE, Vol. 112, No. 10, October, pp. 904-908

Bertin, J. J., and Smith, M. L., (1979), *Aerodynamics for Engineers*, Prentice-Hall, Inc., Englewood Cliffs, N.J.

Biedenharn, D. S., Combs, P. G., Hill, G. J., Pinkard, C. F., Jr., Pinkston, C. B., (1989), "Relationship Between Channel Migration and Radius of Curvature on the red River", Proceedings of the International Symposium on Sediment Transport Modelling, New Orleans, LA, pp. 536-541

Chabert, J., Remillieux, M., and Spitz, I., (1961), "Application de la Circulation Transversale a la Correction des Riviers et a la Protection des Prises d'Eau.", *Proceedings of the Ninth Convention, International Association for Hydraulic Research*, Dubrovnik, Yugoslavia, pp. 1216-1223 (in French)

Chang, H. H., (1988), *Fluvial Processes in River Engineering*, John Wiley & Sons, Inc., New York, N.Y.

Chow, V. T, (1959), *Open-channel Hydraulics*, McGraw-Hill, Inc., New York, N.Y.

Currie, I. G., (1974), *Fundamental Mechanics of Fluids*, McGraw-Hill, Inc., New York, N.Y.

Davinroy, R. D., (1990), "Bendway Weirs, A New Structural Solution to Navigation Problems Experienced on the Mississippi River", *Permanent International Association of Navigation Congresses*, Bulletin 69, Osaka, Japan, pp. 5-19

Derrick, D. L., (1997), "Bendway Weirs Redirect River Flow to Protect Highway Bridge Abutments", U.S. Army Corps of Engineers Waterways Experiment Station, Vicksburg, M.S.

Falcon, M. A., (1979), "Analysis of Flow in Alluvial Channel Bends", thesis presented to the University of Iowa, Iowa City, Iowa, in partial fulfillment of the requirements for the degree of Doctor of Philosophy

Garcia, M. H., (1999), "Sedimentation and Erosion Hydraulics", in *Hydraulic Design Handbook*, L. W. Mays, ed., McGraw-Hill, Inc., New York, N.Y.

Hickin, E. J., and Nanson, G. C., (1975), "*The Character of Channel Migration on the Beatton River, Northeast British Columbia, Canada*", Geological Society of America Bulletin, Vol. 86, pp. 487-494

Hickin, E. J., and Nanson, G. C., (1986), "*A Statistical Analysis of Bank Erosion and Channel Migration in Western Canada*", Geological Society of America Bulletin, Vol. 97, pp. 497-504

Hwang, N. H., and Houghtalen, R. J., (1996), *Fundamentals of Hydraulic Engineering Systems*, Prentice-Hall, Inc., Upper Saddle River, N. J.

Jansen, P. Ph., van Bendegom, L., van den Berg, J., de Vries, M., and Zanen, A., (1979), *Principles of River Engineering*, Pitman Publishing Ltd., London, U.K.

Jarocki, W., (1961), "Effects of Piers on Water Streams and Bed Forms", Proceedings of the ASCE Journal of Waterways and Harbours Division, Vol. 97, HY8, pp. 1165-1180

Joglekar, D. V, (1971), "Manual on River Behavior Control and Training", Publication No. 60, Central Board of Irrigation and Power, New Delhi, India, September

Kwan, T. F., (1988), "A Study of Abutment Scour", Report No. 328, School of Engineering, The University of Auckland, New Zealand

Lamb, H., (1932), "Hydrodynamics", Sixth Ed., Cambridge University Press, Cambridge, U.K.

Laursen, E. M., (1963), "Analysis of Relief Bridge Scour", ASCE, *Journal of Hydraulics Division*, Vol. 89, HY3, pp. 93-118

Leopold, L. B., and Wolman, M. G., (1960), "River Meanders", Bulletin of the Geological Society of America, Vol. 71, pp. 769-794

Leopold, L. B., Wolman, M. G., and Miller, J. P., (1964), *Fluvial Processes in Geomorphology*, W. H. Freeman, San Francisco, California

Matthes, G. H., (1948), "Mississippi River Cutoffs", *ASCE Transactions*, Vol. 113

Melville, B. W., (1975), "Local Scour at Bridge Sites", Report No. 117, School of Engineering, The University of Auckland, New Zealand

Milne-Thomson, L. M., (1966), *Theoretical Aerodynamics*, Dover Publications, Inc., New York, N.Y.

Odgaard, J. A., (1984), "Flow and Bed Topography in Alluvial Channel Bend", *Journal of Hydraulic Engineering*, ASCE, Vol. 110, No. 4, HY 4, April, pp. 521 - 536

Odgaard, J. A., (1986), "Meander Flow Model I: Development", *Journal of Hydraulic Engineering*, ASCE, Vol. 112, No. 12, pp. 1117-1136

Odgaard, J. A, (1989), "River-Meander Model. I: Development", *Journal of Hydraulic Engineering*, ASCE, Vol. 115, No. 11, November, pp.1433-1450

Odgaard, J. A, (1989), "River-Meander Model. II: Applications", *Journal of Hydraulic Engineering*, ASCE, Vol. 115, No. 11, November, pp. 1451-1464

Odgaard J. A., and DeWitt, R. J., (1989), "Sediment Control by Submerged Vanes", *Proceedings of the 20th Annual Conference of the International Erosion Control Association*, Vancouver, BC, Canada

Odgaard, J. A, and Kennedy, F., (1983), "River-Bend Bank Protection by Submerged Vanes", *Journal of Hydraulic Engineering*, ASCE, Vol. 109, No. 8, August, pp. 1161-1173

Odgaard, J. A., and Lee, H. E., (1984), "Submerged Vanes for Flow Control and Bank Protection in Streams", submitted to the Highway Division of the Iowa Department of Transportation and the Iowa

Highway Research Board, Project HR-255, IIHR Report No. 279, Iowa Institute of Hydraulic Research, University of Iowa

Odgaard, J. A., and Mosconi, C. E. (1987), "Streambank Protection by Submerged Vanes", *Journal of Hydraulic Engineering*, ASCE, Vol. 113, No. 4, April, pp. 521-536

Odgaard, J. A., and Spoljaric, A., (1986), "Sediment Control by Submerged Vanes", *Journal of Hydraulic Engineering*, ASCE, Vol. 112, No. 12, December, pp. 1164-1181

Odgaard, J. A., and Spoljaric, A. (1986), "Submerged Vanes for Sediment Control in Rivers", *Proceedings of the ASCE Conference, Water Forum '86: World Water Issues in Evolution*

Odgaard, J. A., and Spoljaric, A., (1989), "Sediment Control by Submerged Vanes: Design Basis", *River Meandering*, American Geophysical Union, Washington, DC, edited by Ikeda, S., and Parker, G., pp. 127 -151

Odgaard, J. A., and Wang, Y., (1990), "Sediment Control in Bridge Waterways", sponsored by the Highway Division of the Iowa Department of Transportation and the Iowa Highway Research Board, Project HR-307, IIHR Report No. 336, Iowa Institute of Hydraulic Research, University of Iowa

Odgaard, J. A., and Wang, Y., (1991), "Sediment Management with Submerged Vanes. I: Theory", *Journal of Hydraulic Engineering*, ASCE, Vol. 117, No. 3, March, pp. 267-283

Odgaard, J. A., and Wang, Y., (1991), "Sediment Management with Submerged Vanes. II: Applications", *Journal of Hydraulic Engineering*, ASCE, Vol. 117, No. 3, March, pp. 283-302, Discussion by Laursen, E. M.

Petersen, M. S, (1963), "Hydraulic Aspects of Arkansas River Stabilization", *Journal of the Waterways and Harbors Division*, ASCE, November

Petersen, M. S., (1986), *River Engineering*, Prentice-Hall, Inc., Englewood Cliffs, N.J.

Potapov, M. V., (1950), "Sochineniya v Trekh Tomakh - I", *Gos Izd. Sel'skokhozyaistvennoi Lit.*, Moscow, the Soviet Union (in Russian)

Potapov, M. V., (1951), "Sochineniya v Trekh Tomakh - II", *Gos Izd. Sel'skokhozyaistvennoi Lit.*, Moscow, the Soviet Union (in Russian)

Potapov, M. V., and Pyshkin, B. A., (1947), "Metod Poperechnoy Tsirkulyatsii i ego Primenenie v Gidrotekhnike", *Izd. Ak. Nayk SSSR*, Moscow, Leningrad, the Soviet Union (in Russian)

Przedwojski, B., Błażejewski, R., and Pilarczyk, K. W., (1995), *River Training Techniques: Fundamentals, Design and Applications*, A.A. Balkema Publishers, Rotterham, Netherlands

Raudkivi, A. J., (1990), *Loose Boundary Hydraulics*, Pergamon Press, Inc., Elmsford, N.Y.

Rozovskii, I. L., (1957), *Flow of Water in Bends of Open Channels*, Academy of Sciences of the Ukranian SSR, Kiev, the Soviet Union (English Translation, Israel Program for Scientific Translation, Jerusalem, Israel)

Sabersky, R. H., and Acosta, A. J., (1964), *Fluid Flow*, MacMillan Publishing Co., Inc., New York, N.Y.

Schiechtl, H. M., and Stern, R., (1997), *Water Bioengineering Techniques: for Watercourse, Bank and Shoreline Protection*, Österreichischer Agrarverlag, Klosterneuburg, Austria, English translation with additions by Blackwell Science Ltd.

Shen, H. W,. Schneider, V. R., and Karaki, S. S., (1966), "Mechanics of Local Scour", US Dept. of Commerce, National Bureau of Standards, Institute of Applied Technology

Shields, A., (1936), "Anvendung der Aenlichkeitsmechanik und der Turbulenzforschung auf die Geshiebebewegung", *Mitteilungen der Preussischen Versuchsanstalt fur Wasserbau and Schiffbau*, Berlin, Germany, Translated to English by W.P. Ott and J.C. van Uchelen, California Institute of Technology, Pasadena, California

Simons, D. B., (1971), "River and Canal Morphology", in *River Mechanics*, H. W. Shen, ed.

Simons, D. B., and Şentürk, F., (1976), *Sediment Transport Technology*, Water Resources Publications, Fort Collins, CO

Sinha, S. K., and Marelius, F., (2000), "Analysis of Flow Past Submerged Vanes", *Journal of Hydraulic Research*, IAHR, Vol. 38, No. 1

Thompson, J. N., and Green, D. L., (1994), "Riparian Restoration and Streamside Erosion Control Handbook", Tennessee Department of Environment and Conservation, Division of Water Pollution Control, Nonpoint Source Program, Nashville, TN

U.S. Corps of Engineers, (1970), "Hydraulic Design of Flood Control Channels," EM 1110-2-1601, Department of the Army, Office of the Chief of Engineers, July

U.S. Army Corps of Engineers, (1981), "The Streambank Erosion Control Evaluation and Demonstration Act of 1974" Section 32, Public Law 93-251, Final Report to Congress, Waterways Experiment Station, Vicksburg, MS, USA

Wang, Y., (1989), "Bank Protection with Submerged Vanes", *Proceedings of the XXIII Congress of the International Association for Hydraulic Research*, Vol. S, pp. 17-23

Wang, Y., (1990), "Sediment Control with Submerged Vanes", thesis presented to the University of Iowa, Iowa City, Iowa, in partial fulfillment of the requirements for the degree of Doctor of Philosophy

Winkley B. R., (1971), "Practical Aspects of River Regulation and Control", in *River Mechanics*, Vol. 1, H.W. Shen, ed.

Yalin, M. S., and Karahan, E. M., (1979), *Mechanics of Sediment Transport*, Pergamon Press, Toronto, Canada

Yang, C. T., (1996), "Sediment Transport: Theory and Practice" McGraw-Hill Co., New York, N.Y.

Yaroslavtziev, J. A., (1954), *Protection of Bridge Supports from Scour*, Moscow Mintranosfoj, USSR

Zimmermann, C., and Kennedy, J. F., (1978), "Transverse Bed Slopes in Curved Alluvial Streams", *Journal of the Hydraulics Division*, ASCE, Vol. 104, No. 1, pp. 33-48

APPENDIX A

EFFECT OF VANE HEIGHT (90° BEND)

A.1 Narrow Vanes (*L/b* = 0.16)

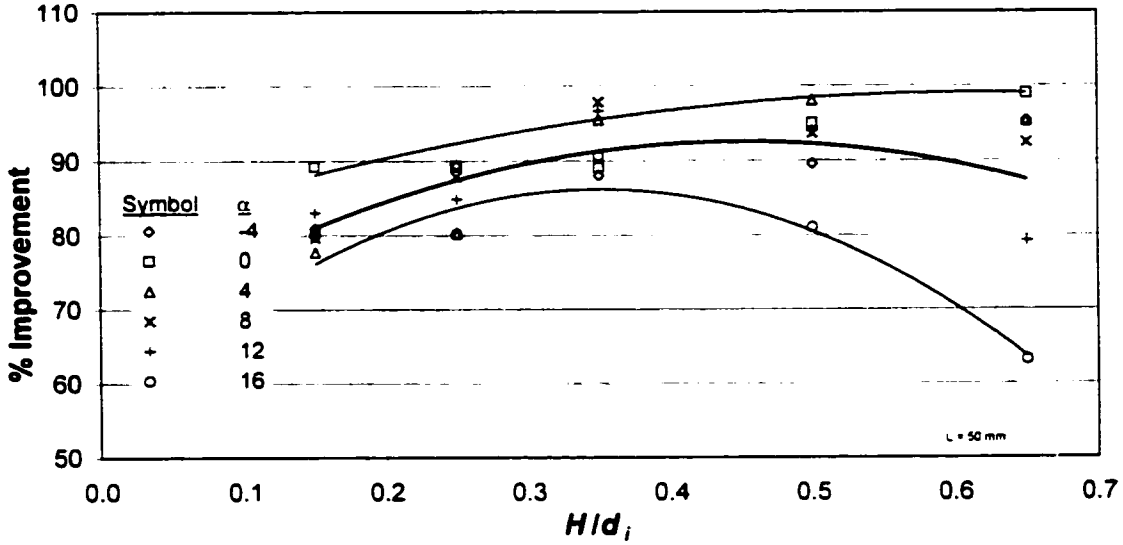

Figure A.1: % Improvement vs. H/d_i ($L/b = 0.16$, $\delta_s/b = 0.98$).

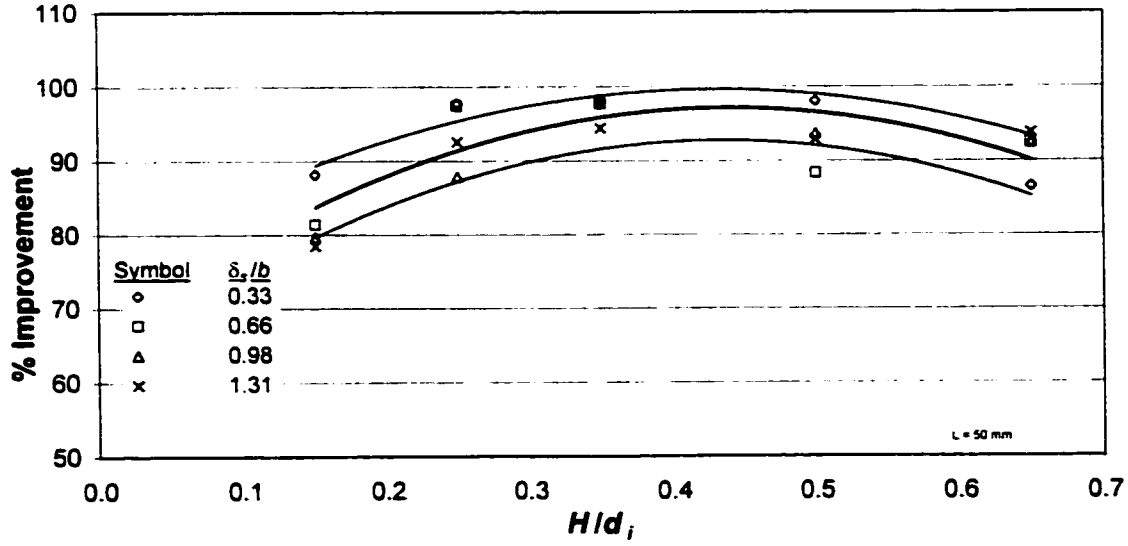

Figure A.2: % Improvement vs. H/d_i ($L/b = 0.16$, $\alpha = 8°$).

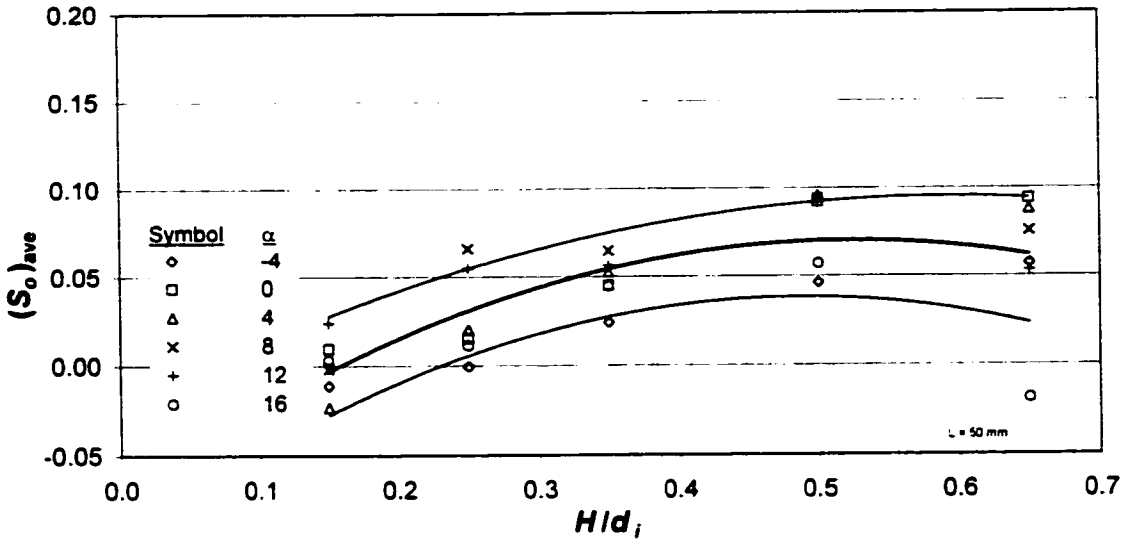

Figure A.3: $(S_o)_{ave}$ vs. H/d_i ($L/b = 0.16$, $\delta_s/b = 0.98$).

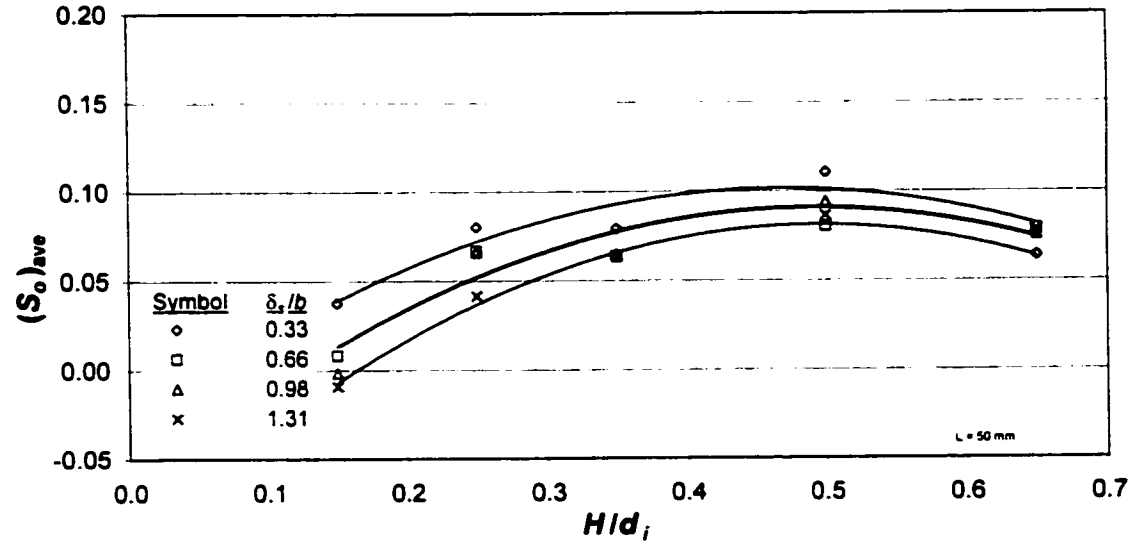

Figure A.4: $(S_o)_{ave}$ vs. H/d_i ($L/b = 0.16$, $\alpha = 8°$).

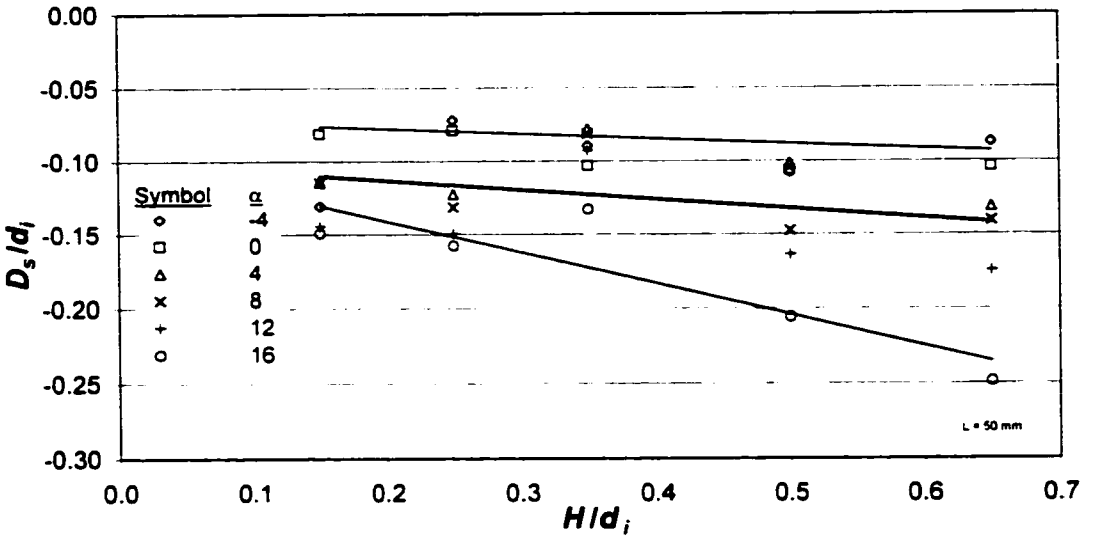

Figure A.5: D_s/d_i vs. H/d_i ($L/b = 0.16$, $\delta_s/b = 0.98$).

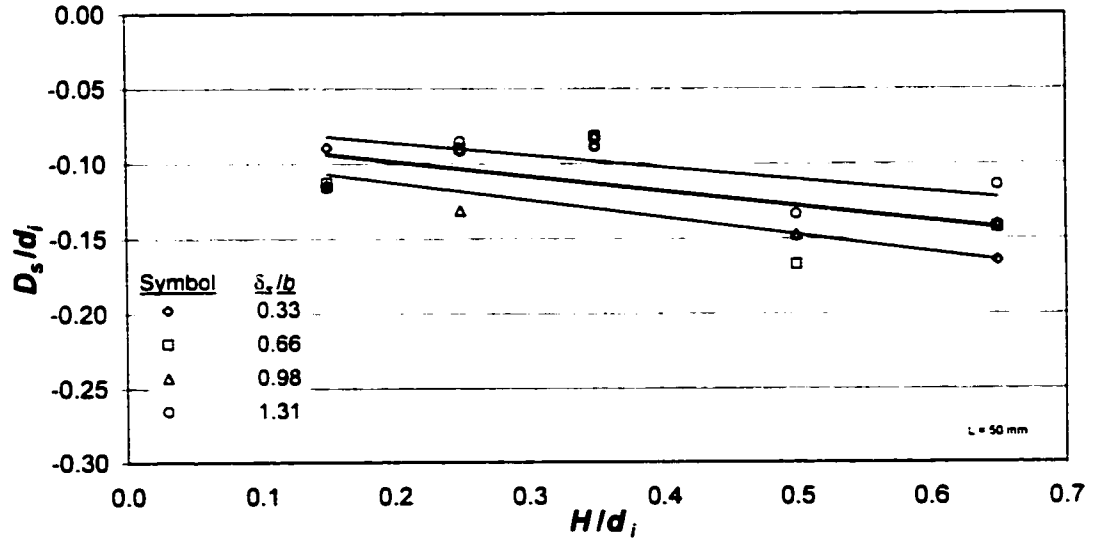

Figure A.6: D_s/d_i vs. H/d_i ($L/b = 0.16$, $\alpha = 8°$).

A.2 Intermediate Length Vanes (L/b = 0.33)

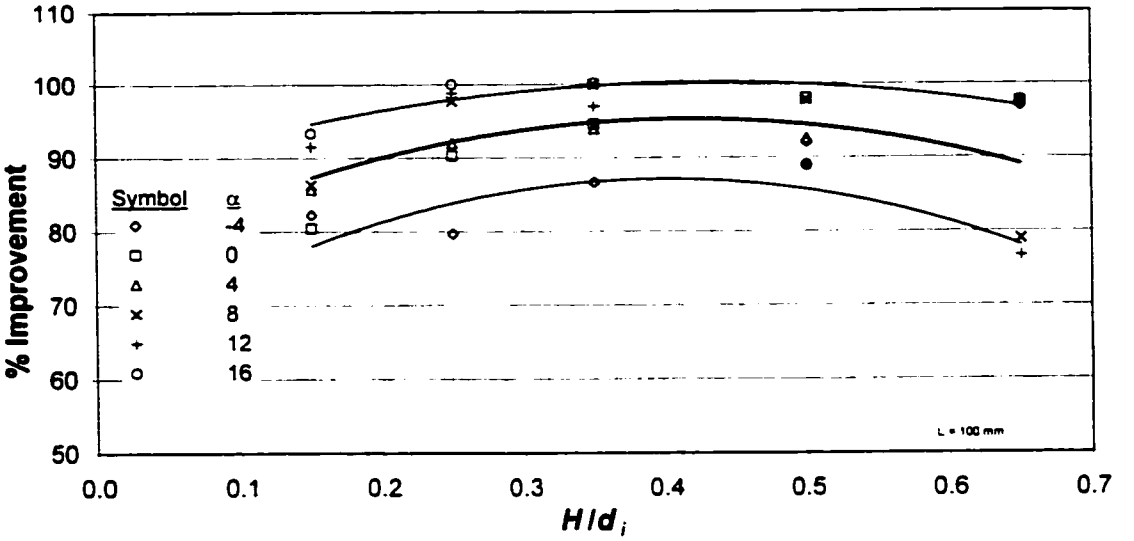

Figure A.7: % Improvement vs. H/d_i (L/b = 0.33, δ_s/b = 0.98).

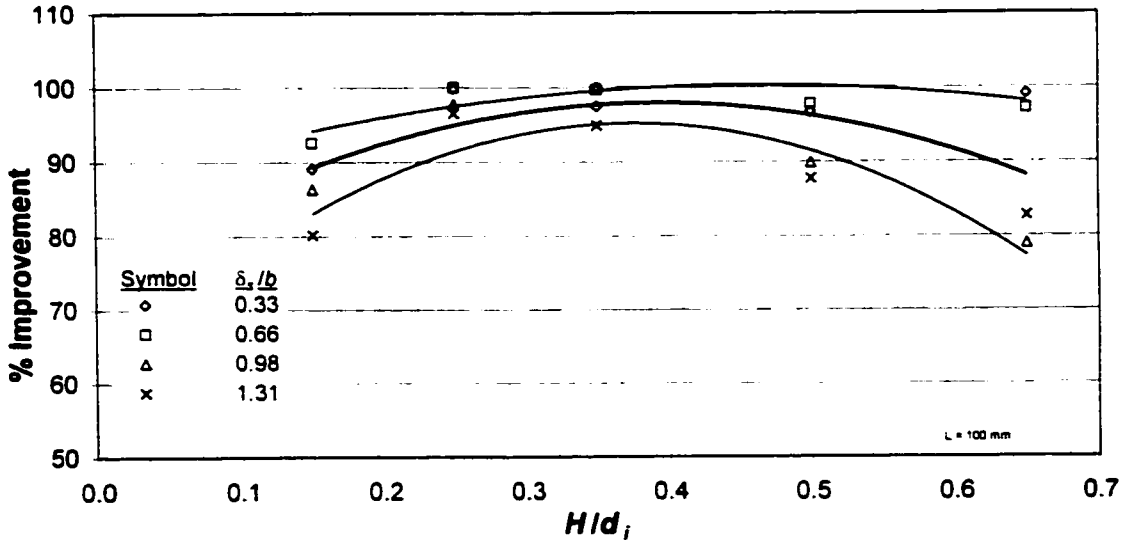

Figure A.8: % Improvement vs. H/d_i (L/b = 0.33, $\alpha = 8°$).

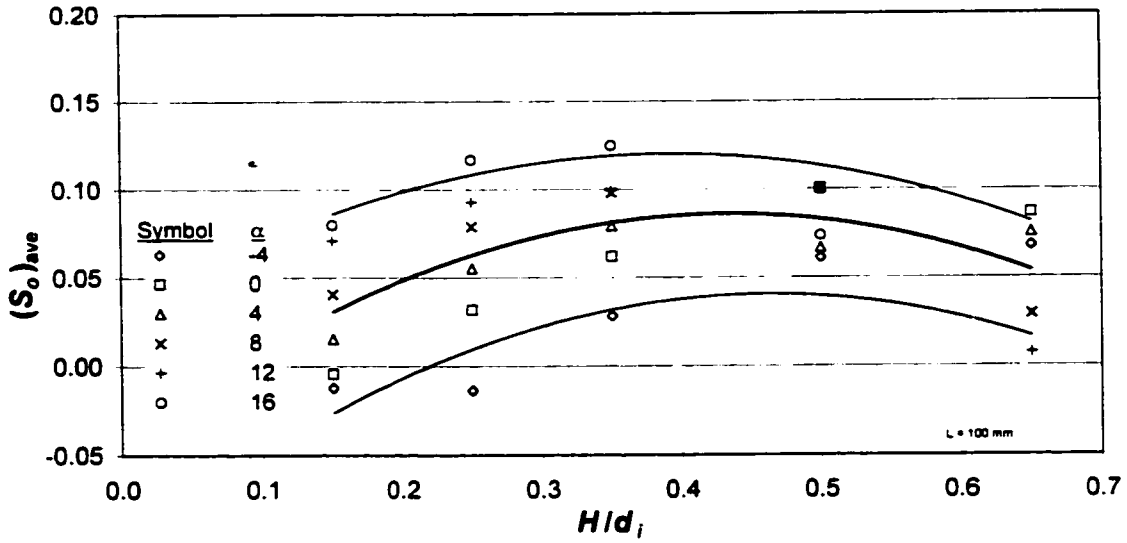

Figure A.9: $(S_o)_{ave}$ vs. H/d_i ($L/b = 0.33$, $\delta_s/b = 0.98$).

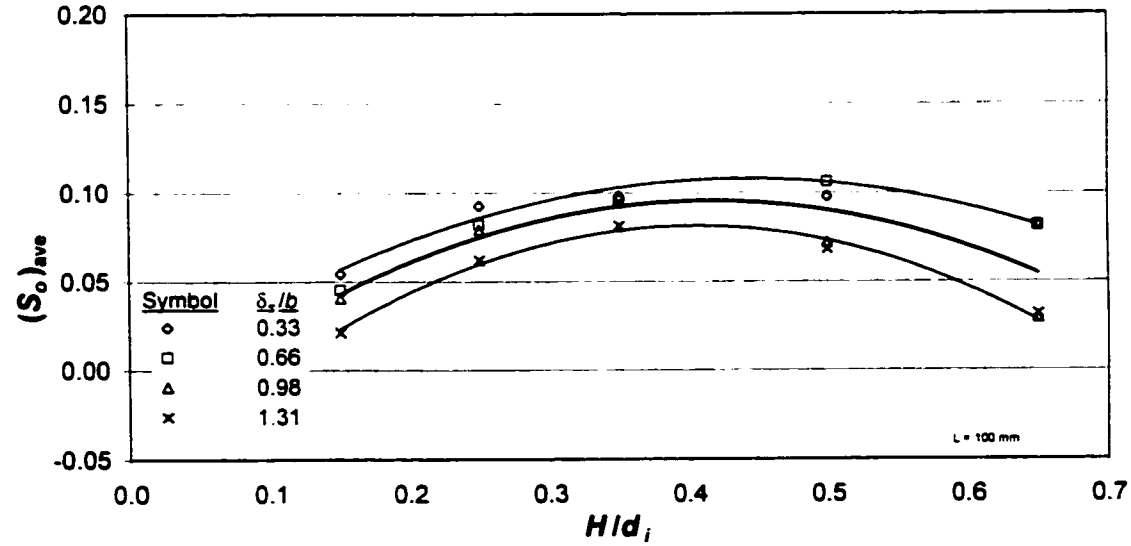

Figure A.10: $(S_o)_{ave}$ vs. H/d_i ($L/b = 0.33$, $\alpha = 8°$).

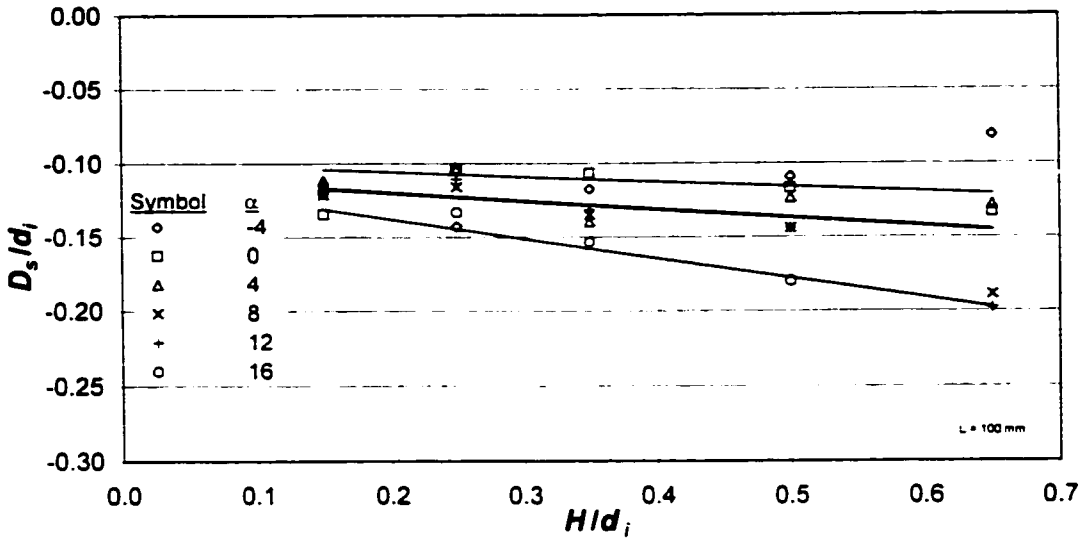

Figure A.11: D_s/d_i vs. H/d_i ($L/b = 0.33$, $\delta_s/b = 0.98$).

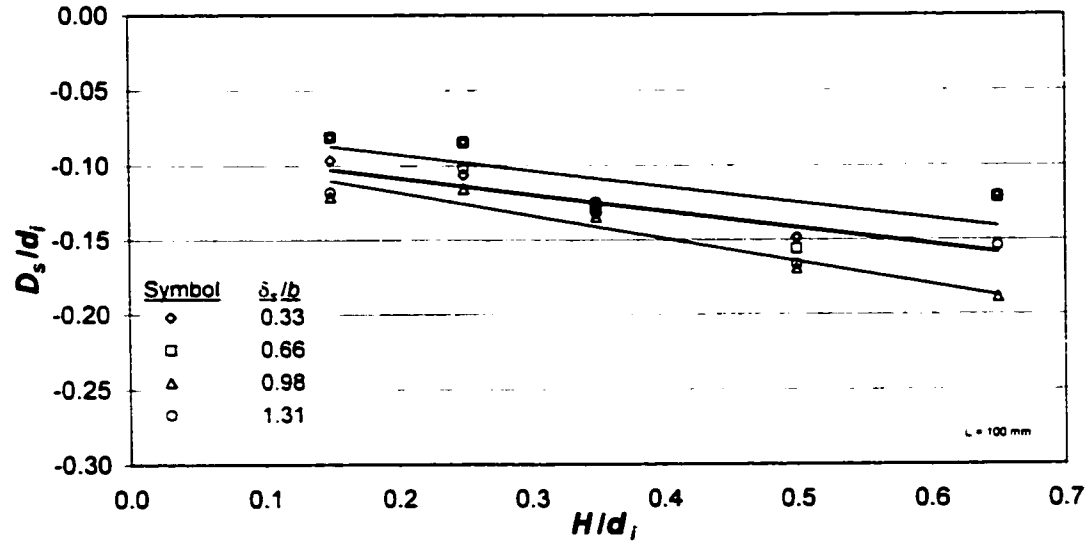

Figure A.12: D_s/d_i vs. H/d_i ($L/b = 0.33$, $\alpha = 8°$).

A.3 Long Vanes (L/b = 0.49)

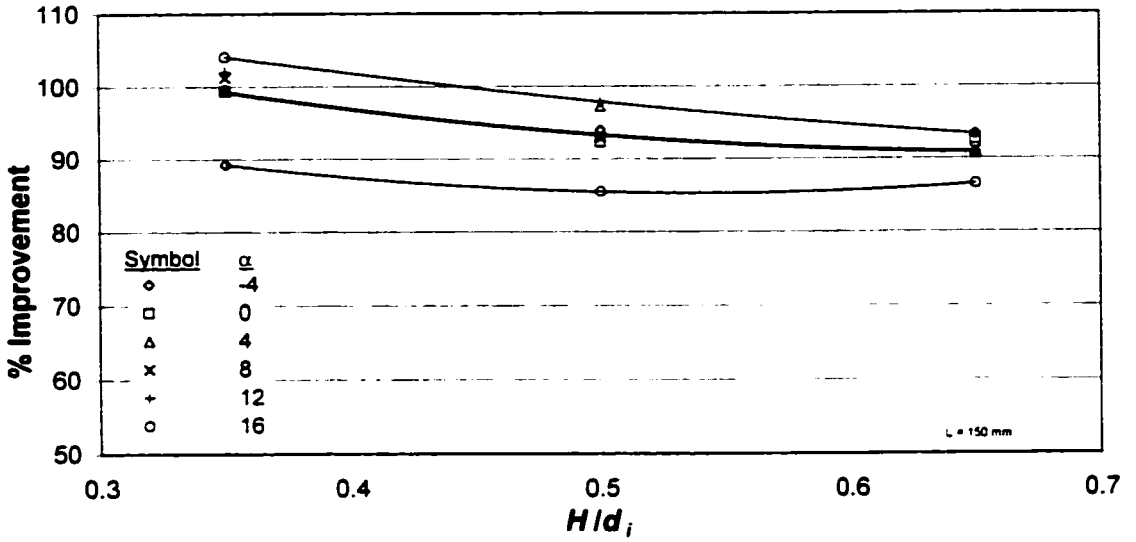

Figure A.13: % Improvement vs. H/d_i (L/b = 0.49, δ_s/b = 0.98).

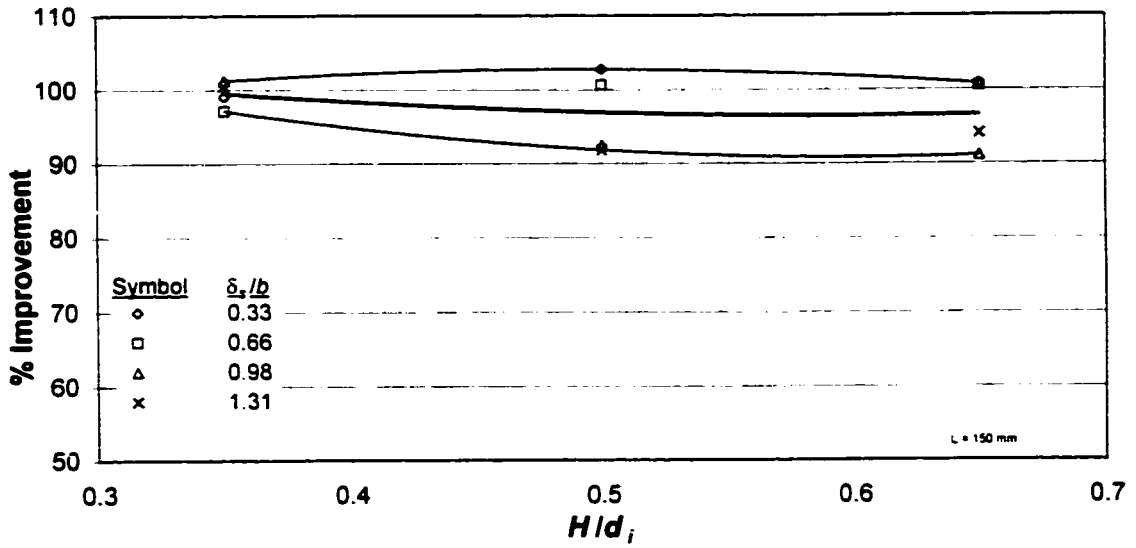

Figure A.14: % Improvement vs. H/d_i (L/b = 0.49, α = 8°).

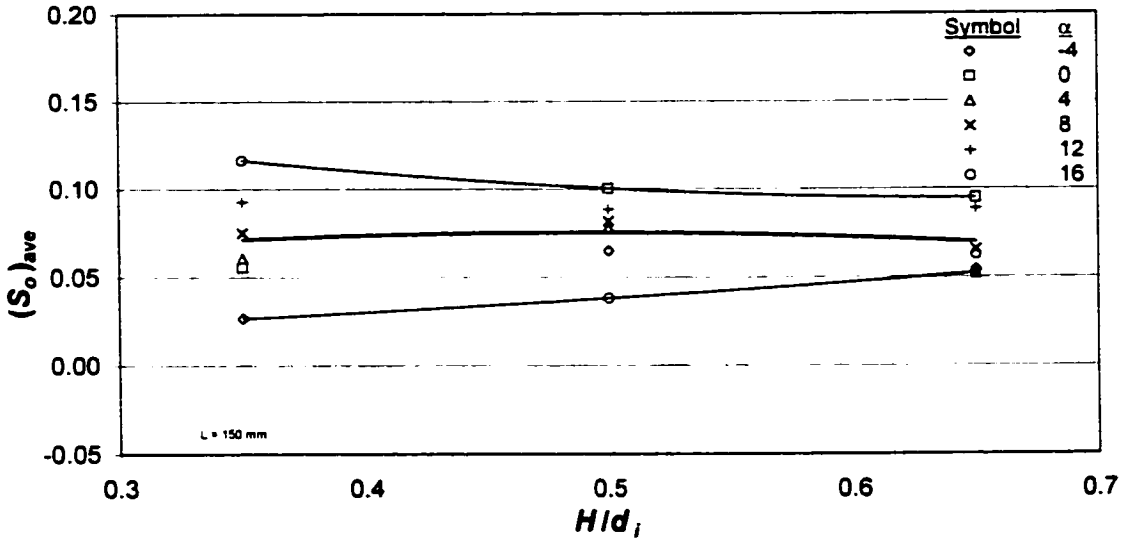

Figure A.15: $(S_o)_{ave}$ vs. H/d_i ($L/b = 0.49$, $\delta_s/b = 0.98$).

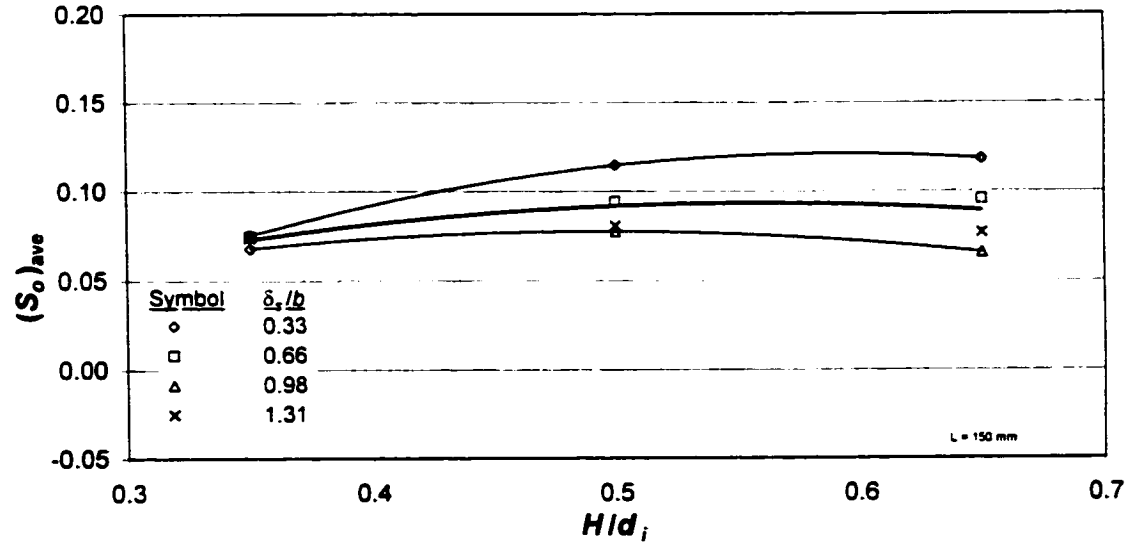

Figure A.16: $(S_o)_{ave}$ vs. H/d_i ($L/b = 0.49$, $\alpha = 8°$).

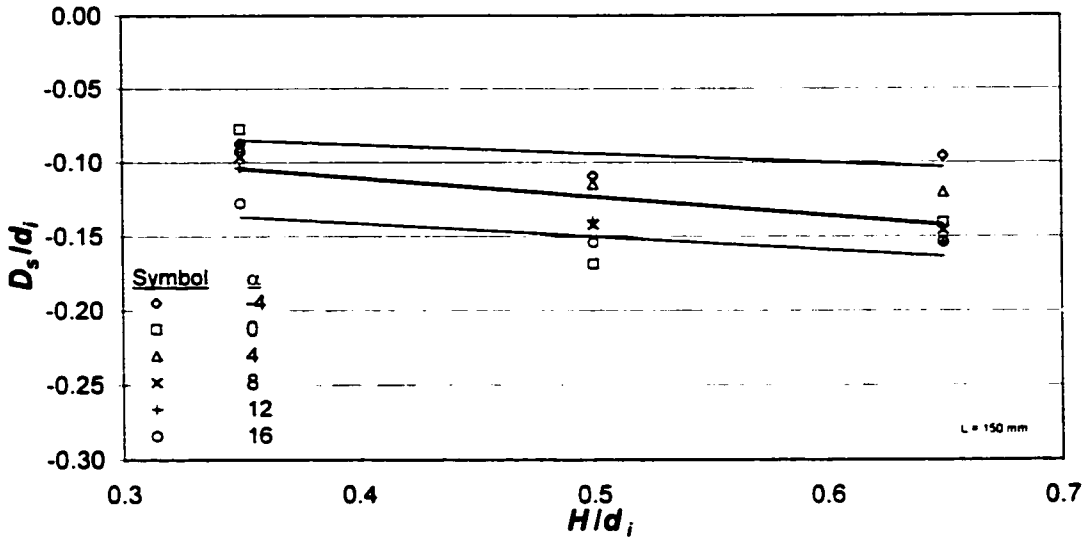

Figure A.17: D_s/d_i vs. H/d_i ($L/b = 0.49$, $\delta_s/b = 0.98$).

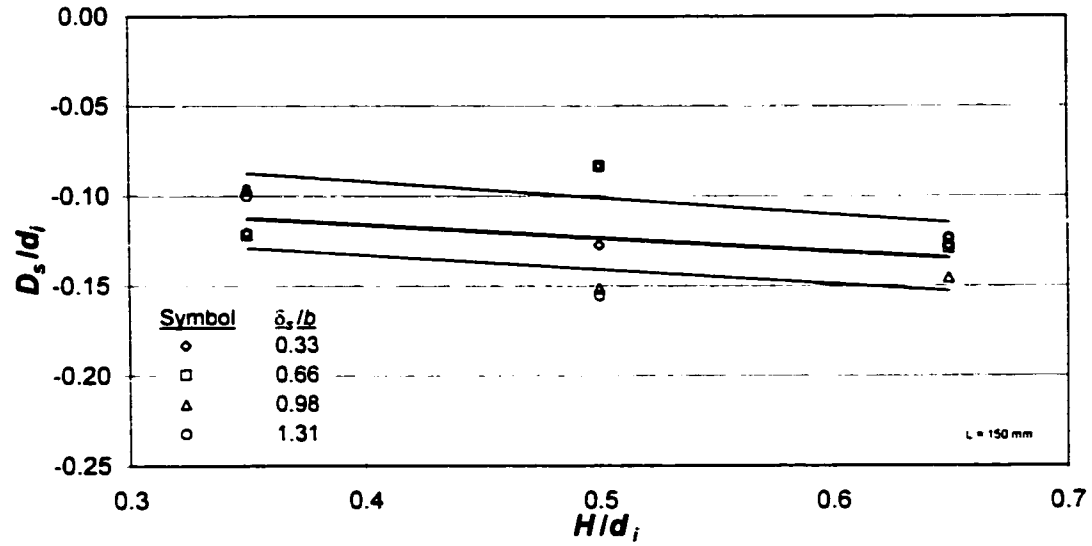

Figure A.18: D_s/d_i vs. H/d_i ($L/b = 0.49$, $\alpha = 8°$).

APPENDIX B

EFFECT OF VANE LENGTH (90° BEND)

B.1 Intermediate Height Vanes ($H/d_i = 0.35$)

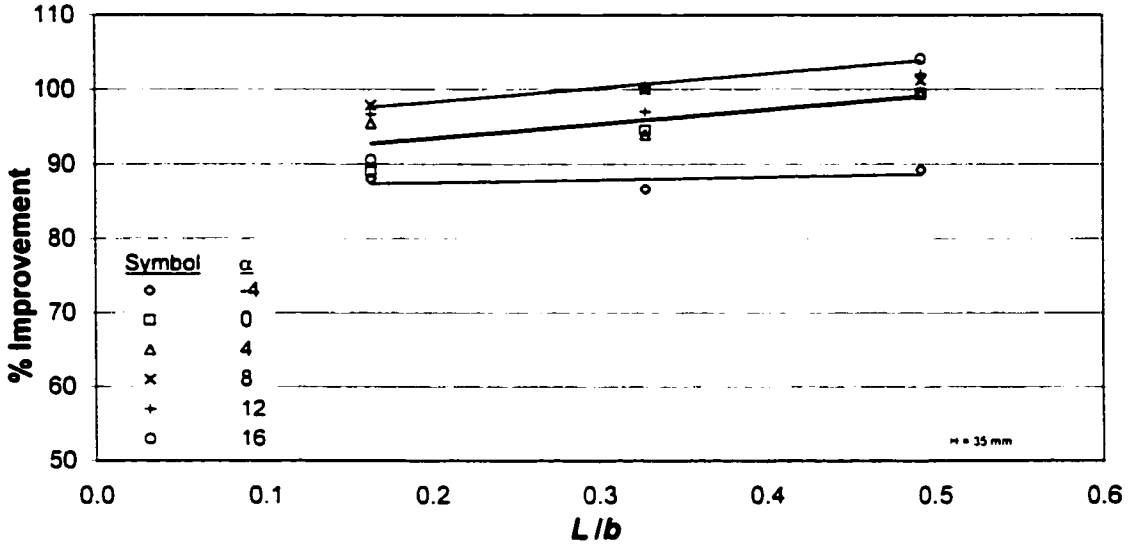

Figure B.1: % Improvement vs. L/b ($H/d_i = 0.35$, $\delta_i/b = 0.98$).

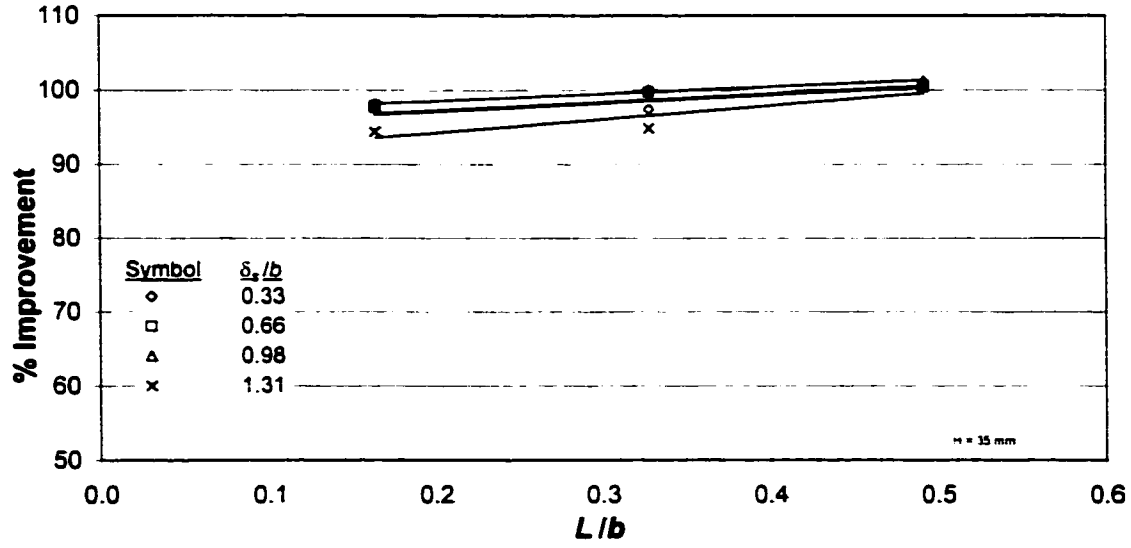

Figure B.2: % Improvement vs. L/b ($H/d_i = 0.35$, $\alpha = 8°$).

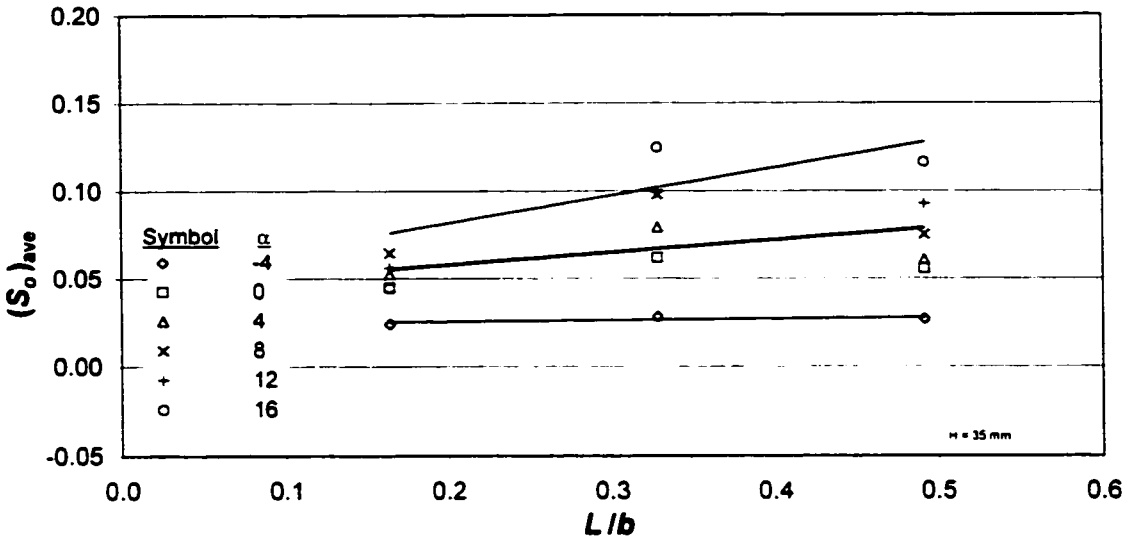

Figure B.3: $(S_o)_{ave}$ vs. L/b ($H/d_t = 0.35$, $\delta_t/b = 0.98$).

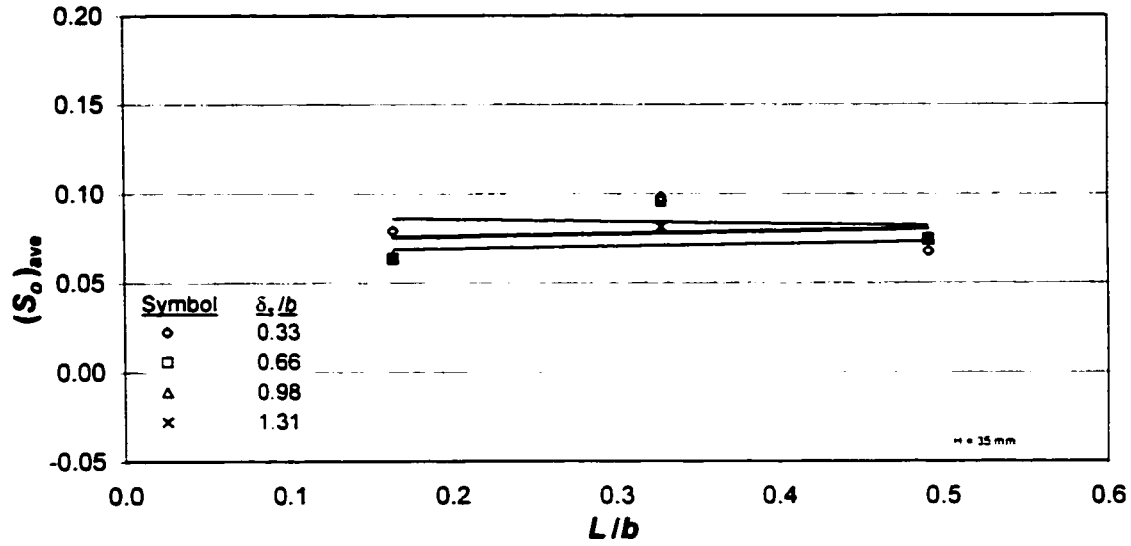

Figure B.4: $(S_o)_{ave}$ vs. L/b ($H/d_t = 0.35$, $\alpha = 8°$).

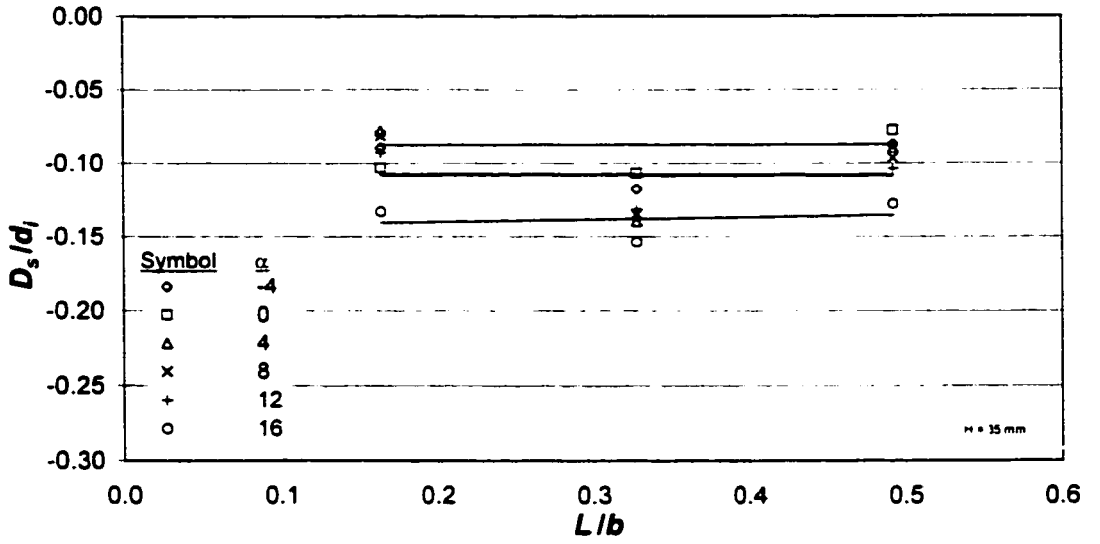

Figure B.5: D_s/d_i vs. L/b ($H/d_i = 0.35$, $\delta_s/b = 0.98$).

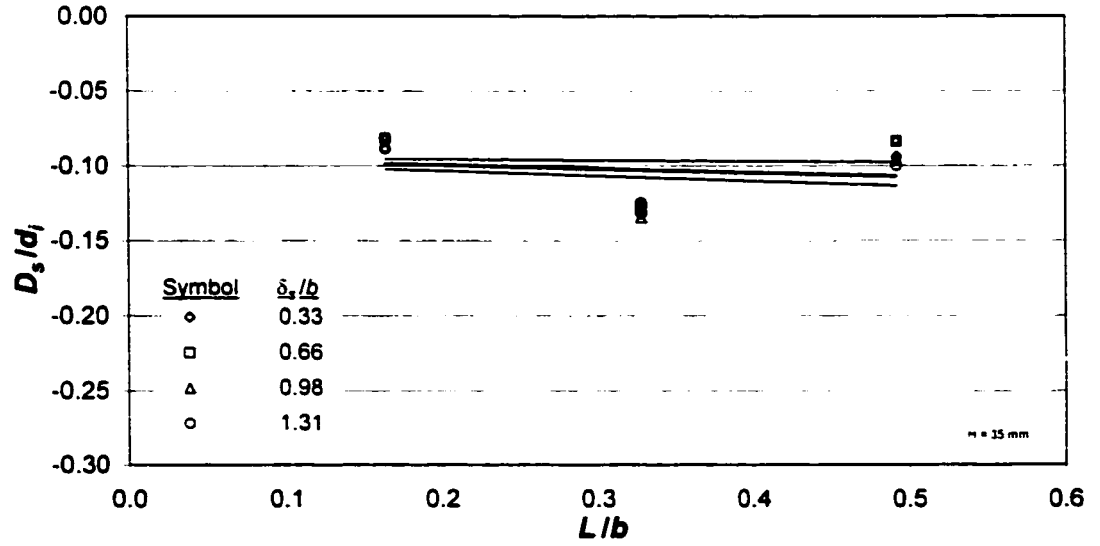

Figure B.6: D_s/d_i vs. L/b ($H/d_i = 0.35$, $\alpha = 8°$).

B.2 Intermediate Height Vanes ($H/d_i = 0.50$)

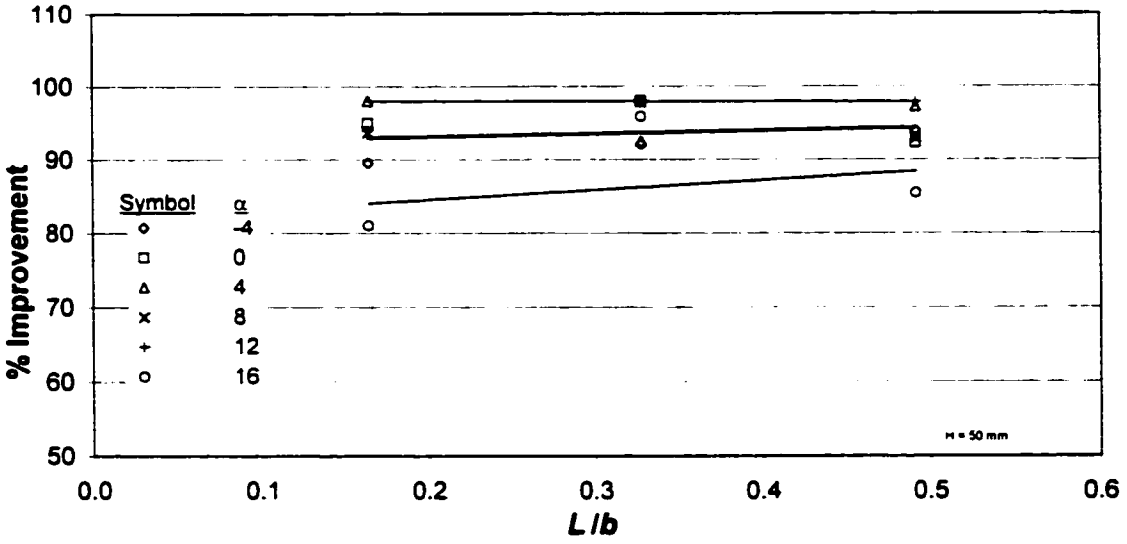

Figure B.7: % Improvement vs. L/b ($H/d_i = 0.50$, $\delta_s/b = 0.98$).

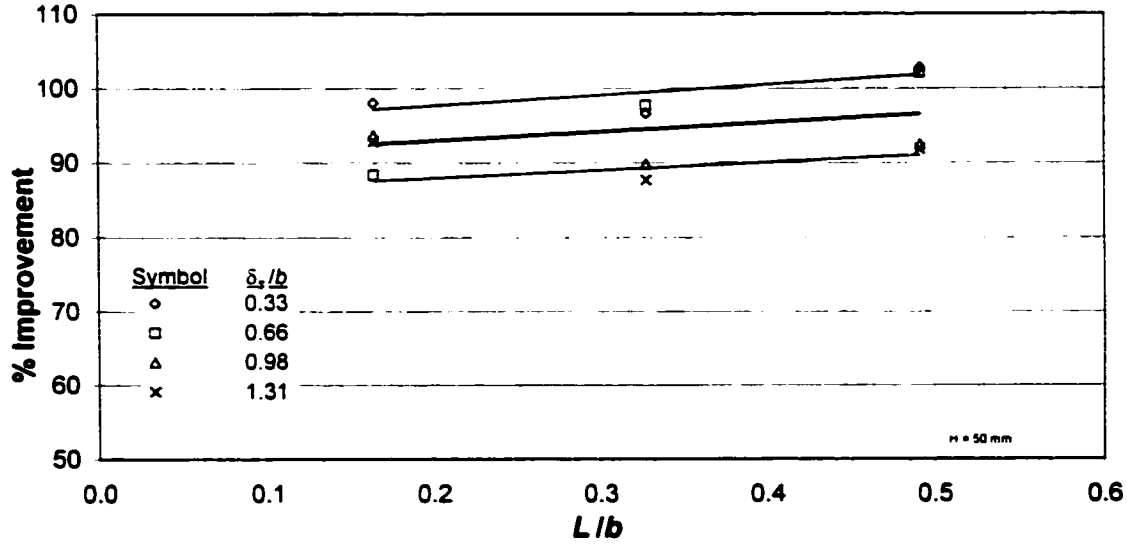

Figure B.8: % Improvement vs. L/b ($H/d_i = 0.50$, $\alpha = 8°$).

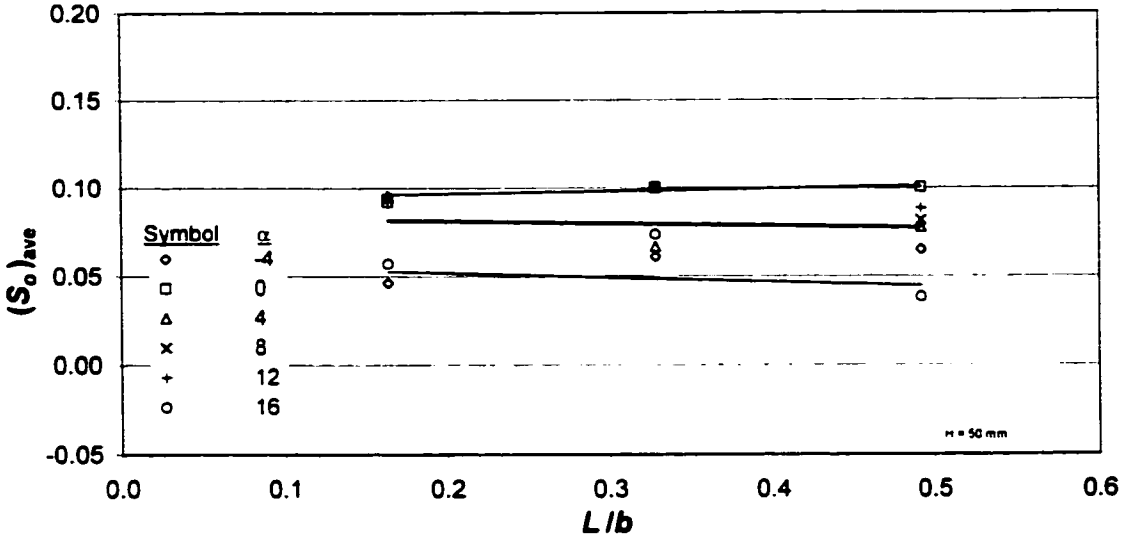

Figure B.9: $(S_o)_{ave}$ vs. L/b ($H/d_t = 0.50$, $\delta_r/b = 0.98$).

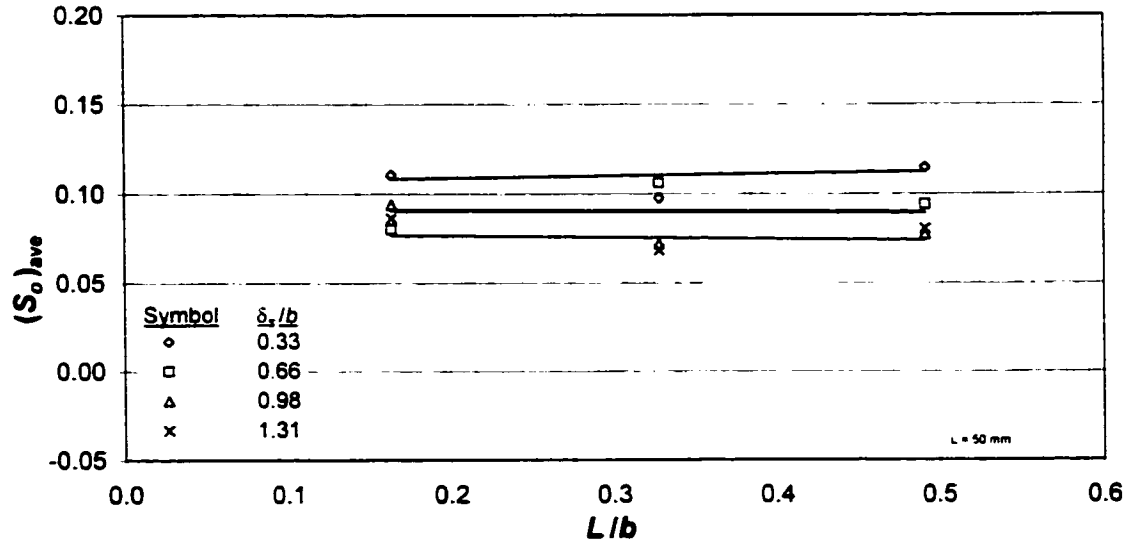

Figure B.10: $(S_o)_{ave}$ vs. L/b ($H/d_t = 0.50$, $\alpha = 8°$).

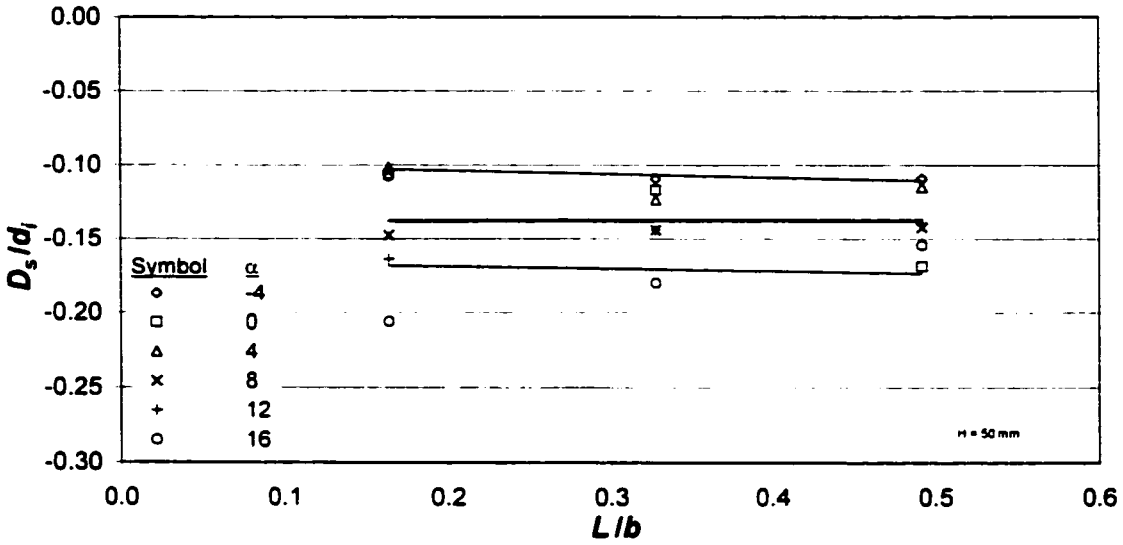

Figure B.11: D_s/d_i vs. L/b ($H/d_i = 0.50$, $\delta_s/b = 0.98$).

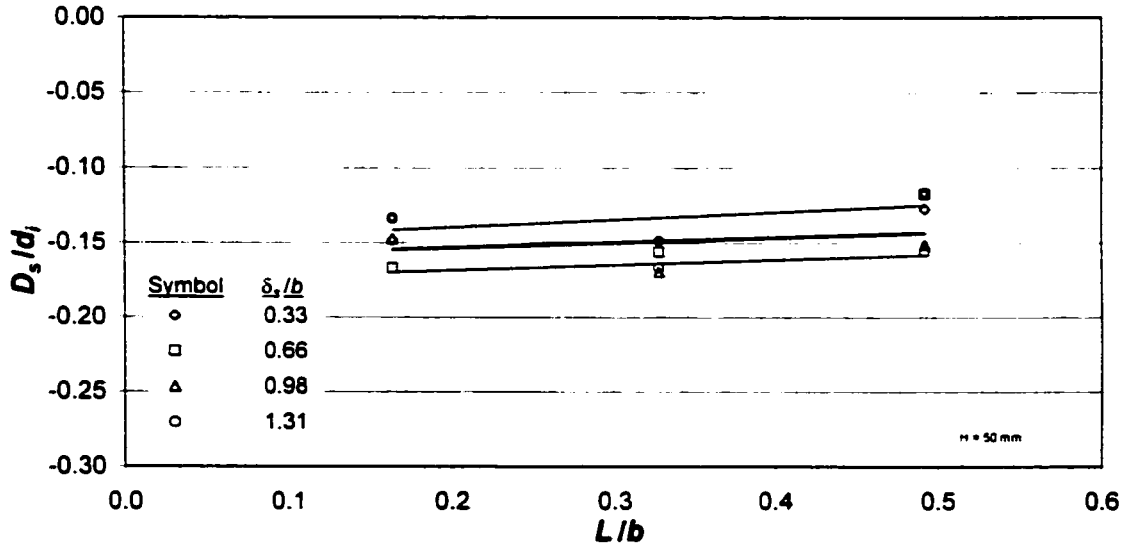

Figure B.12: D_s/d_i vs. L/b ($H/d_i = 0.50$, $\alpha = 8°$).

B.3 Tall Vanes ($H/d_i = 0.65$)

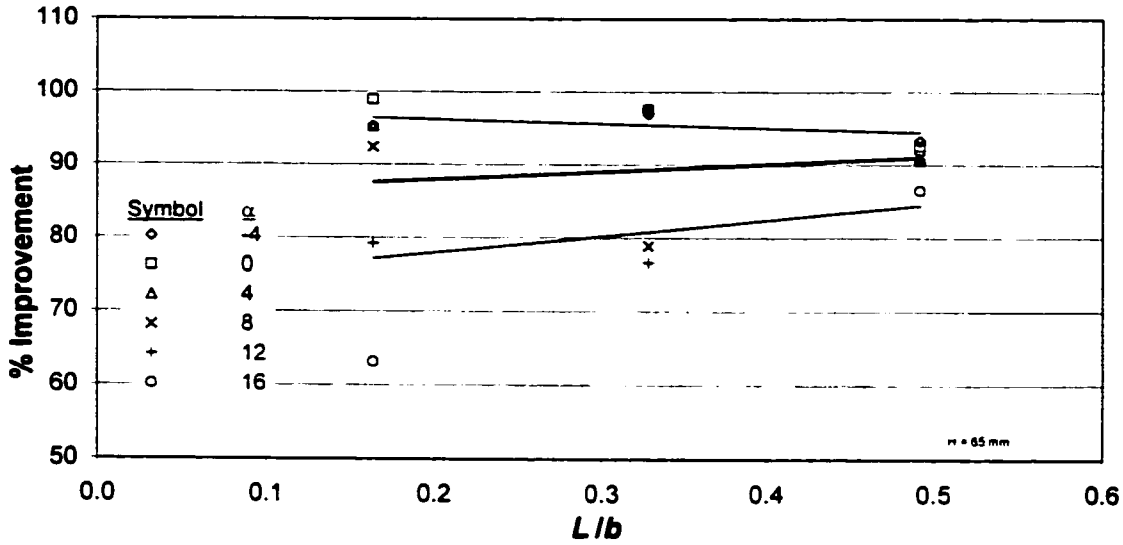

Figure B.13: % Improvement vs. L/b ($H/d_i = 0.65$, $\delta_i/b = 0.98$).

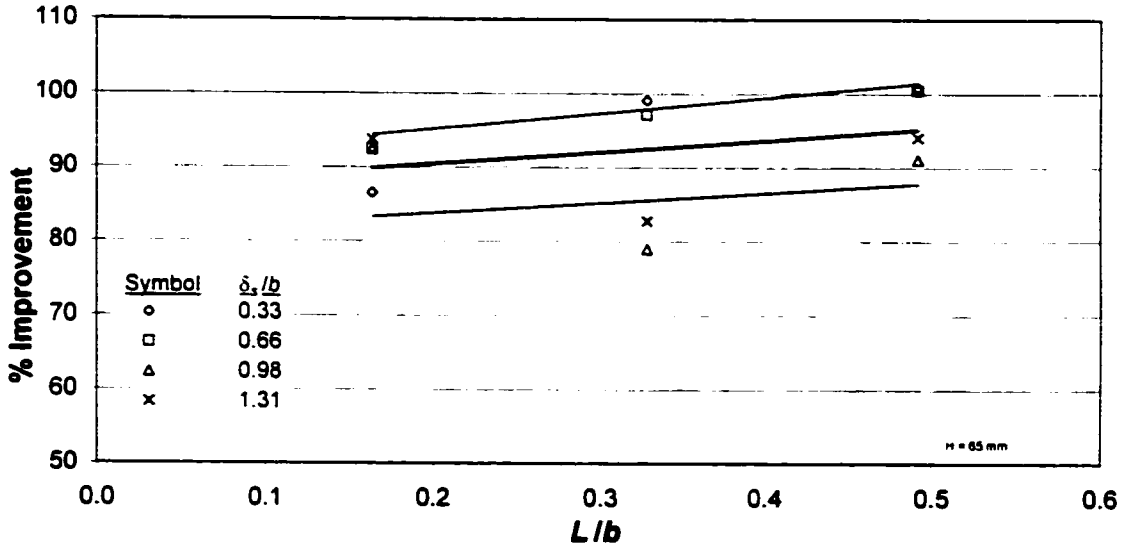

Figure B.14: % Improvement vs. L/b ($H/d_i = 0.65$, $\alpha = 8°$).

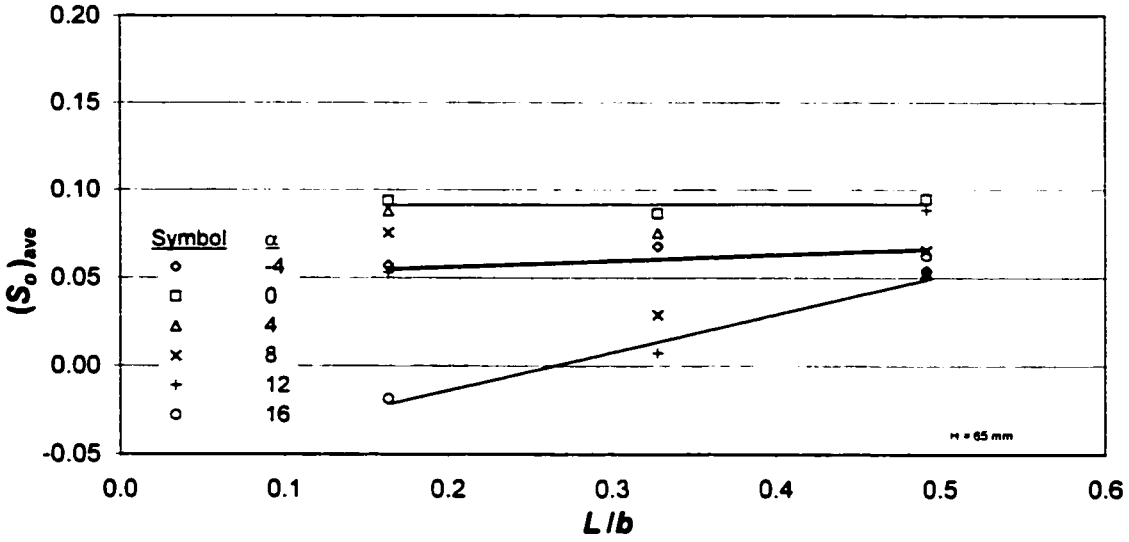

Figure B.15: $(S_o)_{ave}$ vs. L/b ($H/d_i = 0.65$, $\delta_s/b = 0.98$).

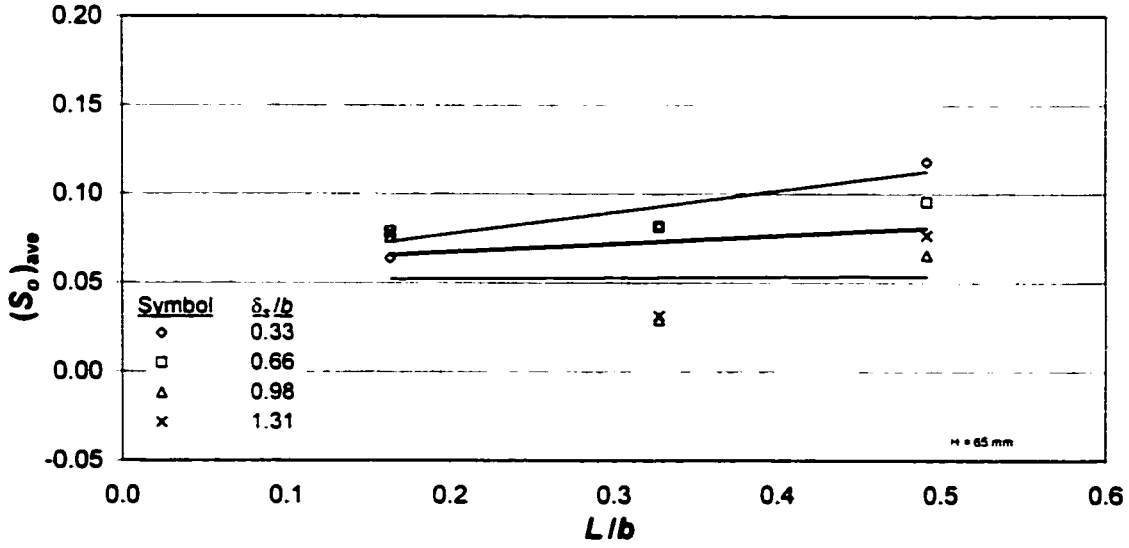

Figure B.16: $(S_o)_{ave}$ vs. L/b ($H/d_i = 0.65$, $\alpha = 8°$).

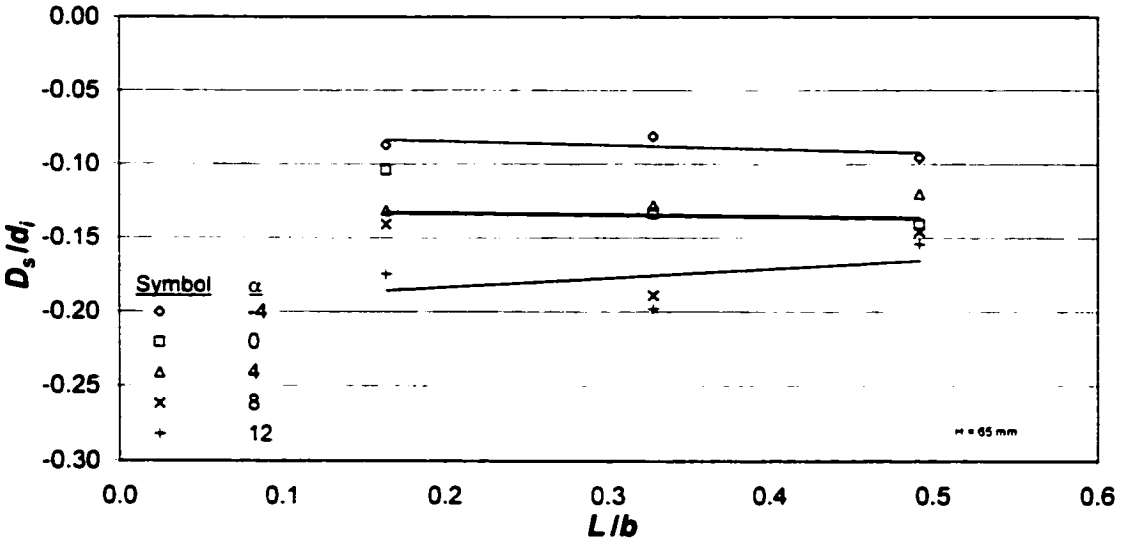

Figure B.17: D_s/d_i vs. L/b ($H/d_i = 0.65$, $\delta_s/b = 0.98$).

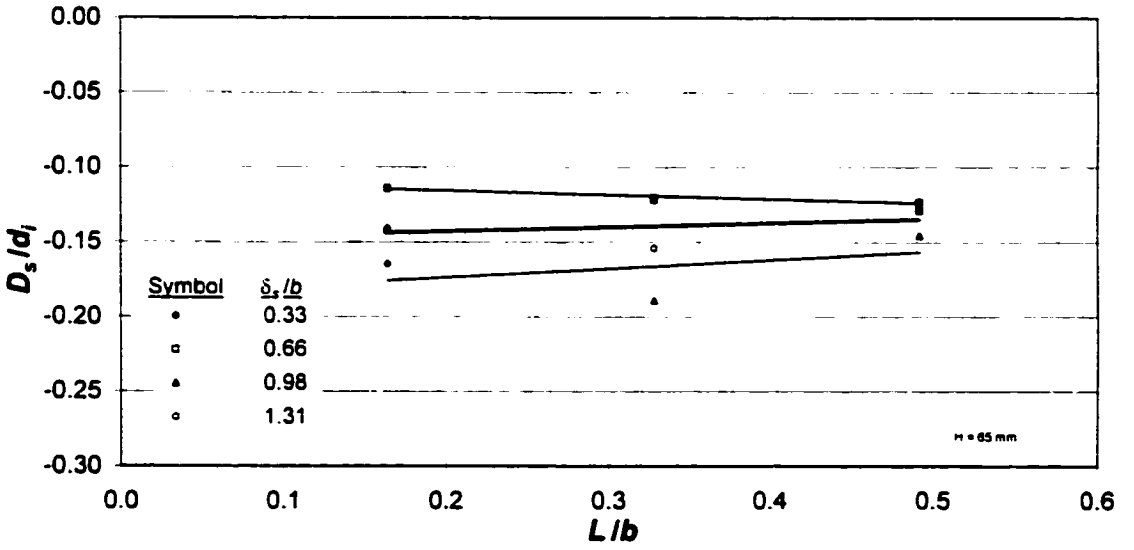

Figure B.18: D_s/d_i vs. L/b ($H/d_i = 0.65$, $\alpha = 8°$).

APPENDIX C

EFFECT OF VANE ANGLE (90° BEND)

C.1 Narrow Vanes (L/b = 0.16)

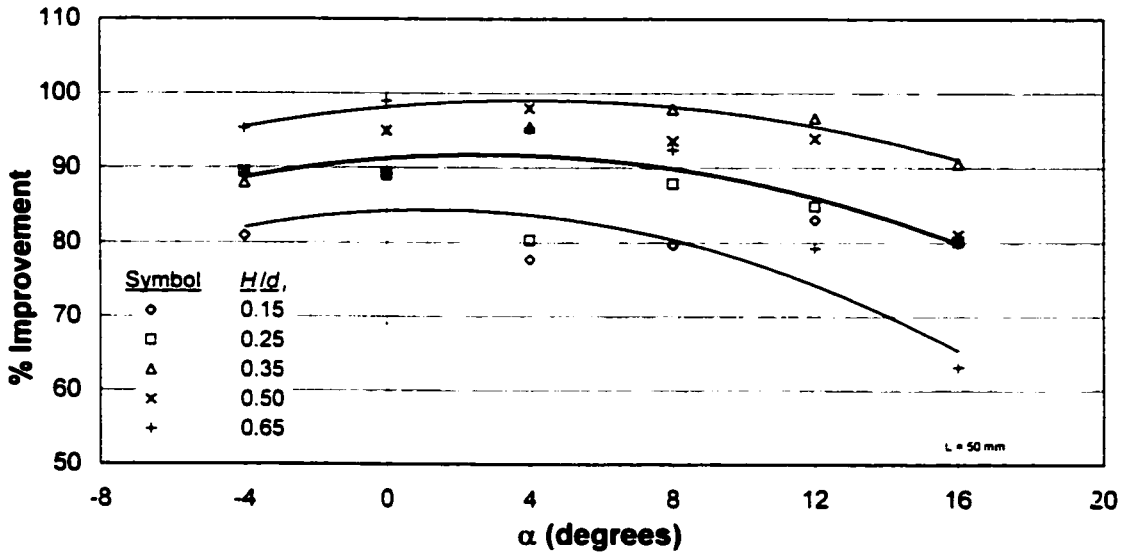

Figure C.1: % Improvement vs. α (L/b = 0.16, δ_i/b = 0.98).

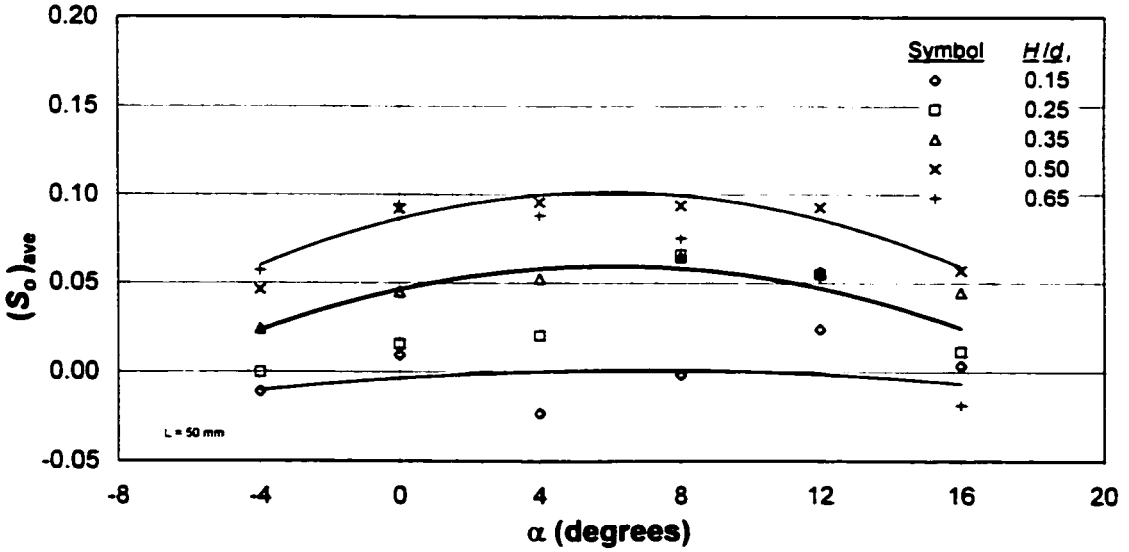

Figure C.2: $(S_o)_{ave}$ vs. α (L/b = 0.16, δ_i/b = 0.98).

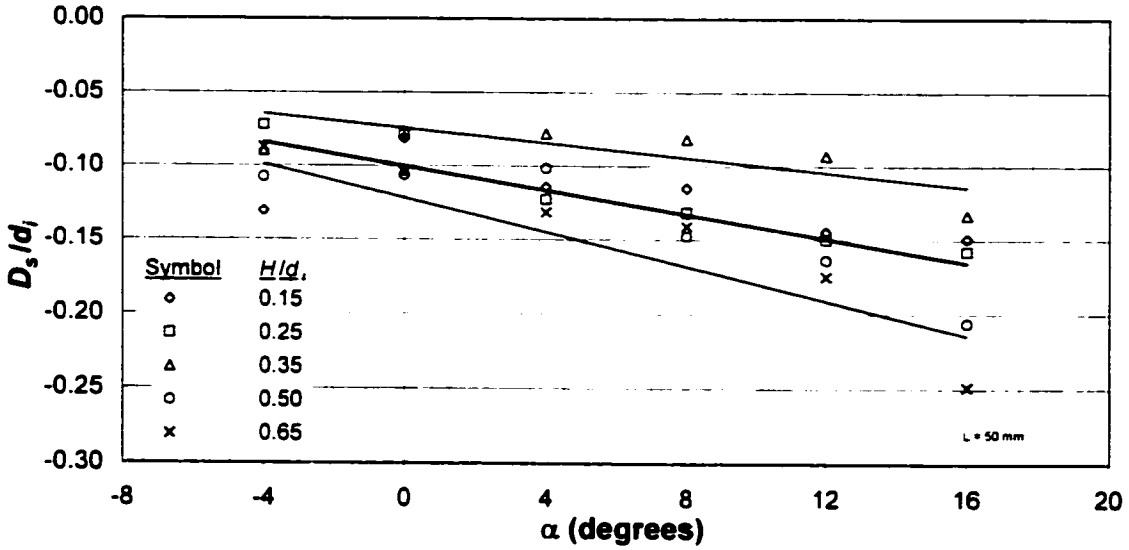

Figure C.3: D_s/d_j vs. α (L/b = 0.16, δ_j/b = 0.98).

C.2 Intermediate Length Vanes (L/b = 0.33)

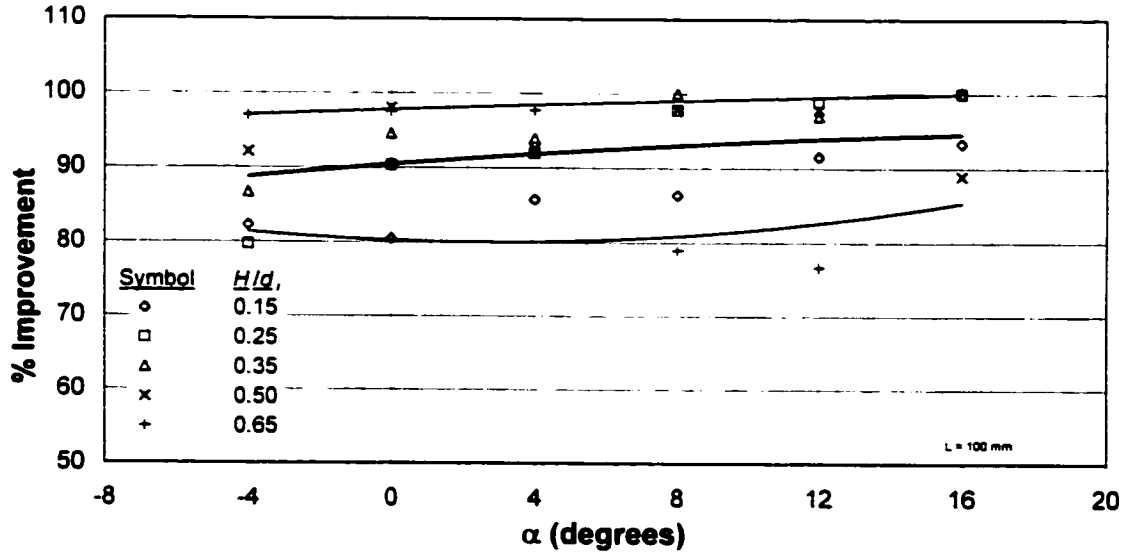

Figure C.4: % Improvement vs. α (L/b = 0.33, δ_j/b = 0.98).

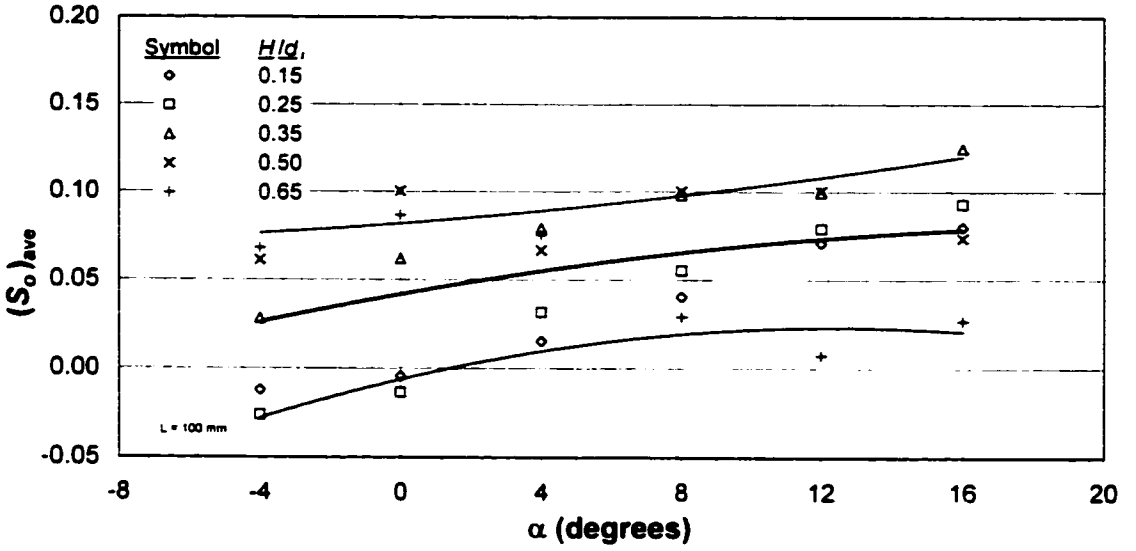

Figure C.5: $(S_o)_{ave}$ vs. α ($L/b = 0.33$, $\delta_i/b = 0.98$).

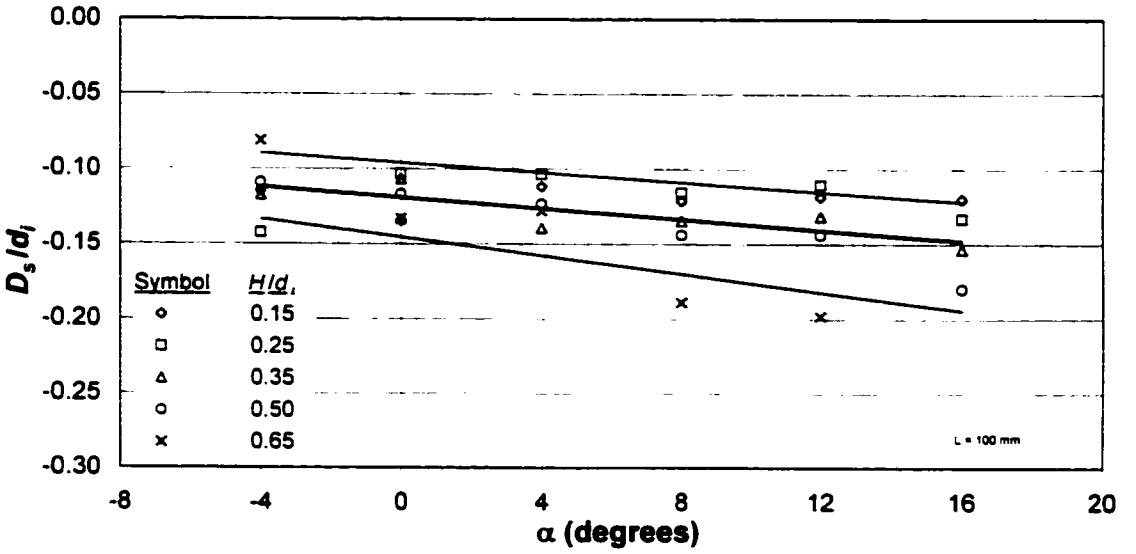

Figure C.6: D_s/d_i vs. α ($L/b = 0.33$, $\delta_i/b = 0.98$).

C.3 Long Vanes (*L*/*b* = 0.49)

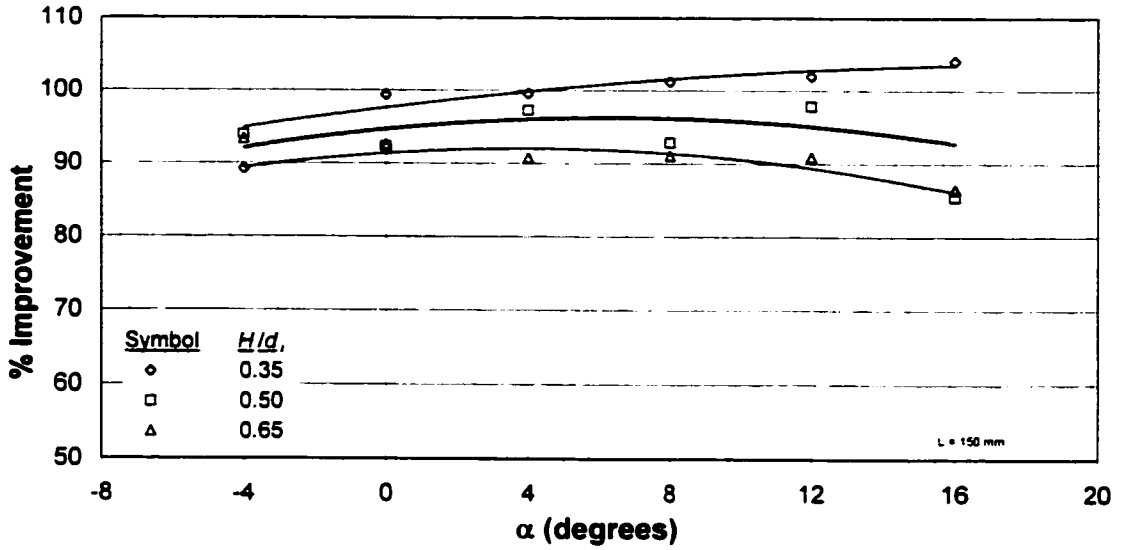

Figure C.7: % Improvement vs. α (*L*/*b* = 0.49, δ_1/b = 0.98).

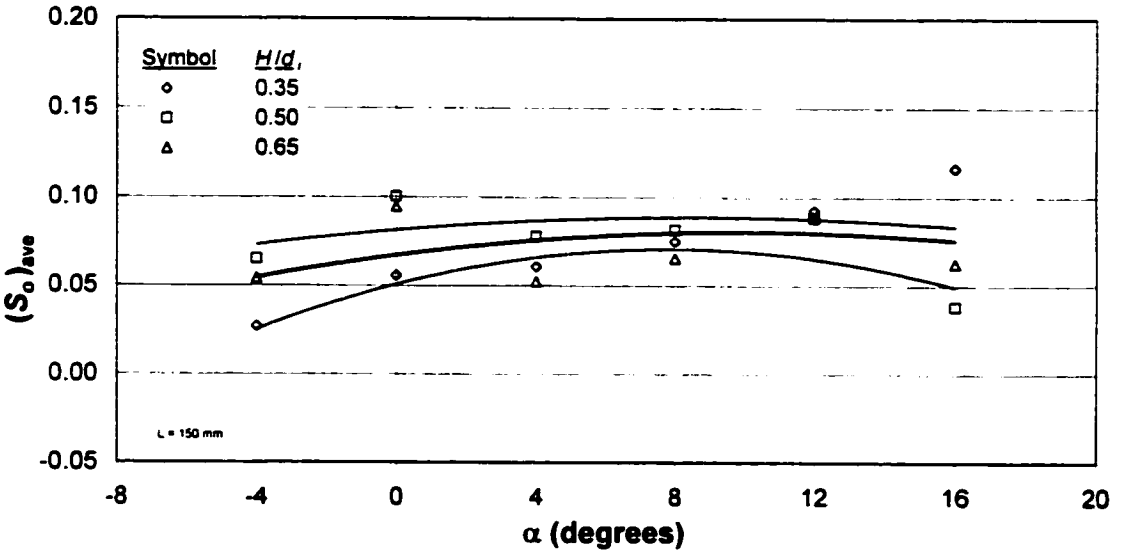

Figure C.8: $(S_o)_{ave}$ vs. α (*L*/*b* = 0.49, δ_1/b = 0.98).

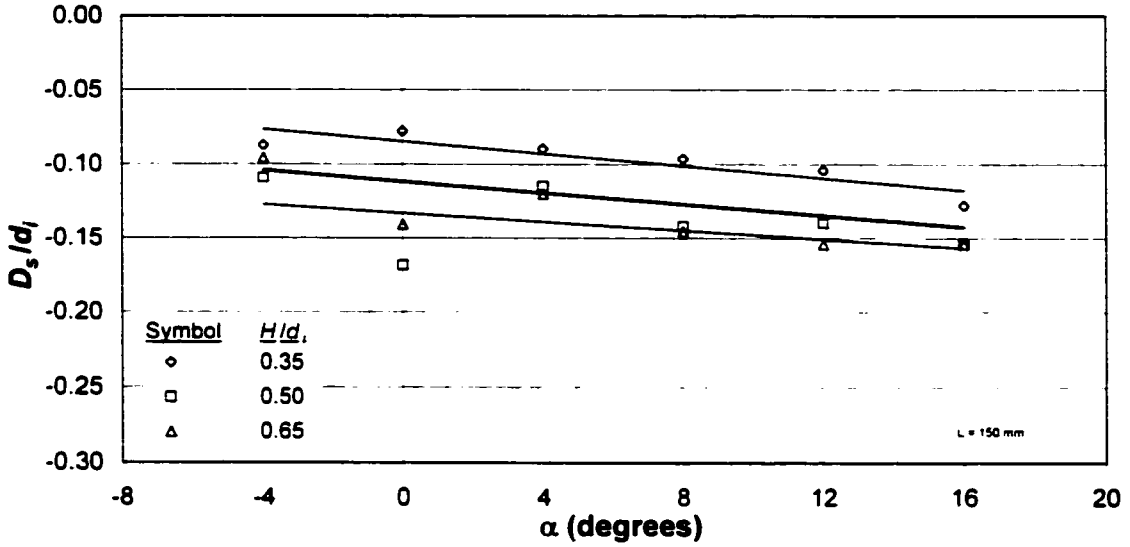

Figure C.9: D_s/d_i vs. α (L/b = 0.49, δ_s/b = 0.98).

C.4 Intermediate Height Vanes (H/d_i = 0.35)

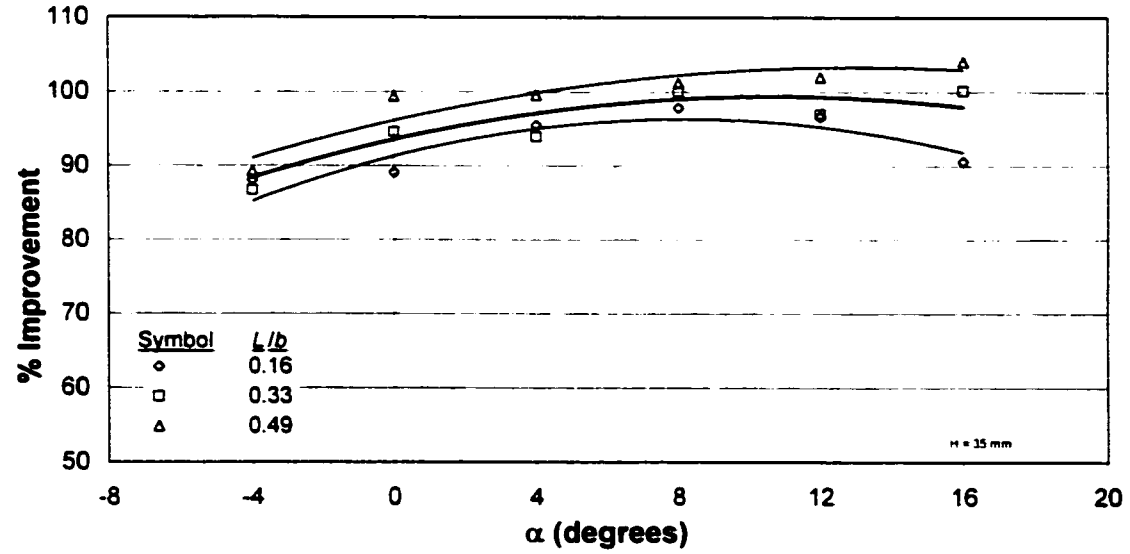

Figure C.10: % Improvement vs. α (H/d_i = 0.35, δ_s/b = 0.98).

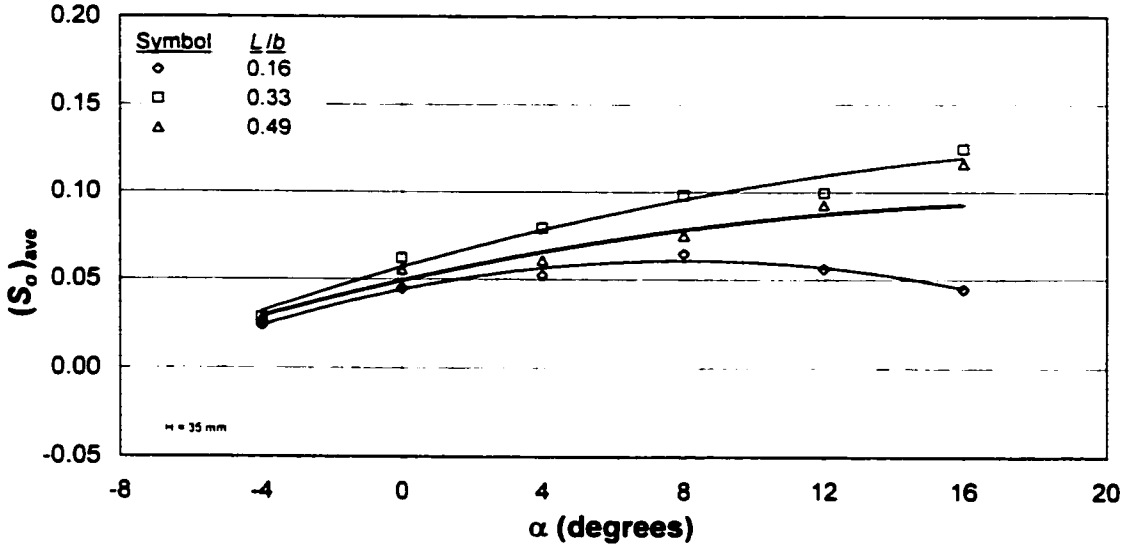

Figure C.11: $(S_o)_{ave}$ vs. α ($H/d_i = 0.35$, $\delta_r/b = 0.98$).

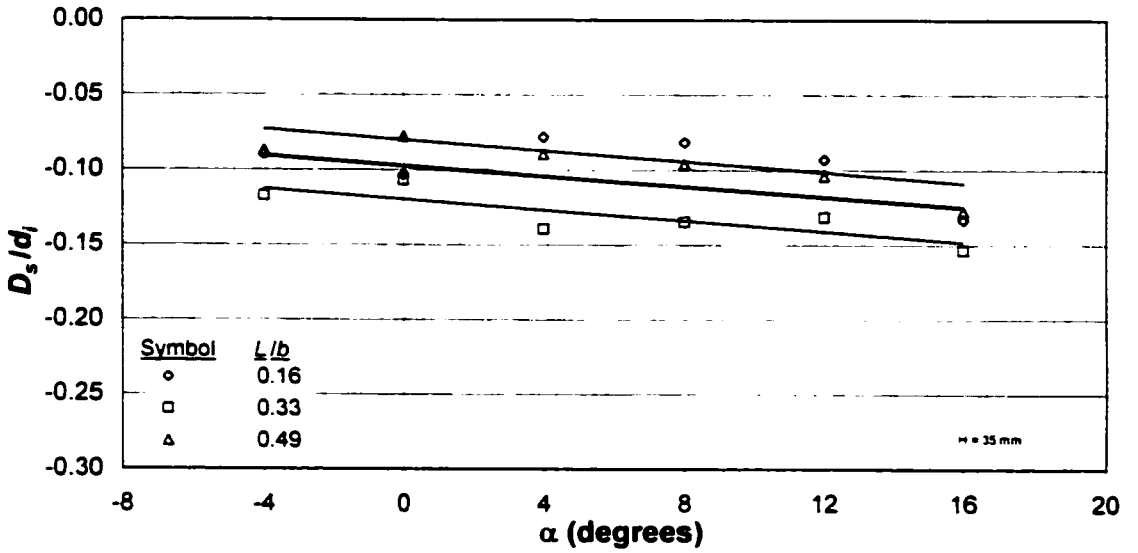

Figure C.12: D_s/d_i vs. α ($H/d_i = 0.35$, $\delta_r/b = 0.98$).

C.5 Intermediate Height Vanes ($H/d_i = 0.50$)

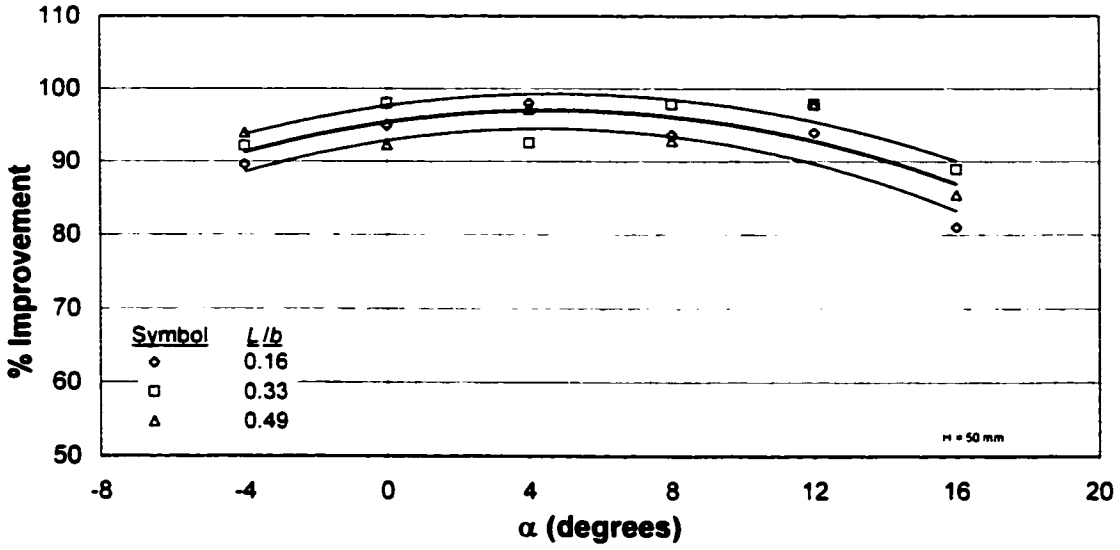

Figure C.13: % Improvement vs. α ($H/d_i = 0.50$, $\delta_r/b = 0.98$).

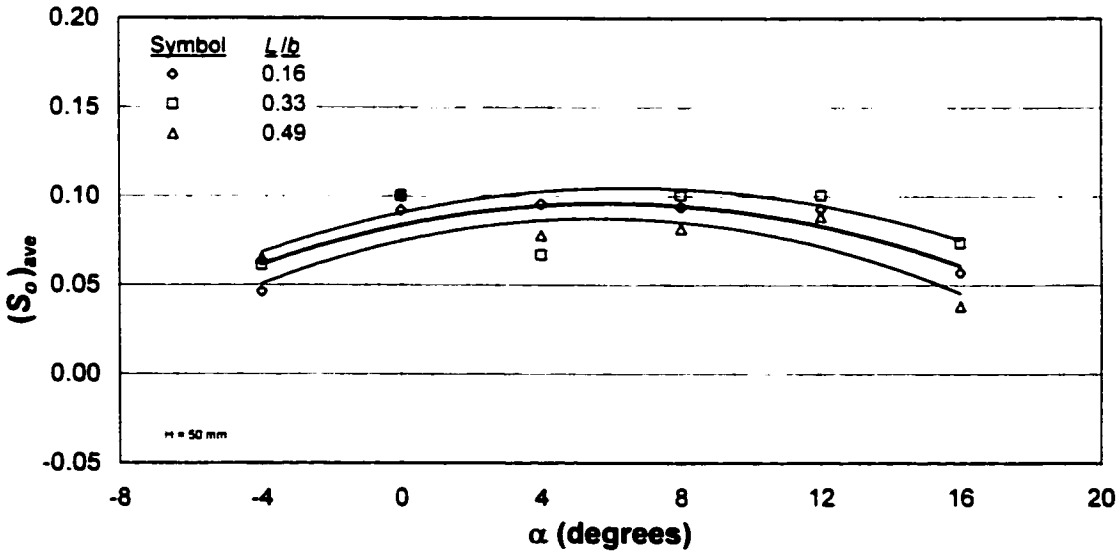

Figure C.14: $(S_o)_{ave}$ vs. α ($H/d_i = 0.50$, $\delta_r/b = 0.98$).

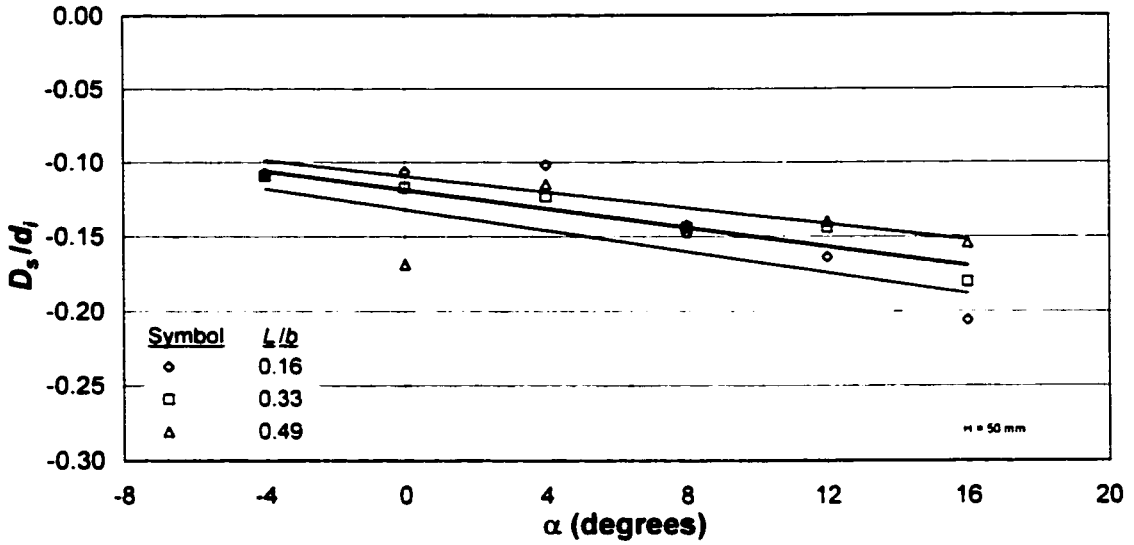

Figure C.15: D_s/d_i vs. α ($H/d_i = 0.50$, $\delta_s/b = 0.98$).

C.6 Tall Vanes ($H/d_i = 0.65$)

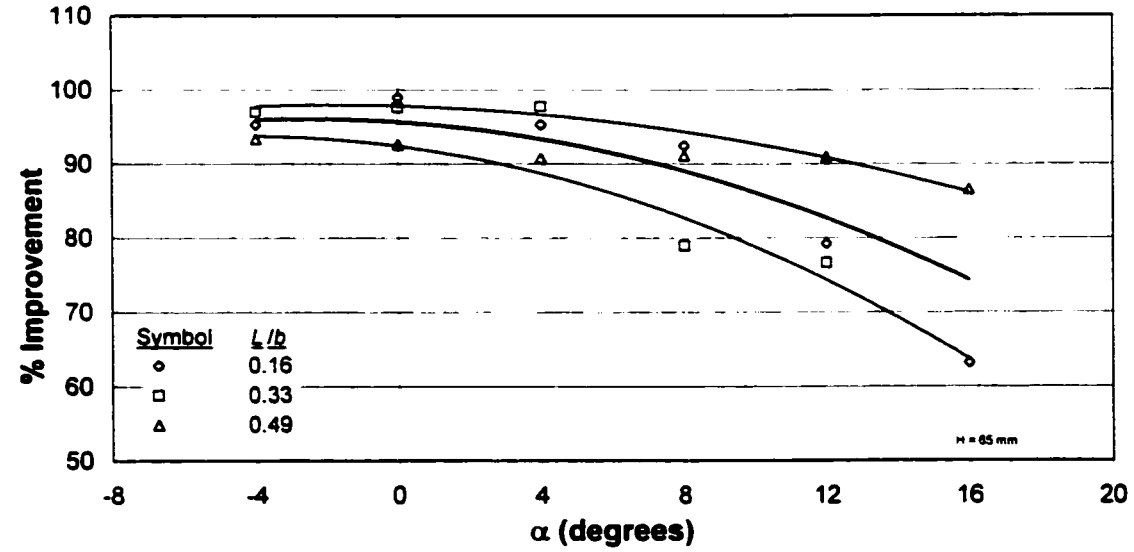

Figure C.16: % Improvement vs. α ($H/d_i = 0.65$, $\delta_s/b = 0.98$).

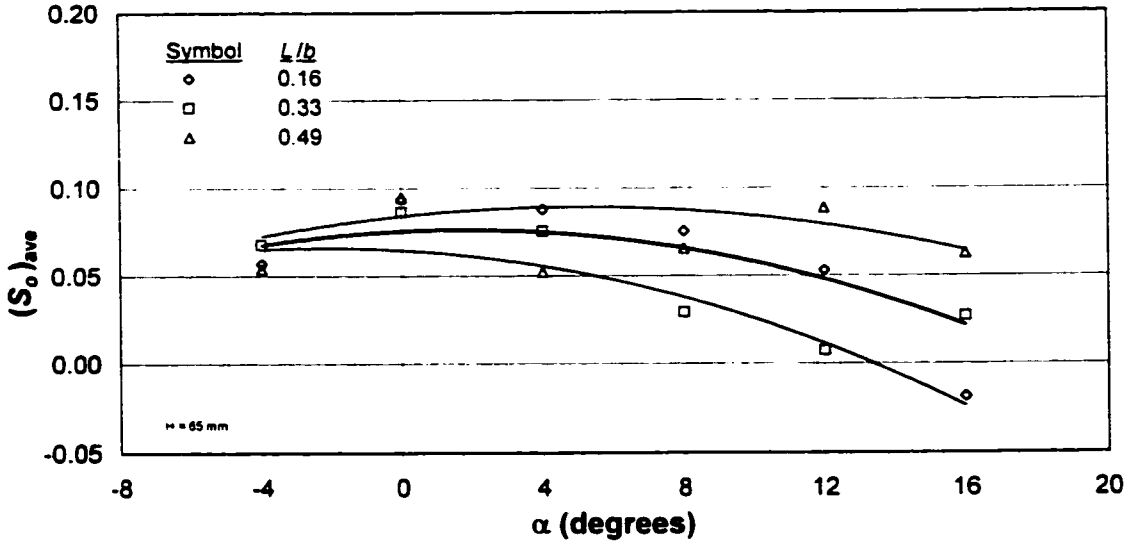

Figure C.17: $(S_o)_{ave}$ vs. α ($H/d_i = 0.65$, $\delta_s/b = 0.98$).

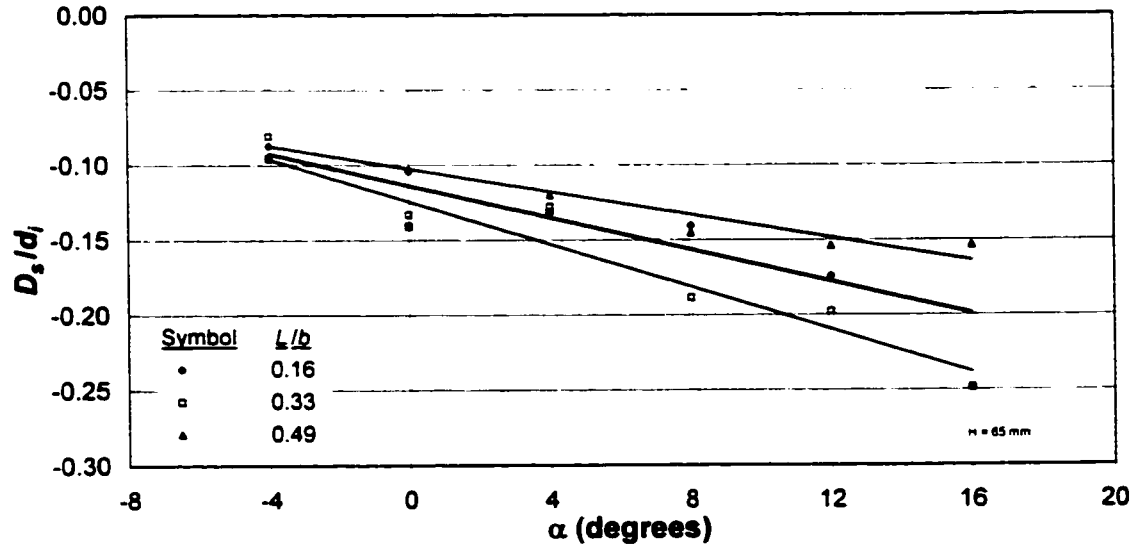

Figure C.18: D_s/d_i vs. α ($H/d_i = 0.65$, $\delta_s/b = 0.98$).

APPENDIX D

EFFECT OF VANE STREAMWISE SPACING (90° BEND)

D.1 Narrow Vanes (*L/b* = 0.16)

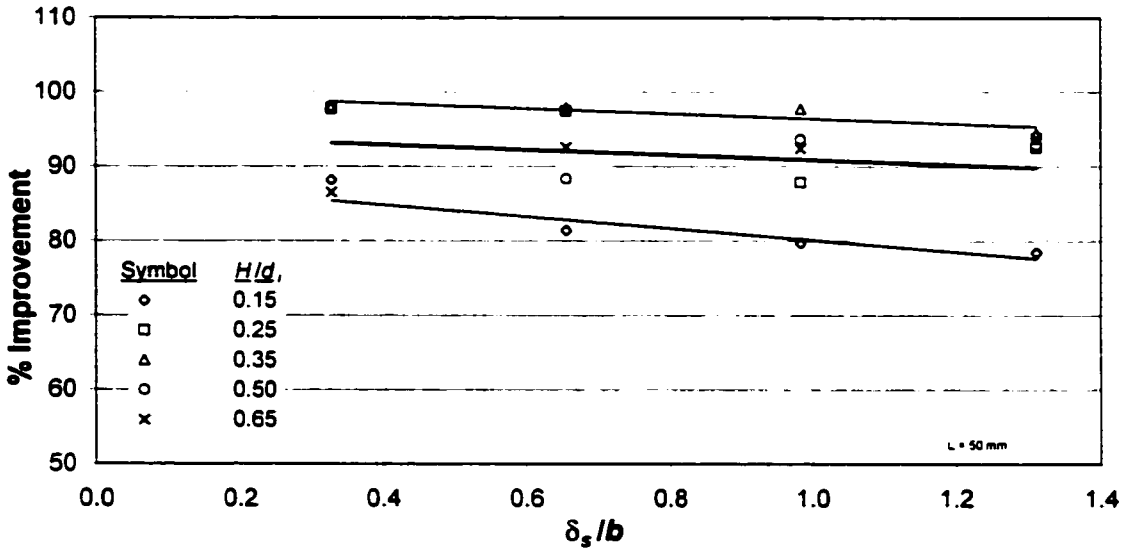

Figure D.1: % Improvement vs. δ_s/b ($L/b = 0.16$, $\alpha = 8°$).

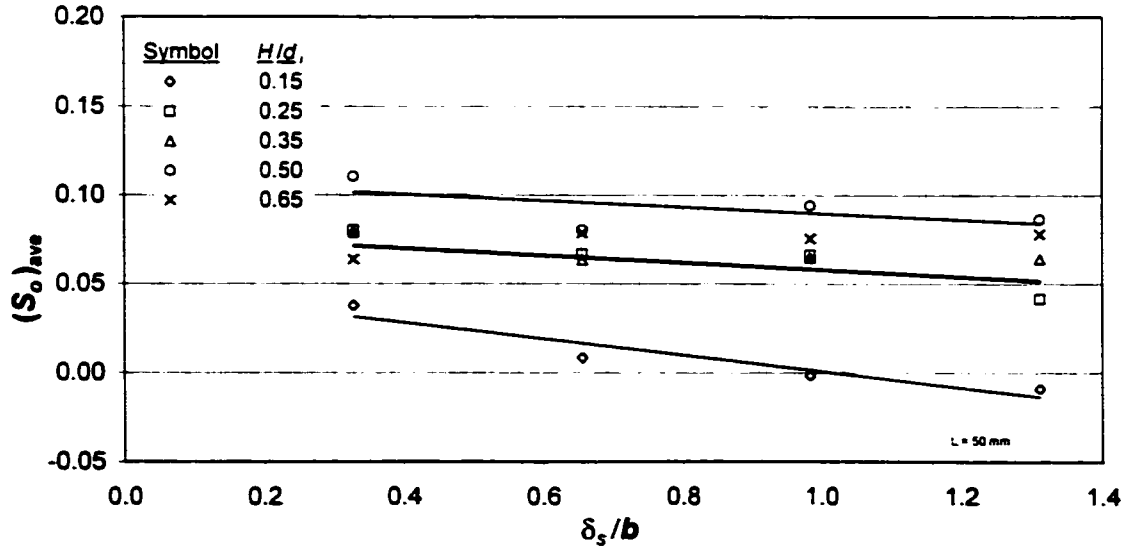

Figure D.2: $(S_o)_{ave}$ vs. δ_s/b ($L/b = 0.16$, $\alpha = 8°$).

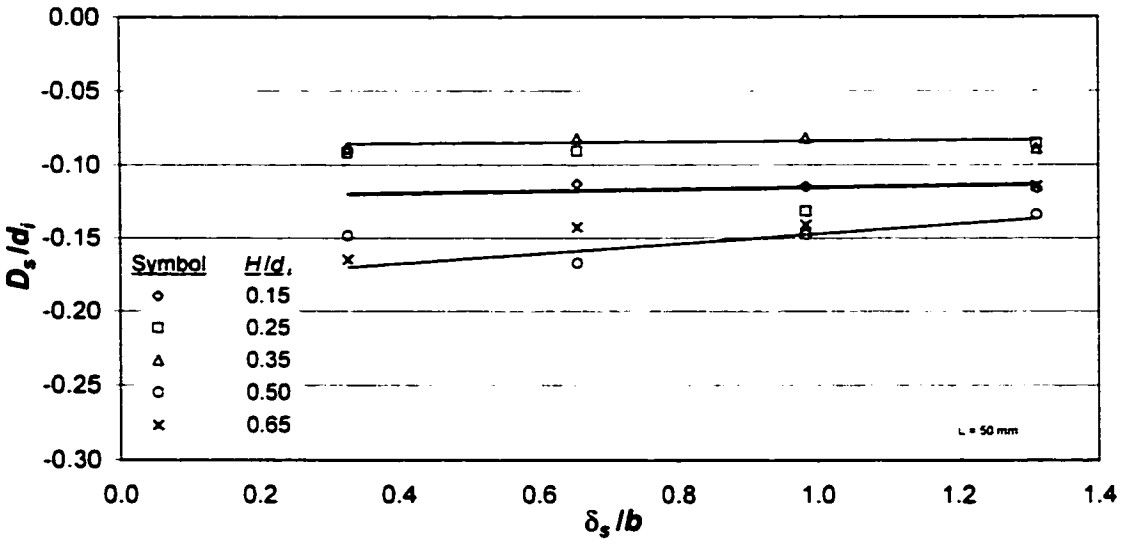

Figure D.3: D_s/d_i vs. δ_s/b ($L/b = 0.16$, $\alpha = 8°$).

D.2 Intermediate Length Vanes ($L/b = 0.33$)

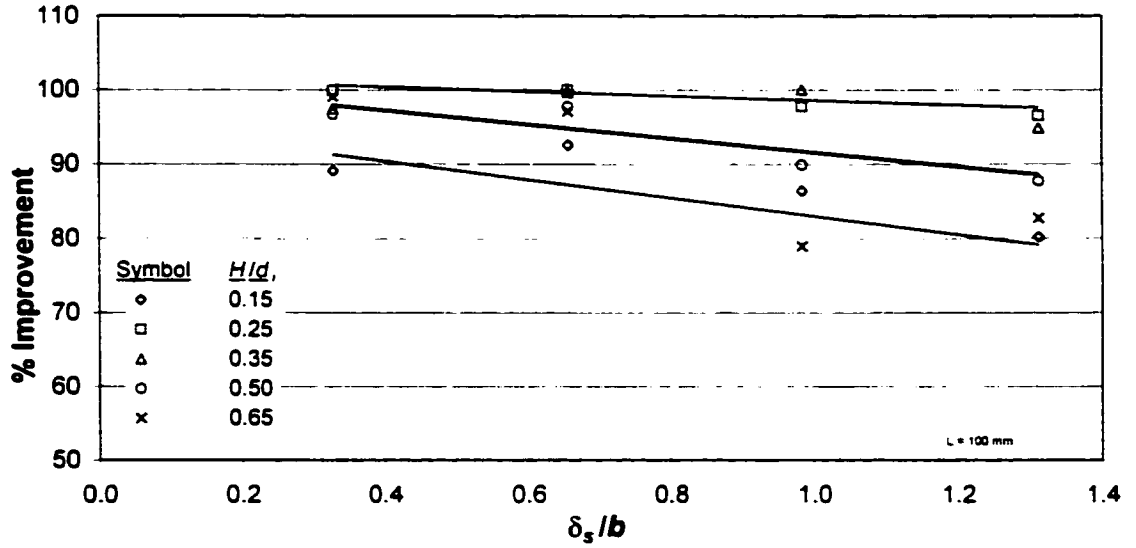

Figure D.4: % Improvement vs. δ_s/b ($L/b = 0.33$, $\alpha = 8°$).

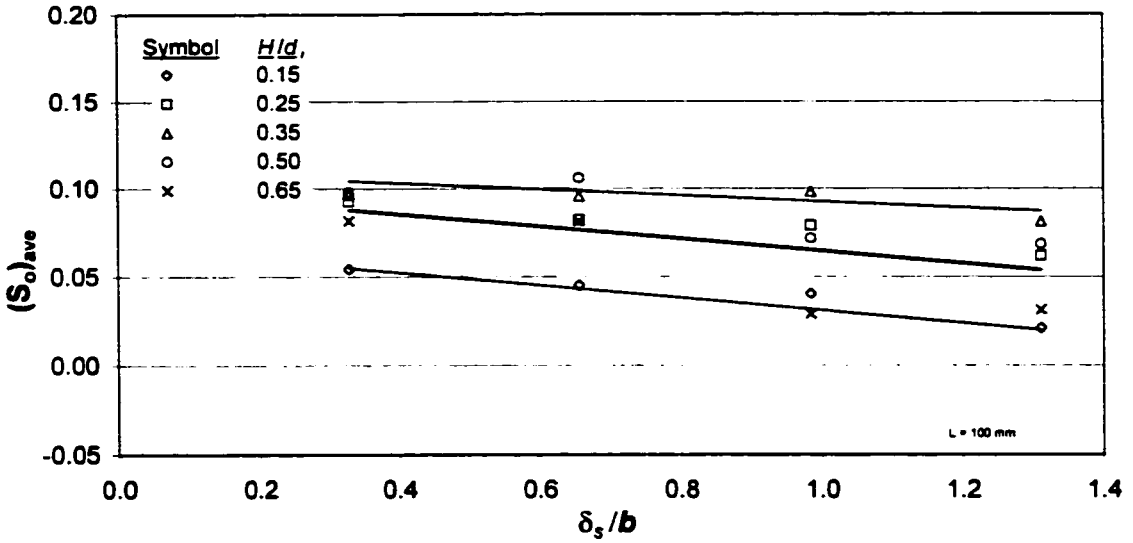

Figure D.5: $(S_o)_{ave}$ vs. δ_s/b ($L/b = 0.33$, $\alpha = 8°$).

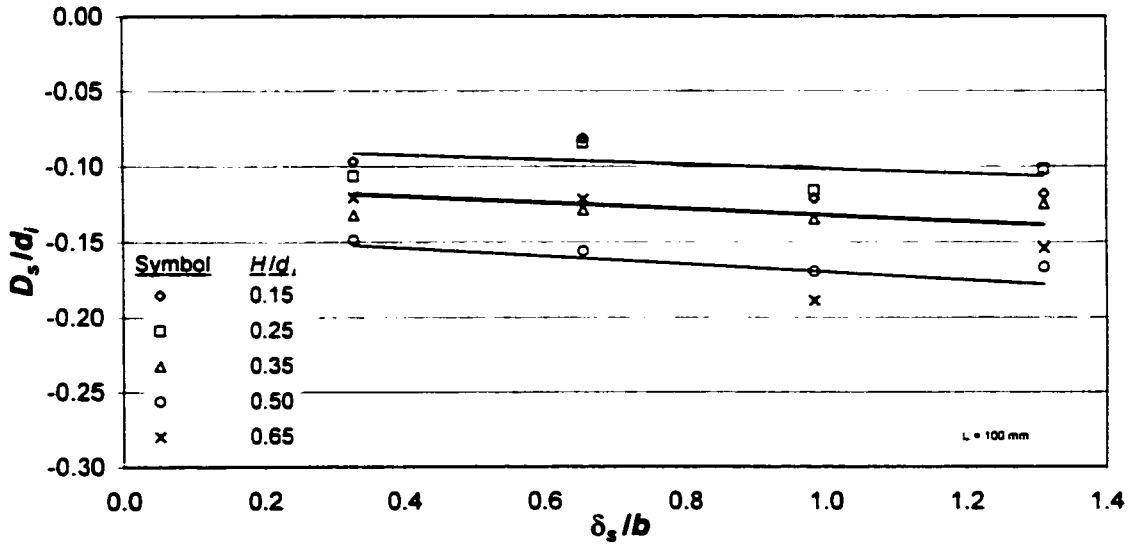

Figure D.6: D_s/d_i vs. δ_s/b ($L/b = 0.33$, $\alpha = 8°$).

D.3 Long Vanes (*L/b* = 0.49)

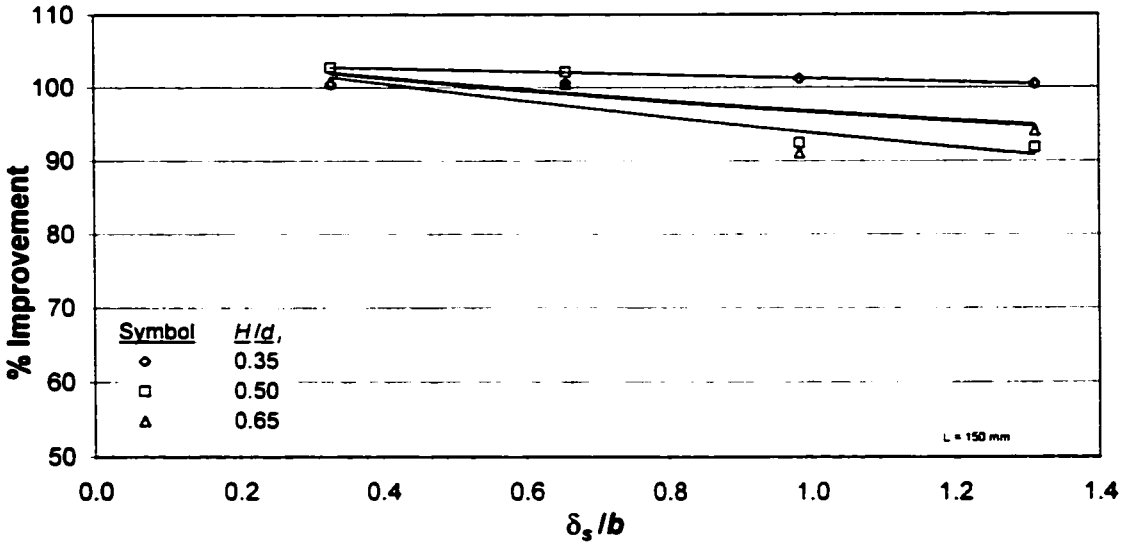

Figure D.7: % Improvement vs. δ_s/b ($L/b = 0.49$, $\alpha = 8°$).

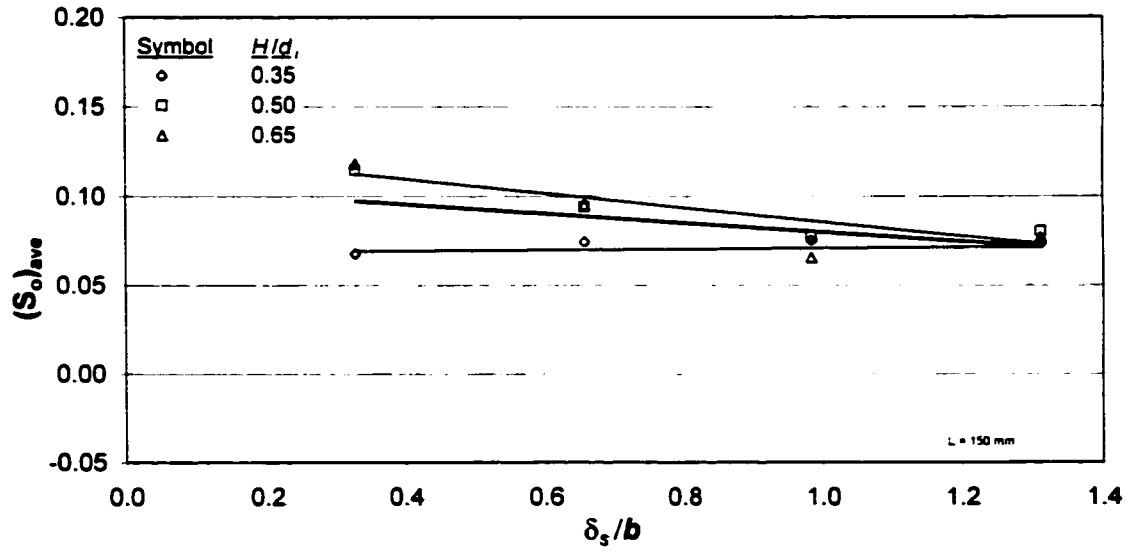

Figure D.8: $(S_o)_{ave}$ vs. δ_s/b ($L/b = 0.49$, $\alpha = 8°$).

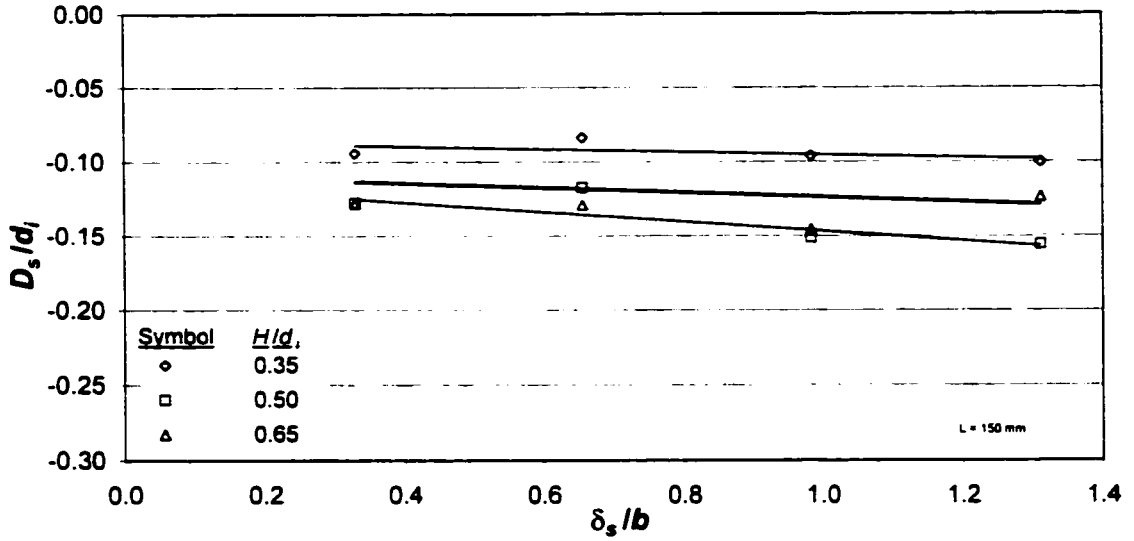

Figure D.9: D_s/d_i vs. δ_s/b ($L/b = 0.49$, $\alpha = 8°$).

D.4 Intermediate Height Vanes ($H/d_i = 0.35$)

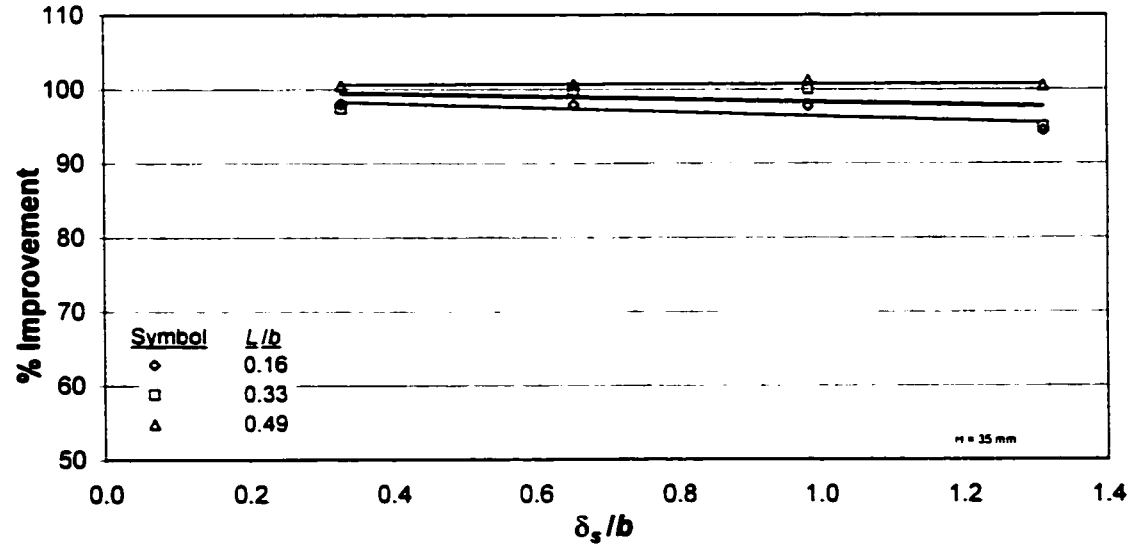

Figure D.10: % Improvement vs. δ_s/b ($H/d_i = 0.35$, $\alpha = 8°$).

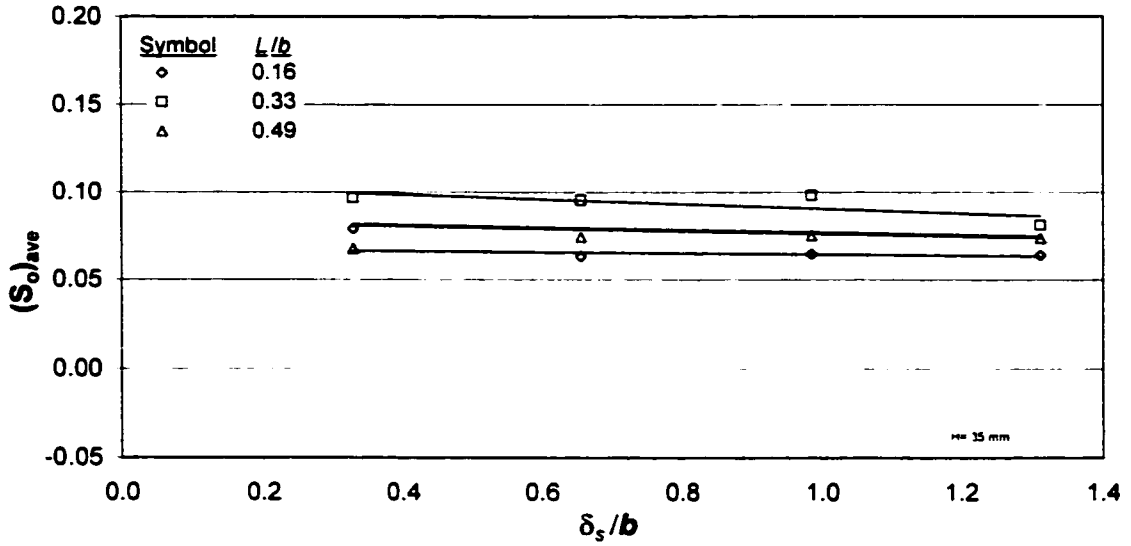

Figure D.11: $(S_o)_{ave}$ vs. δ_s/b ($H/d_t = 0.35$, $\alpha = 8°$).

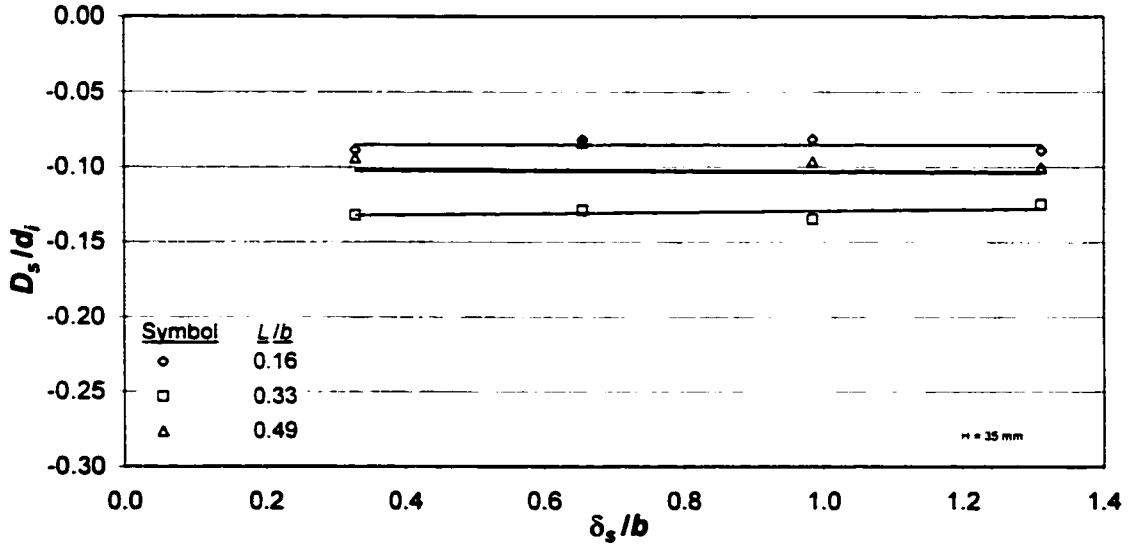

Figure D.12: D_s/d_t vs. δ_s/b ($H/d_t = 0.35$, $\alpha = 8°$).

D.5 Intermediate Height Vanes (H/d_i = 0.50)

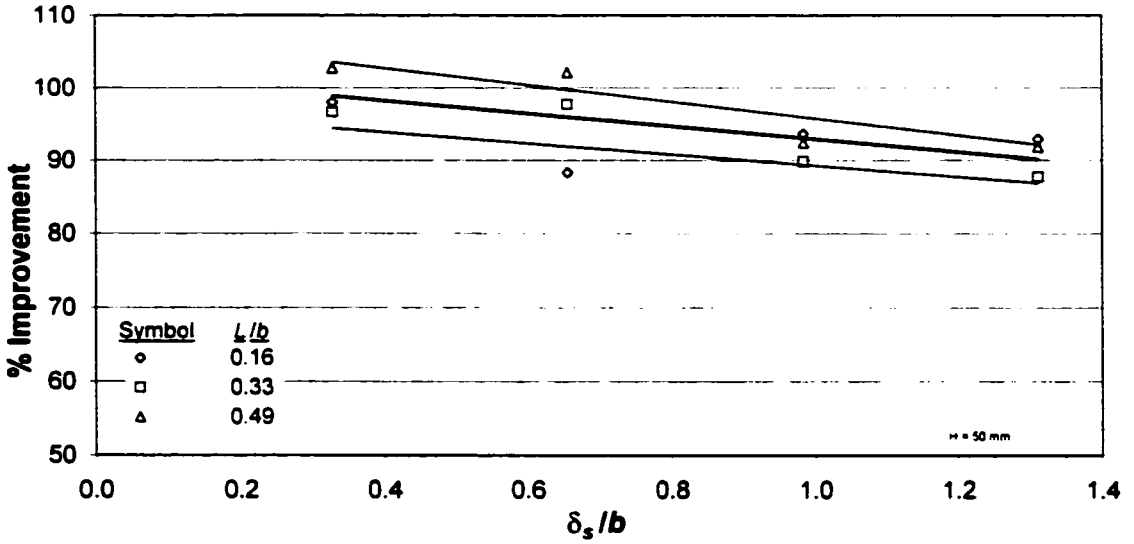

Figure D.13: % Improvement vs. δ_s/b (H/d_i = 0.50, $\alpha = 8°$).

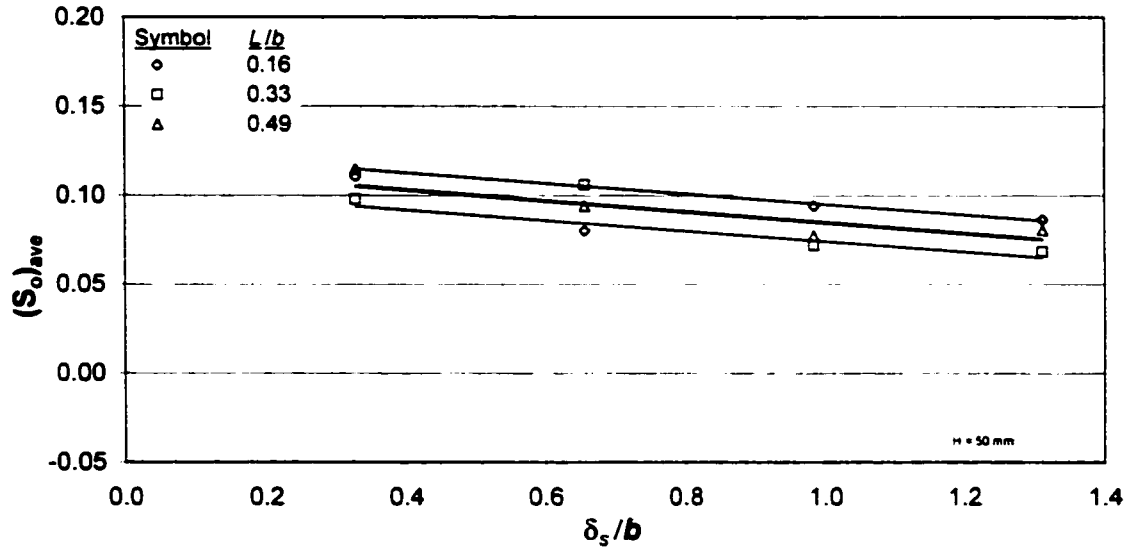

Figure D.14: $(S_o)_{ave}$ vs. δ_s/b (H/d_i = 0.50, $\alpha = 8°$).

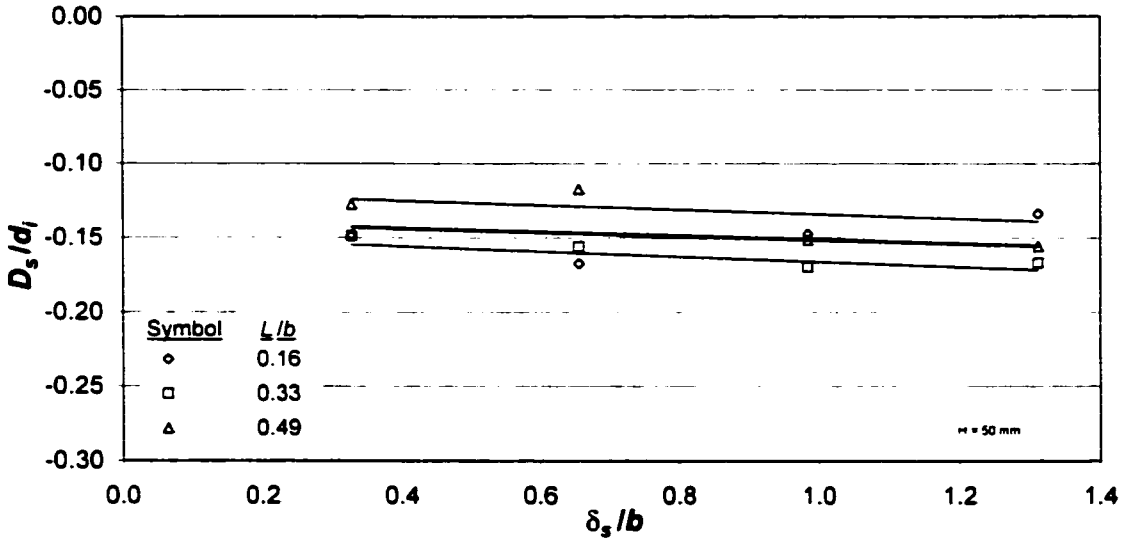

Figure D.15: D_s/d_i vs. δ_s/b ($H/d_i = 0.50$, $\alpha = 8°$).

D.6 Tall Vanes ($H/d_i = 0.65$)

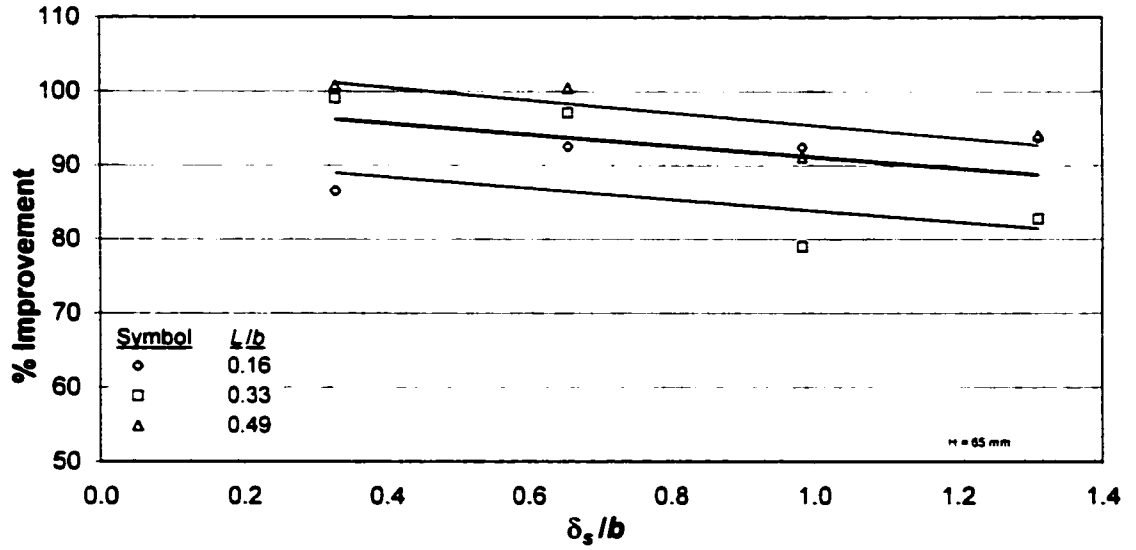

Figure D.16: % Improvement vs. δ_s/b ($H/d_i = 0.65$, $\alpha = 8°$).

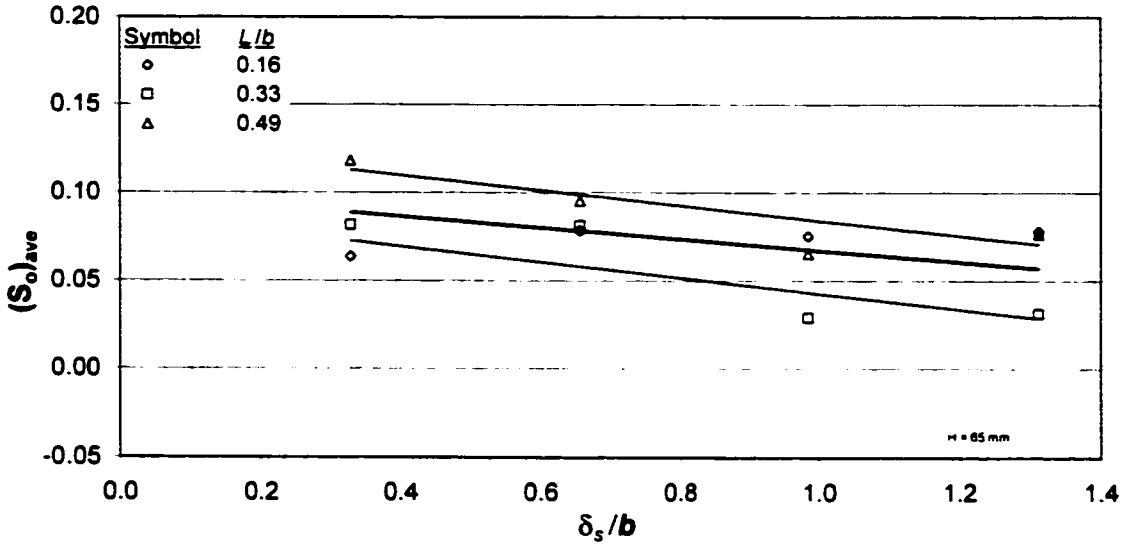

Figure D.17: $(S_o)_{ave}$ vs. δ_s/b ($H/d_j = 0.65$, $\alpha = 8°$).

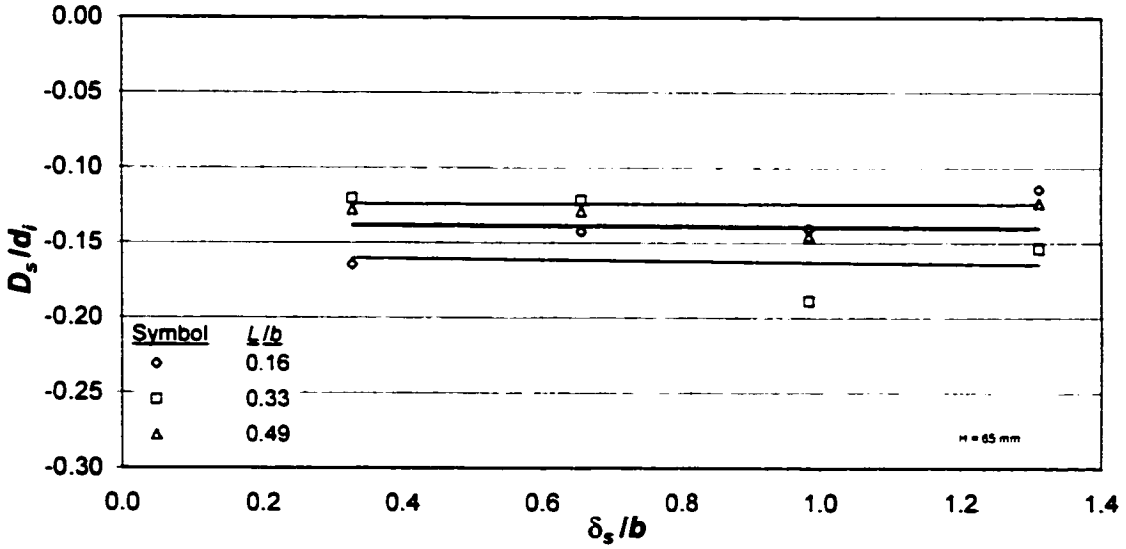

Figure D.18: D_s/d_j vs. δ_s/b ($H/d_j = 0.65$, $\alpha = 8°$).

APPENDIX E

EFFECT OF BEND ANGLE (135°)

E.1 Outer Bank Scour Depth (% Improvement)

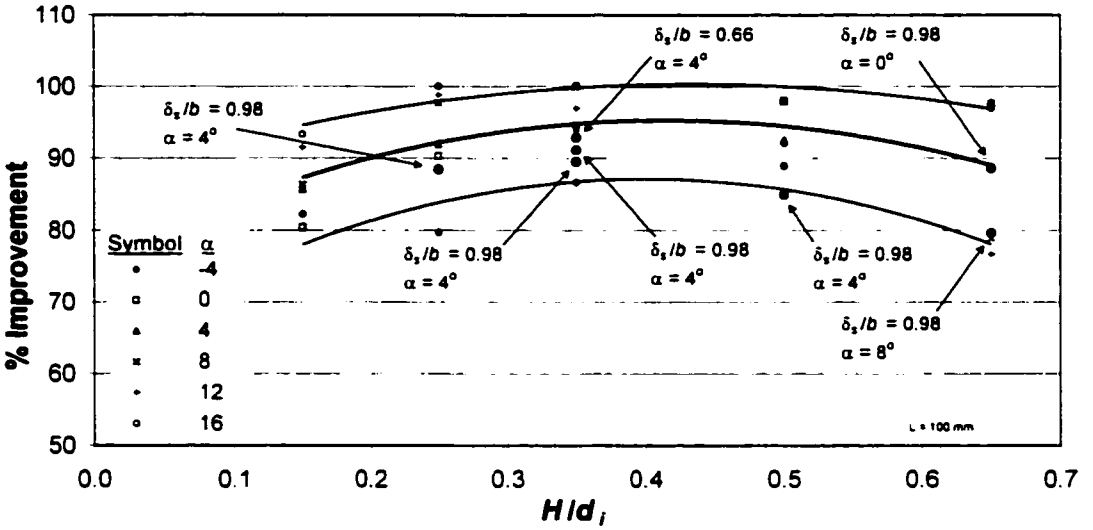

Figure E.1: % Improvement vs. H/d_i for 90° bend with 135° bend data plotted thereon ($L/b = 0.33$, $\delta_s/b = 0.98$).

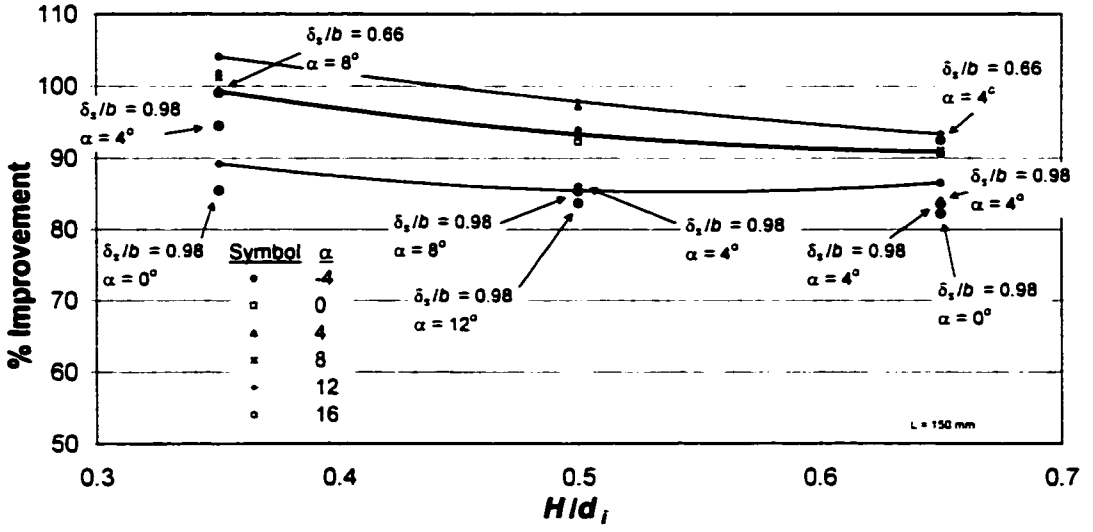

Figure E.2: % Improvement vs. H/d_i for 90° bend with 135° bend data plotted thereon ($L/b = 0.49$, $\delta_s/b = 0.98$).

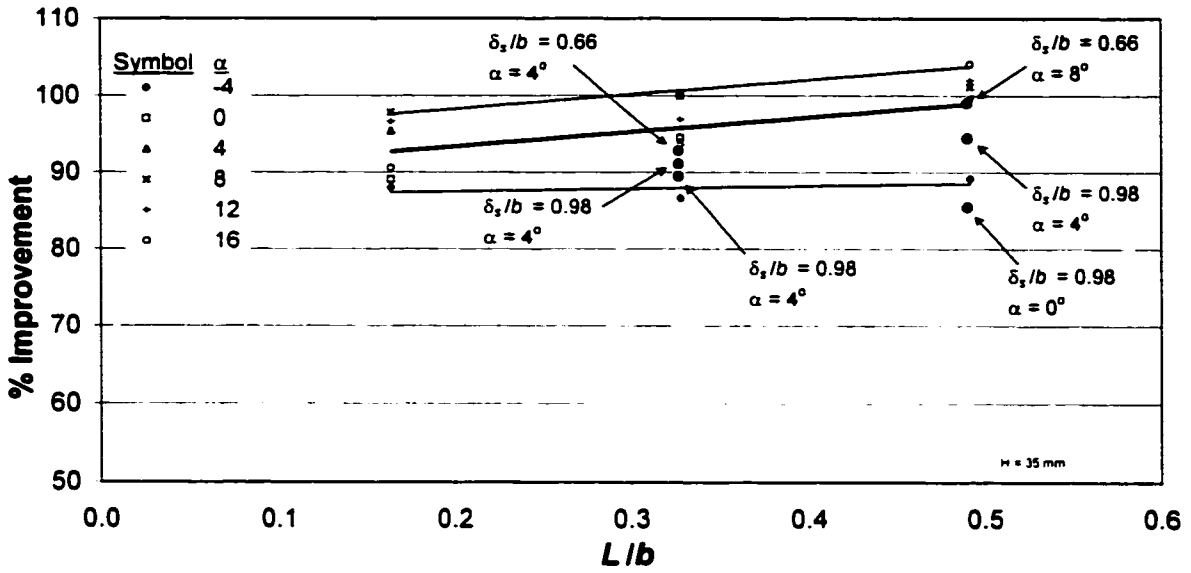

Figure E.3: % Improvement vs. L/b for 90° bend with 135° bend data plotted thereon (H/d_i = 0.35, $\delta_s/b = 0.98$).

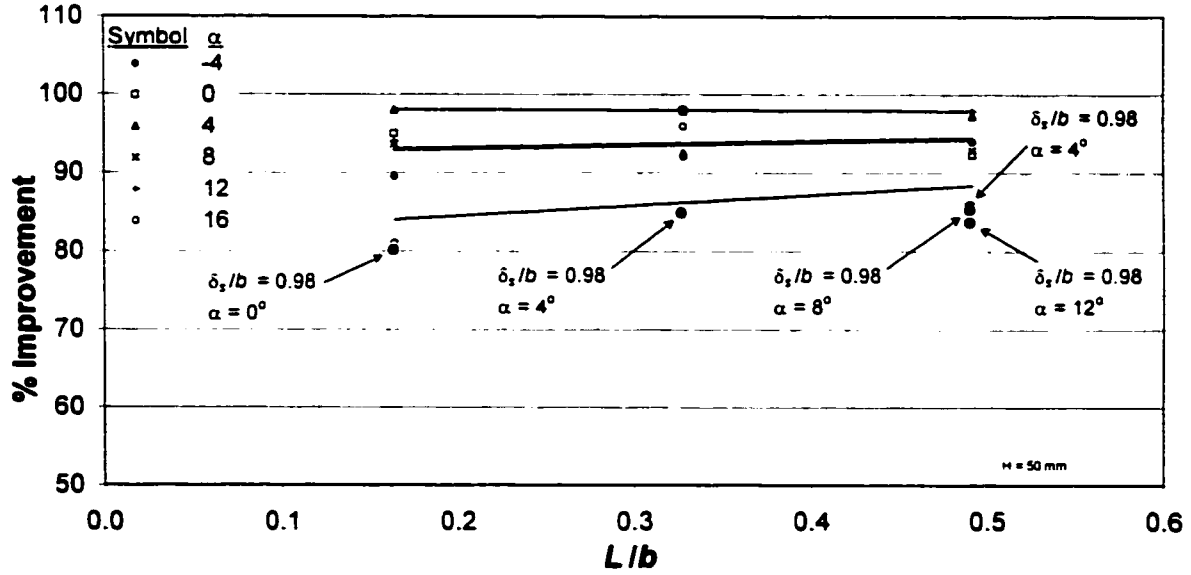

Figure E.4: % Improvement vs. L/b for 90° bend with 135° bend data plotted thereon (H/d_i = 0.50, $\delta_s/b = 0.98$).

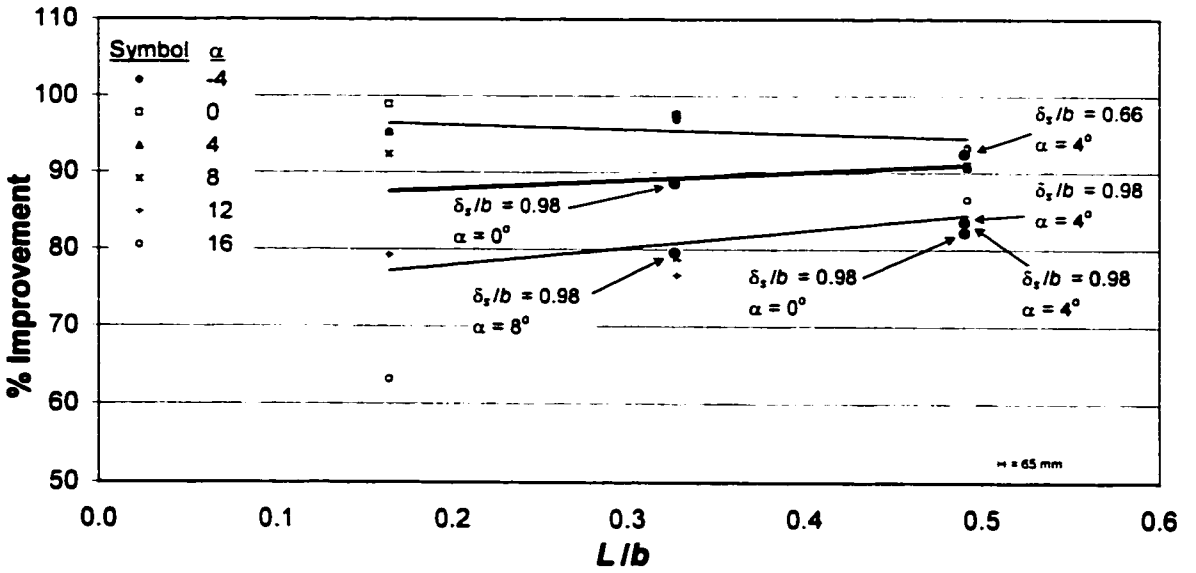

Figure E.5: % Improvement vs. L/b for 90° bend with 135° bend data plotted thereon (H/d_i = 0.65, δ_s/b = 0.98).

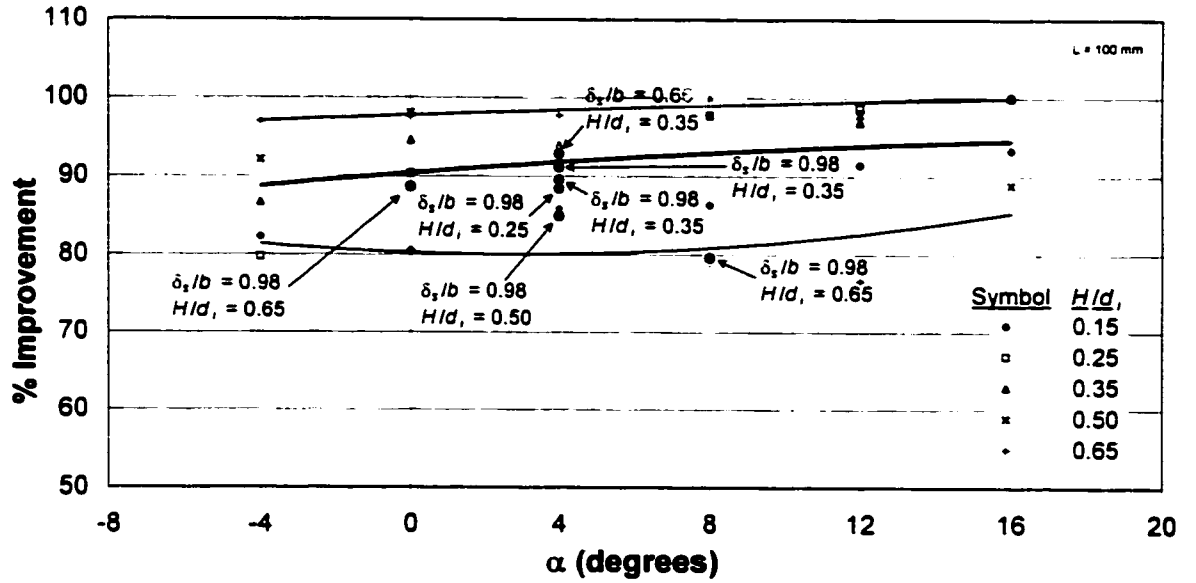

Figure E.6: % Improvement vs. α for 90° bend with 135° bend data plotted thereon (L/b = 0.33, δ_s/b = 0.98).

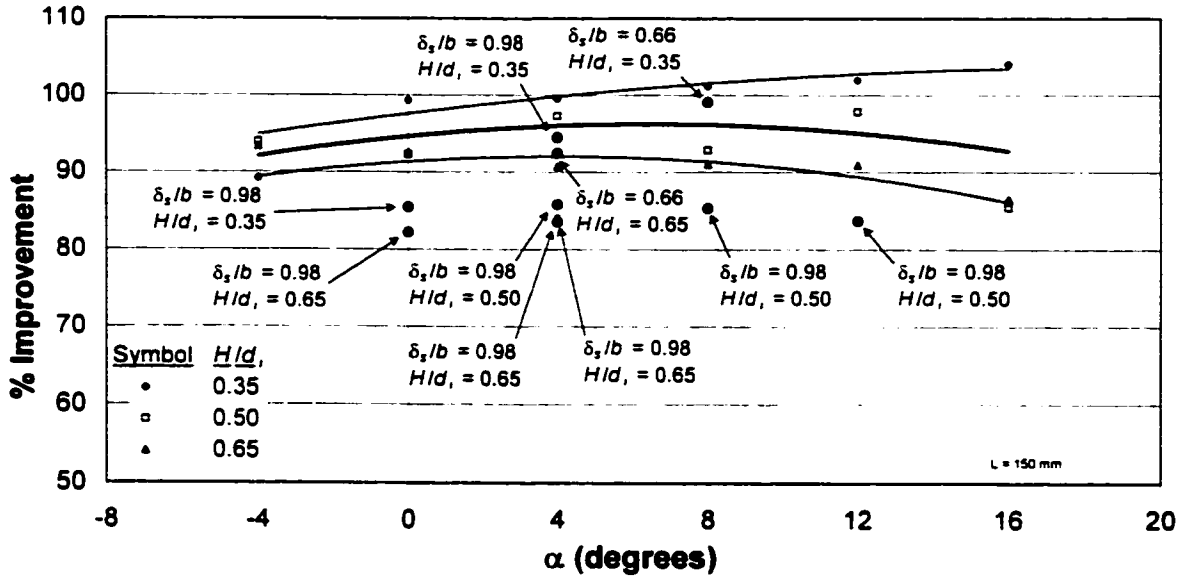

Figure E.7: % Improvement vs. α for 90° bend with 135° bend data plotted thereon ($L/b = 0.49$, $\delta_s/b = 0.98$).

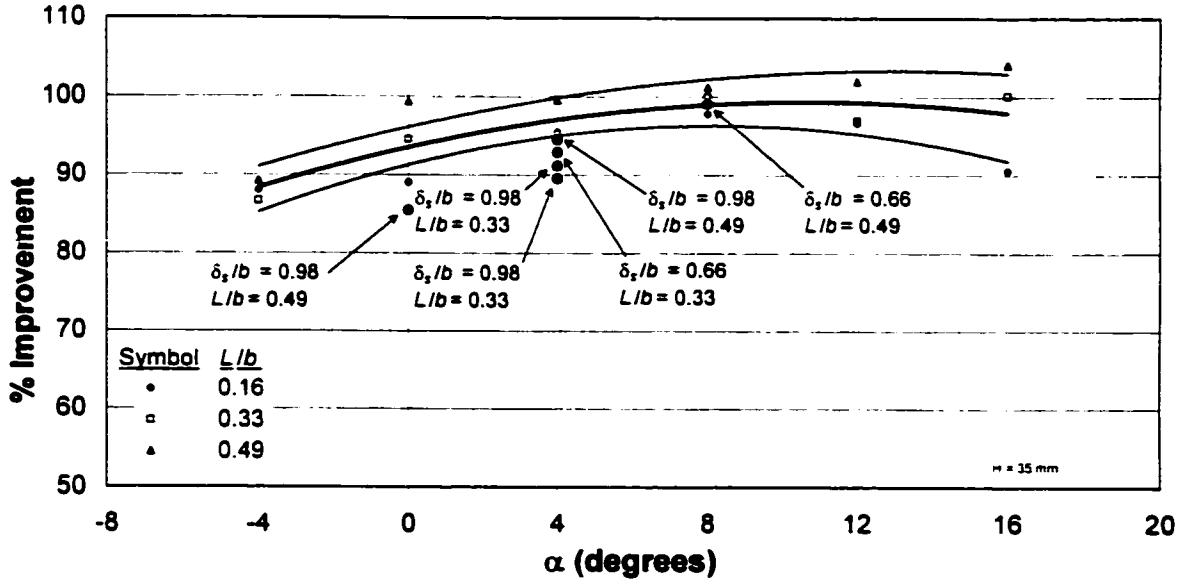

Figure E.8: % Improvement vs. α for 90° bend with 135° bend data plotted thereon ($H/d_s = 0.35$, $\delta_s/b = 0.98$).

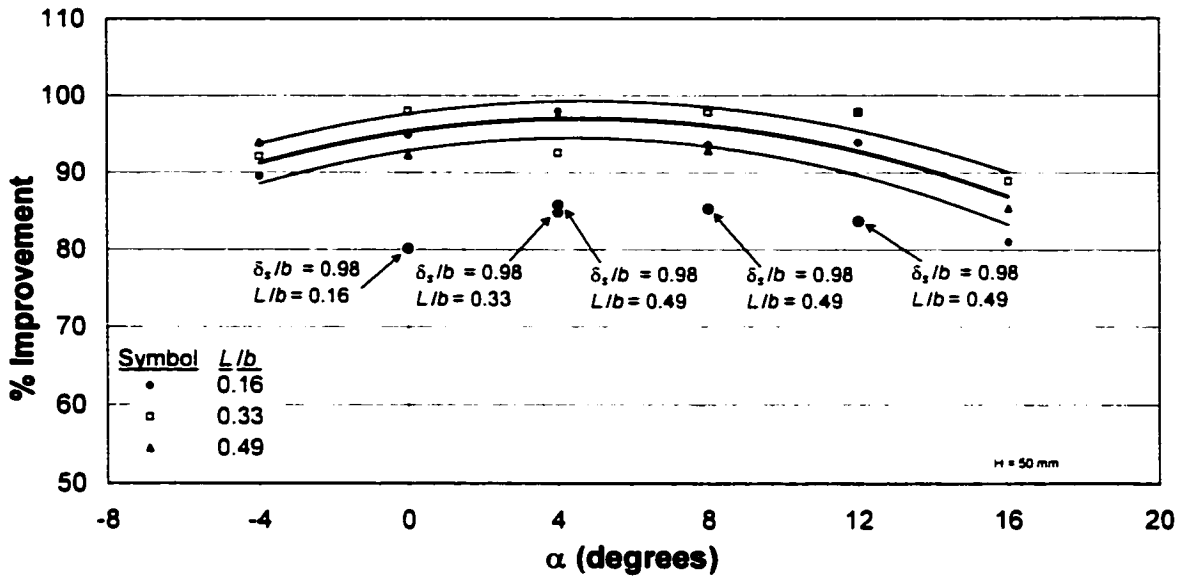

Figure E.9: % Improvement vs. α for 90° bend with 135° bend data plotted thereon ($H/d_t = 0.50$, $\delta_s/b = 0.98$).

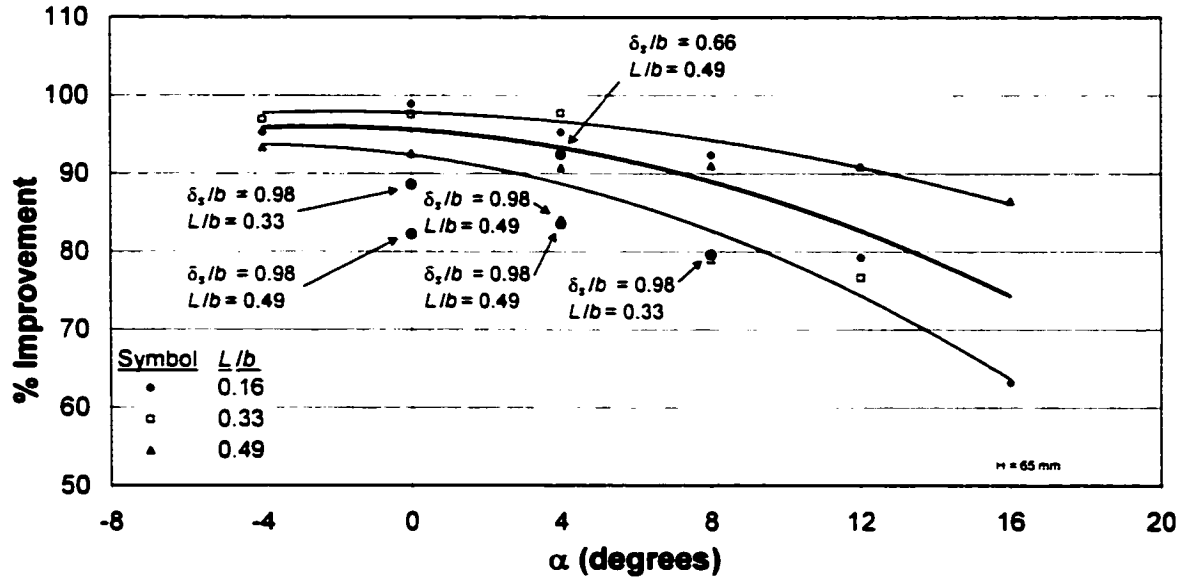

Figure E.10: % Improvement vs. α for 90° bend with 135° bend data plotted thereon ($H/d_t = 0.65$, $\delta_s/b = 0.98$).

E.2 Outer Bank Transverse Bed Slope ($(S_o)_{ave}$)

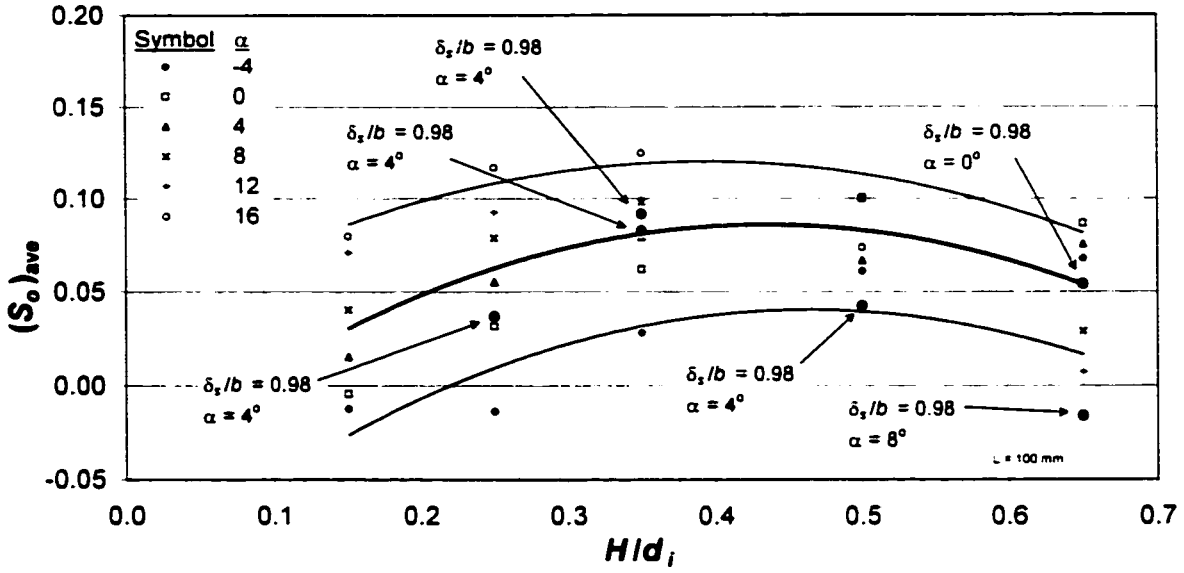

Figure E.11: $(S_o)_{ave}$ vs. H/d_i for 90° bend with 135° bend data plotted thereon (L/b = 0.33, δ_s/b = 0.98).

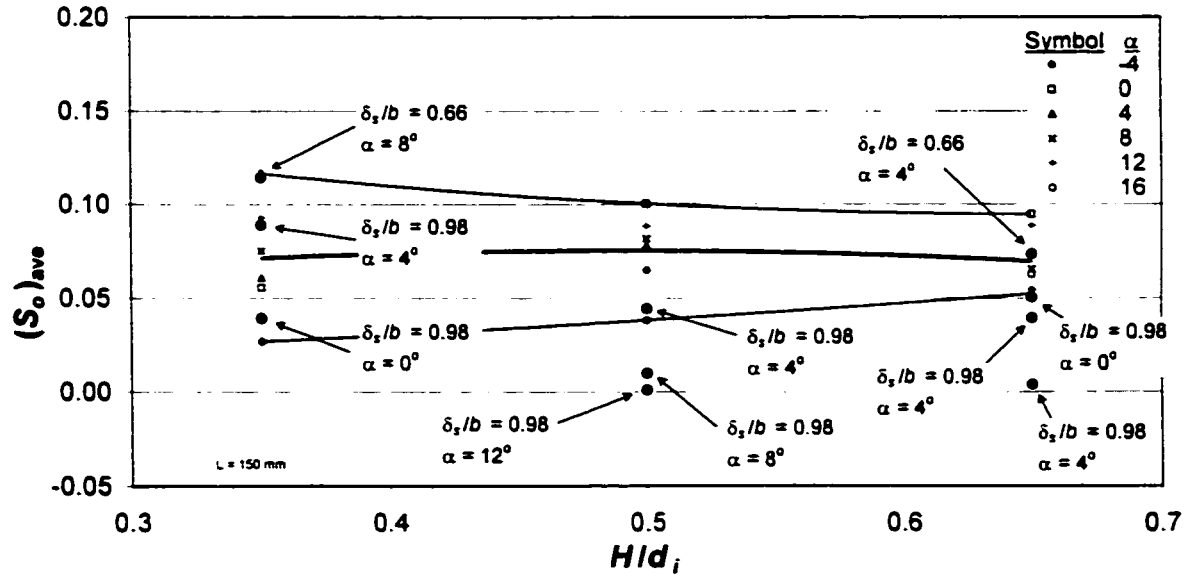

Figure E.12: $(S_o)_{ave}$ vs. H/d_i for 90° bend with 135° bend data plotted thereon (L/b = 0.49, δ_s/b = 0.98).

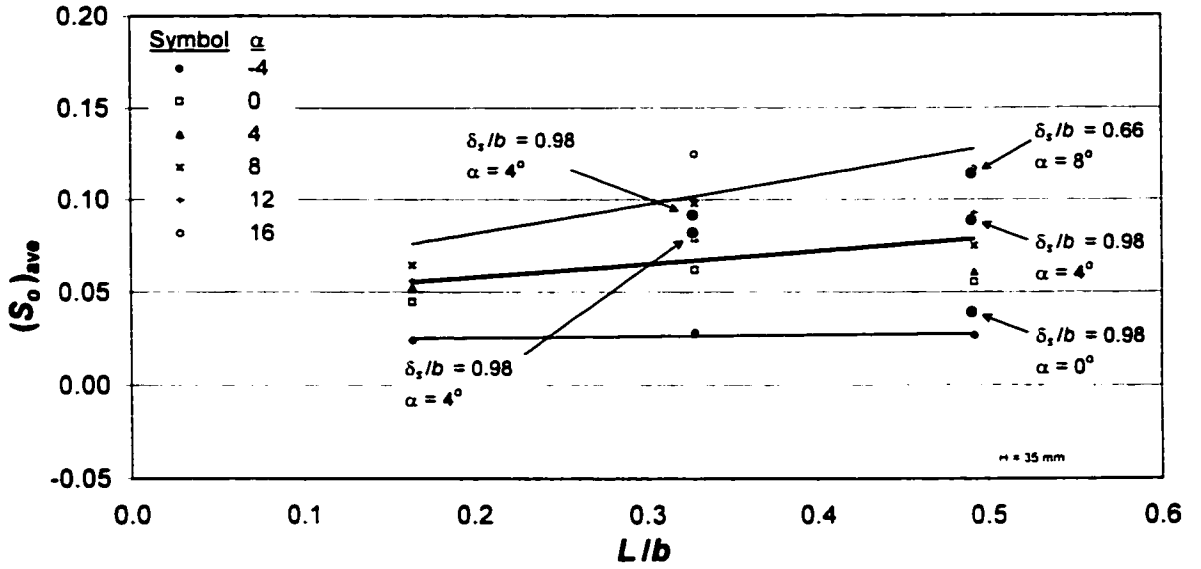

Figure E.13: $(S_o)_{ave}$ vs. L/b for 90° bend with 135° bend data plotted thereon ($H/d_t = 0.35$, $\delta_s/b = 0.98$).

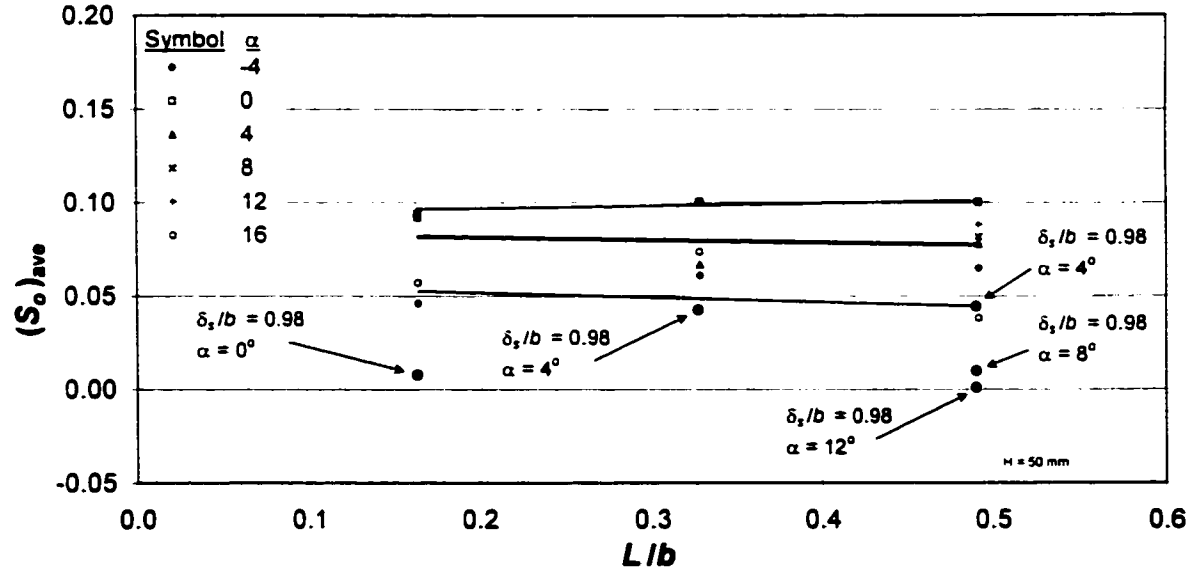

Figure E.14: $(S_o)_{ave}$ vs. L/b for 90° bend with 135° bend data plotted thereon ($H/d_t = 0.50$, $\delta_s/b = 0.98$).

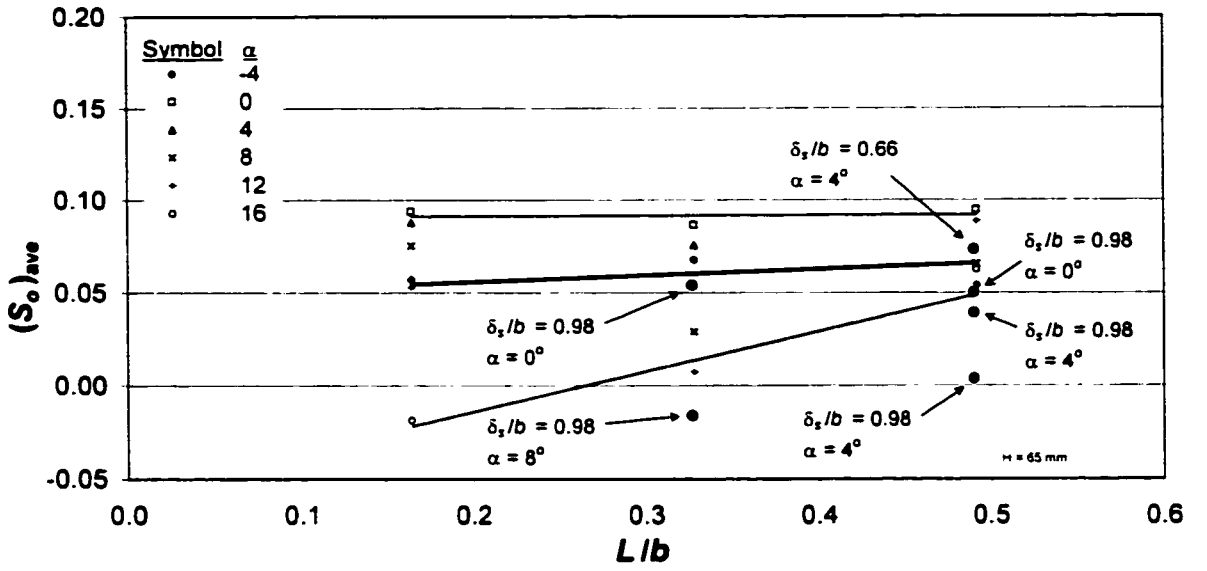

Figure E.15: $(S_o)_{ave}$ vs. L/b for 90° bend with 135° bend data plotted thereon ($H/d_i = 0.65$, $\delta_s/b = 0.98$).

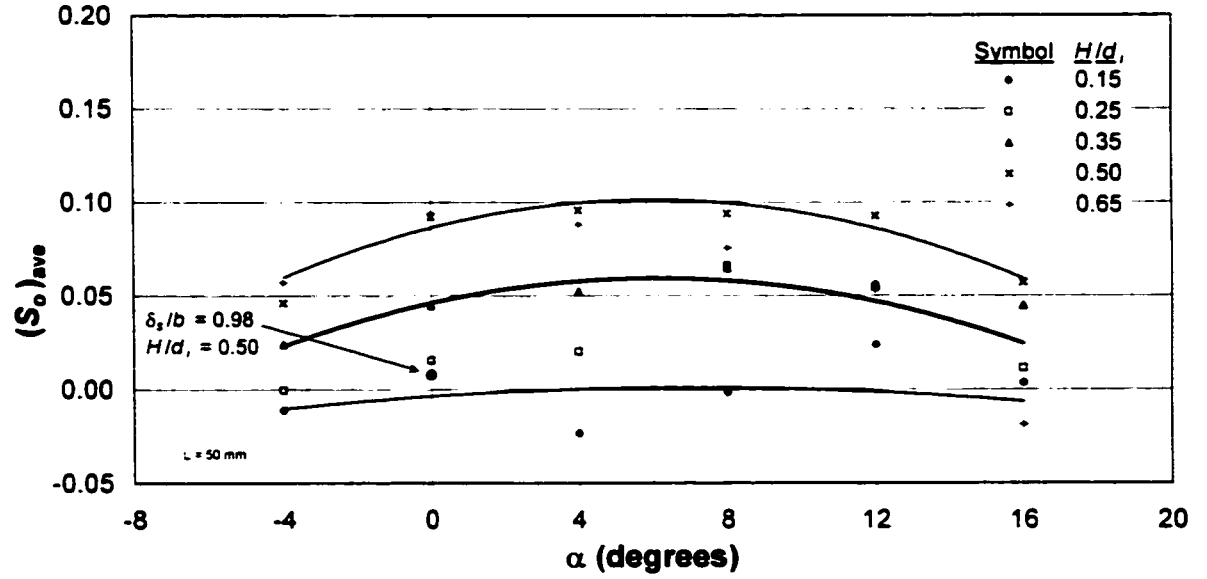

Figure E.16: $(S_o)_{ave}$ vs. α for 90° bend with 135° bend data plotted thereon ($L/b = 0.16$, $\delta_s/b = 0.98$).

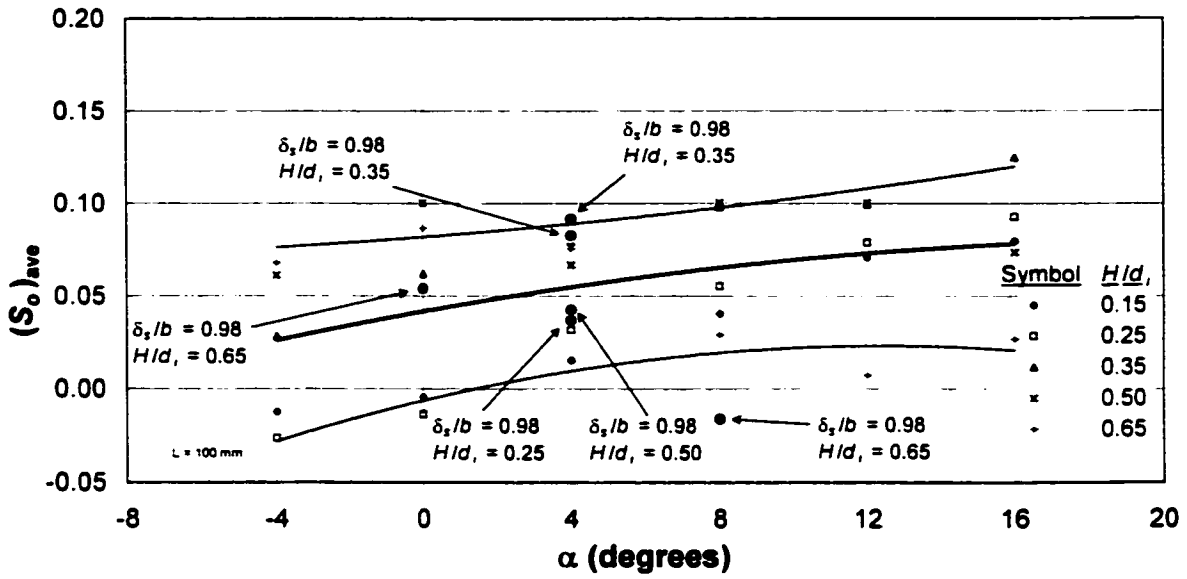

Figure E.17: $(S_o)_{ave}$ vs. α for 90° bend with 135° bend data plotted thereon (L/b = 0.33, δ_s/b = 0.98).

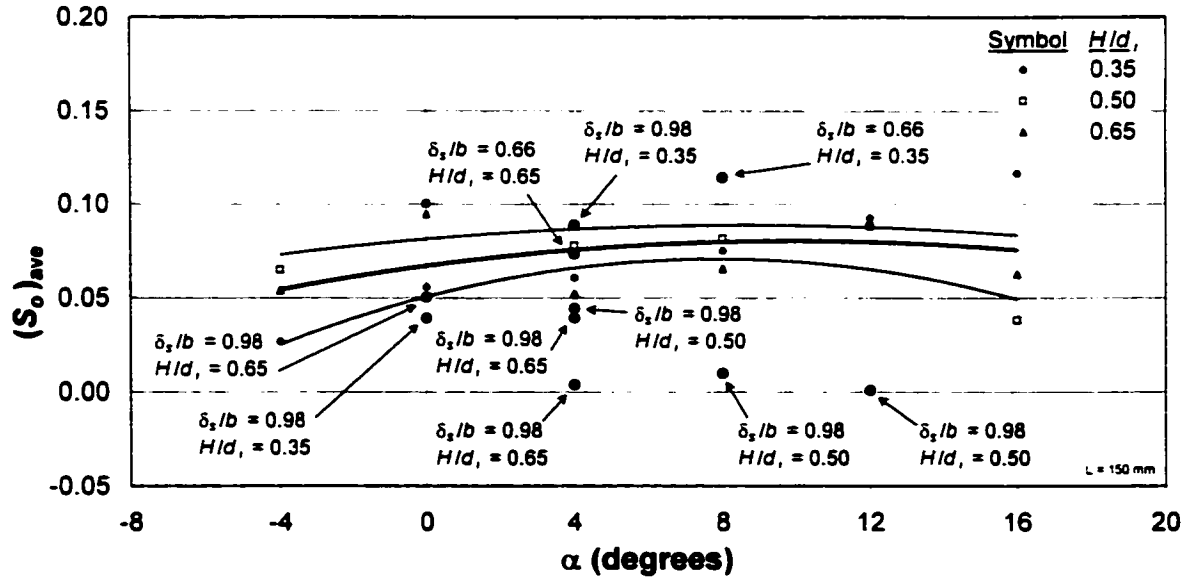

Figure E.18: $(S_o)_{ave}$ vs. α for 90° bend with 135° bend data plotted thereon (L/b = 0.49, δ_s/b = 0.98).

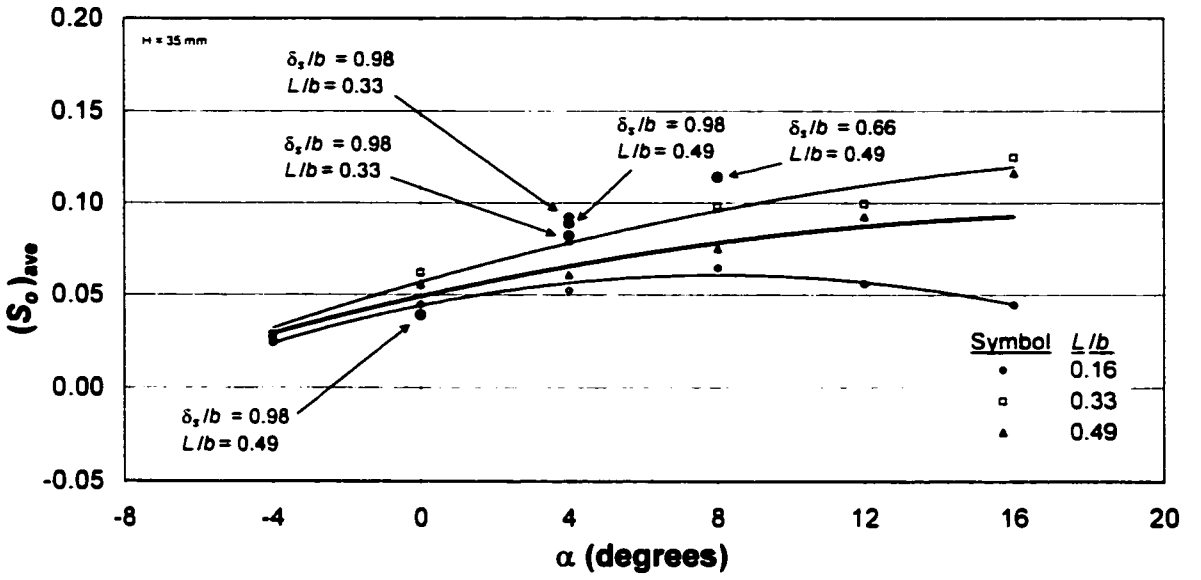

Figure E.19: $(S_o)_{ave}$ vs. L/b for 90° bend with 135° bend data plotted thereon (H/d_t = 0.35, δ_s/b = 0.98).

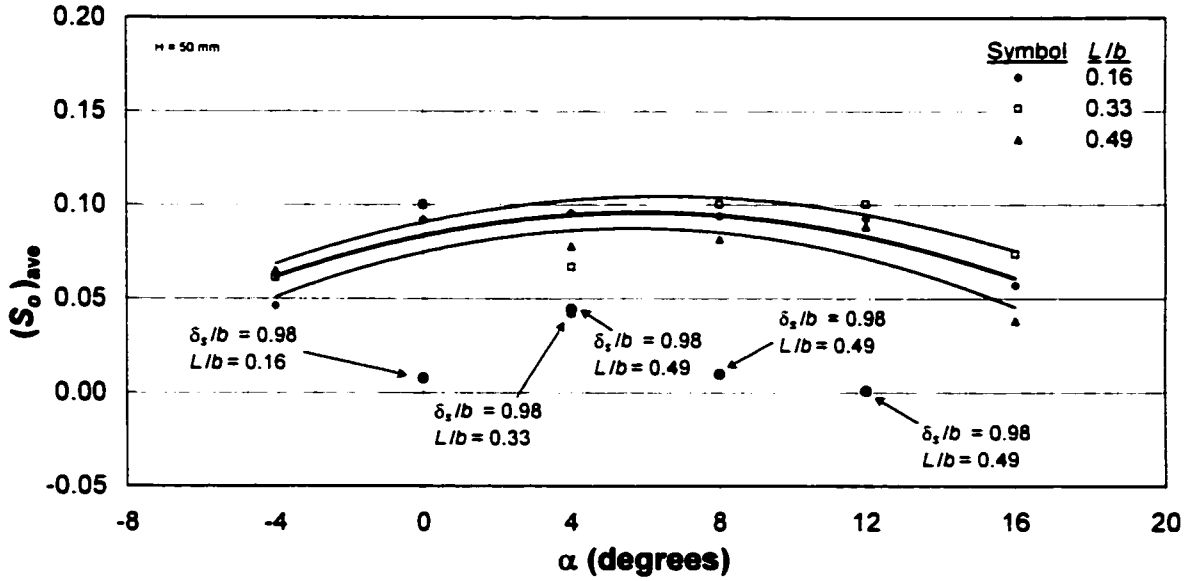

Figure E.20: $(S_o)_{ave}$ vs. α for 90° bend with 135° bend data plotted thereon (H/d_t = 0.50, δ_s/b = 0.98).

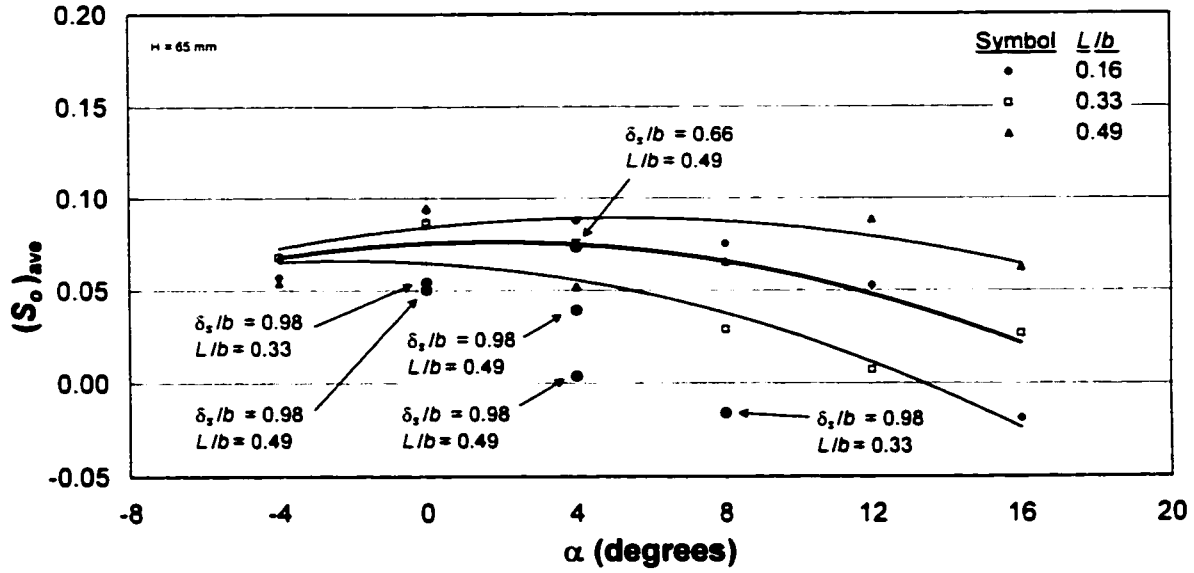

Figure E.21: $(S_o)_{ave}$ vs. α for 90° bend with 135° bend data plotted thereon (H/d_i = 0.65, δ_s/b = 0.98).

E.3 Scour Depth Through Channel (D_s/d_i)

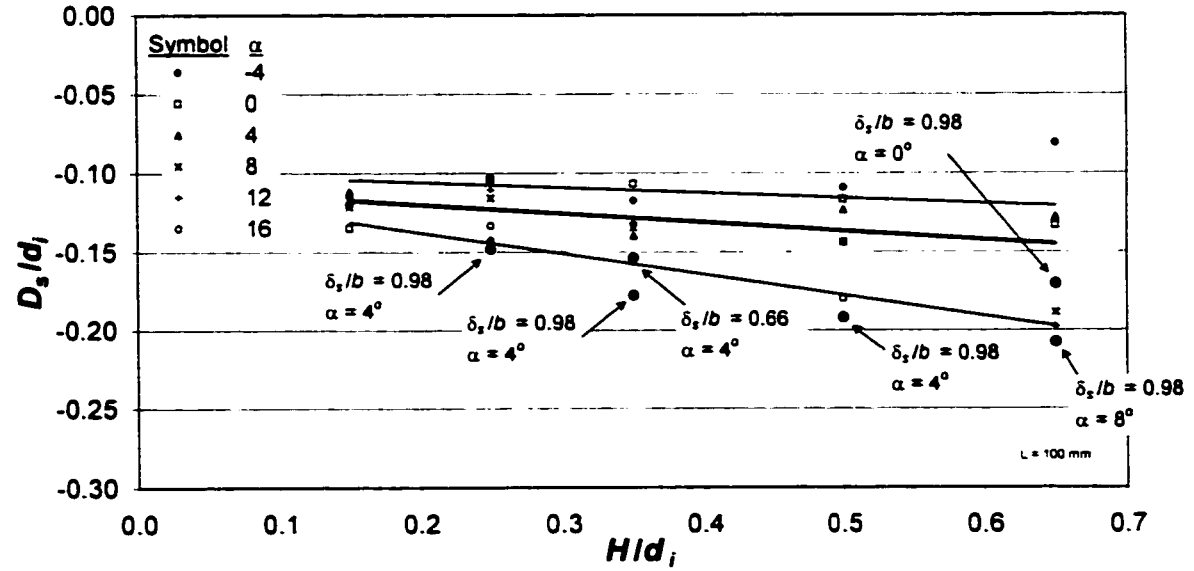

Figure E.22: D_s/d_i vs. H/d_i for 90° bend with 135° bend data plotted thereon (L/b = 0.33, δ_s/b = 0.98).

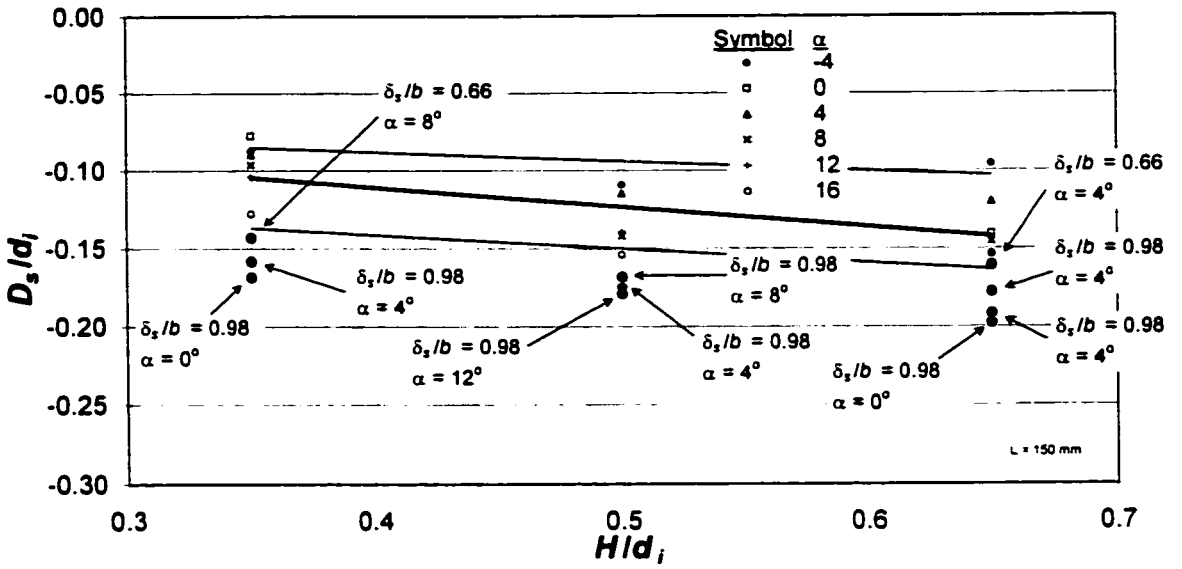

Figure E.23: D_s/d_i vs. H/d_i for 90° bend with 135° bend data plotted thereon (L/b = 0.49, δ_s/b = 0.98).

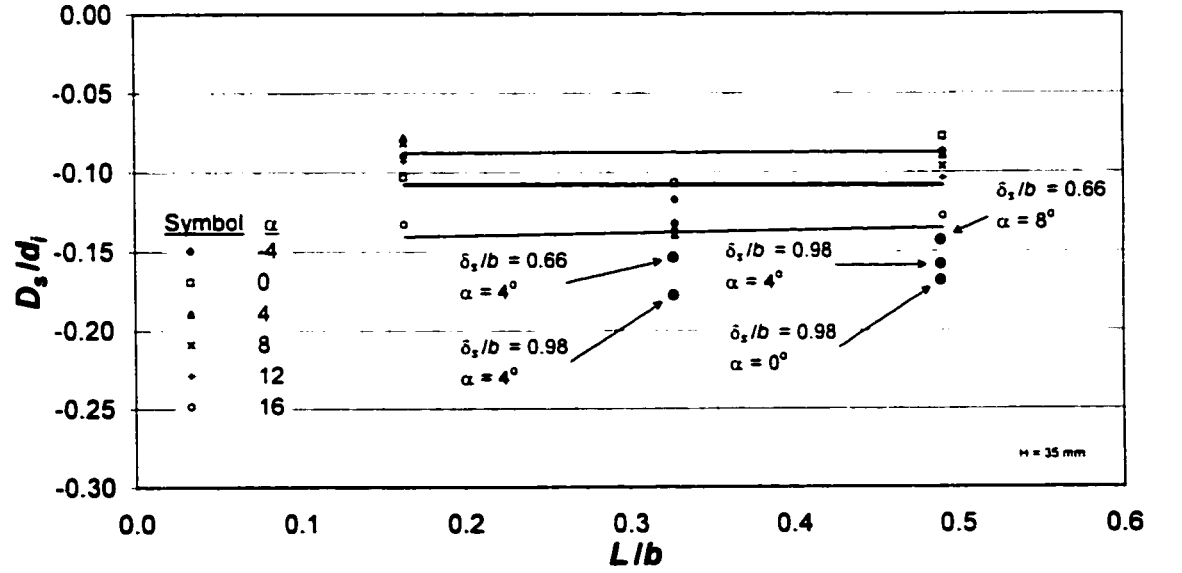

Figure E.24: D_s/d_i vs. L/b for 90° bend with 135° bend data plotted thereon (H/d_i = 0.35, δ_s/b = 0.98).

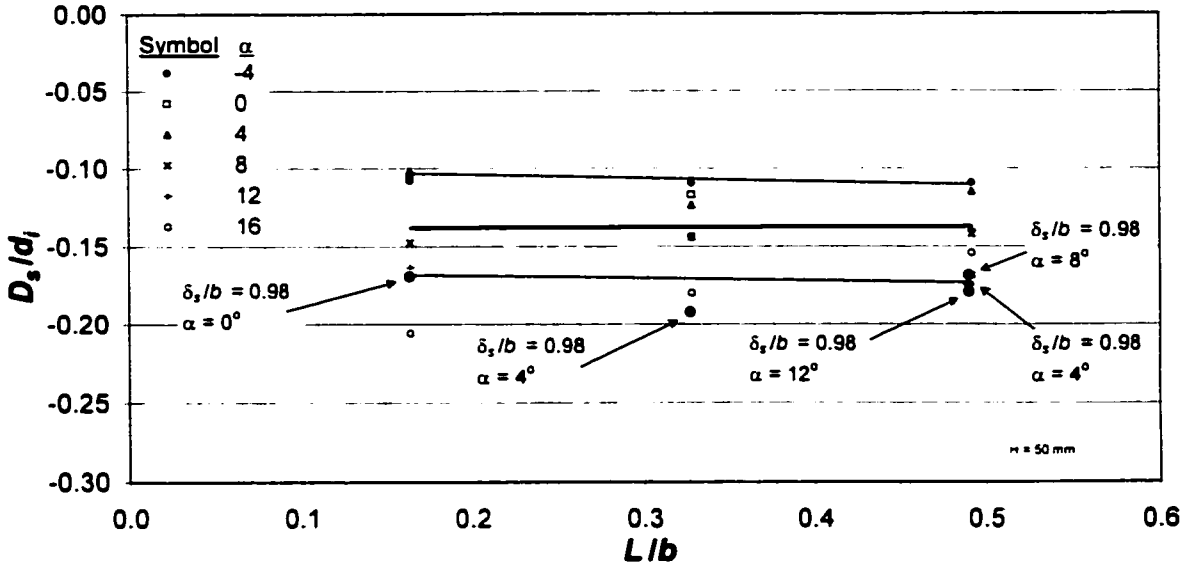

Figure E.25: D_s/d_i vs. L/b for 90° bend with 135° bend data plotted thereon ($H/d_i = 0.50$, $\delta_s/b = 0.98$).

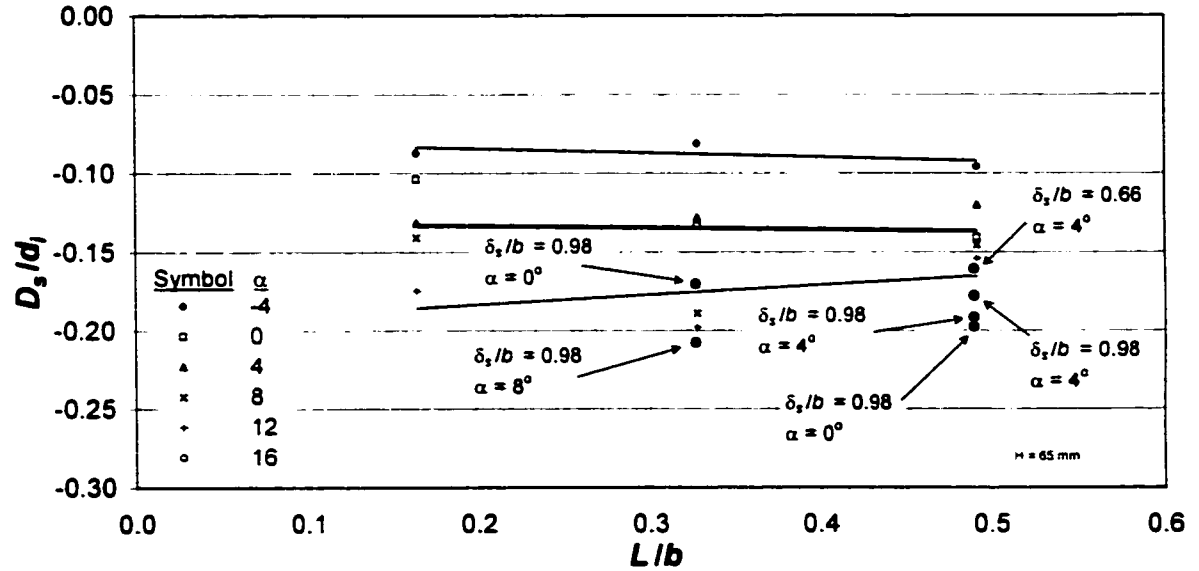

Figure E.26: D_s/d_i vs. L/b for 90° bend with 135° bend data plotted thereon ($H/d_i = 0.65$, $\delta_s/b = 0.98$).

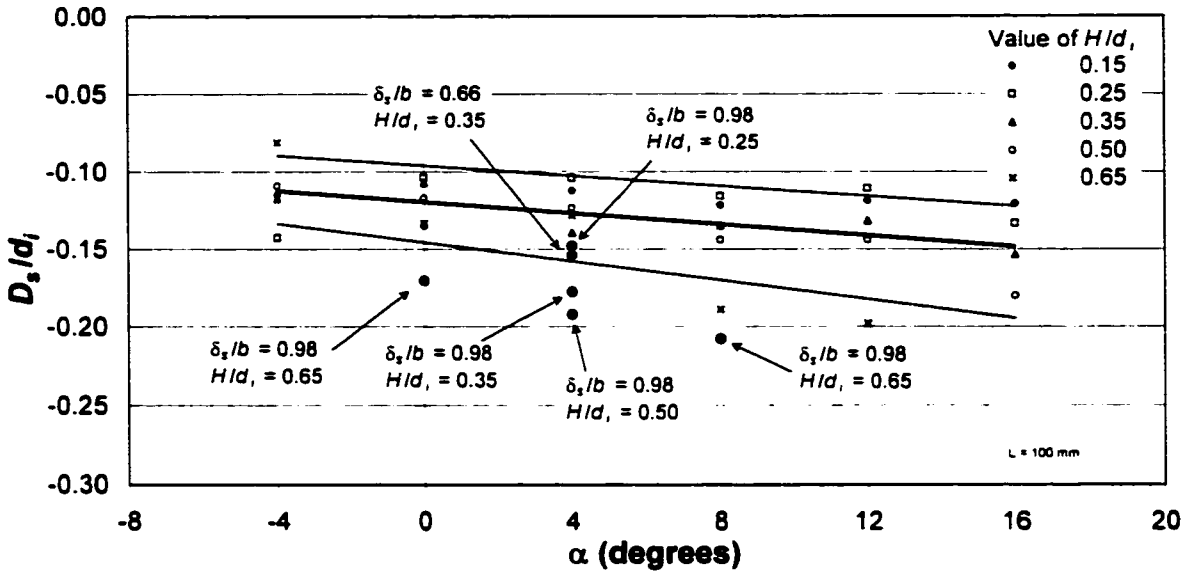

Figure E.27: D_s/d_i vs. α for 90° bend with 135° bend data plotted thereon (L/b = 0.33, δ_s/b = 0.98).

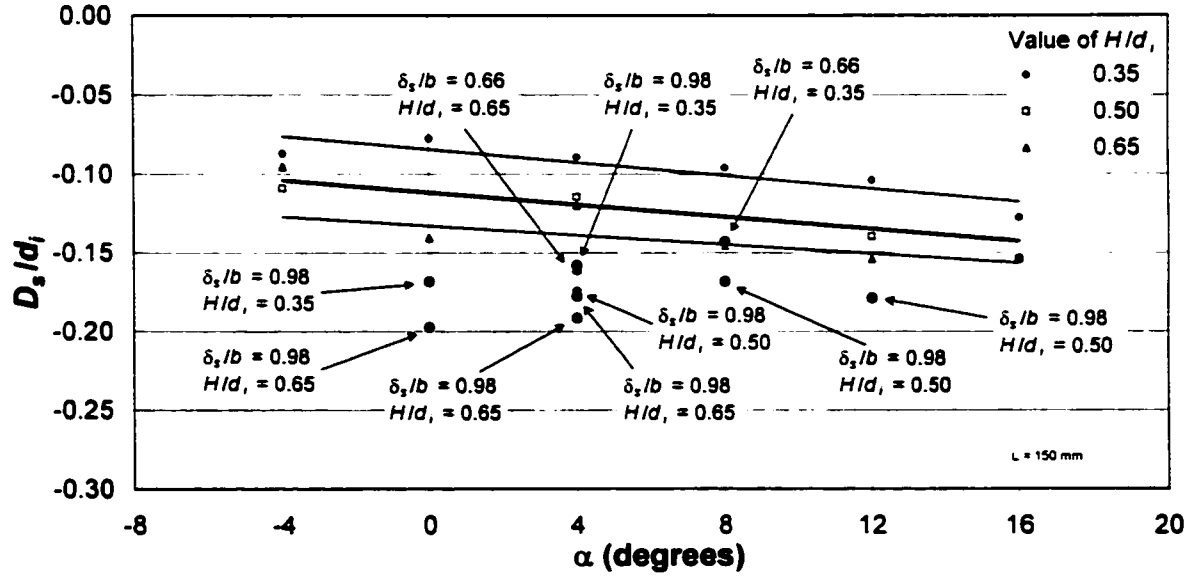

Figure E.28: D_s/d_i vs. α for 90° bend with 135° bend data plotted thereon (L/b = 0.49, δ_s/b = 0.98).

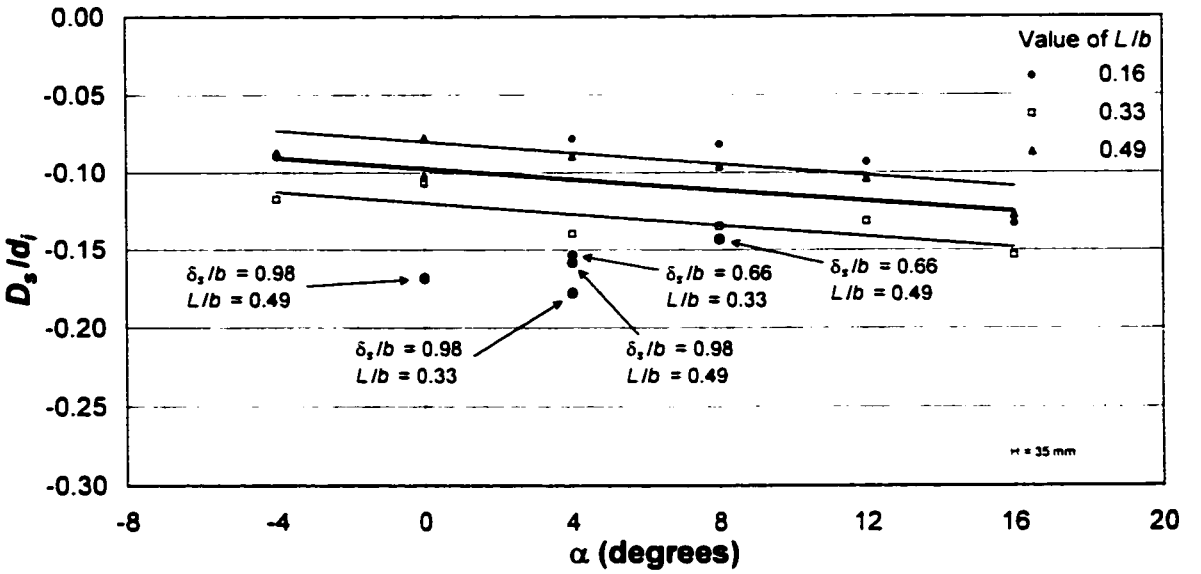

Figure E.29: D_s/d_i vs. α for 90° bend with 135° bend data plotted thereon ($H/d_i = 0.35$, $\delta_s/b = 0.98$).

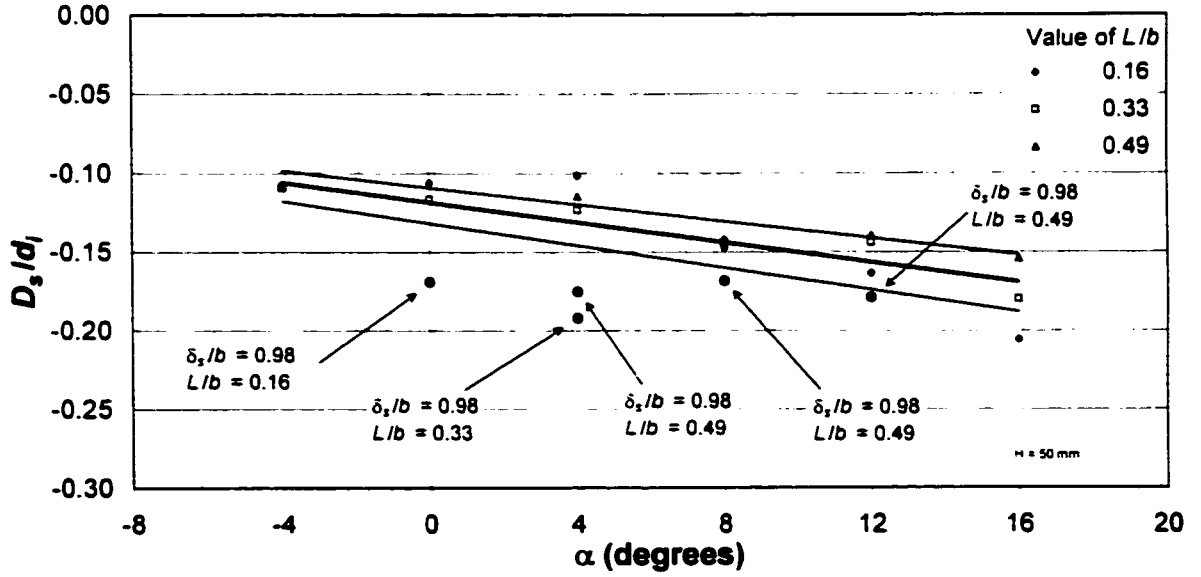

Figure E.30: D_s/d_i vs. α for 90° bend with 135° bend data plotted thereon ($H/d_i = 0.50$, $\delta_s/b = 0.98$).

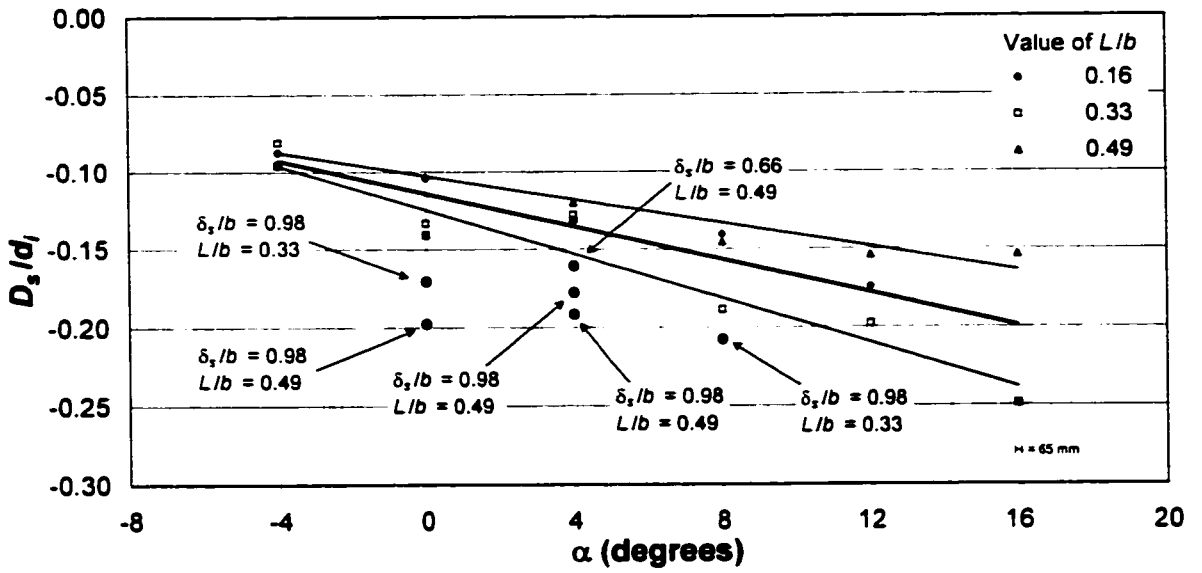

Figure E.31: D_s/d_i vs. α for 90° bend with 135° bend data plotted thereon (H/d_i = 0.65, δ_s/b = 0.98).

APPENDIX F

TOPOGRAPHIC PLOTS

F.1 90° Bend

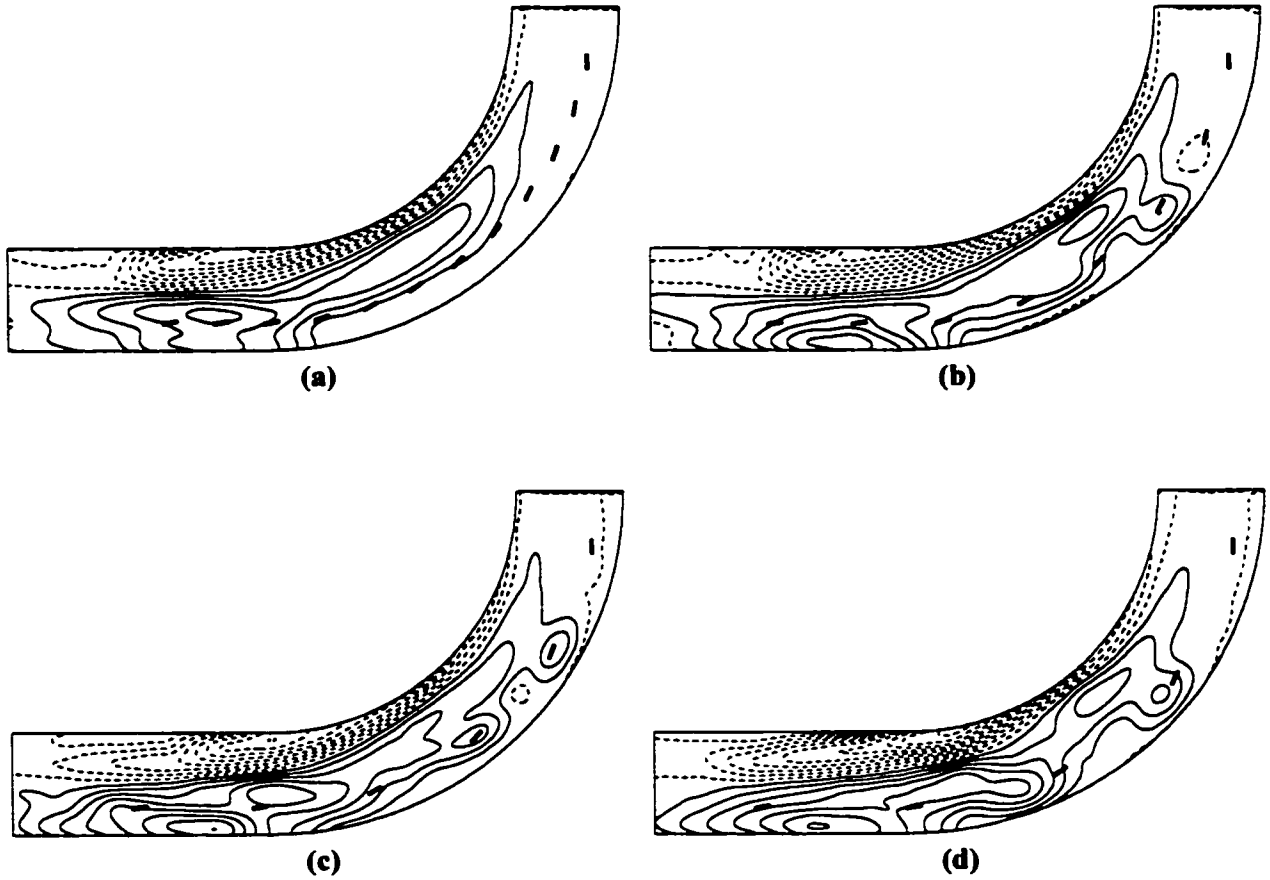

Figure F.1: Topographic plots for:

Fig.	H/d_s	L/b	δ_s/b	α
(a)	0.15	0.16	0.33	8°
(b)	0.15	0.16	0.66	8°
(c)	0.15	0.16	0.98	8°
(d)	0.15	0.16	1.31	8°

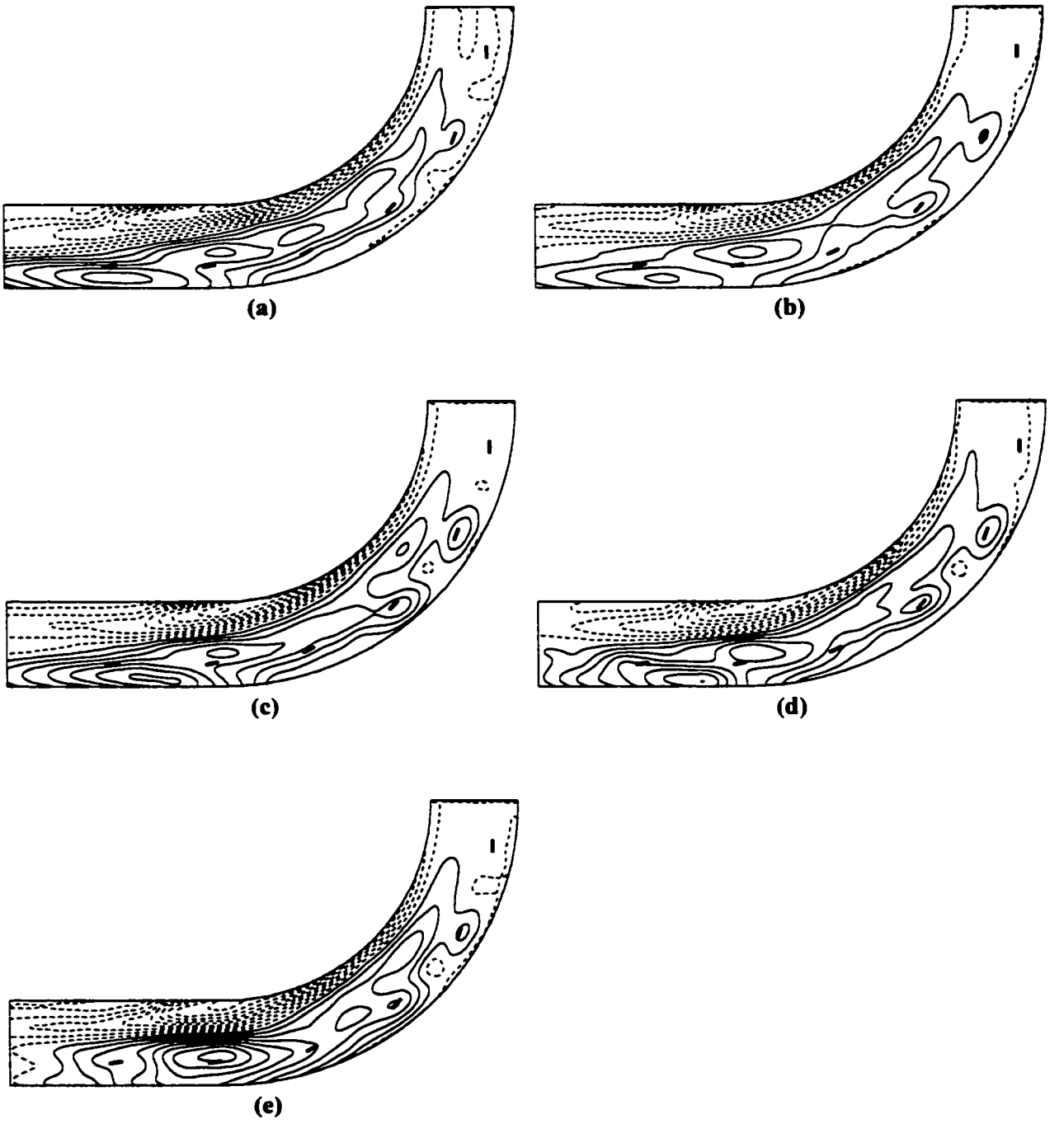

Figure F.2: Topographic plots for:

Fig.	H/d_1	L/b	δ_1/b	α
(a)	0.15	0.16	0.98	-4°
(b)	0.15	0.16	0.98	0°
(c)	0.15	0.16	0.98	4°
(d)	0.15	0.16	0.98	8°
(e)	0.15	0.16	0.98	12°

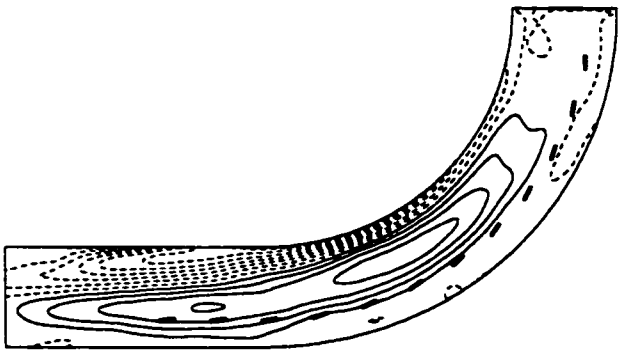

(a)

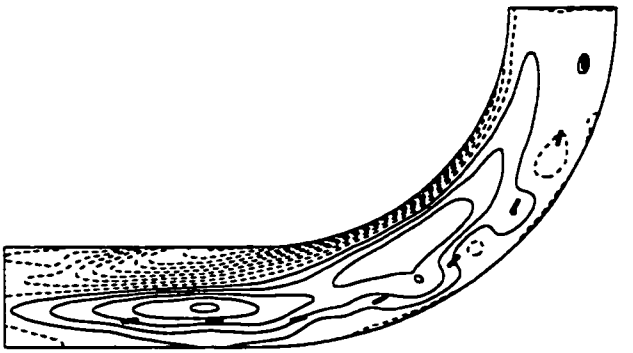

(b)

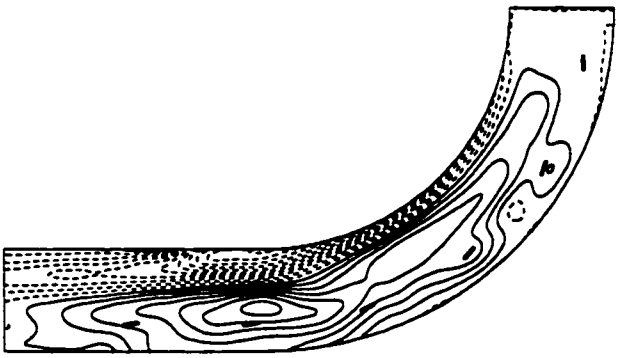

(c)

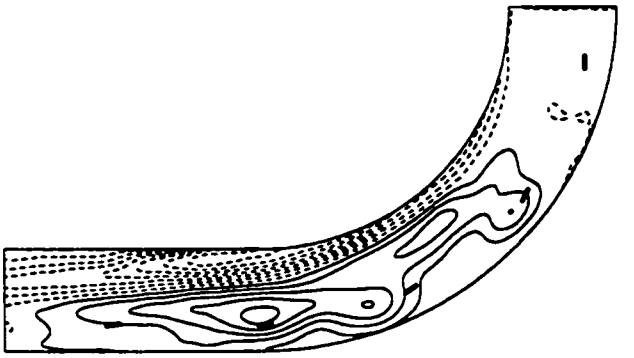

(d)

Figure F.3: Topographic plots for:

Fig.	H/d_t	L/b	δ_t/b	α
(a)	0.25	0.16	0.33	8°
(b)	0.25	0.16	0.66	8°
(c)	0.25	0.16	0.98	8°
(d)	0.25	0.16	1.31	8°

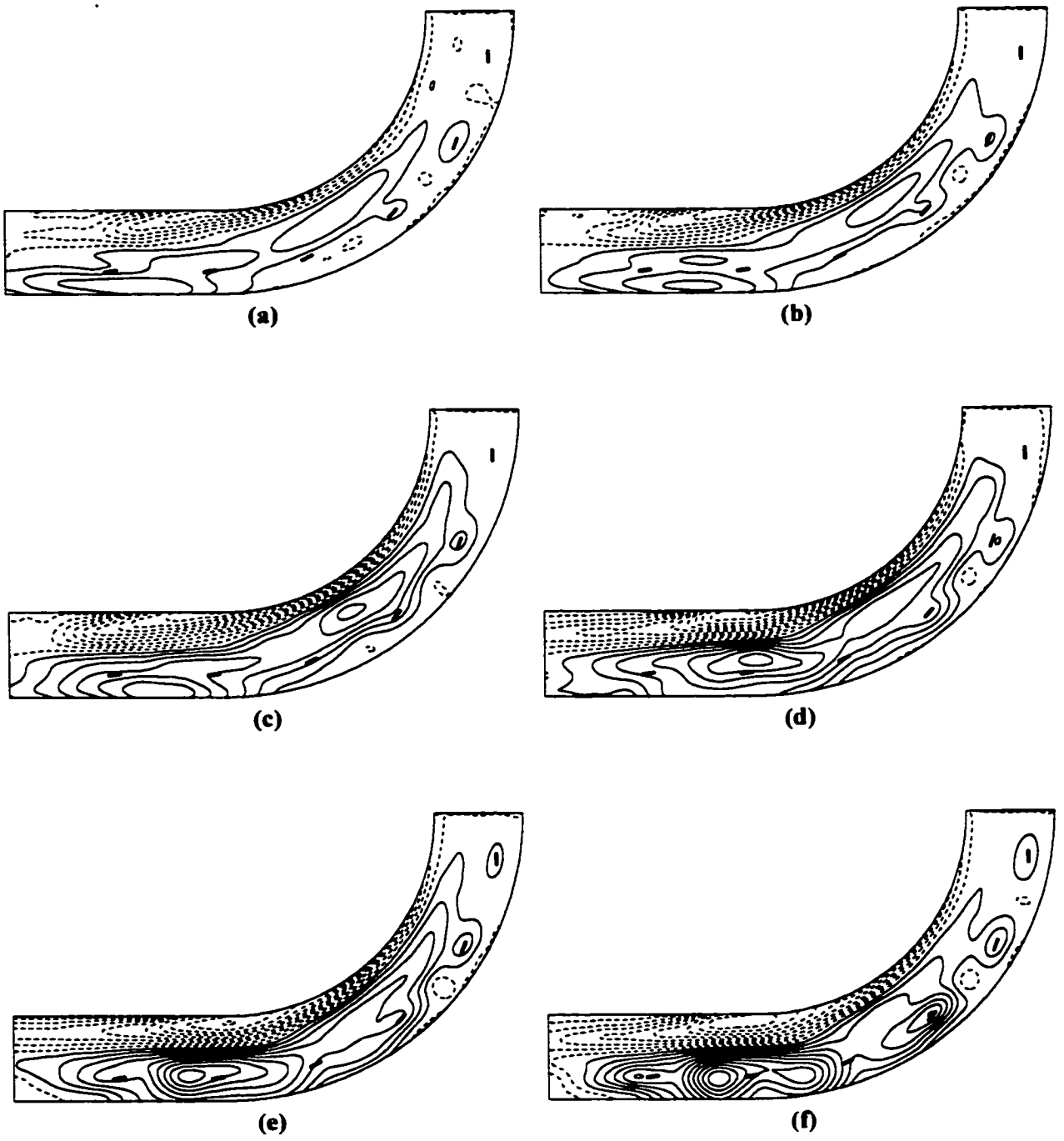

Figure F.4: Topographic plots for:

Fig.	H/d_s	L/b	δ_s/b	α
(a)	0.25	0.16	0.98	-4°
(b)	0.25	0.16	0.98	0°
(c)	0.25	0.16	0.98	4°
(d)	0.25	0.16	0.98	8°
(e)	0.25	0.16	0.98	12°
(f)	0.25	0.16	0.98	16°

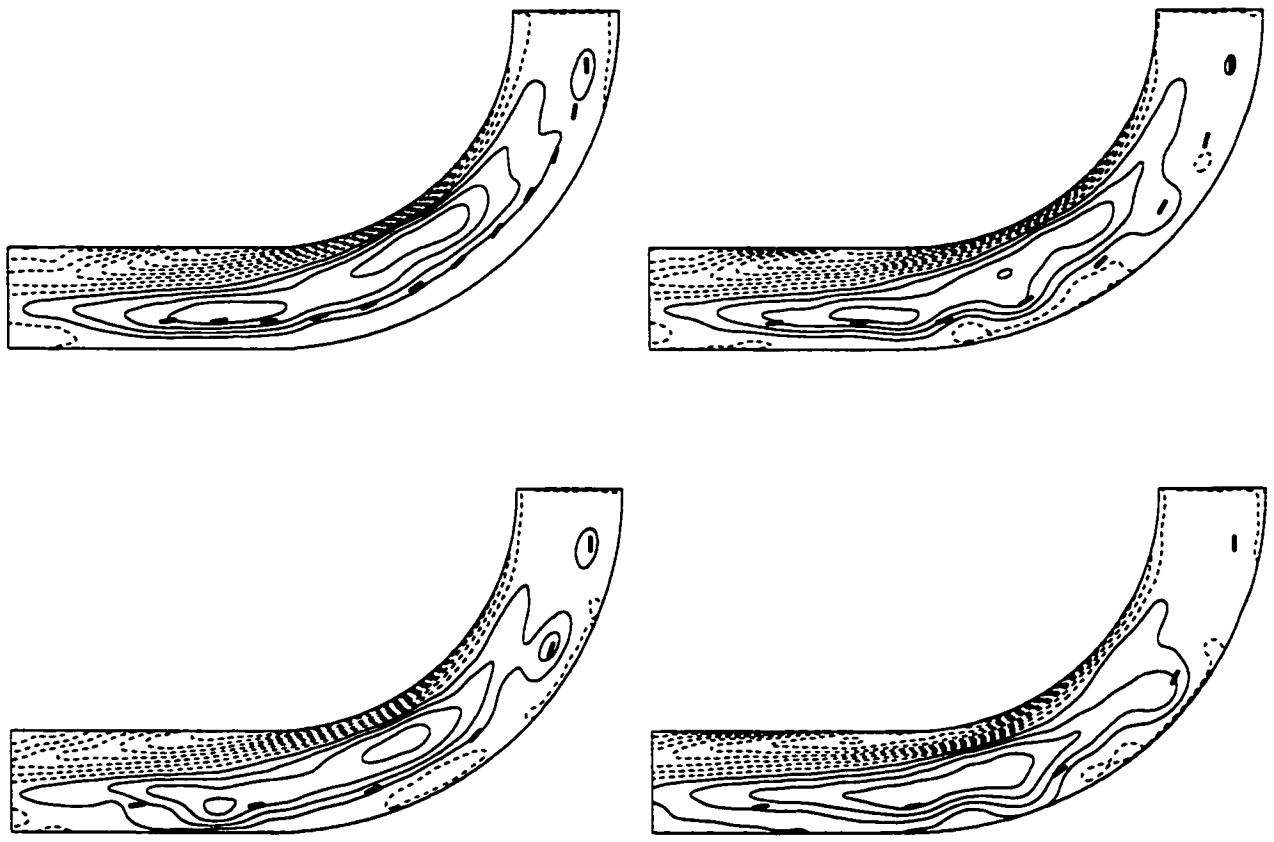

Figure F.5: Topographic plots for:

Fig.	H/d_1	L/b	δ_1/b	α
(a)	0.35	0.16	0.33	8°
(b)	0.35	0.16	0.66	8°
(c)	0.35	0.16	0.98	8°
(d)	0.35	0.16	1.31	8°

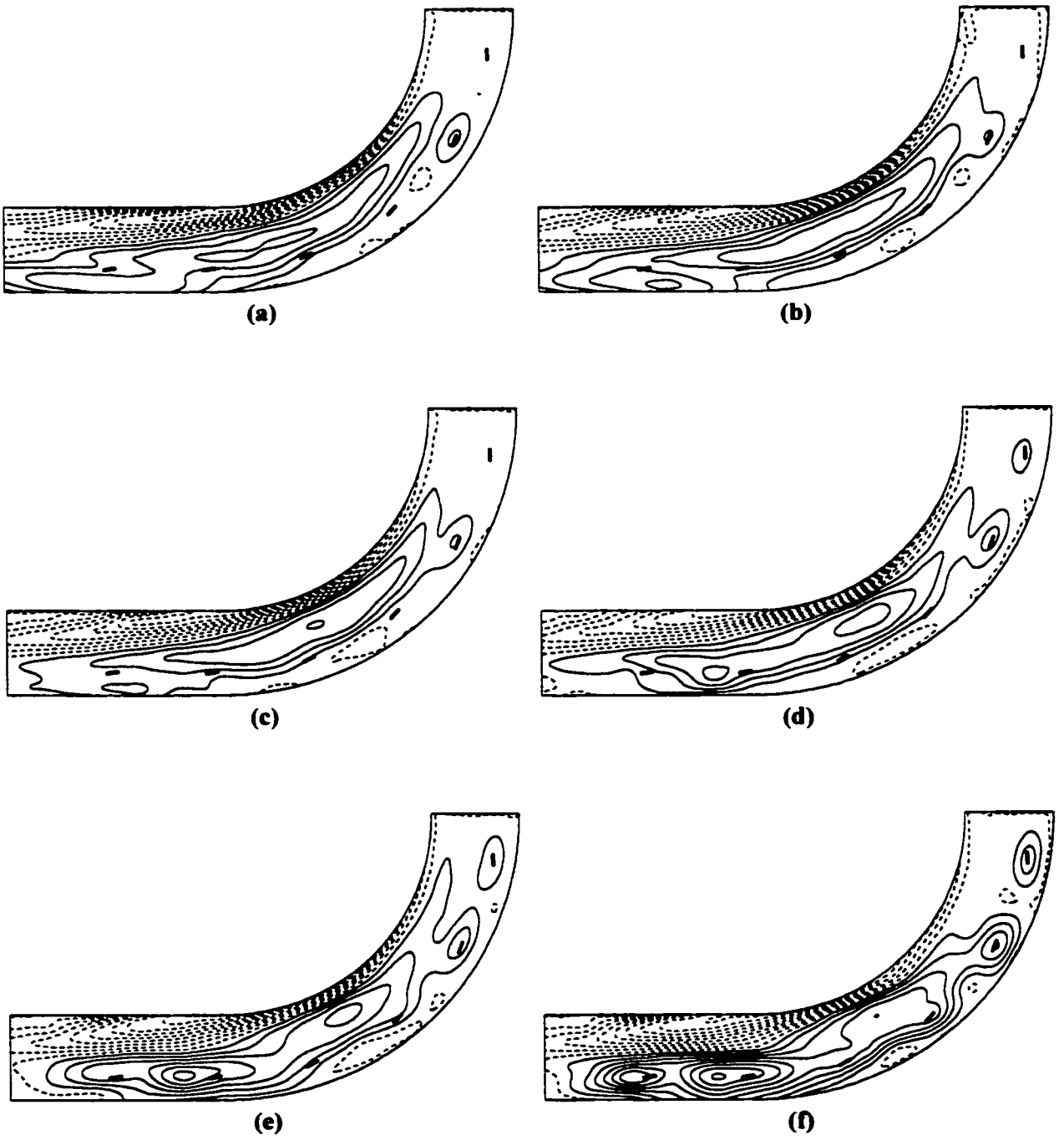

Figure F.6: Topographic plots for:

Fig.	*H/d*,	*L/b*	δ_s/b	α
(a)	0.35	0.16	0.98	-4°
(b)	0.35	0.16	0.98	0°
(c)	0.35	0.16	0.98	4°
(d)	0.35	0.16	0.98	8°
(e)	0.35	0.16	0.98	12°
(f)	0.35	0.16	0.98	16°

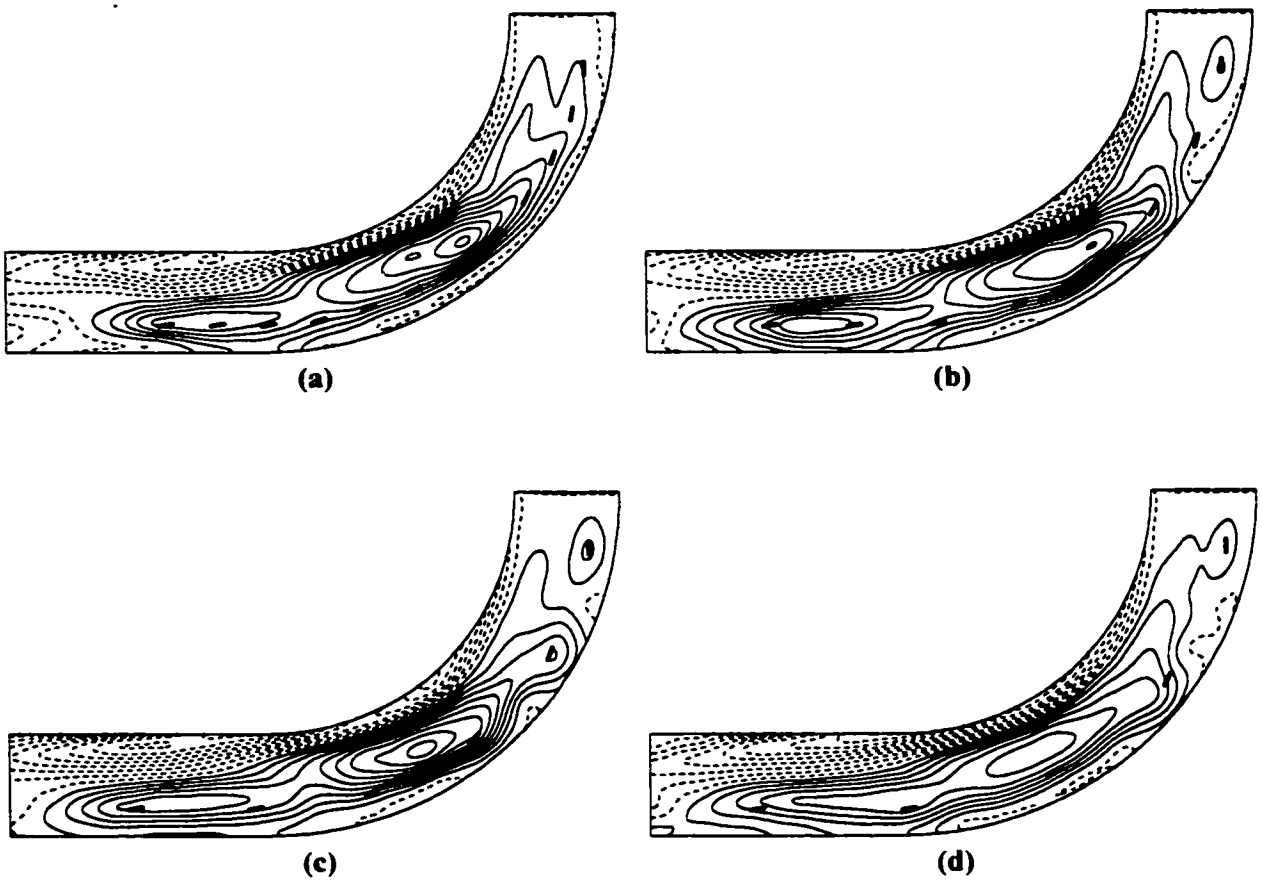

Figure F.7: Topographic plots for:

Fig.	H/d_s	L/b	δ_s/b	α
(a)	0.50	0.16	0.33	8°
(b)	0.50	0.16	0.66	8°
(c)	0.50	0.16	0.98	8°
(d)	0.50	0.16	1.31	8°

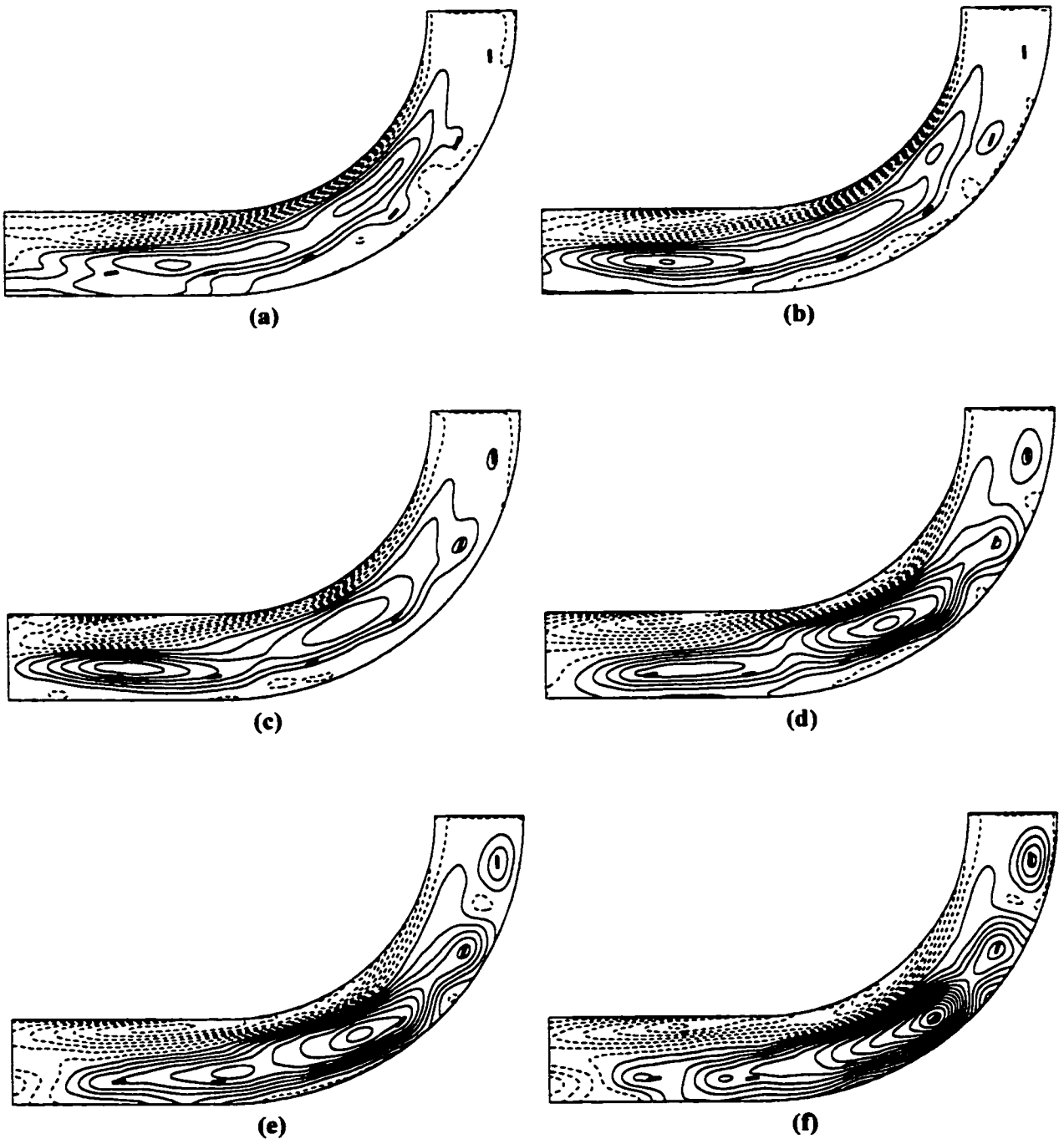

Figure F.8: Topographic plots for:

Fig.	H/d_s	L/b	δ_s/b	α
(a)	0.50	0.16	0.98	-4°
(b)	0.50	0.16	0.98	0°
(c)	0.50	0.16	0.98	4°
(d)	0.50	0.16	0.98	8°
(e)	0.50	0.16	0.98	12°
(f)	0.50	0.16	0.98	16°

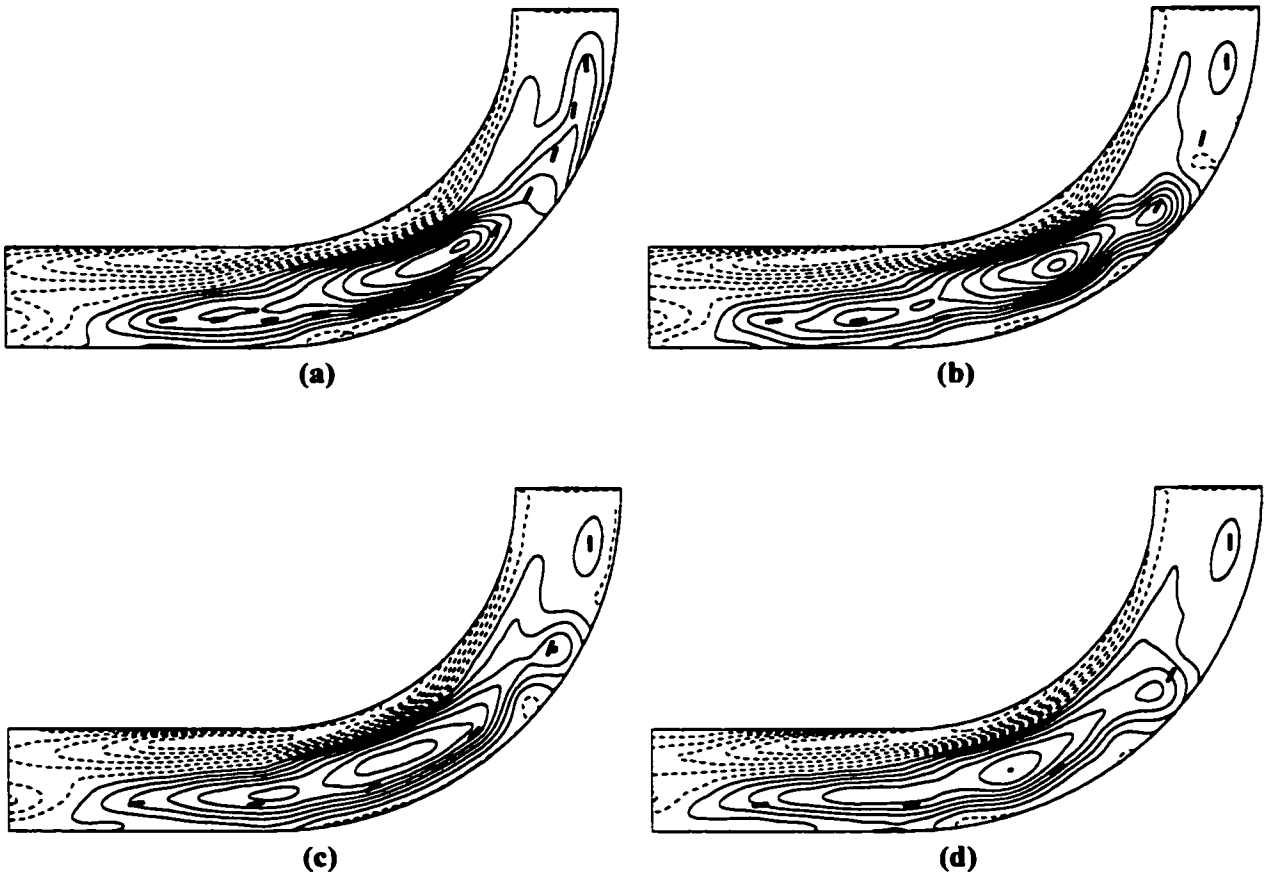

Figure F.9: Topographic plots for:

Fig.	H/d_1	L/b	δ_1/b	α
(a)	0.65	0.16	0.33	8°
(b)	0.65	0.16	0.66	8°
(c)	0.65	0.16	0.98	8°
(d)	0.65	0.16	1.31	8°

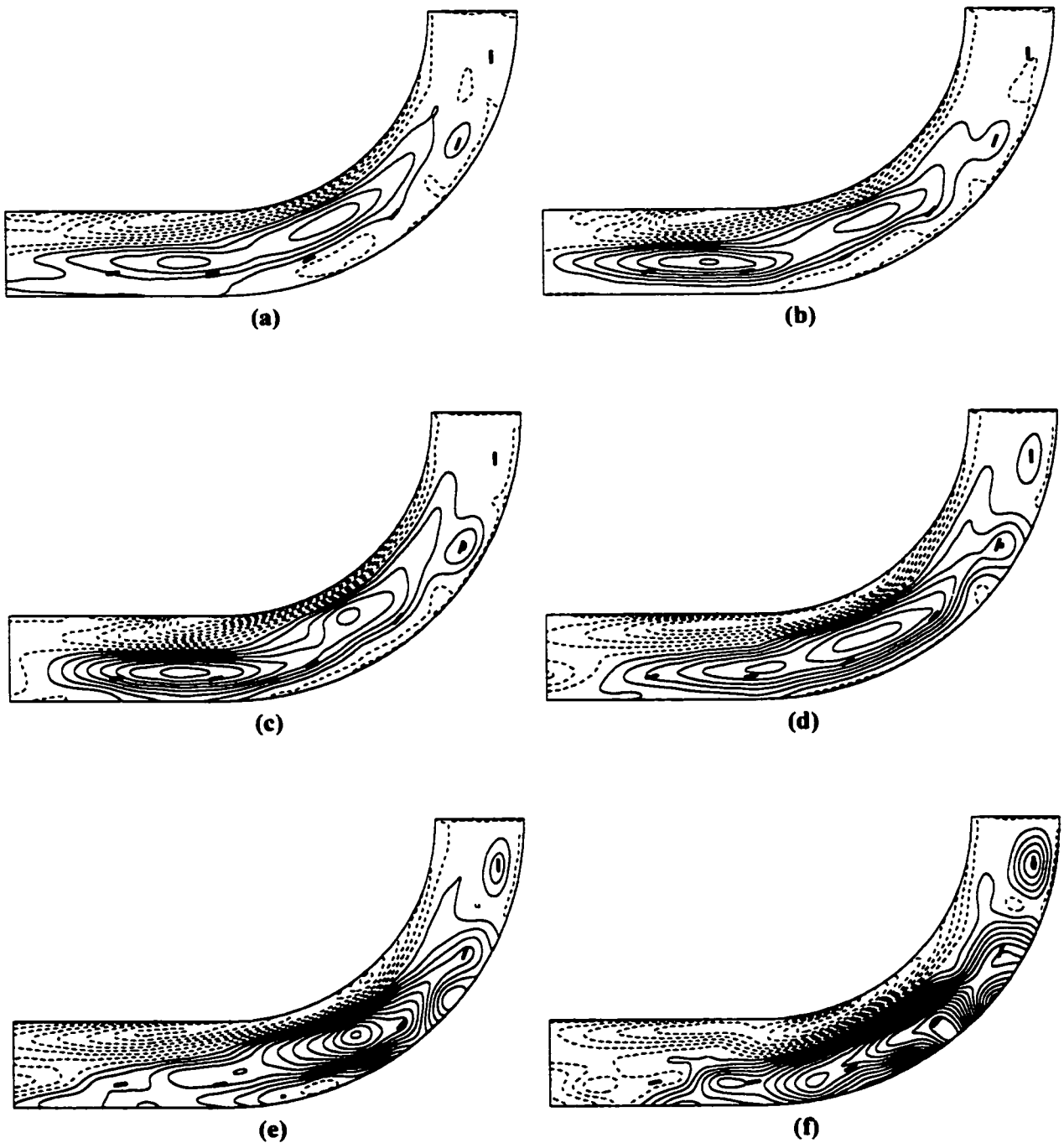

Figure F.10: Topographic plots for:

Fig.	H/d_s	L/b	δ_s/b	α
(a)	0.65	0.16	0.98	-4°
(b)	0.65	0.16	0.98	0°
(c)	0.65	0.16	0.98	4°
(d)	0.65	0.16	0.98	8°
(e)	0.65	0.16	0.98	12°
(f)	0.65	0.16	0.98	16°

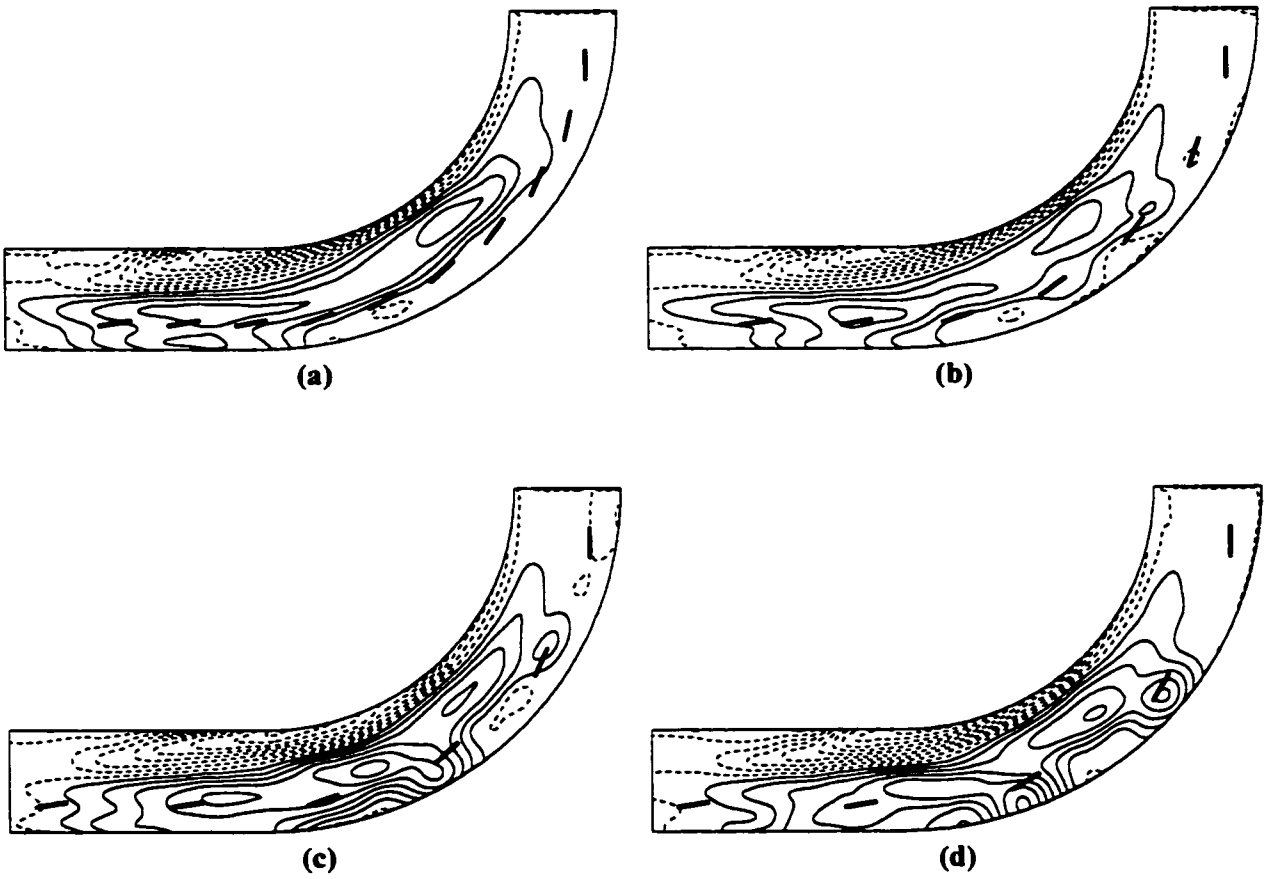

Figure F.11: Topographic plots for:

Fig.	H/d_1	L/b	δ_r/b	α
(a)	0.15	0.33	0.33	8°
(b)	0.15	0.33	0.66	8°
(c)	0.15	0.33	0.98	8°
(d)	0.15	0.33	1.31	8°

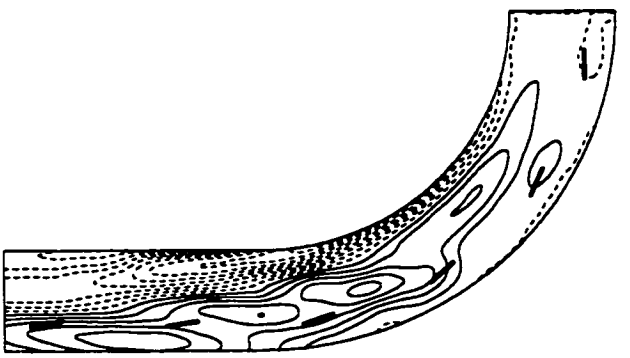

(a)

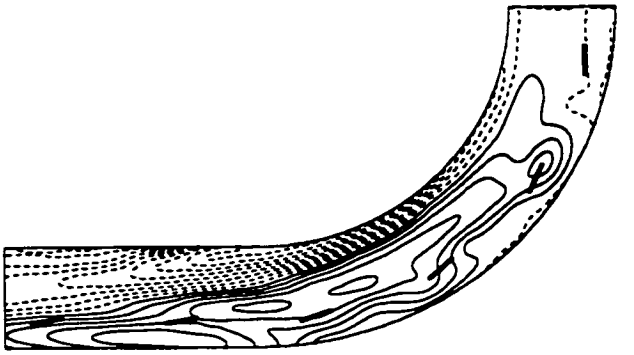

(b)

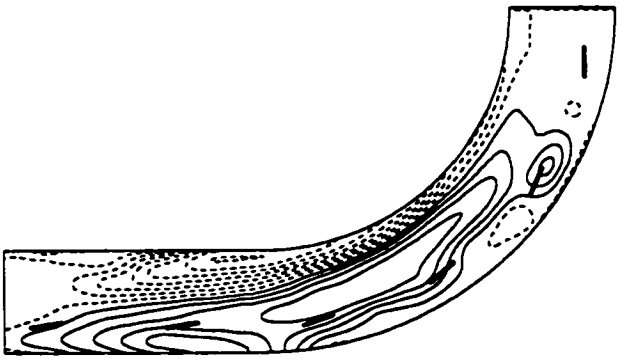

(c)

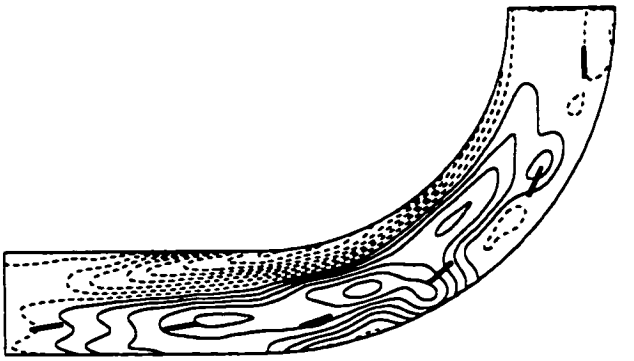

(d)

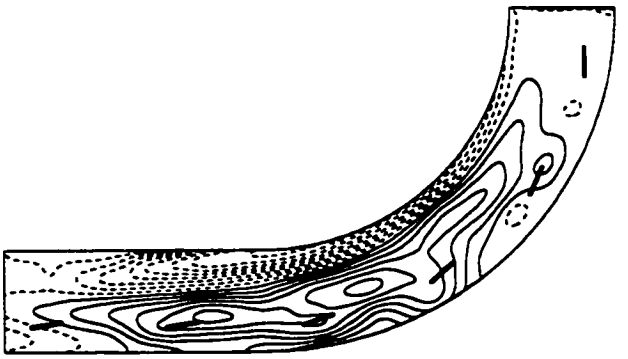

(e)

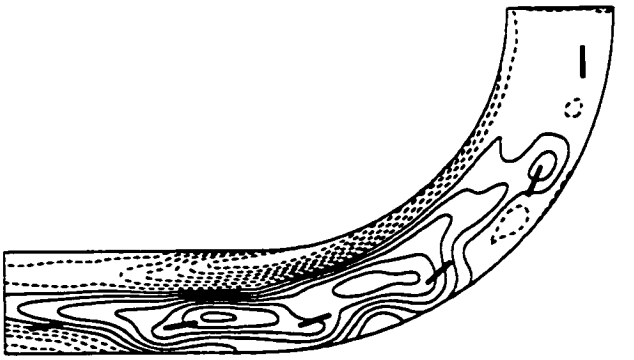

(f)

Figure F.12: Topographic plots for:

Fig.	H/d_s	L/b	δ_s/b	α
(a)	0.15	0.33	0.98	-4°
(b)	0.15	0.33	0.98	0°
(c)	0.15	0.33	0.98	4°
(d)	0.15	0.33	0.98	8°
(e)	0.15	0.33	0.98	12°
(f)	0.15	0.33	0.98	16°

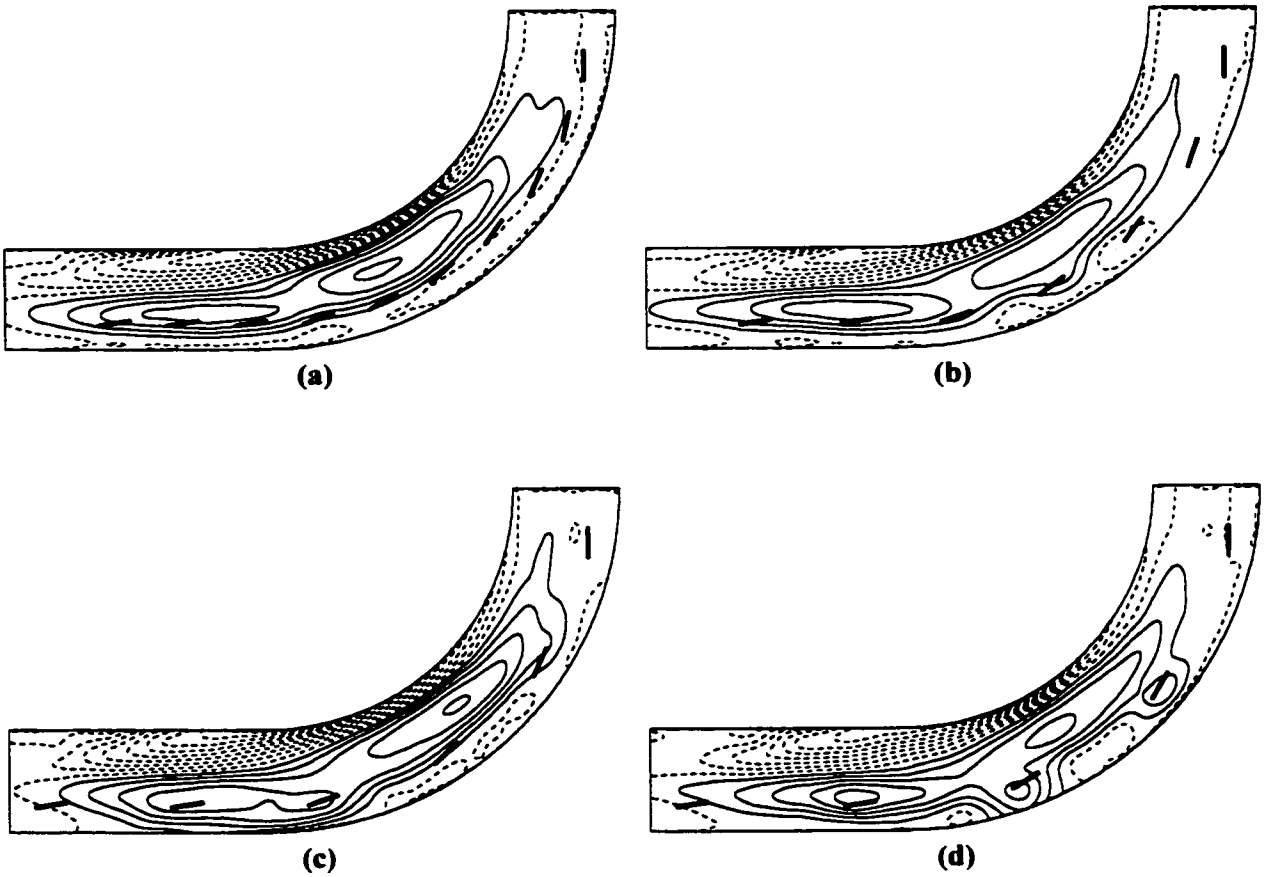

Figure F.13: Topographic plots for:

Fig.	H/d_1	L/b	δ_r/b	α
(a)	0.25	0.33	0.33	8°
(b)	0.25	0.33	0.66	8°
(c)	0.25	0.33	0.98	8°
(d)	0.25	0.33	1.31	8°

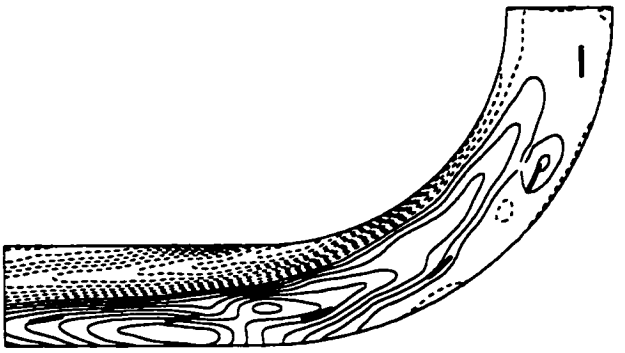

(a)

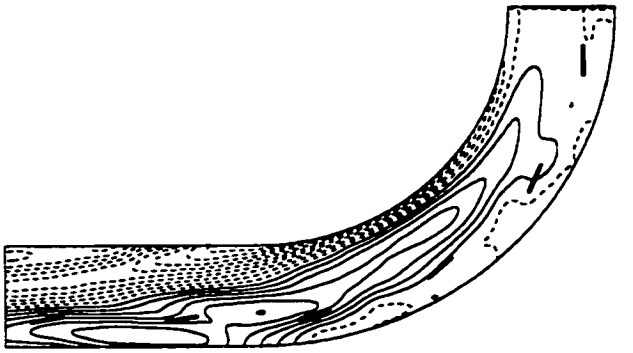

(b)

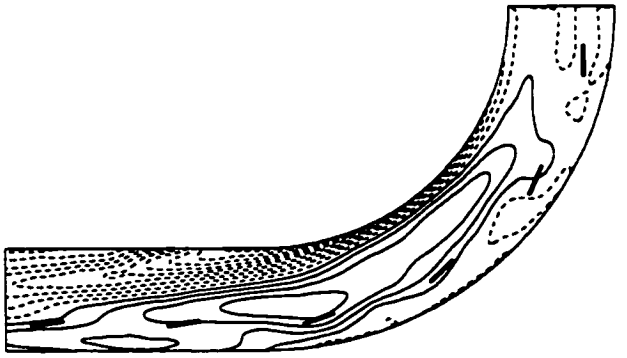

(c)

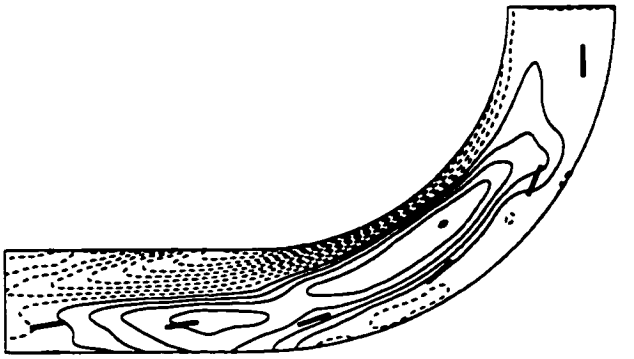

(d)

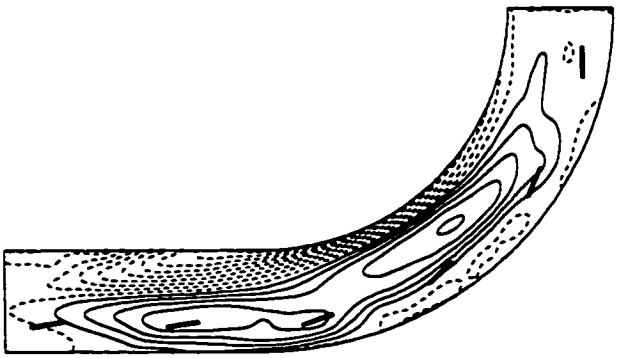

(e)

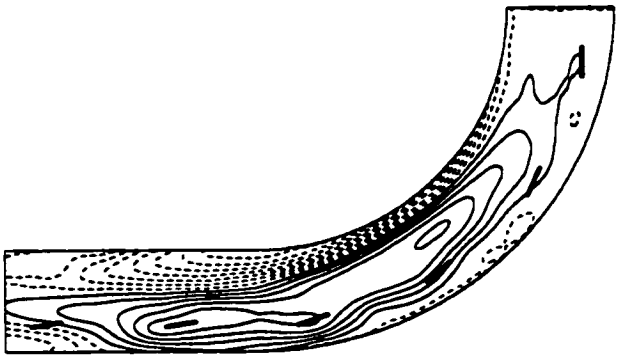

(f)

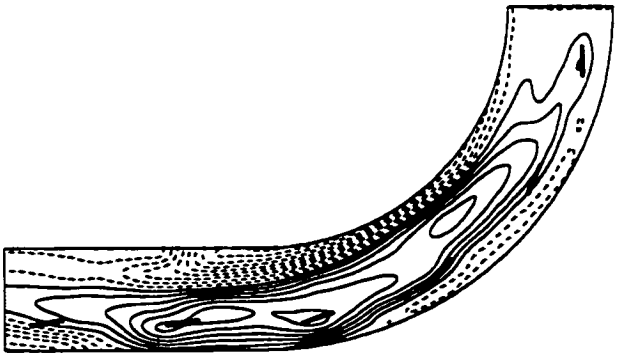

(g)

Figure F.14: Topographic plots for:

Fig.	H/d_s	L/b	δ_s/b	α
(a)	0.25	0.33	0.98	-8°
(b)	0.25	0.33	0.98	-4°
(c)	0.25	0.33	0.98	0°
(d)	0.25	0.33	0.98	4°
(e)	0.25	0.33	0.98	8°
(f)	0.25	0.33	0.98	12°
(g)	0.25	0.33	0.98	16°

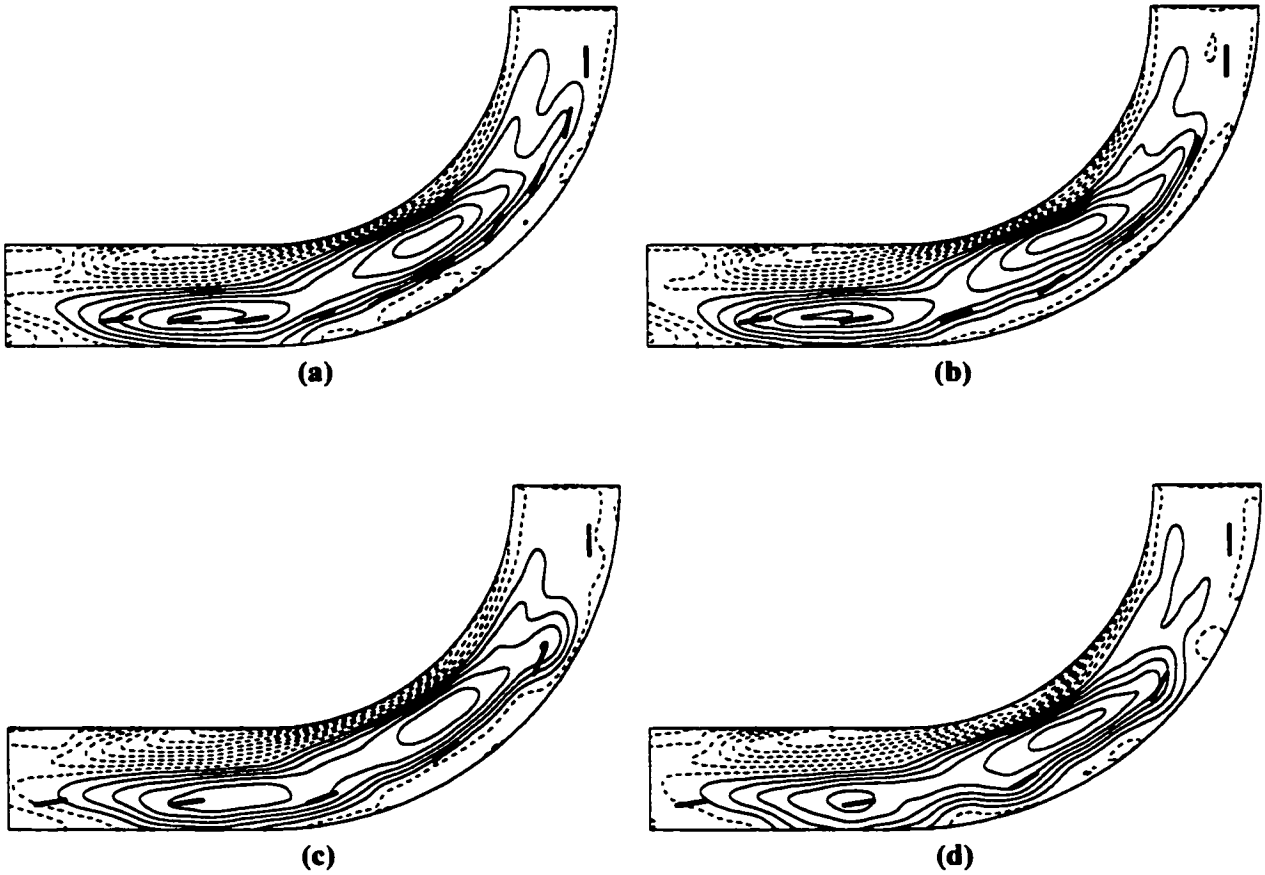

Figure F.15: Topographic plots for:

Fig.	H/d_i	L/b	δ_j/b	α
(a)	0.35	0.33	0.33	8°
(b)	0.35	0.33	0.66	8°
(c)	0.35	0.33	0.98	8°
(d)	0.35	0.33	1.31	8°

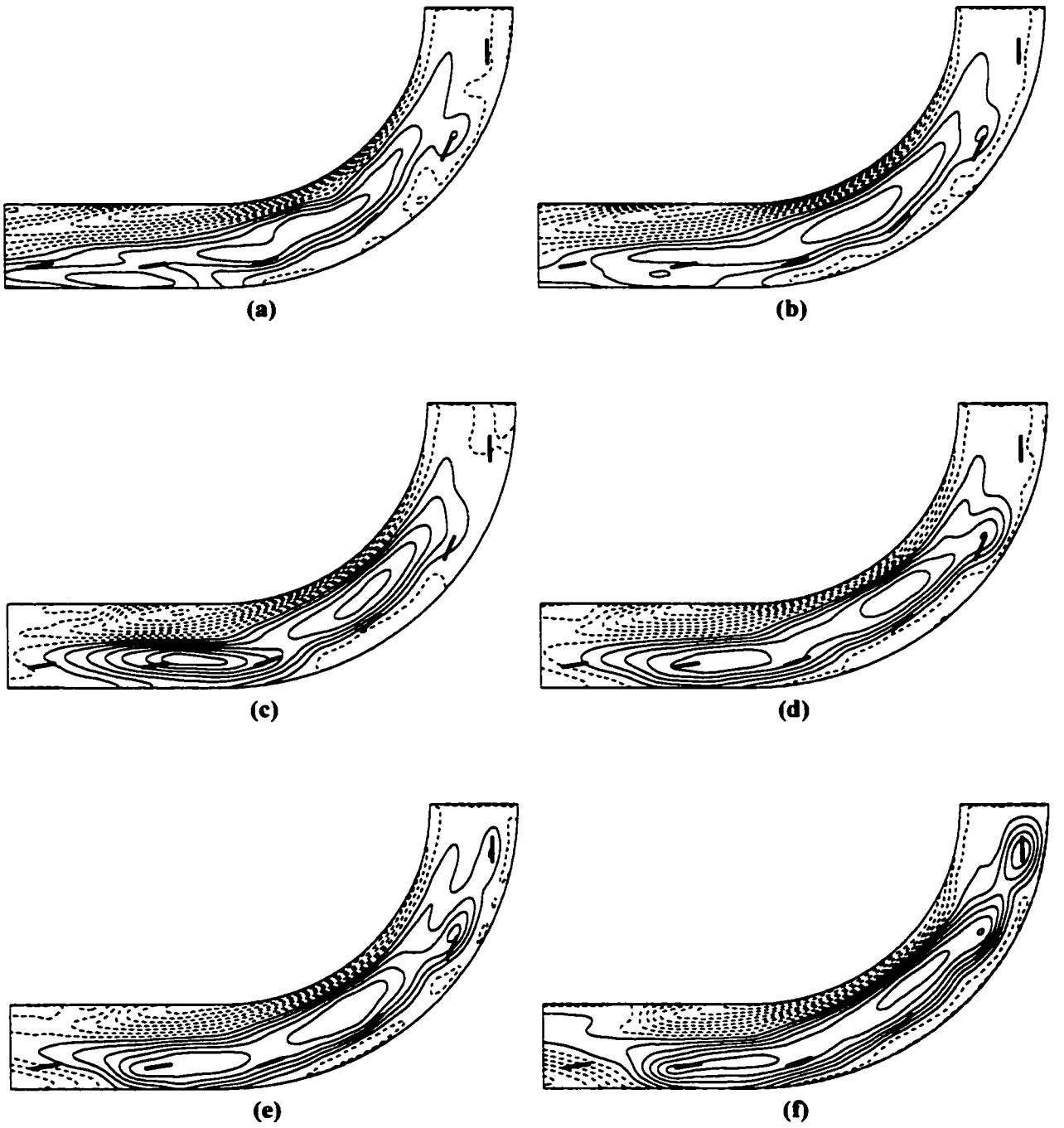

Figure F.16: Topographic plots for:

Fig.	H/d_1	L/b	δ_1/b	α
(a)	0.35	0.33	0.98	-4°
(b)	0.35	0.33	0.98	0°
(c)	0.35	0.33	0.98	4°
(d)	0.35	0.33	0.98	8°
(e)	0.35	0.33	0.98	12°
(f)	0.35	0.33	0.98	16°

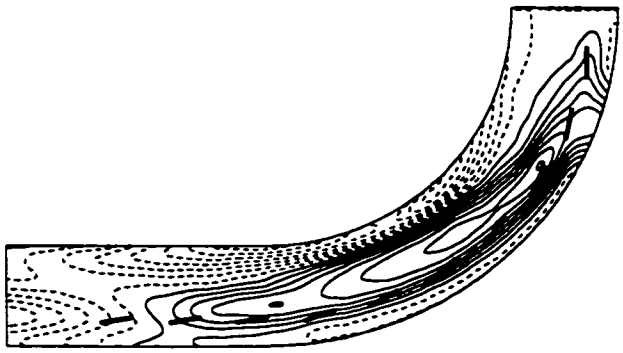

(a)

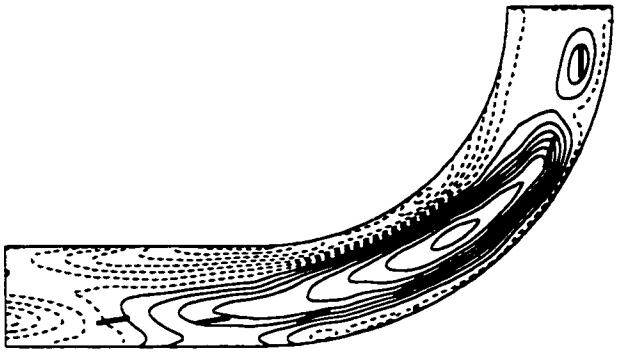

(b)

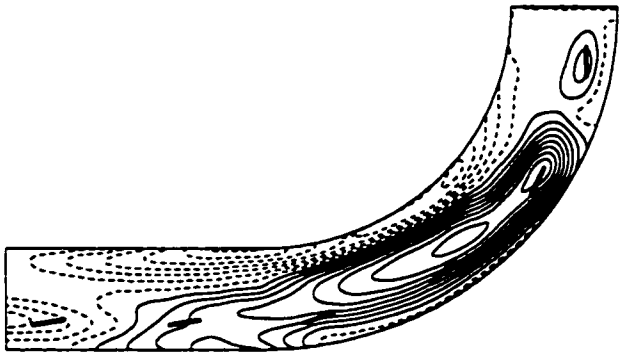

(c)

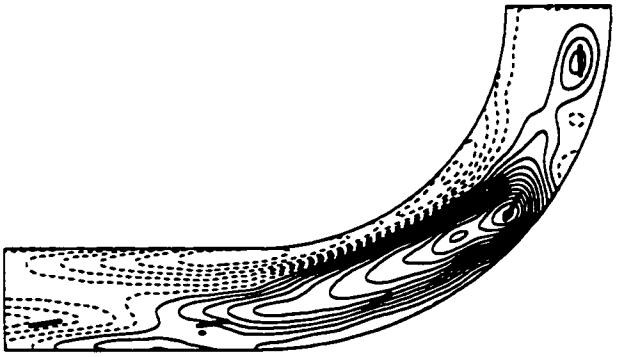

(d)

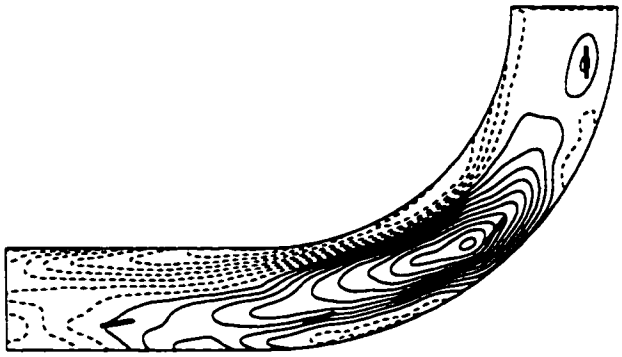

(e)

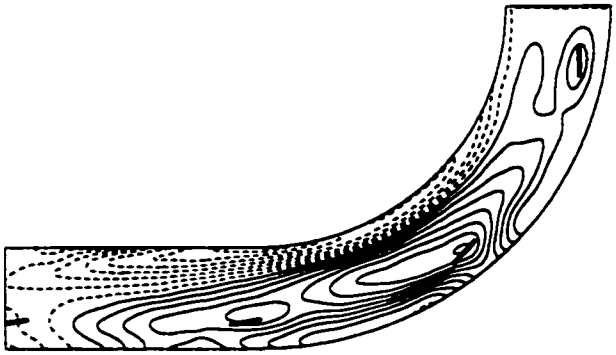

(f)

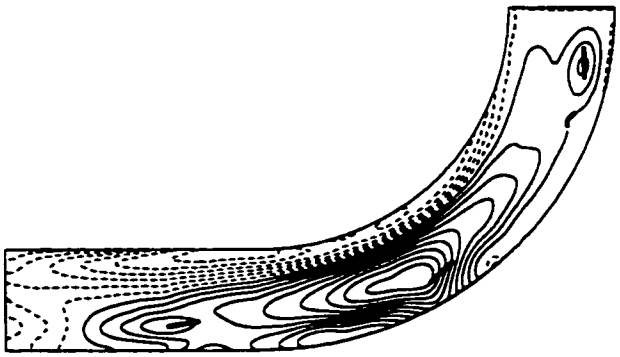

(g)

Figure F.17: Topographic plots for:

Fig.	H/d_1	L/b	δ_1/b	α
(a)	0.50	0.33	0.33	8°
(b)	0.50	0.33	0.66	8°
(c)	0.50	0.33	0.98	8°
(d)	0.50	0.33	1.31	8°
(e)	0.50	0.33	1.63	8°
(f)	0.50	0.33	1.97	8°
(g)	0.50	0.33	2.30	8°

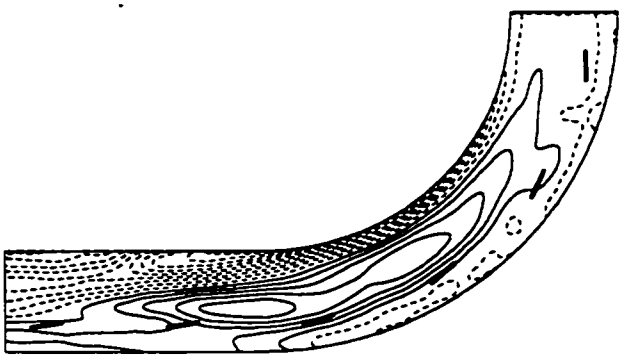

(a)

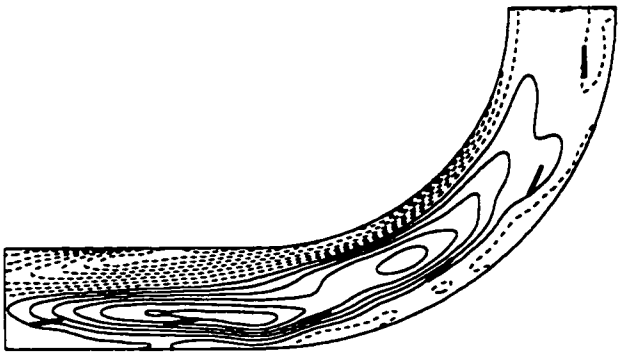

(b)

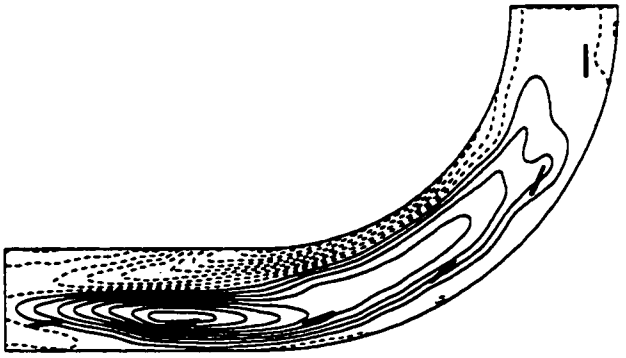

(c)

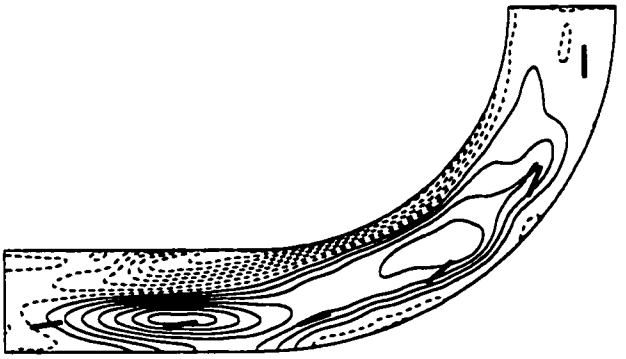

(d)

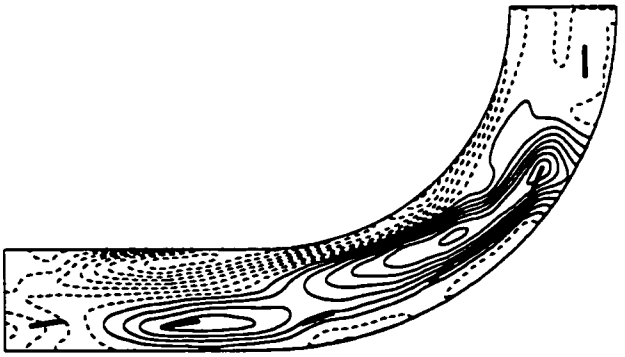

(e)

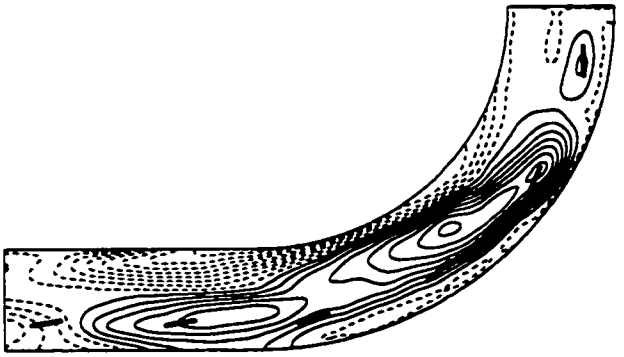

(f)

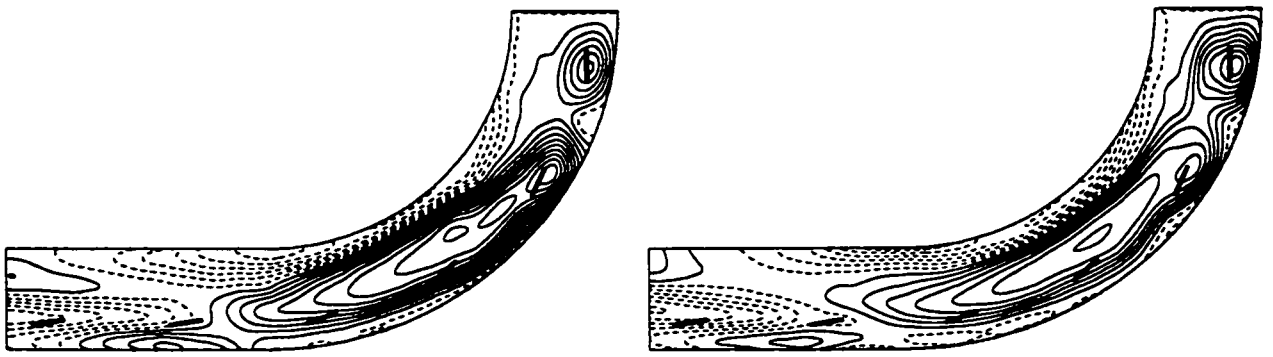

(g) (h)

Figure F.18: Topographic plots for:

Fig.	H/d_1	L/b	δ_1/b	α
(a)	0.50	0.33	0.98	-4°
(b)	0.50	0.33	0.98	0°
(c)	0.50	0.33	0.98	2°
(d)	0.50	0.33	0.98	5°
(e)	0.50	0.33	0.98	8°
(f)	0.50	0.33	0.98	10°
(g)	0.50	0.33	0.98	15°
(h)	0.50	0.33	0.98	18°

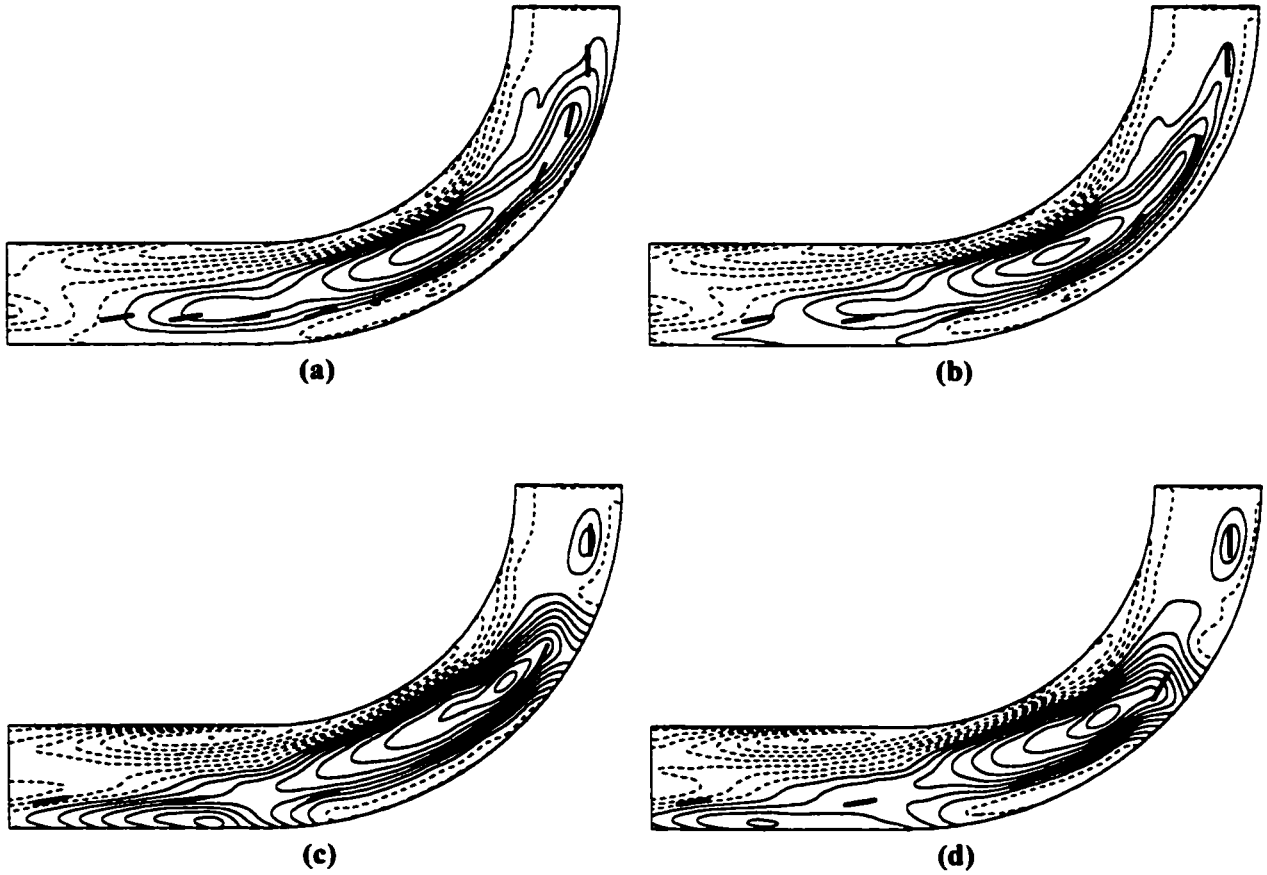

Figure F.19: Topographic plots for:

Fig.	H/d_t	L/b	δ_t/b	α
(a)	0.65	0.33	0.33	8°
(b)	0.65	0.33	0.66	8°
(c)	0.65	0.33	0.98	8°
(d)	0.65	0.33	1.31	8°

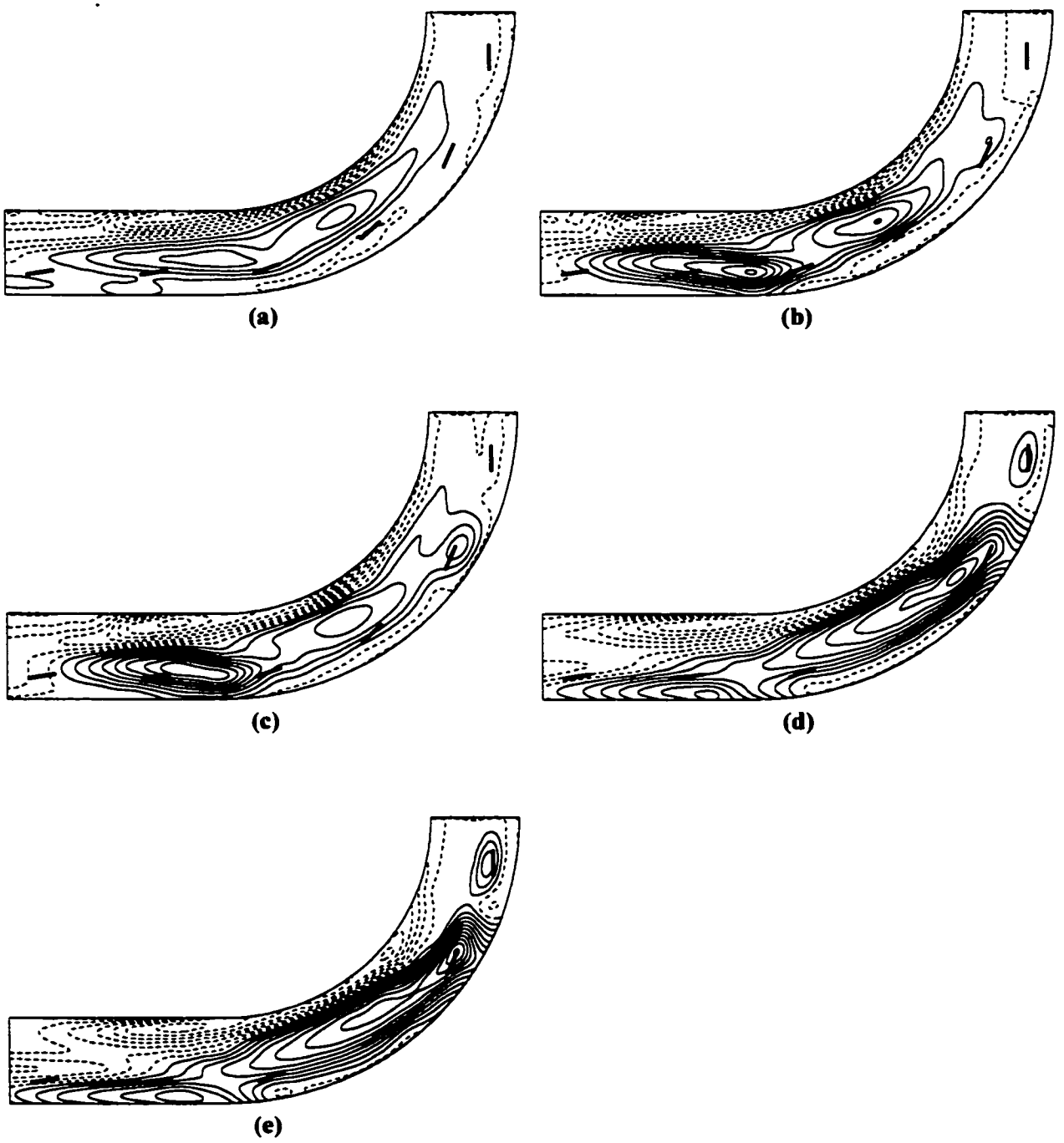

Figure F.20: Topographic plots for:

Fig.	H/d,	L/b	δ/b	α
(a)	0.65	0.33	0.98	-4°
(b)	0.65	0.33	0.98	0°
(c)	0.65	0.33	0.98	4°
(d)	0.65	0.33	0.98	8°
(e)	0.65	0.33	0.98	12°

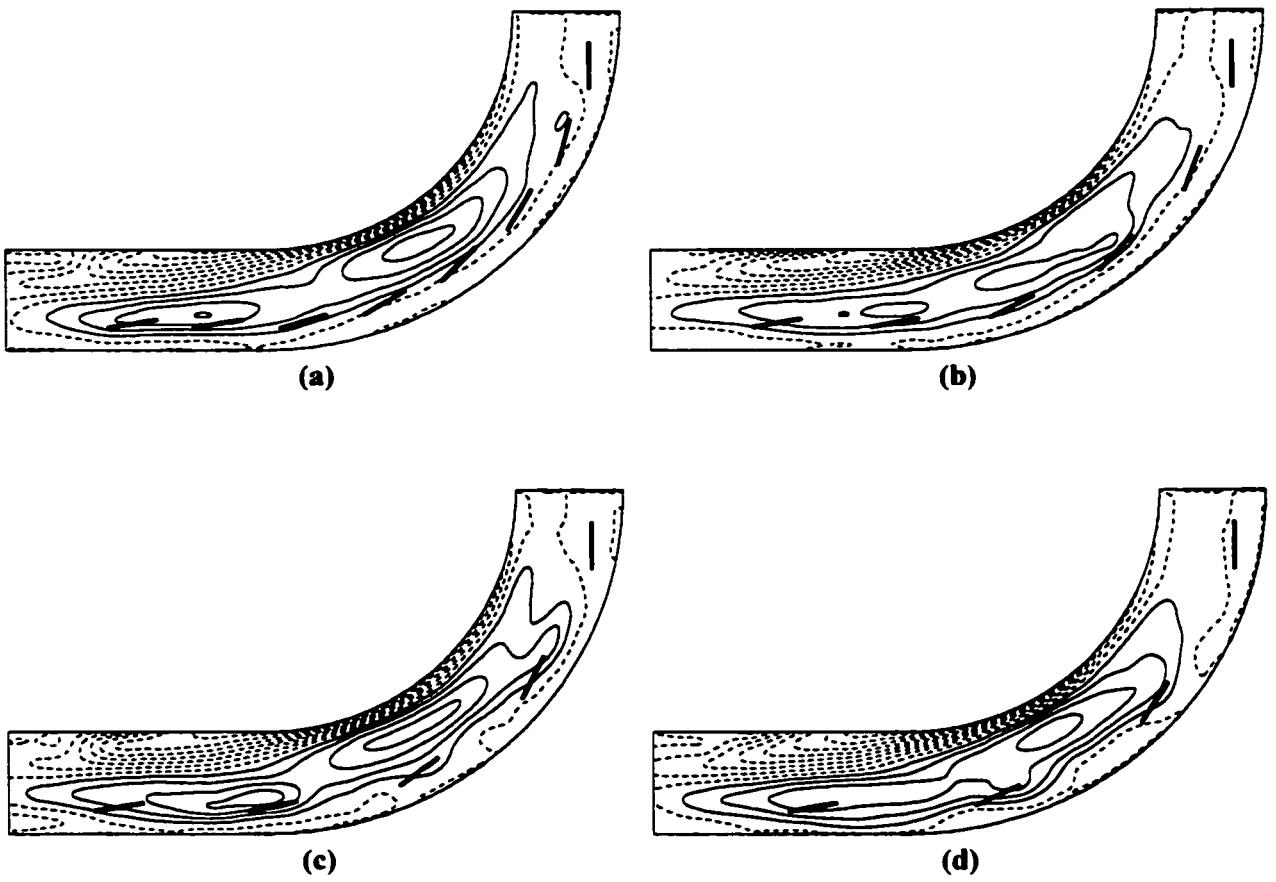

Figure F.21: Topographic plots for:

Fig.	H/d_1	L/b	δ_1/b	α
(a)	0.35	0.49	0.33	8°
(b)	0.35	0.49	0.66	8°
(c)	0.35	0.49	0.98	8°
(d)	0.35	0.49	1.31	8°

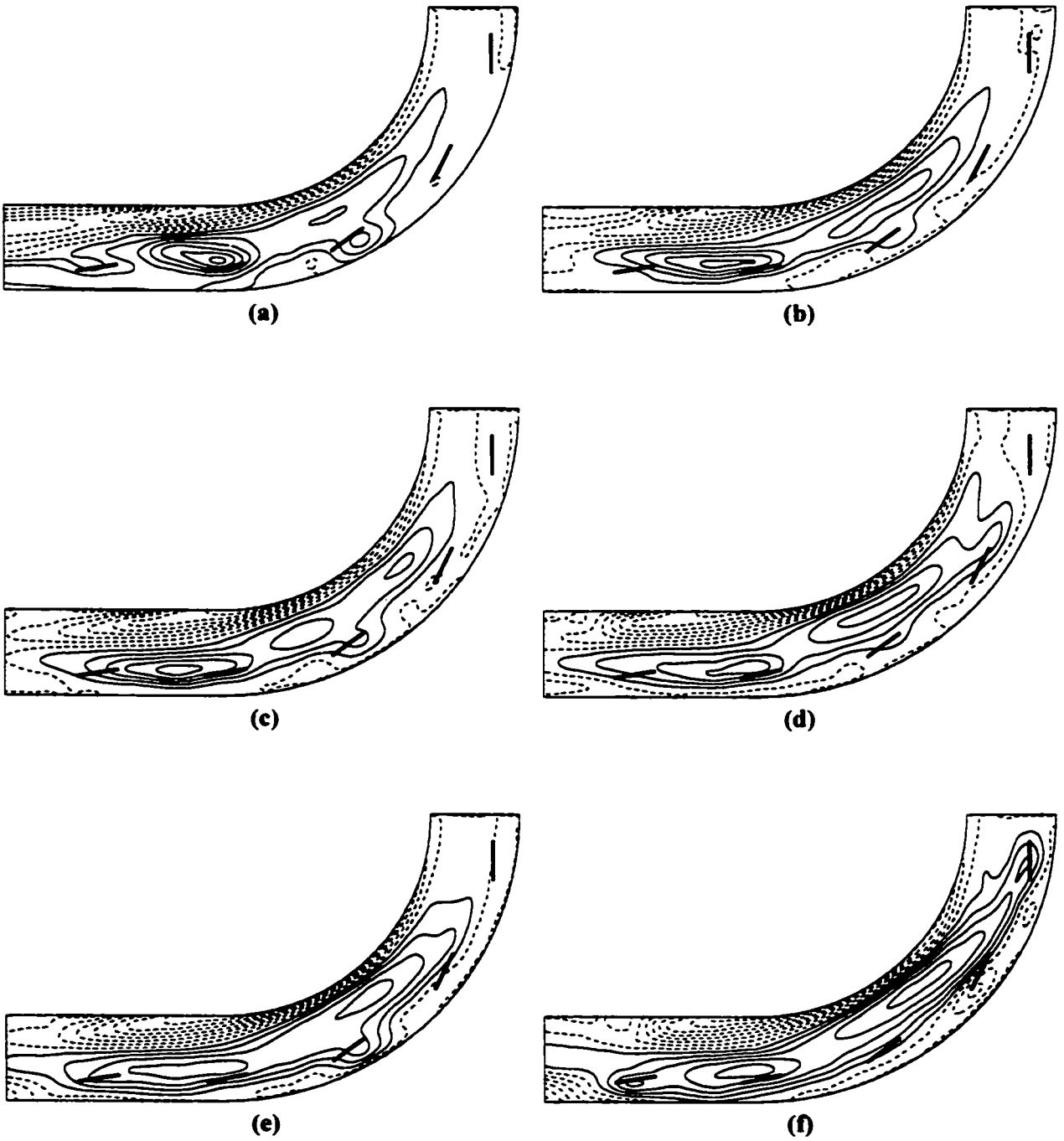

Figure F.22: Topographic plots for:

Fig.	H/d_i	L/b	δ_i/b	α
(a)	0.35	0.49	0.98	-4°
(b)	0.35	0.49	0.98	0°
(c)	0.35	0.49	0.98	4°
(d)	0.35	0.49	0.98	8°
(e)	0.35	0.49	0.98	12°
(f)	0.35	0.49	0.98	16°

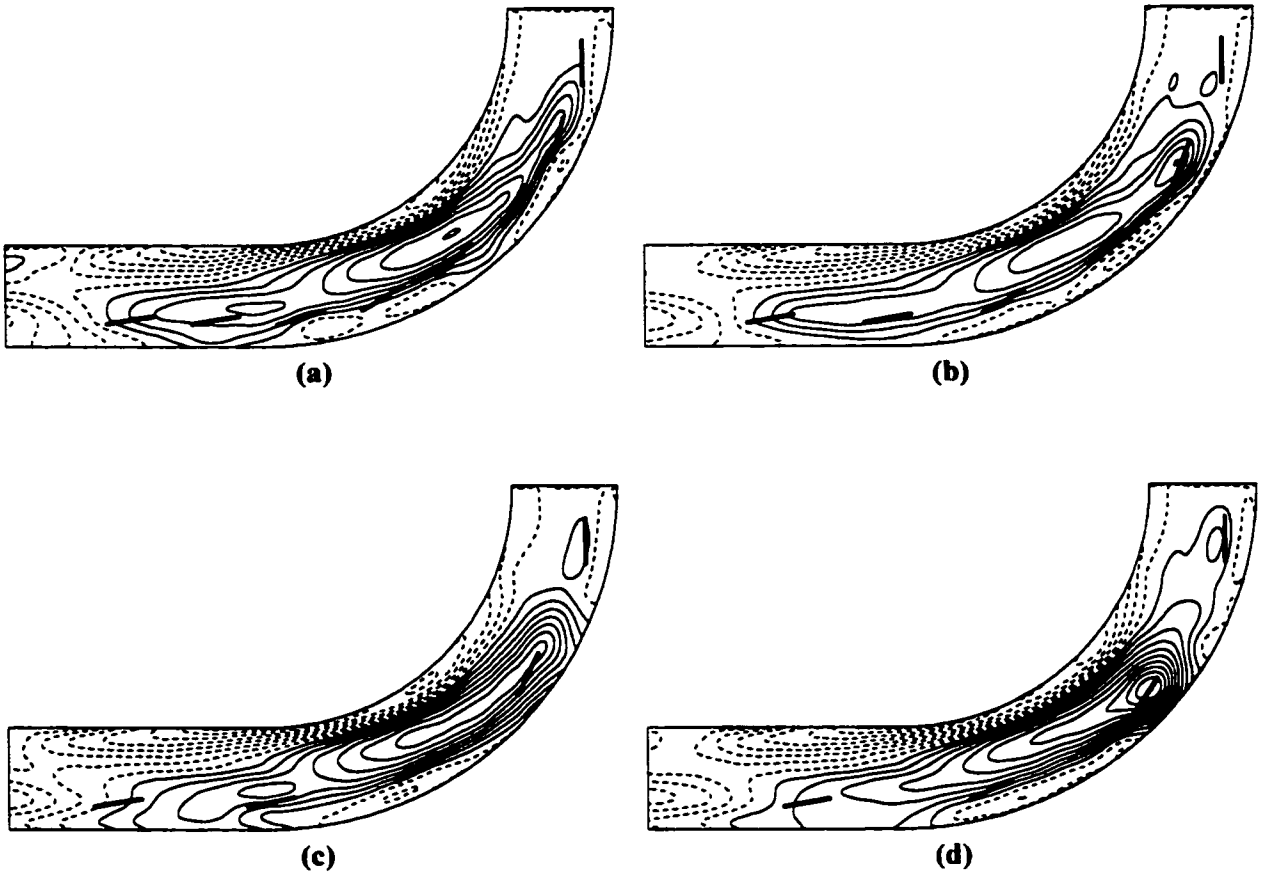

Figure F.23: Topographic plots for:

Fig.	H/d_s	L/b	δ_s/b	α
(a)	0.50	0.49	0.33	8°
(b)	0.50	0.49	0.66	8°
(c)	0.50	0.49	0.98	8°
(d)	0.50	0.49	1.31	8°

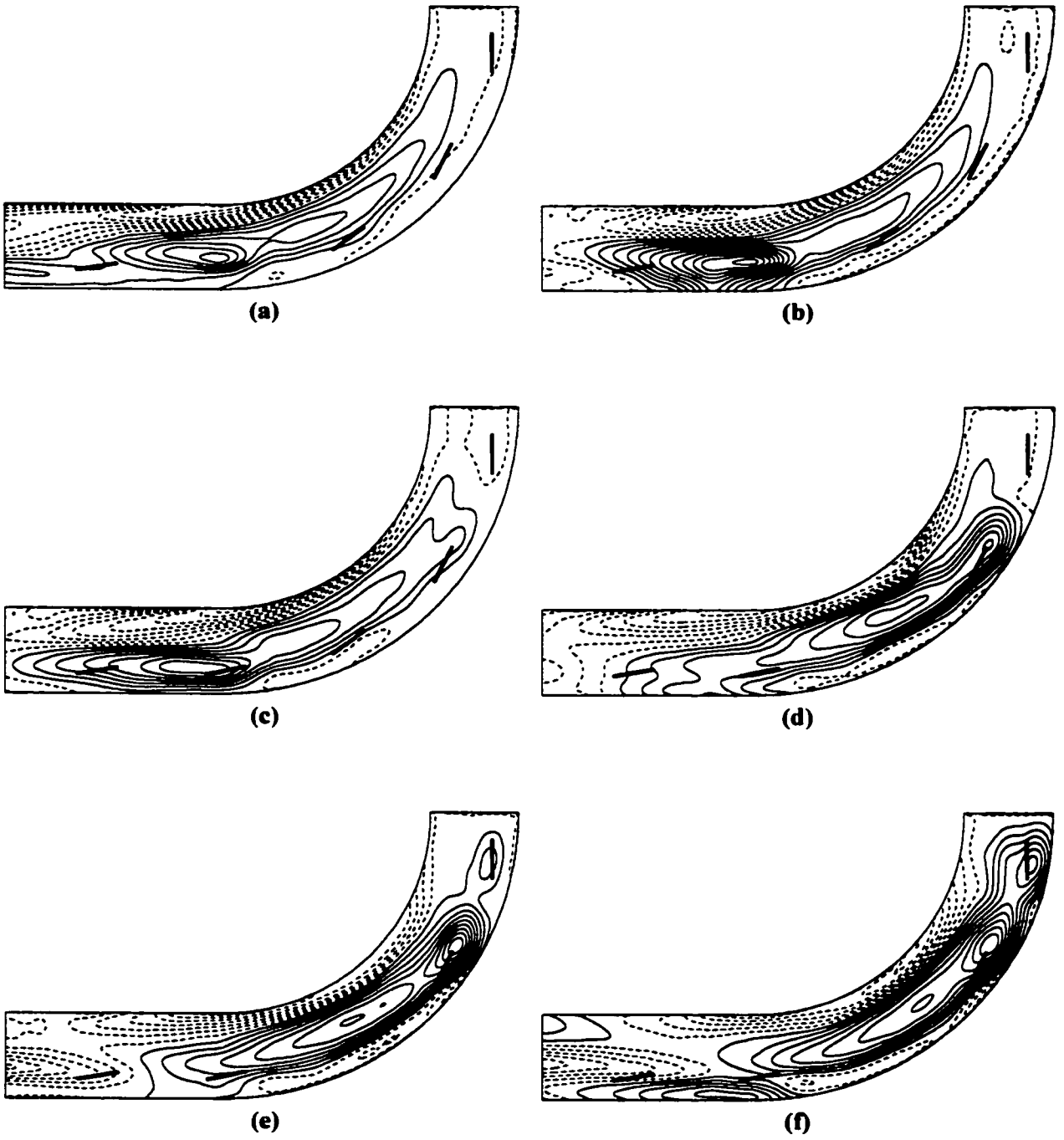

Figure F.24: Topographic plots for:

Fig.	H/d_s	L/b	δ_s/b	α
(a)	0.50	0.49	0.98	-4°
(b)	0.50	0.49	0.98	0°
(c)	0.50	0.49	0.98	4°
(d)	0.50	0.49	0.98	8°
(e)	0.50	0.49	0.98	12°
(f)	0.50	0.49	0.98	16°

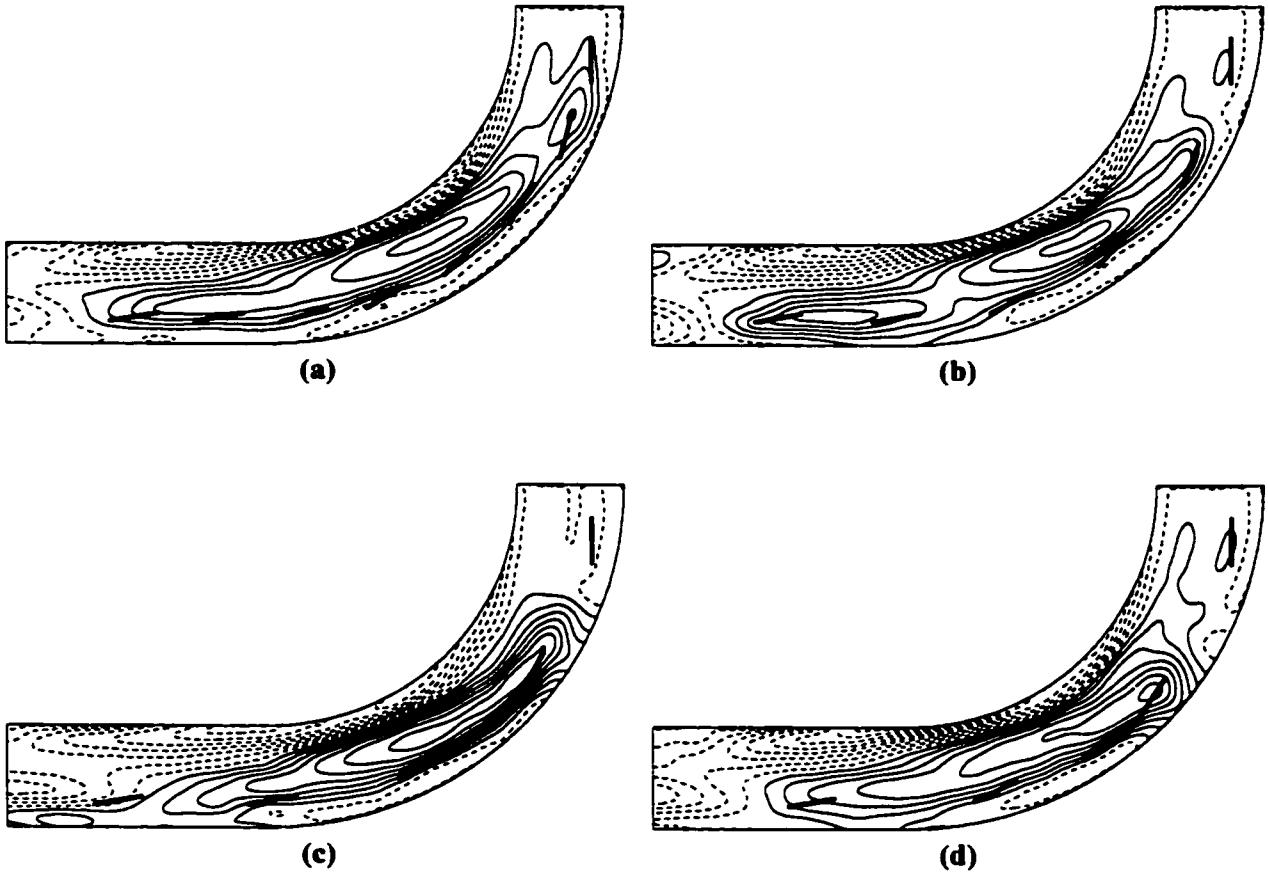

Figure F.25: Topographic plots for:

Fig.	H/d,	L/b	δ/b	α
(a)	0.65	0.49	0.33	8°
(b)	0.65	0.49	0.66	8°
(c)	0.65	0.49	0.98	8°
(d)	0.65	0.49	1.31	8°

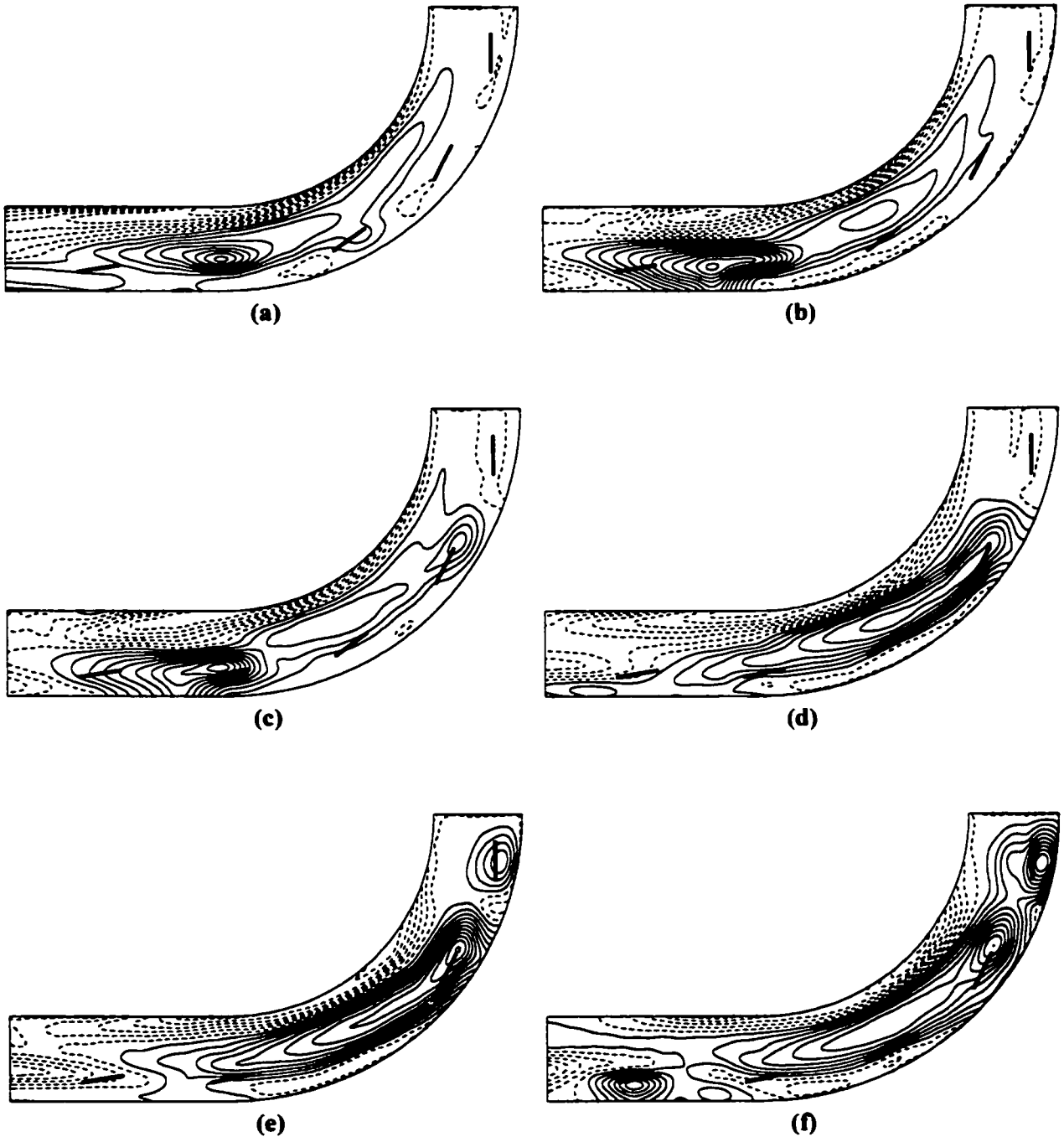

Figure F.26: Topographic plots for:

Fig.	H/d_s	L/b	δ_s/b	α
(a)	0.65	0.49	0.98	-4°
(b)	0.65	0.49	0.98	0°
(c)	0.65	0.49	0.98	4°
(d)	0.65	0.49	0.98	8°
(e)	0.65	0.49	0.98	12°
(f)	0.65	0.49	0.98	16°

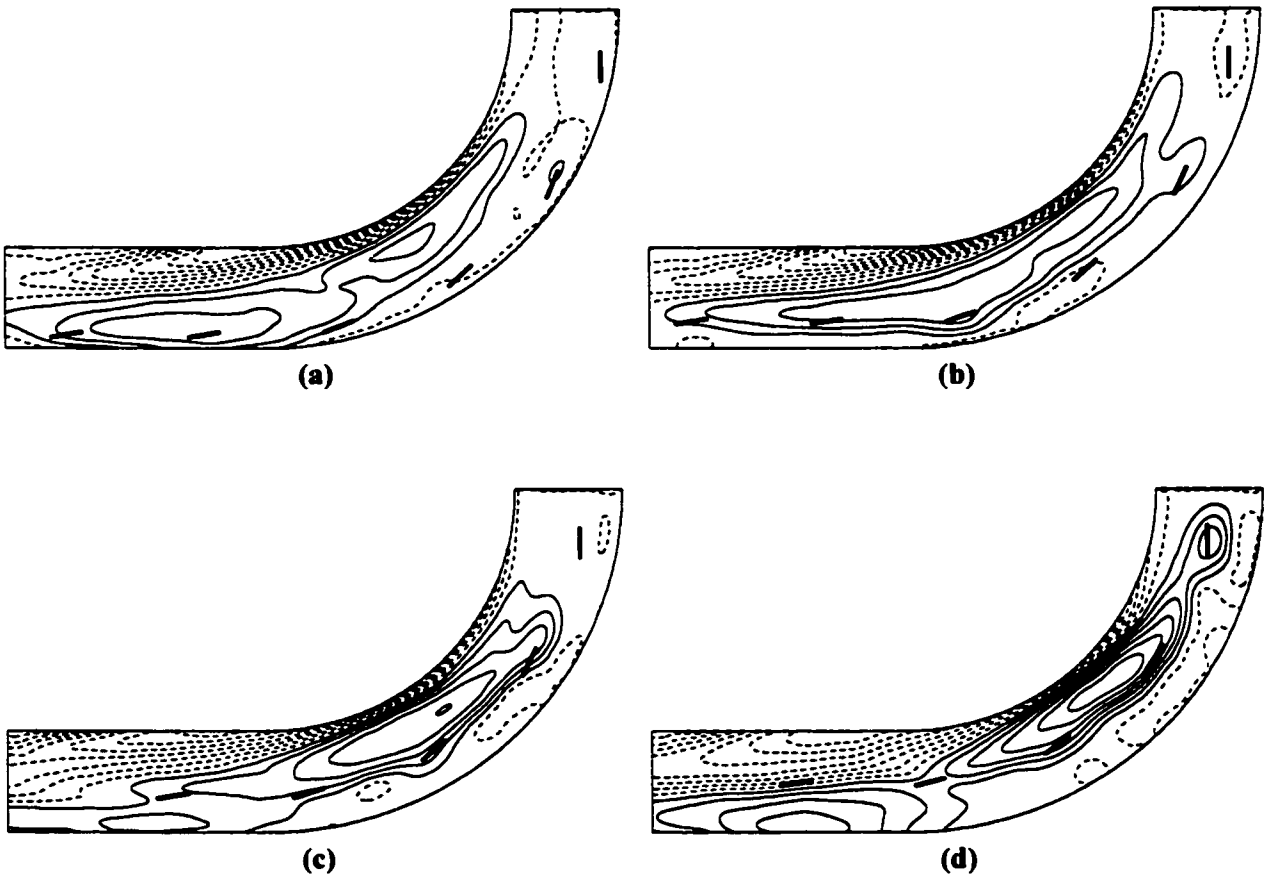

Figure F.27: Topographic plots for:

Fig.	H/d_1	L/b	δ_v/b	δ_h/b	α
(a)	0.35	0.33	0.98	0.13	4°
(b)	0.35	0.33	0.98	0.26	4°
(c)	0.35	0.33	0.98	0.36	4°
(d)	0.35	0.33	0.98	0.49	4°

F.2 135° Bend

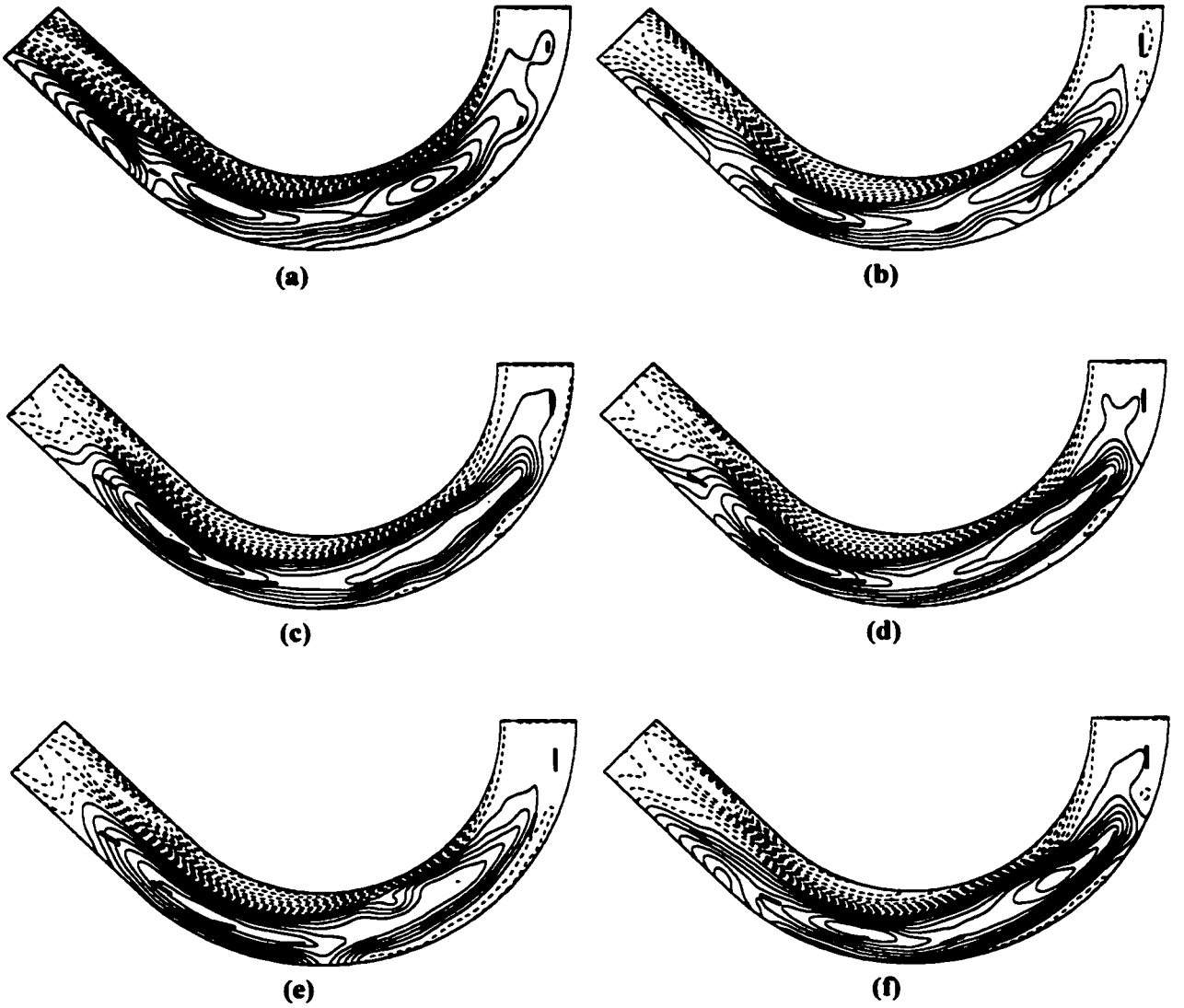

Figure F.28: Topographic plots for:

Fig.	H/d_1	L/b	δ_1/b	α
(a)	0.50	0.16	0.98	0°
(b)	0.25	0.33	0.98	4°
(c)	0.35	0.33	0.98	4°
(d)	0.35	0.33	0.98	4°
(e)	0.35	0.33	0.66	4°
(f)	0.50	0.33	0.98	4°

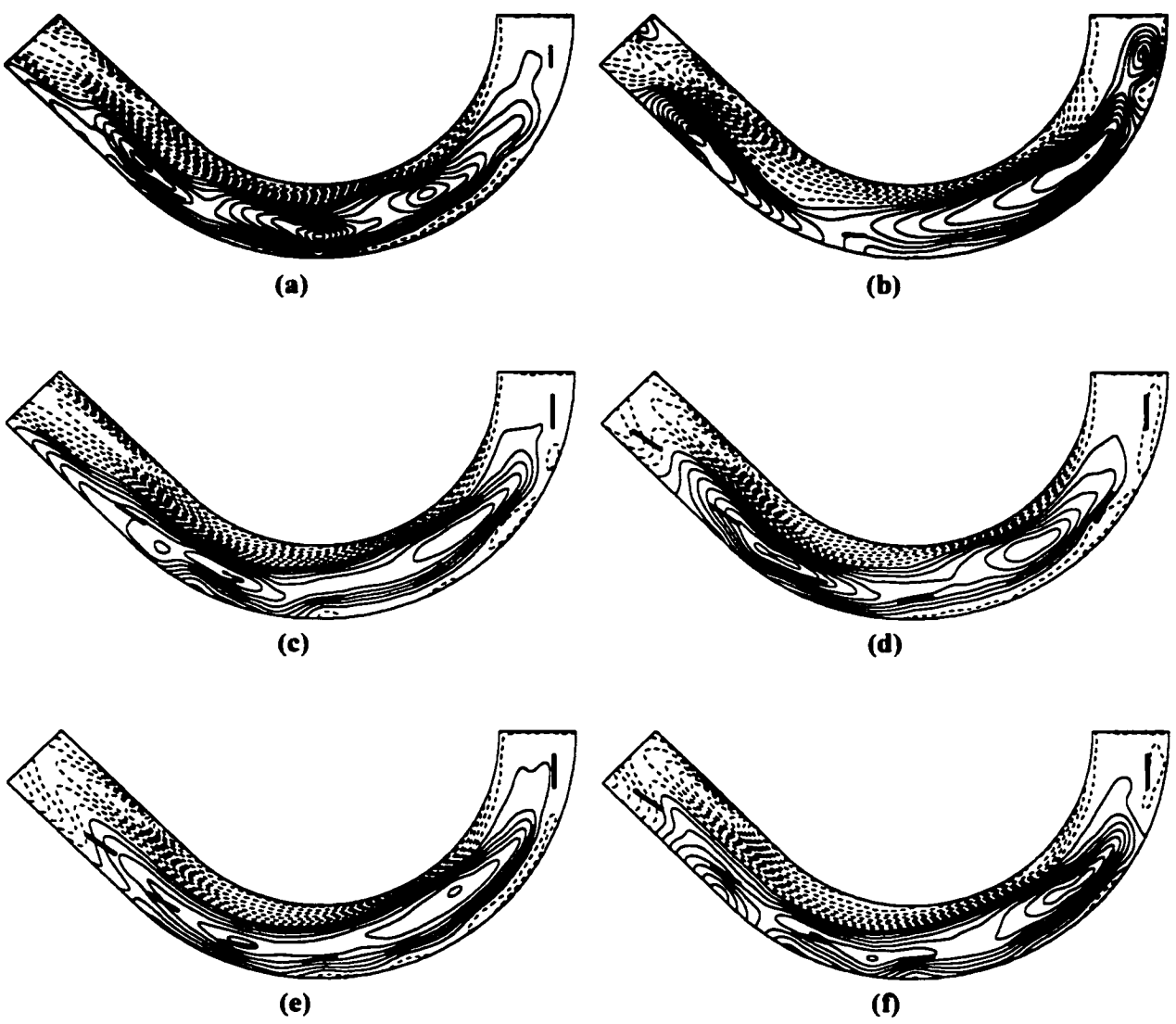

Figure F.29: Topographic plots for:

Fig.	H/d_1	L/b	δ_1/b	α
(a)	0.65	0.33	0.98	0°
(b)	0.65	0.33	0.98	8°
(c)	0.35	0.49	0.98	0°
(d)	0.35	0.49	0.98	4°
(e)	0.35	0.49	0.66	8°
(f)	0.50	0.49	0.98	4°

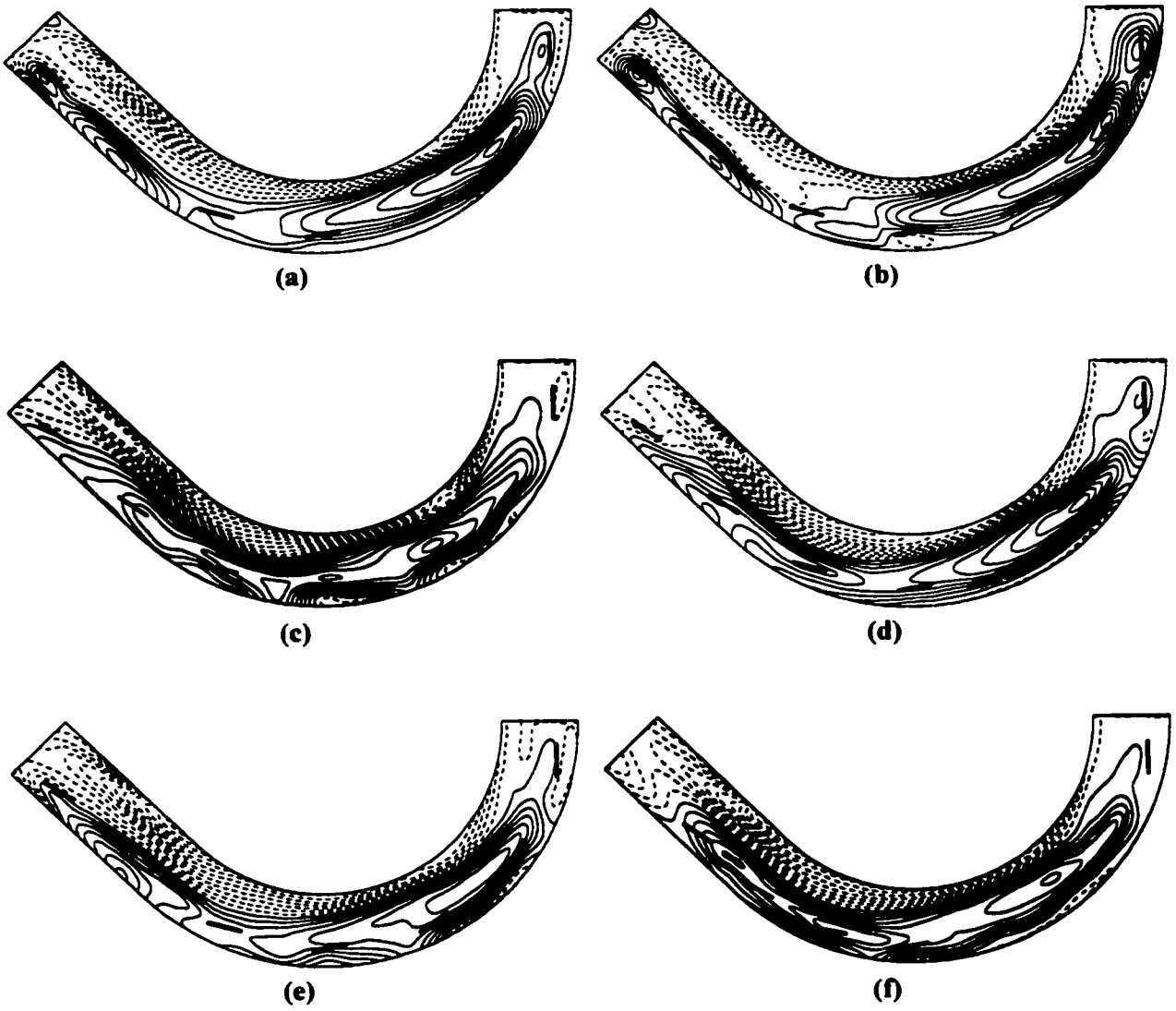

Figure F.30: Topographic plots for:

Fig.	H/d_1	L/b	δ_1/b	α
(a)	0.50	0.49	0.98	8°
(b)	0.50	0.49	0.98	12°
(c)	0.65	0.49	0.98	0°
(d)	0.65	0.49	0.98	4°
(e)	0.65	0.49	0.98	4°
(f)	0.65	0.49	0.66	4°

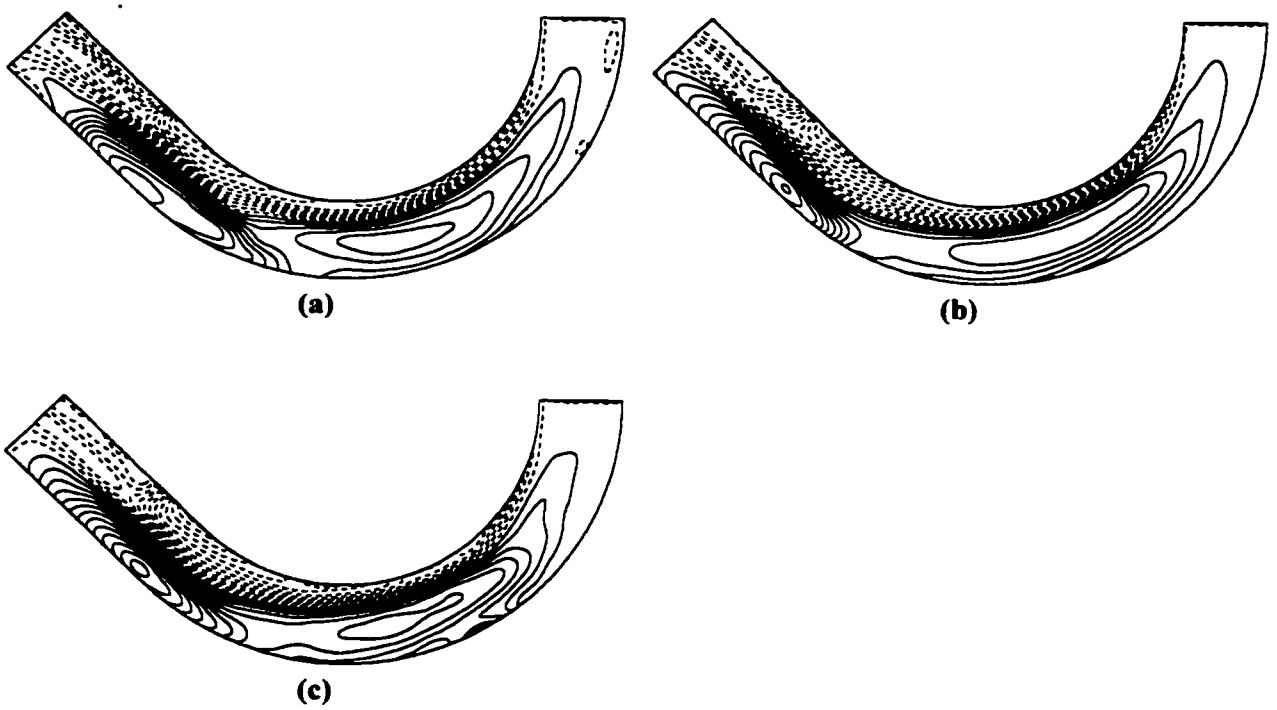

Figure F.31: Topographic plots for:

Fig.	Scenario
(a)	No vanes (at start of experimental program)
(b)	No vanes (at end of experimental program)
(c)	No vanes (uncompacted sand bed)